Technical Report

TURBULENT DIFFUSION IN A
STABLY STRATIFIED BOUNDARY LAYER

by

Stanley Berns Koehler

Fluid Mechanics Program
College of Engineering
Colorado State University
Fort Collins, Colorado

March 1967

CER66-67SBK41

ABSTRACT OF DISSERTATION

TURBULENT DIFFUSION

On a practical level of application the problem studied
in this dissertation is that of the dispersal of a "pollut-
ant" gas in air under inversion conditions. The experimen-
tal work was performed in the U.S. Army Meteorological Wind
Tunnel at Colorado State University. Using helium gas as a
tracer, or "pollutant," diffusion from a point source was
studied within a "two-dimensional" turbulent boundary-layer
flow over a smooth cold plate ($\sim$30°F). Concentration pro-
files downstream from a simulated point source located on
the floor of the wind tunnel were measured using flow veloc-
ities of 5, 6, 7, 10, 20 fps with a $\Delta T=0$ and $\Delta \tilde{T}=-110^{\circ}$F
($\Delta T=T_{wall}-T_{\infty}$) where T_{∞} is the free stream temperature.

Velocity and temperature data were modeled using the
Monin-Obukhov (1954) velocity and temperature profiles:

$$\frac{k(u_r - u_s)}{u_*} = \ln \frac{z_r}{z_s} + \frac{\mathcal{B}}{L} (z_r - z_s) \qquad 3.19$$

and:

$$\frac{k(T_r - T_s)}{T_*} = \ln \frac{z_r}{z_s} + \frac{\mathcal{B}}{L} (z_r - z_s) \qquad 3.20$$

with "universal" constant $\mathcal{B}$ and where k, von Karman's con-
stant, is 0.4; where u_r and T_r are reference velocity and
reference temperature at reference height z_r; and where u_s
and T_s are velocity and temperature at variable height z_s.
A technique is demonstrated by which one may solve for the
"averaged" constants u_*, T_*, $\mathcal{B}$, and L.

Two basic theories were formulated, experimentally verified, and presented in this dissertation. Using a "Lagrangian similarity hypothesis" and the above-mentioned velocity and temperature profiles, a theoretical relationship was developed relating the vertical dispersion of a pollutant to the downwind distance. Then, based on physical and empirical reasoning, the maximum floorline concentration was theoretically related to this same downwind distance. The experimental concentration results agree very well with the two theoretical predictions. These two relationships were numerically solved using a 1620 IBM Computer and are graphically represented.

While additional experimental work would be an interesting adjunct to the work herein presented, the experimental results obtained herein give excellent agreement with the theoretical predictions and serve to show that one may use theoretical models and laboratory experimental work in the increasingly important field of air pollution and its relation to the atmospheric condition known as temperature inversion.

S. B. Koehler, Research Assistant
Fluid Mechanics Program
Civil Engineering Department
Colorado State University
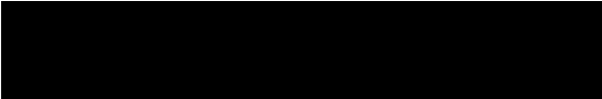Fort Collins, Colorado
March 1967

ACKNOWLEDGMENTS

TABLE OF CONTENTS

LIST OF FIGURES

NOMENCLATURE

Alphabetic Letters

Symbols	Quantity	Dimension
A,B	Constants in eqs 5.19 and 5.20	----
b	Batchelor's constant; exponent in eq 4.2	----
C	Floorline concentration	ppm
C_m, C_o	Floorline maximum concentration	ppm
c	Constant	----
c'	Concentration fluctuation	ppm
c_p	Specific heat at constant pressure	$\dfrac{L^2}{T^2 \theta}$
E	Mean turbulent kinetic energy	$\dfrac{ML^2}{T^3}$
f	Function	----
F	Force per unit volume	$\dfrac{M}{T^2 L^2}$
g	Acceleration of gravity	$\dfrac{L}{T^2}$
g_c	Dimensional constant	$\dfrac{ML}{FT^2}$
H,h	Characteristic height	L
h_t	Coefficient of heat transfer	$\dfrac{M}{T^3 \theta}$
K_i	Diffusion coefficient	$\dfrac{L^2}{T}$
K_{ij}	Diffusion tensor	$\dfrac{L^2}{T}$
K_H	Eddy conductivity	$\dfrac{L^2}{T}$

Alphabetic Letters - continued

Symbols	Quantity	Dimension
K_M	Eddy viscosity	$\dfrac{L^2}{T}$
k	von Karman's constant	----
k_t	Coefficient of thermal conductivity	$\dfrac{ML}{T^3\theta}$
L	Stability length defined in eq 3.18	L
L_c	Characteristic length	L
ℓ	Length characterizing local intensity of turbulent mixing, $\ell = kz$	L
m	Exponent in power laws, exponent	----
N	Macroviscosity $N=u_* z_0$	$\dfrac{L^2}{T}$
n	Sutton's n defined in eq 2.16	----
n_y	Lateral diffusion	L
n_z	Vertical diffusion	L
P	Pressure	$\dfrac{M}{LT^2}$
p,q,r	Exponents in eq 2.42	----
Q	Source strength	$\dfrac{L^3}{T}$
q	Heat flux	$\dfrac{ML^2}{T^2}$
T_*	Friction temperature defined in eq 3.3	θ
T'	Temperature fluctuation	θ
T, T_w, T_∞	Temperature, on floor, freestream	θ

Alphabetic Letters - continued

Symbols	Quantity	Dimension
T_o	Temperature at height z_o	θ
t	Time	T
u_*	Friction temperature	$\dfrac{L}{T}$
$\bar{u}_i, \bar{u}, \bar{v}, \bar{w}$	Mean velocities	$\dfrac{L}{T}$
u_i', u', v', w'	Turbulent velocity fluctuations	$\dfrac{L}{T}$
$\tilde{u}$	Mean velocity defined in eq 3.59	$\dfrac{L}{T}$
$\overline{u'w'}$	Reynolds stress	$\left(\dfrac{L}{T}\right)^2$
w	Work per unit volume	$\dfrac{M}{T^2 L}$
x_o	Adiabatic entry length	L
$x_i; x, y, z$	Components of cartesian coordinate system	L
$\tilde{y}$	Standard deviation for particles moving in crosswind direction $\tilde{y} = (\overline{y^2})^{\frac{1}{2}}$	L
$\tilde{z}$	Mean position of vertical displacement of fluid particles $\tilde{z} = (\overline{z^2})^{\frac{1}{2}}$	L
z_o	Roughness length	L
z	Length	L
$z_r, z_{r'}$	Reference heights	L
$z_s, z_{s'}$	Reference heights	L

Greek Letters

Symbols	Quantity	Dimension
α	Ratio of $\dfrac{K_H}{K_M}$	---
β	Universal constant	---
β_t	Coefficient of thermal expansion	$\dfrac{1}{\Theta}$
Δ or ∇^2	Laplacian operator, $\dfrac{\partial^2}{\partial x_i^2}$	---
γ, γ_t	Exponents in eqs 5.19 and 5.20	---
$\delta, \delta_h, \delta_t$	Momentum boundary layer thickness; heated; thermal	L
Γ	Adiabatic lapse rate	$\dfrac{\Theta}{L}$
ε_p	Representative mean height of surface protuberance	L
ε_d	Dissipation of energy per unit mass of the fluid	$\dfrac{ML^2}{T^3}$
ε_k	Eddy heat conductivity	$\dfrac{ML}{T^2\Theta}$
ε_μ	Eddy viscosity	$\dfrac{M}{LT}$
f, f_o	Stability parameters based on $\dfrac{\bar{z}}{L}$ and $\dfrac{z_o}{L}$	---
$\tilde{n}, n_o$	Stability parameters based on $\dfrac{y}{L}$ and $\dfrac{z_o}{L}$	---
n	Vertical length scale of concentration profile, $\dfrac{C(x,0,n)}{C_m} = 0.5$	L

Greek Letters

Symbols	Quantity	Dimension
α	Ratio of $\dfrac{K_H}{K_M}$	----
β	Universal constant	----
β_t	Coefficient of thermal expansion	$\dfrac{1}{\Theta}$
Δ or ∇^2	Laplacian operator, $\dfrac{\partial^2}{\partial x_i^2}$	----
γ, γ_t	Exponents in eqs 5.19 and 5.20	----
$\delta, \delta_h, \delta_t$	Momentum boundary layer thickness; heated; thermal	L
Γ	Adiabatic lapse rate	$\dfrac{\Theta}{L}$
ε_p	Representative mean height of surface protuberance	L
ε_d	Dissipation of energy per unit mass of the fluid	$\dfrac{ML^2}{T^3}$
ε_k	Eddy heat conductivity	$\dfrac{ML}{T^2\Theta}$
ε_μ	Eddy viscosity	$\dfrac{M}{LT}$
f, f_o	Stability parameters based on $\dfrac{\bar{z}}{L}$ and $\dfrac{z_o}{L}$	----
$\tilde{n}, n_o$	Stability parameters based on $\dfrac{\bar{y}}{L}$ and $\dfrac{z_o}{L}$	----
n	Vertical length scale of concentration profile, $\dfrac{C(x,0,n)}{C_m} = 0.5$	L

NOMENCLATURE - continued

Greek Letters - continued

Symbols	Quantity	Dimension
Θ	Potential temperature, $\Theta = (T + \Gamma z)$	Θ
λ	Half horizontal length scale of concentration profile, $\dfrac{C(x,\lambda,0)}{C_m} = 0.5$	L
μ	Absolute viscosity	$\dfrac{M}{LT}$
ν	Kinematic viscosity	$\dfrac{L^2}{T}$
ρ	Mass density	$\dfrac{M}{L^3}$
τ	Shearing stress	$\dfrac{M}{LT^2}$
τ_o	Shearing stress at wall	$\dfrac{M}{LT^2}$
σ^2	Variance	L^2
ϕ	Function	----
ω	Time defined in eq 3.18	T

Dimensionless Groups

$\tilde{c}$	Maximum floorline concentration	$\dfrac{u_* L^2 C_o}{Qk}$
$\tilde{\varepsilon}$	Downwind distance in eq 3.54	$\dfrac{k^2 \tilde{x}}{L}$
ε	Downwind distance in eq 3.56a	$\dfrac{kb\bar{x}}{L}$

NOMENCLATURE - continued

Dimensionless Groups - continued

Symbols	Quantity	Dimension
Fr	Froude No.	$\dfrac{U^2}{L_c g}$
Gr	Grashof No.	$\dfrac{L_c^3 g \rho^2}{\mu^2}(\beta_t \Delta T)$
Nu	Nusselt No.	$\dfrac{h_t L_c}{k_t}$
Pr	Prandtl No., laminar	$\dfrac{c_p \mu}{k_t}$
Pr_t	Prandtl No., turbulent	$\dfrac{c_p \varepsilon_\nu}{\varepsilon_k} = \dfrac{K_M}{K_H} = \alpha$
Re_δ	Reynolds No. based on boundary layer thickness	$\dfrac{\delta U \rho}{\mu}$
Re_x	Reynolds No. based on downwind distance from leading edge	$\dfrac{x U \rho}{\mu}$
Ri	Gradient Richardson No.	$\dfrac{g\left(\frac{\partial T}{\partial z}\right)}{T\left(\frac{\partial U}{\partial z}\right)^2}$
Rf	Flux Richardson No.	$\dfrac{K_H\, g\left(\frac{\partial T}{\partial z}\right)}{K_M\, T\left(\frac{\partial U}{\partial z}\right)^2}$
Sn	Stability parameter in eq 2.27	$\dfrac{g \theta_*}{T u_*^2}$

CHAPTER I

INTRODUCTION

A. <u>History of Theory</u>

A landmark in the early development of the study of atmospheric turbulence was the formulation of the concept of the "Austausch" (exchange) coefficient by W. Schmidt and G. I. Taylor. This hypothesis adapted the fundamental ideas of the kinetic theory of gases and applied them to turbulence. This new concept was built on ideas then current in the field of aerodynamics and was later used in research by von Karman, Prandtl, and others. An early, practical and notably meteorological investigation by Taylor (1915)[*] was concerned with the formation of fog when warm air flowed over the Great Banks of Newfoundland. Taylor applied the ideas to the vertical diffusion of heat through the lowest layers of a thermally stratified atmosphere.

These beginnings (1,2)[*] served to emphasize that much of the interest in turbulence by the meteorologist and fluid dynamicist lay in the transport properties -- notably in sensible heat, momentum, concentration, and water vapor or heat in latent form.

The small-scale turbulent flux of these quantities in the vertical direction generally far exceeds that in the horizontal direction particularly in the lower

---

[*] Numbers in parentheses refer to "References."

atmosphere. Thus, the vertical flux plays a dominant role in the study of vertical (concentration) diffusion or "spread." The theoretical solution to the small-scale "diffusion" problem has generally evolved around two basic approaches: 1. the classical-approach solution to the diffusion equation, using the concepts of the "Aus-tausch" or K-theory approaches; 2. the statistical approach or the theory of continuous movements. Both these theories are applicable under certain conditions to free stream flow and are not generally valid in the boundary layer flow.

To date, many theoretical and experimental diffusion studies have been in the direction of attempts to modify the above two basic theories so that they might be extended or applied to boundary layer flow. Much of this experimental work has been in the nature of field studies (which are subject to varying atmospheric conditions). A few studies have been made in wind tunnels so that the variables of flow may be more adequately controlled or stabilized.

This dissertation is concerned with <u>Turbulent Diffusion in a Stably Stratified Boundary Layer</u>. Stable flow conditions can be simulated in the wind tunnel by cooling the lower boundary and heating the circulating air. This represents the night-time conditions present in the atmosphere under a temperature inversion. This "stable flow stratification" is also called an inversion or

temperature inversion. This inversion is also one of the primary causes in the containment of air pollutants and the attendant air pollution problems commonly occurring in some of the larger cities of the U.S.A.

To date, work has been done both in the field and in the wind tunnel analyzing neutral and unstable diffusion. There has been some work on stable diffusion that was based on field studies, but to date there has been no published work on turbulent diffusion in a stably strati- fied boundary layer that has been obtained in a wind tunnel. Colorado State University has the only facilities capable of performing such studies at present.

B. Background of Present Theory

The basic theory of this dissertation evolves around the velocity profile as proposed by Monin and Obukhov (1954) and is as follows:

The classical experiments of Nikuradse (1) in the laboratory established the existence of various regimes of flow in a turbulent boundary layer. Buoyancy effects were absent, and shearing stress took place under neutral conditions.

The analysis of flow under turbulent conditions in- volves the shear velocity u_* , defined as:

$$u_* = \sqrt{\frac{\tau_0}{\rho}} \qquad\qquad 1.1$$

where τ_o is the shearing stress at the wall and ρ is the density.

Using the mixing-length hypothesis in relation to the velocity profile in a turbulent boundary layer, Nikuradse (1) obtained the nondimensional form of the profile of the mean velocity to be:

$$\frac{\overline{u}}{u_*} = \frac{1}{k} \ln\left(\frac{u_* z}{\nu}\right) + \text{constant} \qquad 1.2$$

For motion near a smooth wall he (1) found eq 1.2 could be written as:

$$\frac{\overline{u}}{u_*} = \frac{1}{k} \ln\left(\frac{u_* z}{\nu}\right) + 5.5 \qquad 1.3$$

and is used for the mid-region of the three flow regions.

It was also found for smooth and rough surfaces that:

$$\frac{u_* z_o}{\nu} < 0.13 \text{ for smooth flow and that:}$$

$$\frac{u_* z_o}{\nu} > 2.5 \text{ for fully-rough flow where } z_o \text{ is}$$

defined as the roughness length.

In the fully-rough regime the influence of viscosity is negligible. Thus, in terms of the mixing length hypothesis, $\frac{\overline{u}}{u_*}$ must depend only on the lengths z , ℓ , and ε_ρ. The unique length is ℓ , which characterizes the local intensity of the turbulent mixing at some height and may be a function of position and of the mean velocity.

ε_ρ is a representative mean height of the surface

protuberances. Taking ℓ = kz , the velocity profile is now:

$$\frac{\bar{u}}{u_*} = \frac{1}{k} \ell n \frac{z}{\varepsilon\rho} + \text{constant} \qquad 1.4$$

which is usually written in the form:

$$\frac{\bar{u}}{u_*} = \frac{1}{k} \ell n \frac{z}{z_0} \qquad z \gg z_0 \text{ and} \qquad 1.5$$

$z_0 \cong \frac{\varepsilon\rho}{30}$. The two profiles, eqs 1.2 and 1.5, are

similar in form when the γ in 1.2 is replaced by $u_* z_0$, a term which Sutton (1) has named "macroviscosity" or "N."

Whether a surface is rough or smooth, the shape of the adiabatic profile is uniquely given by:

$$\frac{\partial \bar{u}}{\partial z} = \frac{u_*}{kz} \qquad 1.6$$

Following Obukhov (1946), Russian experimenters have used the ratio $\frac{z}{L}$ for the diabatic wind profile where for small

$\frac{z}{L}$, $\frac{z}{L} \propto Ri_{No}$ (Richardson No. to be defined later), and

where L is a length defined by:

$$L = - \frac{u_*^3}{k \frac{g}{T} \frac{q}{c_p\rho}} \qquad 1.7$$

To allow for the effects of stability, one may seek generalization of eq 1.6 by writing:

$$\frac{\partial \bar{u}}{\partial z} = \frac{u_*}{kz} f(\eta) \qquad 1.8$$

where η is a stability parameter = $\frac{z}{L}$ and "f" is the function which remains to be determined. For small values

of n and retaining only the first term in a power-series representation of this function n , eq 1.8 may be express-ed as follows:

$$\frac{\partial \bar{u}}{\partial z} = \frac{u_*}{kz}(1 + \beta \frac{z}{L})$$

1.9

where β may be expected to be a universal constant. This assumption was first introduced by Halstead (1943).

Integration of 1.9 gives:

$$\bar{u}(z) = \frac{u_*}{k}(ln\frac{z}{z_0} + \beta \frac{z}{L})$$

1.10

If the temperature profile is assumed to follow the same form as 1.10, it may be written as:

$$T(z) - T(z_0) = \frac{T_*}{k}(ln\frac{z}{z_0} + \frac{z}{L})$$

1.11

The above discussion is further expanded in the text to follow.

CHAPTER II

LITERATURE SURVEY

A. Introduction

As has been mentioned previously, there are two basic
theories utilized in describing the turbulent diffusion
process. This chapter is devoted to a general review of
these two basic theories. This chapter also cites exten-
sions and modifications to these theories. Also, other
work which makes one aware of the development to date in
the field of neutral and stable diffusion is cited.

One of the basic theories is based on the Eulerian
frame of reference to describe the diffusion process.
This Eulerian viewpoint describes the spatial distribution
of the scalar quantity of concentration. If, in describ-
ing this process of diffusion, an exact analogy is made
with the process of molecular diffusion, then the exchange
coefficients are assumed constant as is done in the Kinet-
ic Theory of Gases (1,2). This is then called the "Fick-
ian Diffusion Theory" or the "K-Theory of Diffusion."

The second basic theory is that formulated by G. I.
Taylor (3) and stems from his classical works based on
statistical methods. It employs a Lagrangian frame of
reference and describes the characteristics of a diffusing
medium in terms of mean, variance, standard deviation and
the like.

B. Semi-Empirical Diffusion Theory

If one assumes that the tracer or "pollutant" gas is neither created nor destroyed, one can write for the conservation of mass of an incompressible fluid as follows:

$$\frac{\partial c}{\partial t} + \nabla \cdot (C \vec{V} - \text{grad } KC) = 0 \qquad 2.1$$

Using Reynolds' rules of time-averaging, neglecting molecular diffusivity in comparison to turbulent diffusivity, assuming an incompressible fluid, and operating on eq 2.1, one obtains for the conservation equation the following expression in tensor notation:

$$\frac{\partial \bar{C}}{\partial t} + \frac{\partial}{\partial x_i} (\bar{C} \bar{u}_i) = \frac{\partial}{\partial x_i} (-\overline{c' u_i'}) + K \frac{\partial^2 \bar{C}}{\partial x_i \partial x_i} \qquad 2.2$$

where the bar represents the mean value and the prime represents the fluctuating value. The first term in the above equation is the local temporal variation of concentration; the second term is the convective transport; the third term is the local velocity-concentration fluctuation correlation which is equated to the turbulent diffusion or turbulent exchange in eq 2.3 below. The last term is the molecular diffusion -- and is neglected in turbulent flow.

The problem of turbulent diffusion is then to solve eq 2.2 for the mean concentration C. But the three terms $\overline{c' u_i'}$ are unknown. In the semi-empirical analysis (as is

similarly done in the heat-conduction theory), one may
use Boussinesq's exchange coefficient method of writing
and use:

$$- \overline{c' u_i'} = K_{ij} \frac{\partial \overline{c}}{\partial x_j} \qquad\qquad 2.3$$

This hypothesis related the mean concentration gradient to
the local velocity-concentration fluctuation correlation.
There is no general validity to Boussinesq's hypothesis,
but it has proved adequate for approximating simple flow
fields, such as fully developed pipe flow.

The nine coefficients K_{ij} define the diffusion tensor
which in general is a function of the spatial coordinates.
In order to solve eq 2.2 with the help of eq 2.3, the
following additional hypotheses are made:

(i) The diffusion phenomenon is steady, i.e., $\frac{\partial \overline{c}}{\partial t} = 0$;

(ii) $\overline{u} = \overline{U} =$ constant, $\overline{V} = \overline{W} = 0$ (i.e., mean flow
is one-dimensional);

(iii) The x- , y- , and z-axes are the principal
axes of the diffusion tensor. Thus, $K_{ij} = 0$, $i \neq j$
$(i,j : 1,2,3)$;

(iv) The diffusion tensor does not depend on x, y,
and z. Thus, $K_{ii} = K_{jj} =$ constant (i.e., Fickian).
Substituting these assumptions into eq 2.3, one obtains:

$$\overline{U} \frac{\partial \overline{c}}{\partial x_i} = K_{ii} \nabla^2 \overline{c} \qquad\qquad 2.4$$

If a simple transformation is made, i.e.:

$$t_1 = \frac{x}{\overline{U}} \quad , \quad x_1 = \frac{x}{\sqrt{K_{xx}}} \quad , \quad y_1 = \frac{y}{\sqrt{K_{yy}}} \quad , \quad z_1 = \frac{z}{\sqrt{K_{zz}}} \qquad 2.5$$

then eq 2.4 is transformed into the classical heat equation:

$$\frac{\partial \overline{c}}{\partial t} = \nabla_1^2 \overline{c} \qquad 2.6$$

If the exchange coefficients K_{ij} are not assumed constant, then one writes eq 2.4 in form:

$$\overline{U} \frac{\partial \overline{c}}{\partial x_i} = \frac{\partial}{\partial x_i} (K_{ii} \frac{\partial \overline{c}}{\partial x_i}) \qquad 2.7$$

This is one of the forms of the basic K-Theory equation. Solutions have also been obtained for eq 2.7 by assuming that the K's vary with height according to some power or other law (1).

In spite of several simple solutions which have been obtained from the modified diffusion equation, these equations 2.4 and 2.7 remain intractable in boundary layer flow. This is due to the fact that these simple expressions do not adequately account for the effect of surface roughness, wind shear, density variation, and time of travel. In closing the above discussion one should note that the essential feature of the Fickian (4) and "K-Theory" equation is that the distribution of the suspended material or gas, with respect to distance from the center

of the "puff" in the case of instantaneous generation at a point or from the line or plane through the line or point source, is predicted to have a Gaussian form with variance:

$$\sigma_i^2 = 2 K_{ii} t = 2 K_{ii} \frac{x}{\bar{U}} \qquad\qquad 2.8$$

C. The Statistical Theory of Turbulent Diffusion

The theory of diffusion by continuous movements as published by Taylor (3) in 1921, like the Fickian and related theories, is restricted to giving a kinematic description of dispersion; but the description is much more adequate because it is based on the turbulent properties of the fluid flow. Taylor's equation for the case of dispersion in a turbulent flow field which is spacially homogeneous and stationary (5) in time with source at (0,0,0), gives the component variances of the particle displacement from the appropriate center of gravity (x,0,0) after a time of travel $t = \frac{x}{\bar{U}}$, to be:

$$\sigma_i^2(t) = \overline{X_i^2(t)} = 2\overline{u_i'^2}\int_0^t (t-\xi)\, R_i(\xi)\, d\xi \qquad\qquad 2.9$$

where $R_i(\xi)$ is the Lagrangian autocorrelation coefficient:

$$R_i(\xi) = \frac{\overline{u_i'(t)\, u_i'(t+\xi)}}{\overline{u'^2}} \qquad\qquad 2.10$$

For small dispersion times the limit of eq 2.10 is unity for $\xi = 0$; and eq 2.10 is effectively zero for large ξ ,

say $\xi > t_1$. Hence, for small t, eq 2.9 reduces to:

$$\sigma_i^2(t) \simeq \overline{u'^2}\, t^2 \qquad\qquad 2.11$$

and for large t, eq 2.10 reduces to:

$$\sigma_i^2(t) = 2\,\overline{u_i'^2}\, L_{t_i}\, t - 2\,\overline{u_i'^2}\int_0^\infty \xi R_i(\xi)\,d\xi \qquad 2.12$$

(where $L_{t_i} = \int_0^\infty R_i(\xi)\,d\xi$ is the Lagrangian time scale of

turbulence); or:

$$\sigma_i^2(t) = 2\,\overline{u_i'^2}\, L_{t_i}\, t - \text{constant} \qquad\qquad 2.13$$

Since for very large times the time t in eq 2.13 is much
larger than the constant in this same equation, 2.13 can
be written as:

$$\sigma_i^2(t) \simeq 2\,\overline{u_i'^2}\, L_{t_i}\, t \qquad\qquad 2.14$$

Equation 2.14 is equivalent to the variance given for the
diffusion equations 2.4 and 2.8 when $\overline{u_i'^2}\, L_{t_i}$ replaces K_{ii}
This theory too is not generally valid in the case of
diffusion in the boundary layer.

D. <u>Sutton's Hypothesis and Others</u>

Practical utilization of the principles set forth in
the Taylor diffusion theory has been accomplished by
Sutton (1947), who derived a set of expressions for
diffusion from a point source from eq 2.9 by making cer-
tain assumptions upon the nature of the autocorrelation

function 2.10. Using dimensional arguments, Sutton (1)

showed that in a layer of air flowing over a smooth

surface, $R_i(\xi)$ could be expressed in form:

$$R_i(\xi) = \left[\frac{\nu}{\nu + (\overline{u_i'^2})\xi}\right]^{-n} \qquad 2.15$$

The exponent n is a stability parameter varying between 0

and 1 in accordance with the wind profile expression:

$$\bar{u}(z) = \bar{u}_1\left(\frac{z}{z_1}\right)^{\frac{n}{2-n}} \qquad 2.16$$

For flow over rough surface Sutton suggested that ν in

eq 2.15 be replaced by the macroviscosity, $N = u_* z_0$.

Upon substituting 2.15 into 2.9 and integrating, Sutton

obtained a combined expression for the three-dimensional

distribution of pollutant concentration that would result

at a point at any time after an instantaneous emission

from a point source emission with a source strength Q :

$$\chi(x,y,z,t) = \left[\frac{Q}{\pi^{3/2}K_x K_y K_z (\bar{U}t)^{3/2(2-n)}}\right]\exp\left[(\bar{U}t)^{n-2}\cdots\right.$$

$$\left.\cdots\left(\frac{x^2}{K_x^2} + \frac{y^2}{K_y^2} + \frac{z^2}{K_z^2}\right)\right] \qquad 2.17$$

where K_i is the diffusion coefficient. This equation has

been extended to different geometries and stabilities by

Sutton by the use of different related expressions. From

2.17, solutions for a continuous point, finite line and

infinite line sources in a uniform wind $\bar{U}$ are obtained by

14

integration. For a continuous point source the solution is:

$$\chi_{(x,y,z)} = \left(\frac{2Q}{\pi K_y K_z \bar{U} x^{2-n}}\right) exp\left[-x^{n-2}\left(\frac{y^2}{K_y^2} + \frac{z^2}{K_z^2}\right)\right] \quad 2.18$$

where the factor two in the numerator accounts for the reflection" of the gas by the impervious ground. For diffusion over level surface with small temperature gradient and with moderate wind, a value of n = ¼ has been used in eq 2.16. This corresponds to the one-seventh "power-law" which wind-tunnel studies have found to characterize the turbulent boundary layer of a smooth plate.

In 1953 Frenkiel (7) derived the following expression for three-dimensional diffusion from an instantaneous point source from the standpoint of statistical theory, basing his treatment upon the Taylor equation:

$$\chi_{(x,y,z,t)} = \frac{Q}{2\pi(\overline{x^2})^{3/2}} exp\left[\frac{-(x^2+y^2+z^2)}{2\,\overline{x^2}}\right] \quad 2.19$$

Here the variance of the displacements of the diffusing particles $\overline{x^2}$ is a function of t determined by Taylor's diffusion equation. Comparing this result with the K-Theory solution for the same problem given by Roberts (8) in 1923:

$$\chi_{(x,y,z,t)} = \frac{Q}{(4\pi Kt)^{3/2}} exp\left[\frac{-(x^2+y^2+z^2)}{4Kt}\right] \quad 2.20$$

it can be seen that the two expressions are identical when $\overline{x^2} = 2Kt$.

In 1962 Cermak (14) applied the Lagrangian similarity hypothesis to diffusion in turbulent shear flow. Basically this hypothesis is based on a Lagrangian description of a fluid particle and also uses the parameters of shear velocity u_*, stability length L. This assumption postulates that the turbulence characteristics of the mean flow are completely determined (21) by the shear velocity u_* and the stability length L and that the roughness length z_o for fixed L and u_* affects only the mean velocity of translation.

Using this basic hypothesis and the definition of the distribution of particle-displacement probability density for an ensemble of single-particle releases, Cermak (14) extended the Lagrangian similarity hypothesis to obtain (for the neutral velocity distribution) the continuous point slope m (tangent to concentration versus downstream distance line) to be:

$$
m = -\left(\frac{kb\overline{x}}{z_o}\right)\left(\frac{1 + 2\ln\frac{\overline{z}}{z_o}}{\frac{\overline{z}}{z_o}\ln^2\frac{\overline{z}}{z_o}}\right) \qquad 2.21
$$

using the logarithmic velocity distribution of eq 1.5.

In the thermally stratified case Cermak (14) obtained for the continuous point source the slope m to be:

$$m = \left[\frac{-b\ell\frac{\bar{x}}{z_0}}{\frac{\bar{\bar{z}}}{z_0}}\right]\left\{\frac{2\ell n\frac{\bar{\bar{z}}}{z_0} + \frac{z_0}{L}\left(\frac{\bar{\bar{z}}}{z_0}-1\right) + \frac{z_0}{L}\left(\frac{\bar{\bar{z}}}{z_0}\right)+1}{\left[\ell n\frac{\bar{\bar{z}}}{z_0} + \frac{z_0}{L}\left(\frac{\bar{\bar{z}}}{z_0}-1\right)\right]\left[\ell n\frac{\bar{\bar{z}}}{z_0} + \frac{z_0}{L}\left(\cdots\right.\right.} \right.$$

$$\left. \frac{}{\cdots\frac{\bar{\bar{z}}}{z_0} + \frac{1}{4}\frac{\bar{\bar{z}}}{z_0}\ell n\frac{\bar{\bar{z}}}{z_0}-1\right)\bigg]}\right\}$$

2.22

using a form (15) of the exponential wind profile (eq 2.49).

E. Effect of Thermal Stability

In general heat-transfer work, three basic dimension-less numbers play a dominant role in describing a convective flow field. They are as follows:

Reynolds Number $\quad = \quad \dfrac{L_c U \rho}{\mu}$ $\qquad$ 2.23

Nusselt Number $\quad = \quad \dfrac{h_t L_c}{k_t}$ $\qquad$ 2.24

Prandtl Number $\quad = \quad \dfrac{c_p \mu}{k_t}$ $\qquad$ 2.25

where L_c is a characteristic length and k_t is the coefficient of thermal conductivity.

If the problem is one of low-speed flow as found in natural or free convection, one can modify the Reynolds number, which is the ratio of inertia forces to the viscous forces, to obtain:

$$Re = \left(\frac{L_c^2 U^2 \rho^2}{\mu^2} \right)^{\frac{1}{2}} \qquad 2.26$$

In this low-speed flow, buoyant forces have been found to be dominant; thus, if the kinetic energy of motion $\frac{\rho U^2}{2}$ is set equal to the work per unit volume required to move a fluid element $[g(\rho \beta_t)(\frac{\Delta T}{2})L_c]$ through a characteristic distance or height L_c , one can solve for U^2 to obtain:

$$U^2 = g \beta_t \Delta T L_c \qquad 2.27$$

where β_t is the coefficient of thermal expansion. Thus is obtained the velocity of motion at which the buoyant forces are dominant.

Now placing eq 2.27 into eq 2.26, one obtains the Grashof number:

$$Gr = \frac{L_c^3 \rho^2 g (\beta_t \Delta T)}{\mu^2} \qquad 2.28$$

which is the ratio of the buoyant forces and inertia forces to the viscous forces.

Using these above-mentioned dimensionless numbers, researchers in heat transfer have investigated the mean velocity distribution in a stably stratified boundary layer. However, they have generally assumed that the

effect of thermal stratification on the mean velocity

(eq 1.4) is negligible, i.e., that the profile for neutral

flow is the same as that for stratified flow. However,

micrometeorologists (who do not use these dimensionless

numbers) have realized that for a sufficiently large

stability number the effect of the stratification can no

longer be ignored; and a number of equations have been

proposed in which the thermal influence on the velocity

distribution is considered.

In the presence of marked density gradients, this

subject has been further examined by Deacon (1948). He

(33) introduced the Richardson number:

$$\text{Ri} = \frac{g}{\bar{\theta}} \frac{\left(\dfrac{\partial \theta}{\partial z}\right)}{\left(\dfrac{\partial \bar{u}}{\partial z}\right)^2} \qquad \qquad 2.29$$

which is the reciprocal of the Froude number squared:

$$\left[\text{Fr}^2 = - \frac{\left(\dfrac{U}{L_c}\right)^2}{\dfrac{g}{T}\left(\dfrac{\Delta T}{L_c}\right)} \right]$$ (i.e., the ratio of inertia forces to

gravity forces) as the basic parameter. In general:

$$\frac{\bar{u}}{u_*} = f(\text{Re}, \text{Ri}, z_0) \qquad \qquad 2.30$$

If the motion is of the fully-rough type (see p.4), the

influence of viscosity, and hence the influence of the

Reynolds number, is negligible; and, if the observations

are always made over the same surface, the roughness may

19

be regarded as constant. Thus, with these assumptions,
$\bar{u}$
— should depend on Ri, which may be expected to play
u_*

much the same part as that exercised by the Reynolds

number in the motion of a homogeneous air stream. If the

case exists such that the temperature gradient is super-

adiabatic, then Ri < 0 ; and for the case such that there

exists an inversion of the potential temperature, then

Ri > 0 .

Stewart (20) gives a stability criteria of Ri $\gtrsim$ 0.25,

i.e., the buoyant forces predominate. Sutton (1) says

that in the shallow layer of relatively dense air near

the ground the gradients of velocity and temperature may

be supposed invariable with height (without large varia-

tion) so that differentials may be replaced by finite

difference and one may write 2.29 in form:

$$Ri = \frac{g}{\theta} \frac{\left(\frac{\Delta \theta}{\Delta z}\right)}{\left(\frac{\Delta U}{\Delta z}\right)^2}$$

2.31

The publication of the preceding theoretical works

provided insight into the field of turbulent diffusion.

Based on this new insight, many workers have been attempt-

ing to analyze theoretically the mechanism of diffusion in

the turbulent surface layer by concepts based on or extensions of the statistical theory of turbulence or the diffusion equation.

With Prandtl's theory of mixing length as the point of beginning, Businger (1955) proposed another theory for the atmospheric surface layer (9). He considered the acceleration due to the frictional part of the turbulence to be dependent on stability. A dimensionless stability number was introduced enabling one to obtain a simple survey of all states of the atmospheric surface layer.

To express his work (1) Businger makes use of Richardson's principle which is expressed thus: the kinetic energy of the turbulence will increase or decrease depending upon the balance between the supply of energy made available by the Reynolds stresses and the rate at which work has to be done against gravity by the turbulence. In this form the Richardson principle neglects certain possible energy transformations and limits its applications to conditions in which the degree of turbulence is small and the flow borders on the laminar state.

The criterion in its original form may be derived as follows: suppose the fluid is one in which P, $\bar{\rho}$, and T are all functions of height z, and consider a volume of fluid moving vertically as a result of the turbulence from a level $z-\ell$ to a new level z, where ℓ is the mixing length. If the volume of fluid rises without mixing the eddy, which

originally had the temperature $\overline{T}(z-\ell) \simeq \overline{T}(z) -\ell\frac{\partial \overline{T}}{\partial z}$, it

will change its temperature adiabatically and will reach

the level z with the temperature $\overline{T}(z) -\ell(\frac{\partial \overline{T}}{\partial z} +\Gamma)$ where Γ

is the adiabatic lapse rate. At the new level its density

will be greater than its environment by the following

amount: $\frac{1}{\overline{T}} \ell\rho\left(\frac{\partial \overline{T}}{\partial z} +\Gamma\right)$. Thus, there is a buoyancy

force brought into being, acting downwards, of magnitude:

$\left(\frac{g\rho\ell}{\overline{T}}\right)\left(\frac{\partial \overline{T}}{\partial z} +\Gamma\right)$. If w' be the eddy velocity, the

mean rate at which work has been done against gravity in

lifting the mass is therefore: $\left(\frac{g\rho\,\overline{w'\ell}}{\overline{T}}\right)\left(\frac{\partial \overline{T}}{\partial z} +\Gamma\right)$

and since we define $\overline{w'\ell} = K_H$ as the eddy conductivity,

then one obtains:

$$\frac{K_H g\rho}{\overline{T}} \left(\frac{\partial \overline{T}}{\partial z} +\Gamma\right) \qquad\qquad 2.32$$

as the expression for the work done per unit volume, which

work must be done at the expense of the energy of the

turbulent motion.

On the other hand, the work which is extracted from

the mean motion by the Reynolds stress and which serves to

maintain the turbulence is:

$$\tau_{zx} \frac{\partial \bar{u}}{\partial z} = K_M \rho \left(\frac{\partial \bar{u}}{\partial z}\right)^2 \qquad\qquad 2.33$$

per unit volume, where K_M is the eddy viscosity or exchange

coefficient. If now $\overline{E}\rho$ denotes the mean turbulent kinetic

energy per unit volume of the fluid, Richardson's principle

states that the time rate of increase of $\overline{E}$ is given by the

difference between eq 2.33 and eq 2.32 or:

$$\frac{\partial \bar{E}}{\partial t} = K_M \left(\frac{\partial \bar{u}}{\partial z}\right)^2 - K_H \frac{g}{\bar{T}} \left(\frac{\partial \bar{T}}{\partial z} + \Gamma\right)$$ 2.34

$$= K_H \left(\frac{\partial \bar{u}}{\partial z}\right)^2 \left\{ \frac{K_M}{K_H} - \frac{g}{\bar{T}} \frac{\left(\frac{\partial \bar{T}}{\partial z} + \Gamma\right)}{\left(\frac{\partial \bar{u}}{\partial z}\right)^2} \right\}$$ 2.35

Since $K_H \left(\frac{\partial \bar{u}}{\partial z}\right)^2$ is essentially positive and different

from zero (except in the trivial case when $\bar{u}$ = constant),

the sign of $\frac{\partial \bar{E}}{\partial t}$ depends on whether the Richardson No:

$$Ri = \frac{g}{\bar{T}} \frac{\left(\frac{\partial \bar{T}}{\partial z} + \Gamma\right)}{\left(\frac{\partial \bar{u}}{\partial z}\right)^2}$$ 2.36

is less or greater than the ratio $\frac{K_M}{K_H}$, the turbulent

Prandtl number. In his original discussion Richardson

assumed K_M = K_H , in which case the criterion becomes:

turbulence increases if Ri $<$ 1

turbulence decreases if Ri $>$ 1

implying the existence of a critical value (Ri$_{crit}$) of

the Richardson number, which in this case is unity.

Usually Ri is expressed by a change of variables to

be:

$$Ri = \frac{g}{\bar{\theta}} \frac{\left(\frac{\partial \bar{\theta}}{\partial z}\right)}{\left(\frac{\partial \bar{u}}{\partial z}\right)^2}$$ 2.37

and $\bar{\theta}$ = potential temperature = $(\bar{T} + \Gamma z)$.

Using the Ri No. of eq 2.37 as a measure of stability of the atmosphere, Businger (9) cites a disadvantage of 2.37 in that the Ri No. varies with height. He defines a new Ri No.:

$$Ri' = \frac{g\left(\frac{\partial \bar{\theta}}{\partial z}\right)}{T_m \left(\frac{\partial \bar{u}}{\partial z}\right)^2} = \frac{g}{T_m}\frac{\theta_*}{u_*^2} R$$

2.38

(T_m = mean absolute temperature)
where one term is constant with height: i.e., $Sn = \frac{g}{T_m}\frac{\theta_*}{u_*^2}$
and a known quantity R , which varies with height. Sn is now used as a stability parameter instead of Ri to describe the flow conditions.

In 1957 Ellison (10) set up dimensional "laws" governing the process of heat and momentum transport from an infinite plane. Then he set up detailed equations for the turbulent energy, the mean square temperature fluctuation, and the covariance of temperature and vertical velocity to make some speculative assumptions concerning the dissipative action of the turbulence from which he derived a series of relations between the turbulent intensities and the Austausch coefficients. One of these relations indicates that the flux form of the Richardson No. (denoted by Rf) is equal to the ratio of the rate at which buoyancy forces extract energy from the turbulence to the rate at which it is supplied by the shear stress. This result is a direct consequence of a simplified energy

equation for the turbulence. Rf may be expressed in the following equivalent ways:

$$Rf = Ri \frac{K_H}{K_M} = \frac{K_H}{K_M} \frac{g}{\overline{T}} \frac{\left(\frac{\partial \overline{T}}{\partial z}\right)}{\left(\frac{\partial \overline{u}}{\partial z}\right)^2} \qquad 2.39$$

or

$$Rf = -\frac{K_H}{K_M} \frac{g}{\overline{\rho}} \frac{\left(\frac{\partial \overline{\rho}}{\partial z}\right)}{\left(\frac{\partial \overline{u}}{\partial z}\right)^2} = \frac{g}{\overline{\rho}} \frac{\overline{\rho' w}}{u_*^2 \left(\frac{\partial \overline{u}}{\partial z}\right)} \qquad 2.40$$

where for P=const : $\frac{1}{\overline{T}}\left(\frac{\partial \overline{T}}{\partial z}\right) = -\frac{1}{\overline{\rho}}\left(\frac{\partial \overline{\rho}}{\partial z}\right)$ and

$$K_H = -\frac{\overline{\rho' w}}{\left(\frac{\partial \overline{\rho}}{\partial z}\right)} \qquad K_M = \frac{u_*^2}{\left(\frac{\partial \overline{u}}{\partial z}\right)} \qquad 2.41$$

Ellison (10) states that under certain specified conditions and from experimental data Rf = 0.15 . He (10) also states that "the small critical value is most remarkable since it implies that in stable conditions the buoyancy forces do not have any great effect on the energy balance."

F. <u>Log + Linear Wind Profile</u>

In the 1950's several Russian workers published a similarity theory for diffusion in the surface layer of the atmosphere. The foremost of those were Monin and Obukhov (1953 and 1954).

The basis of the 1953, 1954 work was described in an article by Monin (1959). He cites that the turbulent regime is completely determined by the parameters u_* (friction velocity) and L (stability length) and says that these are the only scales of velocity and length in the surface layer. This is applicable when the turbulence is stationary and has horizontal homogeneity in the surface layer. Monin describes an average wind velocity profile and universal profile which have been used and modified by others and have been described in this writing previously.

Combining this wind velocity equation with the turbulent energy balance and utilizing several other assumptions gave a result which takes into account the variation of wind velocity with height. This result (11) was one of few at that date.

G. Dependency of β upon L

Monin and Obukhov (1954) determined $\beta = 0.6$ on the basis of experimentally determined wind profiles. Ogura (1952), who obtained the equation for wind speed profile on the basis of the energy balance, gave $\beta = 3$ in the range where the log + linear law holds. However, there is an unknown proportional constant in his equation which is determined by using data from Deacon (1949). In 1959 Yamamoto questioned Monin's (1954) method of obtaining β. Yamamoto believed that the procedure used to determine the

value of β from observations without knowing the exact ex-pression for the wind profile might lead to erroneous re-sults. This is possible in the above situation of Monin because the range of applicability of the approximate formula (eqs 1.10, 1.11) is not certain. Instead, Yama-moto (1959) extended the mixing-length theory to non-adiabatic conditions and obtained β = 10 under unstable conditions and β = 2 under stable conditions in the range where the log + linear law holds. In 1955 Businger reported that β = 2 . Gifford (1961) reports that as a result of studies by Priestly (1959), Taylor (1960), Inoue (1959), Takeuchi (1961), and Panofsky, Blackadar and McVehil (1960), it appears that β should be somewhat larger --- and that the value -- of β = 6 is consistent with results given by most of these authors. However, Takeuchi (1961) found that β changes considerably from 0.2 to about 20, that under stable conditions β becomes larger than under unstable conditions at the same magni-tude of $|L|$, and that β is largest under neutral condi-tions. These studies described above have been the basis of later work by Batchelor (12), Gifford (13), Cermak (14), and Swinbank (15). It was also the basis of a great deal of work on stable flow by several Japanese workers -- notably Inoue (16), Yamamoto (17), Takeuchi (18), and Okamato (19).

One final article should be mentioned in this theo-retical aspect. In 1959 Stewart (20) analyzed the problem

of diffusion in a stratified field. He based his analysis on the work of Corrsin (1956), Ellison (1957) and Townsend (1958) and discussed various assumptions and terms of the Navier-Stokes equations and balance of turbulent energy equation. He finally concludes that when stability becomes very great, it is doubtful if satisfactory results can be obtained by any approach which treats the fluctuating motion as turbulence in the ordinary laboratory sense. In fact he believes that in very stable situations the motion is likely to take the form largely of internal gravity waves. In this case the transfer of momentum is intimately connected with the little understood mechanism of wave generation, while transfer of other properties depends upon the breaking of the waves about which also very little is known.

H. Experimental Work

1. Diffusion

In addition to the theoretical studies described or mentioned above, various workers have done experimental work (or confirmed theory) in turbulent diffusion in a shear boundary layer with stable stratification.

Basing his work on the previously reported work of the Russians (21), Inoue (16) in 1959 estimated the effect of thermal stratification on turbulent diffusion in the atmospheric surface layer by comparing the probable

changes in the turbulent structure under the non-adiabatic conditions from that under the adiabatic conditions. This was done semi-empirically by making use of the so-called (log + linear) law of wind velocity profile which is as cited by Monin to be:

$$\frac{\bar{u}}{u_*} = 5.75 \, \ell n \, \frac{z}{z_0} + \beta \frac{z}{L} \qquad \qquad 2.42$$

The numerical constant β which Monin gives as 0.6 was found by Yamamoto's (17) analysis to be:

$$4\beta = \frac{1}{Ri_{crit}} \qquad \qquad 2.43$$

where Ri (crit) was found to be approximately 0.15 by Ellison (10). Thus, the value of β adapted by Inoue is in the order of unity. Inoue also discussed the effects of stability length L on diffusion phenomena and obtained similarity laws of diffusion based on $\frac{H}{z_0}$ and $\frac{H}{L}$ where H denotes the characteristic height of tunnel source or atmospheric source.

In 1959 Panofsky, Blackadar, and McVehil (22) compared observations at various locations (O'Neill, Nebraska; Melbourne, Australia; and others) with the hypothesis of Ellison concerning the Richardson No. effects. They showed that theory and observations agree well for near-neutral and unstable air; however, they claim that in stable air, factors not considered in the similarity

theory may become important. They further take a value of $\beta = 4.5$ and claim that the range of usefulness of the log-linear (log + linear) wind profile is small.

Barad and Haugen (23) in 1959 evaluated Sutton's hypothesis (1) for diffusion for a continuous point source using data obtained from Project Prairie Grass. They found that the hypothesis predicts the observed concentration distribution only if there are two values of Sutton's n : one to characterize lateral diffusion -- n_y ; and one to characterize vertical diffusion -- n_z .

In 1961 Poreh (24) and Davar (25), in 1962 Malhotra (26), and in 1963 Quraishi (27), all made diffusion studies in a neutral and unstable turbulent boundary layer and expressed their results in the form of:

$$c_{max} \propto x^{-p}$$
$$h \propto x^{q}$$
$$\lambda \propto x^{r}$$

2.44

where x is distance downwind from source, h is the vertical spread (position of 50% maximum decay), and λ is half the horizontal floor spread (position of 50% maximum decay). Some of their data has been used to confirm Cermak's (28) Lagrangian Similarity Hypothesis for neutral and unstable flow, which has been discussed previously.

2. Wind and Temperature Profiles

a. Deacon's Equation

Deacon (1949) was one of the first to use the Richardson number as the basic parameter in describing stable and unstable atmospheres. He found that to a good approximation the wind gradient is a function of the Ri No., the surface roughness being constant. He found that he could model velocity data with the relation:

$$\frac{d\bar{u}}{dz} = A z^{-\gamma} \qquad\qquad 2.45$$

(where A is a constant independent of z and γ is the slope of the velocity-gradient versus z curve when plotted on log-log paper); and:

$\gamma > 1$ for   Ri < 0 superadiabatic

$\gamma = 1$ for   Ri $= 0$ adiabatic or neutral

$\gamma < 1$ for   Ri > 0 inversion

Deacon (33) also found that the relationship expressed in eq 2.45 becomes very uncertain when Ri > 0.1.

Others (1) have extended the applicability of eq 2.45 to temperature gradients to obtain an equation as follows:

$$\frac{d\bar{T}}{dz} = G z^{-\gamma_t} \qquad\qquad 2.46$$

(where G is another constant and γ_t is the temperature-gradient slope).

b. <u>Monin's Use of Stability Parameter $\frac{z}{L}$</u>

In 1964 Monin proposed the use of the stability parameter $\mathscr{S} = \frac{z}{L}$, in addition to the customarily used Ri No., for modeling velocity profiles. If the ratio of the exchange coefficients for heat and momentum are considered constant, then eq 3.29 could be expressed as:

$$Ri = \frac{1}{\alpha \, f'\left(\frac{z}{L}\right)} \qquad\qquad 2.47$$

where $\alpha = \dfrac{K_H}{K_M}$.

In his work he used a reference height of $\frac{L}{2}$ which required different reference heights for different velocities and different stations as L changed with station, velocity and type of flow. Monin also cited the asymptotic behavior of the universal functions by means of the following:

1) neutral flow: $L \rightarrow \infty$ and $f'(\mathscr{S}) = \frac{1}{\mathscr{S}}$
This corresponds to logarithmic law for velocity profile.

2) strong instability: u_* must be omitted from similarity equation and $f'(\mathscr{S}) \simeq -c_1 |\mathscr{S}|^{-4/3}$

3) strong stability: z must be omitted from similarity equation and $f'(\mathscr{S}) \sim c_2$ where:

$$f(\mathscr{S}) = \ell n \, |\mathscr{S}| + 0.6 \, \mathscr{S} + \text{constant} \qquad\qquad 2.48$$

c. Swinbank's Exponential Wind Profile

In 1960 Swinbank modeled field data related to stable velocity profiles using the expression:

$$\bar{u}_s - \bar{u}_r = \frac{u_*}{k} \left\{ \frac{(\exp \frac{z_s}{L} - 1)}{(\exp \frac{z_r}{L} - 1)} \right\} \qquad 2.49$$

This relation, above, is expected to be applicable in all stabilities and to all heights below which the shearing stress and the vertical heat flux remain constant.

A form of the above relation proposed by Swinbank (15) was used by Cermak (14) in his Lagrangian similarity hypothesis for modeling diffusion data taken under thermally unstable flow conditions.

I. Resume

This chapter has been a survey of the literature which is most directly related to turbulent diffusion in a stably stratified boundary layer. This writer has discussed the details of the literature of those authors whose work pertains to the two general theories relating to diffusion in general. The subsequent discussion has been an historical survey of the most significant work relating to this dissertation as determined by this writer. A review of the experimental work in this literature survey has been in confirmation of basic theories and compilation of data for which empirical relationships were

developed. The work of this dissertation has utilized the ideas and concepts of many of the authors discussed in the preceding pages in the development of this dissertation in the hitherto unexplored field of turbulent diffusion in a stably stratified boundary layer.

In closing, the author offers the following quotation which so aptly emphasizes the meaningful application of the preceding theoretical and experimental material to the real world: "...increasing concern about air ... pollution presents a ... challenge .... through basic research to provide the knowledge and techniques needed to solve pollution problems." (6) All the work mentioned heretofore is related in some manner to this very real and challenging problem of air pollution and its solution through research.

CHAPTER III

ANALYSIS OF THEORY

A. Introduction

Current progress in the understanding of wind distri-
bution and of temperature distribution in the atmospheric
boundary layer has resulted from the Monin-Obukhov "Simi-
larity Theory." Their work was based on atmospheric data.
Field studies, however, are limited by the variable natu-
ral weather conditions such as temperature, water vapor,
heat transfer, and wind velocity. Since these parameters
can be controlled in a wind tunnel, results obtained in a
wind tunnel study can be more meaningful.

Flow conditions in the atmospheric boundary layer
can be closely simulated in the wind tunnel by the inner
portion of a boundary layer generated by air flow over a
plane wall. If the rate of production of convective
energy in this layer is negative, then this phenomenon
constitutes a basic flow similar to the atmospheric sur-
face layer which occurs naturally in the night-time
atmosphere (at which time the diffusion of matter becomes
very weak -- hence the occurrence of pollution problems).
Under the inversion conditions stated above a most inter-
esting , feasible and, at present, unlimited field of
study is presented. Similar inversion conditions as those
mentioned above can be simulated in the Colorado State
University wind tunnel. However, one also obtains the

added benefit of practically steady-state flow and temperature conditions. This is done by constant cooling on the boundary from below (cold plate) and by constant heating of the circulating air. This produces a stable layer through the action of a temperature inversion of the flowing air. These changes greatly modify the much-studied neutral boundary layer.

The purpose of this portion of the discussion is twofold: (1) to examine the wind and temperature profiles utilizing a modified logarithmic law and wind tunnel data; and (2) to discuss the characteristics of turbulent diffusion under stable stratification.

B. "Log + Linear" Law

From the similarity theory, where $\frac{z}{L}$ is small, the profiles of wind (air) velocity and of temperature can be expressed by the so-called "log + linear" law and by the universal function. One can assume that, for a wide range of stability the profiles are expressed by that law; and one can make analysis of the data obtained in the wind tunnel in order to determine the range and validity of the law. From the previous section, the profiles of wind (air) velocity and temperature can be expected to be expressed by:

$$\bar{u}(z) = \frac{u_*}{k} \left\{ \ell n \frac{z}{z_o} + \frac{\beta}{L} (z - z_o) \right\} \qquad 3.1$$

$$T(z) - T(z_0) = \frac{T_*}{k} \left\{ \ell n \; \frac{z}{z_0} + \frac{\beta}{L} (z - z_0) \right\} \qquad 3.2$$

when it is assumed that the exchange coefficients for momentum and heat are approximately equal to each other (i.e., $f = f_1$).

To determine the validity of eqs 3.1 and 3.2 in the inner portion of the turbulent boundary layer, the values of β and L are computed by means of the mean wind and mean temperature profiles obtained in the wind tunnel by a technique described below.

Assuming that the turbulent Prandtl No. is approximately one, one can write the equations for the wind and temperature profiles as:

$$\bar{u}(z) = \frac{u_*}{k} f(\zeta) \qquad 3.3$$

$$T(z) - T(0) = \frac{T_*}{k} f(\zeta) \qquad 3.4$$

where f is a universal function.

Combining eqs 3.3 and 3.4, one obtains the ratio of friction temperature to friction velocity to be:

$$\frac{T_r - T(0)}{\bar{u}_r} = \frac{T_*}{u_*} \qquad 3.5$$

and

$$\frac{T_r - T_s}{\bar{u}_r - \bar{u}_s} = \frac{T_*}{u_*} \qquad 3.6$$

Combining eqs 3.5 and 3.6, one finds T_o to be:

$$T_o = T_r - \bar{u}_r \left(\frac{T_r - T_s}{\bar{u}_r - \bar{u}_s} \right)$$

3.7

where T_o or $T(z_o)$ represents the temperature at the height z_o for a rough plate or the temperature at the upper bound-ary of the laminar sublayer δ_s for a smooth plate. Thus, the data are averaged by eq 3.7, and an average $\left(\frac{T_*}{u_*} \right)$ is then obtained from eq 3.5 .

Now, using the definition of friction temperature:

$$T_* = \frac{1}{u_*} \left(- \frac{q}{\rho\, c_p} \right)$$

3.8

one can rewrite eq 1.7:

$$L = \frac{u_*^3}{k \frac{g}{\tilde{T}} \left(- \frac{g}{\rho c_p} \right)}$$

1.7

to read:

$$L = \frac{u_*^2}{\frac{k\, g\, T_*}{\tilde{T}}}$$

3.9

or one may write:

$$L = \left(\frac{\omega'\, u_*}{k} \right)$$

3.10

where:

$$\omega' = \frac{T_*}{g} \left(\frac{u_*}{T_*} \right)$$

3.11

If one uses eqs 3.1 and 3.2 for arbitrary heights r and s, one may modify these equations to read:

$$(\bar{u}_r - \bar{u}_s) = \frac{u_*}{k}\left\{\ln\frac{z_r}{z_s} + \frac{\beta}{L}(z_r - z_s)\right\} \qquad 3.12$$

$$r \neq s$$

or:

$$(\bar{u}_r - \bar{u}_s) = \frac{u_*}{k}\left(\ln\frac{z_r}{z_s}\right) + \frac{\beta}{u^*}(z_r - z_s) \qquad 3.13$$

and solving for $(\frac{u_*}{k})$ to obtain:

$$\frac{u_*}{k} = \frac{(\bar{u}_r - \bar{u}_s) - \frac{\beta}{u^*}(z_r - z_s)}{\ln\frac{z_r}{z_s}} \qquad 3.14$$

If different arbitrary heights from r , s are now selected, one obtains:

$$\frac{u_*}{k} = \frac{(\bar{u}_{r'} - \bar{u}_{s'}) - \frac{\beta}{u^*}(z_{r'} - z_{s'})}{\ln\frac{z_{r'}}{z_{s'}}} \qquad 3.15$$

Setting eq 3.14 equal to eq 3.15, one may solve for $\frac{\beta}{u^*}$ to obtain:

$$\frac{\beta}{u^*} = \frac{\dfrac{(\bar{u}_r - \bar{u}_s)}{\ln\frac{z_r}{z_s}} - \dfrac{(\bar{u}_{r'} - \bar{u}_{s'})}{\ln\frac{z_{r'}}{z_{s'}}}}{\dfrac{(z_r - z_s)}{\ln\frac{z_r}{z_s}} - \dfrac{(z_{r'} - z_{s'})}{\ln\frac{z_{r'}}{z_{s'}}}} \qquad 3.16$$

Note: Using the method of Monin (1962) of employing a fixed reference height of z_r and $z_{r'}$ $(r \neq r')$ and utilizing the fixed reference velocities $u_r \neq u_{r'}$ (at these heights) simplifies the solution of the problem. However, one should note that Monin used a reference height $z = \frac{L}{2}$ which reduces the variations in the differences to:

$$\left\{ \bar{u}_r(z_r) - \bar{u}_s(z_s) \right\} = \left\{ \bar{u}(\tfrac{L}{2}) - \bar{u}_s(z_s) \right\} \qquad 3.17$$

$$\left\{ \bar{u}_{r'}(z_{r'}) - \bar{u}_{s'}(z_{s'}) \right\} = \left\{ \bar{u}(\tfrac{L+1}{2}) - \bar{u}_{s'}(z_{s'}) \right\} \qquad 3.18$$

This method described above also reduces the degree of variation in analyzing the velocity profiles (when using eq 3.13) to some fixed constant. Putting the value of $\frac{\beta}{w}$ back into eqs 3.14 and 3.15, one solves for $\frac{u_*}{k}$. Putting this value of u_* and the value of w from eq 3.11 into eq 3.9, one solves for L.

After values of u_*, T_* and $\frac{\beta}{L}$ are found for each profile for arbitrary heights above the floor, the profiles can be expressed as follows:

$$\left| \frac{k(\bar{u}_r - \bar{u}_s)}{u_*} \right| = \left| \ell n(\frac{z_r}{z_s}) + \frac{\beta}{L} (z_r - z_s) \right| \qquad 3.19$$

$$\left| \frac{k(T_r - T_s)}{T_*} \right| = \left| \ell n(\frac{z_r}{z_s}) + \frac{\beta}{L} (z_r - z_s) \right| \qquad 3.20$$

C. Dependence on Richardson Number and Reference Height

From the above discussion concerning results obtained, one can conclude that one must select reference height and regions of applicability quite carefully when determining β and L. Also, when discussing the Richardson number, one must again carefully select reference heights and applicable regions since Ri is proportional to $\frac{z}{L}$ for small z or large L. This is shown as follows:

Starting with the definition of shear (τ) stress per unit area for motion parallel to the x-axis, one (37) can write:

$$\frac{\tau}{\rho} = (\nu + K_M)\frac{\partial \bar{u}}{\partial z} \cong K_M \frac{\partial \bar{u}}{\partial z} \quad \text{if } \nu \ll K_M$$

$$3.21$$

It is known (41) that one is over-predicting and that a maximum is being used for:

$$K_M \frac{\partial \bar{u}}{\partial z} \cong \frac{\tau}{\rho} = u_*^2 \qquad 3.22$$

The heat transfer in the z-direction is (37):

$$\frac{q}{\rho c_p} = - (k_t + K_H)\frac{\partial \bar{T}}{\partial z} = - K_H \frac{\partial \bar{T}}{\partial z} \quad \text{if } k_t \ll K_H$$

$$3.23$$

One can define a velocity profile as:

$$\bar{u}(z) = \frac{u_*}{k}\left\{ \ln \frac{z}{z_0} + \frac{\beta}{L}(z - z_0) \right\} \qquad 3.1$$

$$= \frac{u_*}{k}\left\{ f_1(\hbar) - f_1(\hbar_0) \right\} = \frac{u_*}{k} f_3(\hbar) \qquad 3.3$$

where $\eta = \frac{z}{L}$ and $\eta_o = \frac{z_o}{L}$; and one can define a temperature profile as:

$$T(z) - T(0) = \frac{T_*}{k}\left\{f_2(\eta) - f_2(\eta_o)\right\}$$

3.4

$$= \frac{T_*}{k} f_4(\eta)$$

If Reynolds analogy holds (i.e., the exchange coefficient for momentum and heat being equal), then $f_3 = f_4 = f$ and $K_M = K_H = K$; and one can write 3.3 and 3.4 as:

$$\bar{u}(z) = \frac{u_*}{k} f(\eta)$$

3.3a

$$T(z) - T(0) = \frac{T_*}{k} f(\eta)$$

3.4a

and so:

$$\frac{\partial \bar{u}}{\partial z} = \frac{u_*}{k} \left(\frac{1}{z} + \frac{\beta}{L}\right) = \frac{u_*}{kz} \left(1 + \beta \frac{z}{L}\right)$$

3.24

$$\text{or} \quad \frac{\partial \bar{u}}{\partial z} = \frac{u_*}{kz} f'(\eta)$$

and:

$$\frac{\partial T}{\partial z} = \frac{T_*}{kz} f'(\eta)$$

3.25

Thus combining 3.24 and 3.22, one obtains:

$$K_M = \frac{u_*^2}{\dfrac{\partial \bar{u}}{\partial z}} = \frac{u_*^2 kz}{u_* f'(\eta)} = \frac{u_* kz}{f'(\eta)}$$

3.26

If one combines 3.23, 3.25, and 3.8, one obtains:

$$K_H = \left(\frac{-q}{\rho C_p}\right)\left(\frac{\partial \bar{T}}{\partial z}\right)^{-1} = T_* u_* \left(\frac{\partial \bar{T}}{\partial z}\right)^{-1} \qquad 3.27$$

$$K_H = \frac{T_* u_* kz}{T_* f'(\lambda)} = \frac{u_* kz}{f'(\lambda)}$$

Using a definition of the Richardson Number, one writes:

$$Ri = \frac{g}{\bar{T}} \frac{\left(\frac{\partial \bar{T}}{\partial z}\right)}{\left(\frac{\partial \bar{u}}{\partial z}\right)^2} = \frac{g}{\bar{T}} \left(\frac{T_*}{u_*^2}\right) \frac{f'(\lambda)kz}{\left\{f'(\lambda)\right\}^2}$$

$$= \frac{z}{L} \frac{1}{f'(\lambda)} = \frac{z}{L}\left(\frac{1}{1 + \beta\frac{z}{L}}\right) \qquad 3.28$$

and when $z \ll L$, then: $Ri \simeq \frac{z}{L}$ $\qquad$ 3.29

Therefore, one can conclude that in the stable boundary layer of the wind tunnel there should exist a portion of the velocity and temperature profiles that can be expressed by the log + linear law. This is possible even though there is a great deal of uncertainty involved in the determination and/or selection of β as has been noted in the preceding discussion of the atmospheric boundary layer found in the published literature of other researchers.

It should be noted here again that in conjunction with $\frac{z}{L}$ and/or $\frac{z_o}{L}$ the stability length L is the only scale length which has been proposed to model wind tunnel data with atmospheric field data.

D. Turbulent Diffusion in Stably Stratified Air

In the foregoing section the author discussed that portion of the boundary layer having constant heat flux and constant total shear ---- and related these parameters by means of the stability length L . As noted previously, such a field presents an attractive situation for study because of its similarity to the naturally-occurring atmospheric boundary layer.

The discussion to follow pertains to shearing flow in a stably stratified fluid (39, 40). If in a flow which is predominantly horizontal the density of the medium diminishes rapidly upwards (as in a mass of air with the temperature increasing upwards), the process of turbulent mixing must cause heavier layers to be moved above lighter layers, and lighter layers to be pushed down below heavier; that is, part of the store of energy available for the maintenance of turbulence (derived from the main flow) is used in working against gravity. Hence, the turbulent motion is diminished and may die out altogether. This is the explanation of the cessation of turbulence and "dying-down" of the wind at night in the lower layers of the atmosphere (the wind still continuing unabated at a higher level, but the shearing stress and turbulence is diminished).

Thus, the stability of a heavy stratified fluid, if the velocity varies with height, tends to hinder turbulence, since the vertical motions of individual fluid particles

shift heavier material upwards and lighter material down-
wards, and in <u>both</u> cases work is done.

Now, it is essential to have a length which may be
interpreted as the diameter of fluid particles which move
as a whole and also as the path traversed by these parti-
cles relative to the rest of the fluid before they lose
their individuality again by mixing with the turbulent
fluid by which they are surrounded. One cannot say <u>a</u>
<u>priori</u> that these two lengths are exactly the same; one
may expect, however, that they -- broadly speaking -- will
be proportional to each other. The assumption is also
made that the flow is such that the velocity varies in a
direction at right angles to the stream-lines.

Assuming that the fluid is incompressible, the length
discussed above is proportional to z ; and, utilizing
Archimides' principle, the work done in raising a fluid
particle of unit volume is then found. This is done by
solving for the force which is in equilibrium in a layer
$z = z_1$ in relation to the downward force at $z = z_2$ (i.e.,
buoyancy force) and is (39):

$$F = g(\rho_1 - \rho_2) = \frac{g \, d\rho}{dz}(z_1 - z_2) \qquad 3.30$$

so that the work is:

$$-\int_{z_1}^{z_1 + \ell} F \, dz_2 = g \frac{d\rho}{dz} \frac{z^2}{2} \qquad 3.31$$

where $\ell = cz$, c is taken to be one, and $g \frac{d\rho}{dz}$ is
essentially constant.

Thus, the mean work of many particles is:

$$\frac{1}{2} \, \rho g \left(\frac{1}{\rho} \frac{d\rho}{dz} \right) \overline{z^2}$$ 3.32

The rate at which work is done is therefore:

$$\frac{1}{2} \, \rho g \left(\frac{1}{\rho} \frac{d\rho}{dz} \right) \frac{d}{dt} \left(\overline{z^2} \right)$$ 3.33

where $\overline{z^2}$ is identical with the variance in the theory of diffusion by continuous movements (3) and is shown as:

$$\overline{z^2} = \overline{(z_1 + z_2 + z_3 + \cdots z_n)^2}$$ 3.34

When the turbulent energy is not decreasing, this work must be done by the Reynolds stresses. The rate at which the Reynolds stress does work when the mean flow is two-dimensional is:

$$\rho \, \overline{u'w'} \left(\frac{d\bar{u}}{dz} \right)$$ 3.35

The relations expressed by 3.33 and 3.35 can be combined to make an energy balance in the turbulent field and can be denoted as follows:

$$-\overline{u'w'} \left(\frac{d\bar{u}}{dz} \right) + \frac{1}{2} g \left(\frac{1}{\rho} \frac{d\rho}{dz} \right) \frac{d(\overline{z^2})}{dt} - \phi = 0$$ 3.36

where ϕ represents the mechanism necessary to balance the turbulent energy equation. For instance, ϕ should include the divergence of turbulent energy and the dissipation of turbulent energy.

It is known that the shear stress can be defined as:

$$\tau_{xz} = \tau = \mu \frac{\partial \bar{u}}{\partial z} - \rho \overline{u'w'} \qquad 3.37$$

and that the heat transfer at the wall can be expressed as:

$$q_w = q = -k_t \frac{\partial \bar{T}}{\partial z} + c_p \rho \overline{T'w'} \qquad 3.38$$

Equations 3.37 and 3.38, however, are considered constant in the atmospheric surface layer (31).

In practice, within the region of interest for atmospheric modeling /that is, everywhere except very close to the ground -- i.e.:

$$\frac{z}{\bar{T}} (\frac{\tau}{\rho})^{\frac{1}{2}} \geq 100 \qquad 3.39\underline{7},$$

the first term in each of eqs 3.37 and 3.38 is negligible (1, 31). This is so because the turbulence is responsible for the great majority of the momentum and heat flux. Since the momentum flux and total heat effectively set the conditions of the problem in the boundary layer of the atmospheric surface layer, they are used as scaling parameters by setting:

$$(\frac{\tau}{\rho})^{\frac{1}{2}} = u_* \qquad 1.1$$

where u_* is the shear velocity, and for symmetry by setting:

$$(\frac{-q}{\rho c_p}) \frac{1}{u_*} = T_* \qquad 3.8$$

where T_* is the friction temperature.

As an approximation the following (empirical) relations are used:

$$u_*^2 \overset{\sim}{=} - \overline{u'w'} \qquad 3.40$$

and:

$$\frac{-q}{\rho \, c_p} = T_* u_* = \overline{T'w'} \qquad 3.41$$

If a perfect gas is assumed with constant pressure, one obtains:

$$g \frac{d\rho}{\rho} = - \frac{d\overline{T}}{\overline{T}} \qquad 3.42$$

and 3.36 may now be denoted by:

$$u_*^2 \frac{d\overline{u}}{dz} - \frac{1}{2\,\overline{T}} (\frac{d\overline{T}}{dz}) \frac{d(\overline{z^2})}{dt} - \emptyset = 0 \qquad 3.43$$

On the other hand the balance of turbulent kinetic energy in equilibrium under thermally non-neutral motion can be represented by the following relation (1, 32):

$$\overset{I}{u_*^2 \frac{d\overline{u}}{dz}} + \overset{II}{\frac{q}{\overline{T}} \, \overline{T'w'}} - \overset{III}{\frac{\partial}{\partial z}\left\{\frac{1}{2} \overline{(u'^2 + v'^2 + w'^2)w'} + \frac{1}{\rho}\overline{P'w'}\right\}} = \mathcal{E}_d \qquad 3.44$$

where $\mathcal{E}_d$ is the rate at which turbulent kinetic energy is being converted to heat by the action of viscosity. The first term of eq 3.44 represents production of turbulent energy by transfer from the mean flow. The third term represents diffusive transport of turbulent energy and practically means loss of turbulent energy in the boundary

layer where shearing stress is constant (Townsend, 1956).
The second term represents production or loss of turbulent
energy through work done by or against buoyancy forces
according to unstable or stable conditions. Lumley (31)
writes that the left side of term III is usually neglected
near the ground and the right side of term III, which has
never been measured, is also usually neglected near the
ground.

Using a definition of turbulent heat flux represented
by eq 3.41, one can insert 3.41 into 3.44 and equate this
new relation 3.43 to obtain a relation between the move-
ment of the fluid particles in the field of stable air
flow to read:

$$\frac{1}{2}\frac{\overline{dz^2}}{dt} = - \frac{\frac{q}{\rho c_p}}{\frac{d\overline{T}}{dz}} \qquad\qquad 3.45$$

Again using the definition of heat flux as represented
by eq 3.41, one may now express 3.45 in the form as shown
below:

$$\frac{1}{2}\frac{\overline{dz^2}}{dt} = \frac{T_*u_*}{\frac{d\overline{T}}{dz}} \qquad\qquad 3.46$$

Equation 3.46 can also be derived on the basis of eddy
diffusivity.

In a statistical sense one may assume that $(\overline{z^2})^{\frac{1}{2}}$
corresponds to a certain characteristic height for the
upward movement of the fluid particles; so, if one defines

$\tilde{z} = (\overline{z^2})^{1/2}$, in which $\tilde{z}$ corresponds to the mean position for the vertical displacement of the fluid particles, eq 3.46 can be expressed as follows:

$$d(\tilde{z}) = \frac{1}{2} (\overline{z^2})^{-1/2} d(\overline{z^2})$$

or:

$$d(\overline{z^2}) = 2 d(\tilde{z})(\overline{z^2})^{1/2} = 2\tilde{z} d(\tilde{z})$$

and:

$$\tilde{z}(\frac{d\tilde{z}}{dt}) = \frac{T_* u_*}{\frac{d\bar{T}}{dz}}$$

which can be expressed as:

$$\frac{d\tilde{z}}{dt} = \frac{T_* u_*}{\tilde{z}(\frac{d\bar{T}}{dz})} \qquad\qquad 3.47$$

Assuming:

$$\tilde{z} = c z ;$$

and if c is taken to be one, or solving at $z = \tilde{z}$, one can express 3.47 as:

$$\frac{d\tilde{z}}{dt} = \frac{T_* u_*}{\tilde{z}(\frac{d\bar{T}}{d\tilde{z}})} = \frac{T_* u_*}{\frac{d\bar{T}}{d\ell n\tilde{z}}} \qquad\qquad 3.48$$

Thus, Batchelor's constant b (Batchelor, 1964) should correspond to the term $\dfrac{T_*}{\frac{d\bar{T}}{d\ell n\tilde{z}}}$ of eq 3.48 above. However, it may be expressed by von Karman's constant k under

inversion "flow"; so one would expect b to change (14) with stability under thermally stratified flow. Now, returning to 3.48 the average statistical vertical velocity of a marked fluid particle, released at time t=0 from a ground-level continuous point source, is (Ito, 1965) found by the following procedure.

One can write:

$$\frac{d\tilde{z}}{dt} = \frac{T_* u_*}{\dfrac{\tilde{z}\ d\tilde{T}}{L d\left(\frac{\tilde{z}}{L}\right)}} \qquad\qquad 3.49$$

or:

$$\frac{d\tilde{z}}{dt} = \frac{T_* u_*}{\tilde{\hbar}\ \dfrac{d\tilde{T}}{d\tilde{\hbar}}} \qquad\qquad 3.50$$

Now, using the temperature distribution corresponding to the mean height of the movement of the marked particles:

$$T(\tilde{z}) - T(o) = \frac{T_*}{k}\left\{ f(\tilde{\hbar}) - f(\hbar_o) \right\} \qquad 3.51$$

where $f(\tilde{\hbar}) = \ln \tilde{\hbar} + \beta\tilde{\hbar}$ and $f(\hbar_o) = \ln \hbar_o + \beta\hbar_o$ so that the right side of 3.51 may be written as:

$$f(\tilde{\hbar}) - f(\hbar_o) = \left[\ln \frac{\tilde{\hbar}}{\hbar_o} + \beta(\tilde{\hbar} - \hbar_o)\right] \qquad \text{and}$$

$$\frac{d\tilde{T}}{d\tilde{\hbar}} = \frac{T_*}{k}\frac{d}{d\tilde{\hbar}}\left\{ f(\tilde{\hbar}) - f(\hbar_o)\right\} = \frac{T_*}{k}\left\{ f(\tilde{\hbar}) - f(\hbar_o)\right\}'$$

and thus:

$$\frac{d\tilde{z}}{dt} = \frac{T_* u_*}{\tilde{\lambda} \frac{T_*}{k} \left\{ f(\tilde{\lambda}) - f(\tilde{\lambda_0}) \right\}'}$$

or:

$$\frac{d\tilde{z}}{dt} = \frac{k\, u_*}{\tilde{\lambda} \left\{ f(\tilde{\lambda}) - f(\tilde{\lambda_0}) \right\}'} \qquad 3.52$$

where f is the universal function, $\tilde{\lambda} = \frac{\tilde{z}}{L}$, and the "prime" indicates differentiation.

The average horizontal velocity of a marked fluid particle after a short relaxation time is at any point equal to the assumed mean wind (air) velocity at that point and can be written as follows:

$$\frac{d\tilde{x}}{dt} = \frac{u_*}{k} \left\{ f(\tilde{\lambda}) - f(\tilde{\lambda_0}) \right\} \qquad 3.53$$

The relationship between $\tilde{x}$ and $\tilde{z}$ is shown to be as follows:

$$\frac{d\tilde{x}}{d\tilde{z}} = \frac{\tilde{\lambda}}{k^2} \left\{ f(\tilde{\lambda}) - f(\tilde{\lambda_0}) \right\} \left\{ f(\tilde{\lambda}) - f(\tilde{\lambda_0}) \right\}' \qquad 3.54$$

or:

$$\frac{d\tilde{\epsilon}}{d\tilde{\lambda}} = \tilde{\lambda} \left\{ f(\tilde{\lambda}) - f(\tilde{\lambda_0}) \right\} \left\{ f(\tilde{\lambda}) - f(\tilde{\lambda_0}) \right\}' \qquad 3.55$$

where $\tilde{\epsilon} = k^2 \frac{\tilde{x}}{L}$. One can integrate $\tilde{\epsilon}$ in eq 3.55 to obtain:

$$\tilde{\epsilon} = \int_{\lambda_0}^{\tilde{\lambda}} \left\{ \tilde{\lambda} [f(\tilde{\lambda}) - f(\lambda_0)][f(\tilde{\lambda}) - f(\lambda_0)]' \right\} d\tilde{\lambda} \qquad 3.56$$

Equation 3.56 is similar to one that has been developed and derived by the Lagrangian similarity method provided that Batchelor's constant b is allowed to change (14) with stability under thermally stratified flow.

Introducing the log + linear law for the universal function, one integrates eq 3.56 to obtain:

$$\tilde{\mathcal{E}} = \hat{n}^2 \ell n \frac{\hat{n}}{n_0} - \left(\hat{n} - n_0\right) + \frac{\beta}{2}\left(\hat{n}^2 - n_0^2\right) - n_0\left(\hat{n} - n_0\right) + \cdots$$

$$\cdots \frac{\hat{n}^2}{2} \ell n \frac{\hat{n}}{n_0} - \frac{1}{4}\left(\hat{n}^2 - n_0^2\right) + \frac{\beta}{3}\left(\hat{n}^3 - n_0^3\right) - \frac{\beta}{2} n_0\left(\hat{n}^2 - n_0^2\right)$$

$$3.57$$

Solutions of eq 3.57 were obtained by programming it for the IBM 1620 Computer and solving for different values of β, $\hat{n}$, and n_0 to obtain $\tilde{\mathcal{E}}$.

Equations 3.56 and 3.57 can be compared to Gifford's (1961) solution to Monin's (11) work which is as follows:

$$F(\mathcal{f}, \mathcal{f}_0) = \mathcal{E} = \frac{kb\bar{x}}{L} = \int_{\mathcal{f}_0}^{\mathcal{f}} \frac{\{f(\mathcal{f}) - f(\mathcal{f}_0)\}}{\left\{1 - \frac{1}{f'(\mathcal{f})}\right\}^{1/4}} d\mathcal{f} \qquad 3.58$$

where:

$$f(\mathcal{f}) = \ell n\, \mathcal{f} + \beta \mathcal{f} \qquad\qquad 3.58a$$

$$f(\mathcal{f}_0) = \ell n\, \mathcal{f}_0 + \beta \mathcal{f}_0 \qquad\qquad 3.58b$$

and:

$$\mathcal{f} = \frac{\bar{z}}{L} \quad,\quad \mathcal{f}_0 = \frac{z_0}{L} \quad,\ \text{and}\ f'(\mathcal{f}) = \left(\frac{1}{\mathcal{f}} + \beta\right).$$

One may then rewrite eq 3.58 to read:

$$\varepsilon = \int_{\mathcal{P}_0}^{\mathcal{P}} \left\{ \frac{\ln \frac{\mathcal{P}}{\mathcal{P}_0} + \beta(\mathcal{P}-\mathcal{P}_0)}{\left(\frac{1+\beta\mathcal{P}-\mathcal{P}}{1+\beta\mathcal{P}}\right)^{1/4}} \right\} d\mathcal{P} \qquad 3.59$$

Equation 3.59 can be solved either by graphical or computer means, and in this case the computer was used. The computer solutions of 3.57 and 3.59 are discussed with data points in Chapter V.

E. The Mean Concentration at Ground Level

One can assume that the tracer gas or diffusive material does not influence the dynamical behavior of the surrounding fluid, in which case the state of the gas or material may be as described below.

Cramer et al (1957) have shown that their calculated atmospheric axial gas concentrations agree closely with their measured values based on the assumption that the smoke or gas approximates a normal distribution. If one follows the same approximation, one can assume that the gas or effluent is normally distributed (with some error) along the y and z coordinates. Thus, it follows from the geometry (35) that the downwind ground gas concentration of a ground-level continuous point source (with reflection) is:

$$C_{axis} = \frac{2Q}{2\pi(\frac{y}{L})(\frac{z}{L}) \bar{u} L^2} \qquad 3.60$$

in which $\tilde{y} = (\overline{y^2})^{1/2}$ has the meaning of the standard deviation for the particles moving in the crosswind direction. The velocity, $\tilde{u}$, is defined as follows:

$$\frac{k\tilde{u}}{u_*} = \frac{1}{\tilde{n}} \int_{n_o}^{\tilde{n}} \left\{ \ln \frac{\tilde{n}}{n_o} + \beta(\hat{n} - n_o) \right\} d\tilde{n} \qquad 3.61$$

If one assumes that $\frac{\tilde{y}}{L} \propto \frac{\tilde{z}}{L}$ or $\frac{\tilde{y}}{L} = c\,\tilde{n}$, one can replace the variables of $\tilde{u}$ and $\frac{\tilde{y}}{L}$ from eq 3.60 by their respective values to obtain:

$$\frac{u_* L^2 C_{axis}}{Q k} = \frac{constant}{\pi \tilde{n}^2 \left\{ \ln \frac{\tilde{n}}{n_o} - 1 + \frac{\beta}{2}\left(\tilde{n} - 2n_o + \frac{n_o^2}{\tilde{n}}\right) + \frac{n_o}{\tilde{n}} \right\}} \qquad 3.62$$

$$= \frac{constant}{\pi \tilde{n}^2 F(\tilde{n}, n_o, \beta)}$$

where C_{axis} is the floorline maximum concentration and Q is the volumetric injection flow rate.

Equation 3.62 is similar to the one developed by Gifford (1961), in which he assumes the following:

$$\frac{C}{Q} \propto \frac{k}{\bar{z}^2 u_* \left\{ f(\zeta) - f(\zeta_o) \right\}} \qquad 3.63$$

and using eqs 3.58a and 3.58b mentioned before, one can derive:

$$\frac{u_* L^2 C}{Q k} \propto \frac{1}{\zeta^2 \left\{ \ln \frac{\zeta}{\zeta_o} + \beta(\zeta - \zeta_o) \right\}} \qquad 3.64$$

Equation 3.64 was solved by another computer program.
Then, the dimensionless downwind distance ε was plotted
against the dimensionless maximum floorline (stable flow)
concentration as expressed by the right side of eq 3.62.
The right side of eq 3.64 was similarly plotted against
the definition of ε . Both results are shown in
Chapter V.

From the above results one can model meteorological
phenomena in the wind tunnel using the parameters $\frac{z}{L}$ and
$\frac{z_0}{L}$. This is possible providing the thermal and momentum
stable boundary layers are thicker than the diffusion
boundary layer, as was found to be true in the U.S. Army
Meteorological Wind Tunnel located at Colorado State
University .

CHAPTER IV

EXPERIMENTAL EQUIPMENT AND PROCEDURE

A. Introduction

The experiments were performed in the large U.S. Army
Meteorological Wind Tunnel located in the Fluid Dynamics
and Diffusion Laboratory at Colorado State University.
The wind tunnel has been described in detail by Plate and
Cermak (1963). The instruments used are part of the
standard laboratory equipment with the exception of the
MS-9 (mass spectrometer) leak detector (29). The wind
tunnel and instruments used are hereby described.

B. The Wind Tunnel

The wind tunnel is of the recirculating type. It is
shown in Fig. 1. The injector was placed directly on the
smooth floor of the wind tunnel and was located 40 ft
downstream from the inlet of the test section for the
initial work. For other work the probe was set at x=65 ft.
The boundary layers along the walls of the tunnel were
artificially tripped (Fig. 2) to become turbulent by a
heavy sawtooth fence followed by a four-foot section of
3/8 in. gravel fastened all around the exit portion of the
transition section. The entry length of 40 ft was an
adiabatic 6 ft X 6 ft section and was similar to the 40 ft
length of aluminum-floored test section except for its
wooden floor.

The air speed in this wind tunnel is controlled with a variable-speed, variable-pitch aircraft propeller. The temperature of the ambient air is maintained at a constant value by means of an air-conditioning system for neutral conditions and by electrical heaters for stable conditions. The floor is maintained at a constant temperature by means of a brine system for the stable flow conditions. The pressure in the test section was kept "constant" by adjusting the ceiling of the 6 X 6 ft^2 cross sectional area to obtain a "zero" pressure gradient. A large contraction ratio of 9:1 in conjunction with a set of 4 damping screens yields an ambient turbulence level of about .04%.

C. Instrumentation

The measurements consisted of velocity measurements for mean velocities, temperature measurements for mean temperature, and concentration measurements for mean concentrations.

1. Velocity Measurements

The velocity distributions were measured with a pitot static tube of the standard (Prandtl) design. The two pressure parts of the tube were connected to the two parts of an electronic differential pressure transducer (Transonic Equibar Type 120), which provides a DC output proportional to the differential pressure. This DC voltage was applied to the Y-axis of an X-Y plotter (Moseley Type 135). To the other axis of the plotter, a voltage

was applied which was obtained across a potentiometer. This potentiometer was geared to the drive screw of a motor-driven positioning device and thus provided a resistance proportional to the distance of the probe from the smooth (floor) plate. In this manner, continuous profiles were obtained of the dynamic pressure.

The pressure transducer was calibrated against a water manometer which was used as a primary standard. The position potentiometer and amplifier of the X-Y plotter x-axis were calibrated against measured distances before each run, or before each set of runs, if no interruption of the test sequence was required.

Assuming a perfect-gas relationship for the air, the following relationship based on Bernoulli's equation is obtained:

$$\bar{u}_s = c \sqrt{\Delta h} \qquad 4.1$$

where c is a "constant" dependent on the tunnel ambient air temperature and pressure plus the floor temperature. The variable boundary layer density which is included in c was "averaged" using these two temperatures. These three parameters were measured and recorded for each experiment. The pressure transducer or Transonic error was less than 1% of the full-scale deflection when compared to the inclined manometer mentioned above.

The positioning error of the vertical carriage signal was found to be less than 1/16 of an inch.

2. Temperature Measurements

The temperature distributions were measured with a standard ice-junction thermocouple circuit in conjunction with a precision potentiometer. Select copper constantan wire ($\pm .5^{\circ}$F guarantee) was used for the ambient thermocouple as well as the cold-junction (32°F reference point) thermocouple. These thermocouples were calibrated at two temperatures -- the ice point (32°F) and the boiling point of water at local ambient pressure and temperature. For the mean measurements involved, a linear relationship between these two points was assumed to be sufficiently accurate. Point by point temperature measurements were taken with this thermocouple setup since the time-response of it was not sufficiently rapid to allow continuous temperature recording.

3. Concentration Measurements

The gas feed and sampling system is shown schematically in Fig. 3. The continuous point source was supplied with helium (99.99% pure helium) directly from the pressurized tank. The flow rate of helium was controlled by using a pressure regulator at the bottle outlet and by passing the gas through a calibrated Brooks flowmeter. The exit velocity of the gas was set at an approximately fixed velocity regardless of mean ambient local velocity conditions in the air surrounding the injector.

However, different fixed injection velocities were used
with different mean ambient free stream velocities.

The air was sampled continuously by means of a probe
to which a vacuum pump applied negative pressure. A
calibrated Matheson flow-meter was set in the line prior
to the vacuum pump so that a fixed suction or negative
pressure could be maintained. The suction line was con-
nected through a T-section to the inlet leak ("standard
calibrated leak" or orifice) of the mass spectrometer.
The leak detector (mass spectrometer) continuously sampled
the helium content of the gas-air flow and gave an elec-
trical (DC-voltage) output which was applied to the X-axis
of an X-Y plotter. The Y-axis of the recorder was cali-
brated against distance as was done for the velocity
measurements. However, because of the slow response of
the leak detector, continuous profiles could not be taken.
(This is discussed in more detail in Appendix B.) Instead,
the X-amplifier of the plotter was switched to the time
base; and a plot of output voltage from the leak detector
vs. time was obtained for selected elevations and/or
horizontal positions.

Typical results are shown in Figs. 4 and 5. The
experimental results in output volts of the mass spectro-
meter were converted into concentrations by means of a
calibration chart. An example of this calibration using
three different helium-nitrogen standard gas mixtures and
three different standard calibrated leaks is shown in

Fig. 6. The manufacturer's two constitutent gases (helium-
nitrogen) were checked chromatographically and were found
to be close to the guaranteed concentrations. It was
found by this writer in the initial study (as is discussed
in Appendix B) that a drift in the mass spectrometer out-
put due to "dirtying" of the filament of the "Vee"-tube
and other components caused a change in the magnitude of
the concentration measurements which resulted in a fairly
parallel shift of the calibration curve on log-log paper.
Therefore, before and after each run, calibration points
were obtained with the standard gas (helium-nitrogen mix-
ture -- .05%, .2%, and .5%). The calibration curves were
extended to lower and higher values of the calibrated con-
centration points by assuming that a linear relationship
existed outside the calibration points as did within the
calibration points. It was found that the scale reading
or "SR" versus concentration graph (see Fig. 6) could be
expressed by an equation of form:

$$y = ax^b + c \qquad\qquad 4.2$$

where:

y = scale reading of MS-9

x = concentration in ppm

b = exponent to be found (slope)

a = constant to be found; different with
changing conditions of MS-9

The constant b was found to be approximately one; so, this equation could be written as:

$$y = ax + c \qquad\qquad 4.3$$

4. Sampling and Injection Probes

The sampling probe was made of thin wall 1/16" I.D. stainless steel tubing and was clamped onto the vertical traversing mechanism. Tygon tubing joined the probe to the suction unit.

The injection probe was centered on the floor and was made of a piece of 3"-long, .07in. I.D. brass tubing. It was similarly joined to the gas injection unit by tygon tubing.

5. Calibration of Injection and Suction Flow-Meters

The injection flow-meter with black ball (Brooks Sho-Rate; tubes 2-66-AMM, 6.5 cm scale) was calibrated twice by the well-known water-displacement method, and the calibration points checked within $\pm 1\%$. The meter was further checked using the "soap-bubble" method. The calibration points of both methods agreed within $\pm 3\%$. The results of these calibrations are shown in Fig. 7.

A Matheson Flowmeter No. 203 (with sapphire ball) was used for the suction. The calibration of this flow-meter was verified for a few points only, since the flow-meter had been calibrated previously by other experimenters at the Colorado State University Fluid Dynamics

and Diffusion Laboratory. The recalibrated points agreed with the previous results within the range of allowable experimental variation. The graph of the original calibration for this meter can be found in Reference 27.

CHAPTER V

ANALYSIS OF DATA

A. General Discussion

1. Introduction

This section is concerned with the experimental
results obtained in this work. To date there have been
very few studies of this nature undertaken in any wind
tunnel (except for this facility) or in the manner per-
formed during the work of this dissertation. Therefore,
this topic was particularly intriguing and open to origi-
nal investigation and exploration both experimentally and
theoretically.

2. Stable Atmosphere

To determine what velocity should be used for
stably stratified flow, eq 2.29 was solved for $(\Delta U)^2$ to
obtain:

$$(\Delta U)^2 \quad = \quad g(\frac{\Delta \Theta}{\Theta})(\frac{\Delta z}{Ri}) \qquad\qquad 5.1$$

where Θ is the potential temperature ($^\circ$R). Assuming no
slip at wall, i.e., $u_w = 0$, $Ri = 0.25$, and also using an
average air temperature of 100°F and $\Delta z = 15"$, one ob-
tains $U_o = 6$ fps and for $\Delta z = 30"$, $U_o = 6.9$ fps.

Based on above calculations, an inversion with flow
velocity of 6 fps was utilized as a basic flow for the
stable stratification study.

From neutral flow theory it is known that the logarithmic profile law is valid away from the wall. It was apparent from studying the forms of the velocity profiles under temperature inversion that this same law with modification above should be valid in the same region. This is so because the form of the curve is unaffected by considerable changes in temperature gradient.

From this writer's previous unpublished work it was found that the stability length L was approximately 4 to 15 inches at 6 fps. Various reference heights were experimented with. However, rather than taking a fixed percentage of L for the reference height as was done by Monin ($\frac{L}{2}$), five inches was arbitrarily selected based on the previously mentioned unpublished work. This selection of five inches as the reference height allowed one reference position to be used for all the velocity profiles at 6, 10 and 20 fps. This method reduced the computational work a great deal.

Using this reference height of 5 inches, Figs. 8, 9, and 10 (x = 60, 70, 78 ft) show the Monin-Obukhov velocity model comparison for velocities of 6, 10, 20 fps in confirmation of eq 3.19. It was found from these plots that the wind tunnel data matches or confirms the "log + linear" law very well from 1/2 inch to 18 inches. As was also found from these same graphs and data points, there is a very small area of deviation from the ideal, which occurs

when data is obtained extremely close to the wall and very far from the wall as could be expected.

In addition, whereas other experimenters have used field data in confirmation of the "log + linear" law, the work of this author represents the first over-all confirmation of the "log + linear" law using wind-tunnel boundary-layer data.

Using this same reference height of 5 inches, Figs. 11, 12, and 13 (x = 60, 70, 78 ft) show the Monin-Obukhov temperature model comparison for 6, 10, and 20 fps using eq 3.20. As can be seen from these plots, the confirmation in the Colorado State University wind tunnel is not comparable to the velocity modeling. This poorer agreement is due to the fact that the thermal boundary layer is still rapidly growing at the same velocity stations. However, one can note that the agreement improves as the stations go downstream from 60 ft (Fig. 11) to 78 ft (Fig. 13). The modeling for these temperature profiles was generally valid from 3 inches to 12 inches (Fig. 11, x = 60 ft) and from 2½ inches to 15 inches (Fig. 13, x = 78 ft). The ambient entry region is 40 ft (x_o = 40 ft) in all six figures.

Generally, both the friction velocity u_* and friction temperature T_* are variable quantities (i.e., functions of x, the downwind distance) near the inception of their respective boundary layers. However, if measurements are taken well downstream of the inception regime, then u_* and

T_* are fairly constant. The profiles with the above quantities, however, can be adequately expressed by the log + linear "law" even in such cases where the respective boundary layers are not yet fully developed as can be seen in Figs. 11, 12, and 13. Thus, it is found that data obtained in the wind tunnel can be adequately expressed with the log + linear "law" for the middle portion of the inversion boundary layer. This same relationship has been used by others (14) to confirm the data in the atmospheric boundary layer.

B. Discussion of Results

1. Velocity and Temperature Profiles

As shown in Chapter III, the modeling of the log + linear "law" required the solving of many simultaneous equations to get average values of u_* , T_* , β , and L for the inversion temperature-velocity profiles.

In the growing region of the boundary layer the friction velocity u_* is found to be a function of the downwind distance x both for neutral and inversion type flow. Similarly, the friction temperature T_* is found to be a function of x for the rapidly growing thermal boundary layer. However, using the method of averaging these simultaneous equations, the values of u_* , T_* , β , and L are averaged from the velocity and temperature profiles for a fixed x-position even though these values change with downwind distance as mentioned before.

The above-mentioned simultaneous equations are solved for $(\frac{T_*}{u_*})$ by eq 3.6, $(\frac{u_*}{k})$ by eq 3.14, and $(\frac{\beta}{w})$ by eq 3.16. Then β is obtained from 3.16 in conjunction with 3.11 for w. L is obtained by solving eq 3.10 with the value of w, which was previously obtained from eq 3.11 and with the value of $(\frac{u_*}{k})$ from eq 3.14. Upon solving for u_*, T_*, β, and L, one can then model eq 3.19 for velocity profiles and eq 3.20 for temperature profiles. Even though u_*, T_*, and L are averaged to obtain a constant value for a fixed x-position in the growing boundary layer, they are known to be variable with x; but far enough downstream these parameters should be fairly constant with height and x-position for a fixed velocity and inversion. Since L is directly related to u_* as shown in eq 3.10, L is also a function of x in the wind tunnel boundary layer. The experimental data confirms this.

The velocity profile of 6 fps was studied for inversion flow conditions. In addition a velocity of 10 fps was studied for near "stable" flow conditions. Then a velocity of 20 fps was studied to demonstrate the effects, if any, of a high velocity on the velocity profiles with temperature inversion.

Neutral velocity profiles of 6, 10, and 20 fps were also studied in order to compare the similarities and differences between the two types of flow. In Fig. 14 can be seen the relation between L and x for 6, 10, 20 fps.

The average L's for 6, 10, and 20 fps was found to be 14 inches, 33 inches, and 110 inches respectively.

In Figs. 15 and 16 are seen the relationship between u_* and x for neutral and inversion type flow for 6, 10, and 20 fps. For the neutral case the average friction velocities for 6, 10, 20 fps were found to be 0.27, 0.45, and 0.77 fps respectively. For the inversion-type flow they were found to be 0.25, 0.41, and 0.64 fps. As can be seen on both graphs, u_* decreases with downwind distance. On log-log paper the slope of the u_* vs. x relationship was found to be approximately:

$$u_* \propto x^{-0.14} \qquad\qquad 5.2$$

By plotting the neutral velocity profile of log z vs. $\bar{u}$ on semi-log paper and utilizing a curve of best-fit through the points, the average roughness length z_0 was found to be approximately 0.0011 inches or 0.0001 ft. By taking the intercept of the log z axis where $\bar{u} \cong 0$, the slope of this curve was similarly used to solve for u_*. Since all tests were run in the same tunnel, z_0 should be independent of flow conditions. Solving for z_0 for inversion conditions gave values similar to those above.

In Figs. 17 and 18 can be seen the relationship between u_* and T_* and between u_* and L. As can be seen on both graphs, T_* and L increase with increasing u_*. In Fig. 19 can be seen the relationship between T_* and x. Here T_* increases with downwind distance for all velocities.

In Fig. 20 are seen values of β vs. L under inversion (stable) flow conditions of 6, 10, 20 fps in the Colorado State University large wind tunnel. Thus, it can be seen that β increases with increasing L in agreement with the results found by Takeuchi (18). This wind tunnel velocity profile results also showed an average β = 0.99 for 6 fps, β = 1.33 for 10 fps, and β = 5.96 for 20 fps. When using these results to confirm the diffusion data, an average value of β = 1.0 was used for 6 and 10 fps. An average value of β = 6.0 was used for 20 fps. As noted before, an average β for 6 fps was found to be about 0.99, and an average β for 10 fps to be about 1.33. This gave an average β for both velocities of about 1.2. The average β for 20 fps was found to be 5.96. If one were to average the β for all three velocities, an average β of 2.8 is obtained.

Using these values of u_*, T_*, β , and L as shown on the various graphs, the "log + linear" relationship as presented previously for the velocity profiles was confirmed by the tunnel data from 1/2 inch to 18 inches. An attempt to model the temperature data by a similar "log + linear" law was found to be not as adequate and was only confirmed from 3 inches to 12 inches. These results are all shown on Figs. 8 through 13.

2. Richardson Number

Using temperature-height gradients and velocity-height gradients obtained from temperature velocity profiles under inversion flow conditions, plots of (see Fig. 21) Richardson number as a function of velocity and momentum boundary layer growth were obtained. The definition of the Richardson number as indicated by a form of eq 5.3 was used. It is:

$$Ri = \frac{g}{\overline{T}} \frac{(\frac{\partial \overline{T}}{\partial z})}{(\frac{\partial \overline{u}}{\partial z})^2} \qquad 5.3$$

Fig. 21 also shows that the Ri No increases with downstream distance for the increasing momentum boundary layer and thermal boundary layer. Also, it can be seen from the same figure that the position of the maximum Ri No for the same x-position decreases with decreasing free stream velocity. The Ri No for all velocities and positions starts at a low value near the floor, reaches some maximum value at about 4 to 6 inches up, and then starts to decrease again with height.

Using Figs. 14 and 21, a cross-plot was obtained (see Fig. 22) to show the relationship between Ri_{max} and $\frac{1}{L}$. This was plotted as L vs. $\frac{1}{Ri_{max}}$ and confirms eq 3.29 for small z or large L. It was found that the height for the maximum Ri No for a fixed position was within 3% for the different velocities so that the z in

eq 3.29 could be considered a constant; and thus, eq 3.29 can be expressed as:

$$L \propto \frac{1}{Ri_{max}}$$

5.4

which is a linear relation for the data.

3. Boundary Layer Growth

In Figs. 23 and 24 are plotted dimensionless neutral boundary layer growth versus dimensionless velocity at two different stations. As can be seen from these two figures, there is very little difference in the profiles of 6, 10, and 20 fps for this neutral turbulent flow. In Figs. 25 and 26 are plotted the same type dimensionless parameters for inversion-type flow for the same two stations. As can be seen from these two plots, the profiles become less fully developed with decreasing velocity or decreasing L and increasing Ri No. The profile for inversion 20 fps is practically similar to the same plot for neutral 20 fps. The inversion 10 fps is slightly displaced from the neutral 10 fps, but the inversion 6 fps is greatly displaced from the neutral 6 fps showing the effects of decreased turbulence.

Reynolds et al (36) developed a semi-empirical equation to show the relationship between the thermal boundary layer and the momentum boundary layer for a flat plate with a step temperature distribution (unheated or adiabatic starting length) as a function of downstream

distance. They (36) made the following assumptions:

(a) the viscous effects, ν , as well as thermal effects,

k_t , are negligible in the turbulent boundary layer;

(b) the eddy diffusivity for heat, K_H , is equal to the

eddy diffusivity for momentum, K_M , (Reynolds analogy).

Since assumption (a) is assumed to hold everywhere in the

boundary layer, except at the wall, assumption (b) implied

that the Prandtl number is 1 . (c) The velocity profile

may be assumed to be represented by an expression of the

form:

$$\frac{\bar{u}}{\bar{u}_\infty} = \left(\frac{z_s}{\delta}\right)^{\frac{1}{m}} \qquad\qquad 5.5$$

where m is the familiar exponent of the "power-law" used

to characterize the turbulent boundary layer for a flat

plate. (d) The temperature profile is similar to the

velocity profile, based on its own boundary-layer thick-

ness which is:

$$\Theta = \frac{\bar{T}}{\bar{T}_\infty} = \left(\frac{z_s}{\delta_t}\right)^{\frac{1}{m}} \qquad\qquad 5.6$$

Starting with the energy equation for the boundary

layer, neglecting dissipation and assuming the temperature

difference ($\Delta T = T_w - T_\infty$) is constant in the region of

interest, plus using the four other conditions cited above,

Reynolds et al (36) obtained the following equation

(corrected from ref 36):

$$\left(\frac{\delta_t}{\delta}\right) = \left(\left\{1 - \frac{\delta(x_o)}{\delta(x)}\right\}^{\frac{m+2}{m+1}}\right)^{\frac{m}{m+2}} \qquad 5.7$$

where $\delta(x_o)$ is the momentum boundary thickness at $x = x_o$ and x_o is the adiabatic entry length. The exponent m is as defined in eq 5.5 .

In the range $10^4 < Re_x < 10^7$ the boundary layer thickness δ varies as $x^{4/5}$, and eq 5.7 may be written as (corrected from ref 36):

$$\left(\frac{\delta_t}{\delta}\right) = \left\{1 - \left(\frac{x_o}{x}\right)^{\frac{4(m+2)}{5(m+1)}}\right\}^{\frac{m}{m+2}} \qquad 5.8$$

The neutral and inversion velocity profiles for 6, 10, and 20 fps were normalized and plotted on log-log graph paper to determine the slope of their curves which also is the value of the exponent m in eq 5.5 and eq 5.8 . In all the neutral flow profiles the average m was found (see Fig. 24) to be 7. In the inversion 20 fps, m was 7 (see Fig. 25). In the 10 fps inversion the average m was 6.9 . In 6 fps inversion the average m was found to have a value of 5.4 (see Fig. 25).

In Fig. 27 is shown on arithmetic grid the theoretical line for the turbulent boundary layer growth as postulated by Reynolds et al (36). Also on the same figure are shown laminar lines of Olson (37) and Eckert and

Drake (30). These men (30, 37) obtained two different laminar curves as they assumed slightly different shaped velocity profiles. The experimental data as obtained for the Colorado State University wind tunnel is also shown on this same plot. To obtain a better picture of the theory and data relation, Fig. 27 was put on a log-log plot to obtain Fig. 28. Using a value of m = 7 in eq 5.8 gives:

$$\left(\frac{\delta_t}{\delta}\right) = \left\{ 1 - \left(\frac{x_o}{x}\right)^{\frac{9}{10}} \right\}^{\frac{7}{9}} \qquad\qquad 5.9$$

and for m ≃ 5 , eq 5.8 gives:

$$\left(\frac{\delta_t}{\delta}\right) = \left\{ 1 - \left(\frac{x_o}{x}\right)^{\frac{14}{15}} \right\}^{\frac{5}{7}} \qquad\qquad 5.10$$

These two equations 5.9 and 5.10 are shown plotted on Fig. 28 with the data points between them. It is to be noted on Fig. 28 that the agreement between theory and data improves as the boundary layers become more fully developed.

4. Monin Log + Linear (Velocity Profile) "Law" with Attendant Similar "Law" for Temperature Profile

As mentioned before, Monin's work (1954), the log + linear "law" for velocity profiles (eq 3.19), was used as a basis to model the velocity data obtained in this research. Therefore, it was feasible to investigate how this velocity relationship would match a temperature

relationship (eq 3.20) based on the same reasoning. This
was done for three stations for the three different
velocities (6, 10, 20 fps), using the left-hand sides of
eq 3.19 for the dimensionless velocities and eq 3.20 for
the dimensionless temperatures. These plots are shown as
Figs. 29, 30, and 31, and the solid lines represent the
theory. The raw data points indicated that the matching
is poor at the wall and far from the wall. In between it
was noted that good matching is obtained so that the use
of these relationships is valid for use with wind tunnel
data as has been indirectly pointed out in Figs. 8 through
13 in the region as noted.

5. Diffusion Data

a. Vertical Spread Data

Using assumed values of β , $\tilde{\mathcal{R}}$, and $\mathcal{R}_o$,
theoretical equation 3.56 of this dissertation was solved
as detailed in Chapter III. Equation 3.56 relates the
dimensionless theoretical vertical diffusion to the di-
mensionless downwind distance. The similar relation
(eq 3.59) of Monin (11), expanded by Gifford (13), was
similarly solved by a computer program for the same
values of β , $\int$, and $\int_o$. The Monin-Gifford theoreti-
cal relationship is graphically exhibited in Figs. 34
(where $\beta = 1$) and 38 (where $\beta = 6$). The theoretical
relationship of this dissertation is graphically portrayed
in Figs. 32 (where $\beta = 1$) and 36 (where $\beta = 6$).

Graphically, the greatest difference between these two

equations, aside from the derivations, is found in the

pattern of the spreads downwind from the point of injec-

tion. Graphically, the theory presented in this disserta-

tion shows that away from the point of injection the

vertical dispersion is less than that shown by Gifford's

theory (13). On the other hand, fairly close to the point

of injection, it can be seen that the pattern of the

vertical dispersion for both theories is fairly similar.

On Figs. 33, 35, 37, and 39 are plotted the data

points with roughness data line for 6, 10, and 20 fps as

obtained in this study. In order to locate the dimension-

less vertical spreads of these data points, one must solve

for the dimensionless downwind distance $\tilde{\varepsilon} = \dfrac{kb\tilde{x}}{L}$, where

k is von Karman's constant equal to 0.4, and b is Batche-

lor's constant (12), the value of which has not been

firmly established as yet. Gifford (13) suggests in his

paper that b is equal to the ratio of the mean vertical

velocity of a particle under adiabatic conditions to the

friction velocity u_* . Cermak (14) used a value of b = 0.1

for his neutral and unstable data and got good agreement

with his theory using that value. However, in this dis-

sertation for the work related to inversion flow, the

value of Batchelor's constant was taken to be 0.4. This

b-value of 0.4 was proposed by Ellison (34), provided that

a K-theory of diffusion is valid such that $K = K_M = ku_*z$.

This value of 0.4 gave good agreement with the research data. The raw concentration data for the vertical spread (z at 50% C_{max} or z_{50}) is shown on Figs. 48 and 49.

Using the appropriate values of L and β (see Figs. 14 and 20), as discussed previously, along with the vertical spread data and roughness z_o of the Colorado State University large wind tunnel, the results were obtained as shown on Figs. 33, 35, 37, and 39. Looking at these same figures, one can note that there is fairly good agreement with the theory for the vertical spread of the 10 and 20 fps velocity-concentrations. The 5 and 6 fps do not give as good agreement, and this could indicate that a value of b = 0.4 is too large for the lower velocities. However, it is to be noted that the data has the same slope as the theoretical curve for dimensionless roughness of 6 fps whereas this same data is in much poorer agreement with the roughness data line calculated by use of Gifford's theoretical equation. Here, as the theoretical spread becomes larger with downwind distance, the difference becomes greater between the theoretical line and the data for 5 and 6 fps. The vertical dispersion points for 5, 6, 10, and 20 fps velocities are shown for downwind distances of x equal to 50, 60, 70, and 78 ft. The 5 and 6 fps have some intermediate points at 65 and 75 ft also. In addition to averaged values of β and L in the vertical direction, averaged values of L and z_{50} in the downwind direction were used as shown in Figs. 14, 48, and 49.

b. **Maximum Floorline Concentration Decay Data**

Using assumed values of β , $\tilde{\mathcal{R}}$, and $\mathcal{R}_o$,
equation 3.62 -- which represents the theoretical mean
concentration at ground level as a function of downwind
distance, as presented in a dimensionless form in this
study -- was solved as detailed in Chapter III. The
similar relation, eq 3.64 of Gifford (13), was similarly
solved by a computer program for the same values of β ,
$\mathcal{J}$, and $\mathcal{J}_o$. Using the averaged values of β = 1 for
6 and 10 fps and the averaged value of β = 6 for 20 fps,
the above results are graphically shown on Figs. 40, 42,
44, and 46. In Figs. 40 and 42 the slopes of the curves
are fairly similar. However, it is to be noted that as
the value of the dimensionless roughness becomes larger,
the dimensionless concentration lines in Gifford's work
are more affected than those in this present work. When
β = 6, Fig. 46 of Gifford's theory shows that the larger
roughness value affects concentration lines to an even
greater extent. Fig. 44 of this analysis shows that β = 6
has an opposite effect, and the dimensionless concentra-
tion lines come closer together or undergo a reverse
effect.

The theoretical concentration points for 5, 6,
and 7 fps and 5, 6, 10, and 20 fps are shown on Figs. 50
and 51. The concentration data for 5, 6, 7 fps was taken
with the injection probe at x = 65 ft and a separation
distance of up to 10 feet. The concentration data for 5,

6, 10, and 20 fps was taken with the injection probe at
x = 40 ft and a separation distance of up to 38 ft. Using
averaged values of β , L, and u_* in the vertical direc-
tion -- as well as averaged values of L, u_* , and C_0 in the
downstream direction -- as shown on Figs. 14, 18, 50, and
51, the experimental peak floorline concentration data
points were plotted on Figs. 41, 43, 45, and 47. Compar-
ing the graphical analysis shown in Fig. 41 with that of
Gifford's shown in Fig. 43 for 5, 6, 7, and 10 fps, one
can note that the agreement of the data with the theories
are approximately equivalent. It is to be noted that the
data fall on the low side of the dimensionless roughness
line for this theory and fall on the high side of the same
roughness line for Gifford's (13). However, when com-
paring Fig. 45 with 47 for β = 6, one can note that the
data is more in agreement with this theory than with
Gifford's.

It is to be noted further that at the higher veloci-
ties (i.e., 20 fps) when the flow with temperature-inversion
has a negligible effect on the turbulence, the value of β
is no longer in agreement with the values obtained at 6 and
10 fps.

Complete velocity profiles were taken for 6, 10, and
20 fps. Then, the values of u_* , L, and β were computed
for all those velocities. Those that were obtained for 6
fps and 10 fps were extrapolated for the 5 and 7 fps con-
centration data since there were no velocity profiles

taken for 5 and 7 fps. The values of those extrapolated parameters that were obtained from 6 fps and 10 fps were determined to be suitable for the 5 and 7 fps runs. This determination was based on a study of vertical spread and floorline maximum concentration decay data of the 5, 6, and 7 fps runs after noting the closeness of all concentration values at similar locations.

CHAPTER VI

CONCLUSIONS

This study of turbulent diffusion in a stable boundary layer over a smooth surface in the wind tunnel was used to develop a vertical diffusion theory. This theory is based on the hypothesis of Lagrangian similarity as applied to a turbulent atmospheric surface layer in which the flow characteristics are all determined entirely by the friction velocity u_* and a length L as defined in eq 1.7.

This Lagrangian similarity concept in conjunction with a log + linear "law" for both temperature and velocity profiles as shown by eqs 3.51 and 3.53 was used to solve a form of the turbulent energy equation in order to obtain eq 3.56 which predicts the dimensionless vertical spread (height) as a function of the dimensionless downwind distance. This equation 3.56 is similar to one that has been developed and derived by Gifford, who used the Lagrangian similarity method.

Similarly, based on physical reasoning (40) and some of the above-mentioned concepts concerning u_* , L , and log + linear relations, a theory of mean concentration decay was developed. This is presented as eq 3.62 which relates the dimensionless concentration to the dimensionless downwind distance.

From the agreement between theory and data as shown in this work, one can reasonably predict the vertical spread and maximum ground level decay of a gas or pollutant under inversion conditions. This can now be done experimentally in the wind tunnel using the same scaling parameters determined previously with field data.

A method of averaging simultaneous equations was used to solve for the values of u_*, T_*, β, and L using the log + linear relationships for velocity and temperature. Then, using these calculated values, it was shown that it is possible to confirm the work of Monin and Obukhov with wind tunnel data as had been previously done with field data.

REFERENCES

1. Sutton, O. G. 1953: Micrometeorology. McGraw-Hill, New York. 336p.

2. Priestly, J. B. 1965, rev. ed.: Turbulent Transfer in the Lower Atmosphere. U. of Chicago Press. 130p.

3. Taylor, G. I. 1921: Diffusion by continuous movements. Proc. Roy. Soc. (London). A20, 196-212.

4. Pasquill, F. 1962: Atmospheric Diffusion. Van Nostrand, London. 297p.

5. Baldwin, L. V. and W. R. Mickelsen. 1963: Turbulent diffusion and anemometer measurements. Am. Soc. Civil Engrs. 128: 1595-1631.

6. Baldwin, L. V. Air, water pollution challenge, in Affairs of CSU. 5:No.2, June 1966. Colo. State University, Fort Collins, Colo.

7. Frenkiel, F. N. 1953: Turbulent diffusion, in Advances in Applied Mechanics. v.3. von Mises, R. and T. von Karman, eds. Academic Press, New York. p.61.

8. Roberts, O. F. T. 1923: The theoretical scattering of smoke in a turbulent atmosphere. Proc. Roy. Soc. (London). A104:640-654.

9. Businger, J.A. 1959: A generalization of the mixing-length concept. J. Meteorol. 16:516-522.

10. Ellison, T. H. 1957: Turbulent transport of heat and momentum from an infinite rough plane. J. Fluid. Mech. 2:456-466.

11. Monin, A. S. 1959: Smoke propagation in the surface layer of the atmosphere, in Advances in Geophysics. v.6. Frenkiel, F. N. and P. A. Sheppard, eds. Academic Press, New York. p.331.

12. Batchelor, G. K. 1964: Diffusion from sources in a turbulent boundary layer. Archuvum Mechanikj Stosowanej. 3:16.

13. Gifford, T. A. 1962: Diffusion in the diabatic surface layer. J. Geophys. Res. 67:3207-3212.

14. Cermak, J. E. 1963: Lagrangian similarity hypothesis applied to diffusion in turbulent shear flow. J. Fluid. Mch. 15:49-64.

15. Swinbank, W. C. 1964: The exponential wind profile. Quart. J. Roy. Meteorol. Soc. 90:119-135.

16. Inoue, E. 1959: The effects of thermal stratification on turbulent diffusion in the atmospheric surface layer. Advances in Geophysics. v.6. Frenkiel, F. N. and P. A. Sheppard, eds. loc. cit. 319-329.

17. Yamamoto, G. 1959: Theory of turbulent transfer in non-neutral conditions. J. Meteorol. Soc. Japan. 37:60-69.

18. Takeuchi, K. 1961: On the structure of the turbulent field in the surface boundary layer. J. Meteorol. Soc. Japan. 39:346-367.

19. Okamoto, M. 1963: A note on the wind and temperature profiles in the diabatic atmosphere near the ground. Japan Meteorol. Agency, Tokyo. 505-514.

20. Stewart, R. W. 1959: The problem of diffusion in a stratified fluid. Advances in Geophysics. v.6. Frenkiel, F. N. and P. A. Sheppard, eds. loc. cit. 303-311.

21. Monin, A. S. and A. M. Obukhov. 1954: The basic laws of turbulent transport in the ground layer of the atmosphere. Tr. Geophys. Inst. Acad. Sci. USSR. No. 24:151,163-181.

22. Panofsky, H. A., A. K. Blackadar and G. E. McVehil. 1960: The diabatic wind profile. Quart. J. Roy. Meteorol. Soc. 86:390-398.

23. Barad, M. L. and D. A. Haugen. 1959: A preliminary evaluation of Sutton's hypothesis for diffusion from a continuous point source. J. of Meteorol. 16:12-20.

24. Poreh, M. 1961: Diffusion from a line source into a turbulent boundary layer. Ph.D. Dissertation. Colo. State Univ., Fort Collins, Colo. 100p.

25. Davar, K. S. 1961: Diffusion from a point source within a turbulent boundary layer. Ph.D. Dissertation. Colo. State Univ., Fort Collins, Colo. 161p.

26. Malhotra, R. C. 1962: Diffusion from a point source in a turbulent boundary layer with unstable density stratification. Ph.D. Dissertation. Colo. State Univ., Fort Collins, Colo. 171p.

27. Quraishi, A. A. 1963: Diffusion in a turbulent boundary layer. Ph.D. Dissertation. Colo. State Univ., Fort Collins, Colo. 190p.

28.   Veeco, Complete Mass Spectrometer. Series MS9. Principles of Operation. Vacuum-Electronics Corp. Long Island, N.Y.

29.   Mass Spectrometer Leak Detector, Models MS9A, MS9AB, MS9ABC. Operation and Maintenance Manual. Vacuum-Electronics Corp. Long Island, N.Y.

30. Eckert, E. and R. Drake. 1959: Heat and Mass Transfer. McGraw-Hill, New York. p.217.

31. Lumley, J. L. and H. A. Panofsky. 1964: The structure of atmospheric turbulence. Interscience Publishers. 237p.

32. Calder, K. L. 1949: The criterion of turbulence in a fluid of variable density with particular reference to conditions in the atmosphere. Quart. J. of Roy. Meteorol. Soc. 75:71-78.

33. Deacon, E. L. 1949: Vertical diffusion in the lowest layers of the atmosphere. Quart. J. of Roy. Meteorol. Soc. 75:89-103.

34. Ellison, T. H. 1959: Turbulent diffusion. Science Progress. 47:495-506.

35. Gifford, F. 1966: Personal communications. Feb. 3 and Feb. 22, 1966.

36. Reynolds, W. C., W. M. Kays, and S. J. Kline. 1958: Heat transfer in the turbulent incompressible boundary layer II-step wall-temperature distribution. NASA,Washington,D.C. Memo 12-2-58W.

37. Olson, R. M. 1961: Essentials of Engineering Fluid Mechanics. International Textbook Co., Scranton, Pa.

38. Monin, A. S. 1962: Empirical data on turbulence in the surface layer of the atmosphere. J. of Geophysical Research. 68:No.8,3103-3109.

39. Prandtl, L. 1952: Essentials of Fluid Dynamics.
    Blackie & Son, Ltd., London and Glascow.

40. Goldstein, S. 1965: Modern Developments in Fluid
    Mechanics. v.I. Aeronautical Research Com-
    mittee et al, ed. by S. Goldstein. Dover
    Publications, New York.

41. Sandborn, V. A. 1967: Personal communication.
    Colorado State University. Feb. 17, 1967.

A P P E N D I C E S

APPENDIX A

CONFIRMATION OF VELOCITY PROFILES

I. Deacon's Equation

In Fig. 52 is presented a graph of eq 2.45 showing a comparison based on data obtained by Deacon and by this author. It is to be noted that there is fairly close agreement in the two sets of data points.

On Fig. 53 are shown the velocity-gradient slopes and temperature-gradient slopes as a function of downwind distance as obtained in this study. The average value for γ (velocity-gradient slope) for 6 fps was 0.77; for 10 fps, 0.78; and for 20 fps, 0.93. The average value for γ_t (temperature-gradient slope) for 6 fps was 0.72; for 10 fps, 0.73; for 20 fps, 0.90. Both the $\frac{d\bar{T}}{dz}$ and $\frac{d\bar{u}}{dz}$ slopes were obtained from the $\bar{T}$-z and $\bar{u}$-z profiles at distances of about one-half to one inch to about 7 to 8 inches from the floor of the wind tunnel. Beyond 8 inches the slopes obtained from the data points deviated greatly from the general trend of the points and could not be used to obtain the curve (slope) of best fit.

II. Monin's Stability Parameter $\frac{z}{L}$

Based on Monin's presentation described below, the velocity profile data for inversion flow of 6, 10, and 20 fps for three different stations in the Colorado State University wind tunnel are shown in Figs. 54, 55, and 56. These data are plotted as $\frac{k}{u_*} (\bar{u}_s - \bar{u}_r)$ vs. $\frac{z}{L}$ where $\bar{u}_r$ is the reference velocity at a reference height of 5 inches as used in this study and $\frac{z}{L}$ is a stability parameter suggested by Monin. The universal curve:

$$\frac{k}{u_*} \left\{ \bar{u}(z) - \bar{u}(\tfrac{L}{2}) \right\} = \left\{ f(\mathcal{S}) - f(-\tfrac{1}{2}) \right\} \qquad \text{A-1}$$

is shown on all three plots, Figs. 54, 55, and 56, as a solid line. As can be seen from the plots, all three velocities give three different curves. This is due to using a fixed reference height z . If a reference height was used that was a fixed percentage of L, all curves would intercept the x-axis at the same point and the curves would coincide over a great portion of their arcs. As can be seen on Fig 56, as the stability length L approaches twice the value of the reference height, the data points coincide with Monin's theoretical curve mentioned above. This is so for 6 fps.

III. Swinbank's Equation

Swinbank's experimental curve, eq 2.49, is plotted
on semi-log paper on Figs. 57, 58, and 59 as solid lines.
Based on the reference height of 5 inches, the velocity
difference of zero for each velocity profile again gave
three different curves for the three velocities (data) as
were similarly obtained using Monin's work cited previous-
ly (Appendix A-II). If a reference height that was a
proportion of L was used, these three curves on each
graph would intercept the y-axis at the same point, and
the curves would merge as one. Looking at all three
figures, one can see that the data from velocity profiles
of 6 and 10 fps confirm Swinbank's curve that he previous-
ly confirmed with field data. In all three plots it can
be noted that the 20 fps is not as good a match to the
theoretical curve as are the plots at 6 and 10 fps.

APPENDIX B

PRELIMINARY EXPERIMENTAL STUDIES

I. Concentration Studies

   A. Introduction

        Prior to the use of the mass spectrometer type of
leak detector, this writer had to develop in the labora-
tory a program to check for the stability, response, and
accuracy of the mass spectrometer and related equipment.
Foremost of all, this writer had to determine the feasi-
bility of using this machine and had to determine how the
results obtained with it compared with the then in use
chemical analysis method using ammonia gas. It was found
in all counts that the use of the mass spectrometer was
more reliable, accurate, stable, less time-consuming, and
less arduous.

   B. Operation of MS9 (Mass Spectrometer)

        Basically, the mass spectrometer is a two-vacuum
system -- a high vacuum and a low vacuum. The vee-tube
is in the low vacuum side, which has a cold trap filled
with liquid nitrogen to condense any condensable gases
and vapors and allow the fore pump to operate more effi-
ciently. The cold trap also makes for more efficient
evacuating of the "vee" tube, which depends on a high
ionizing voltage to ionize the gases and accelerate the
ions toward the counter. A schematic of the MS9 and vee

tube is shown in Figs. 6 and 29 of the Mass Spectrometer Handbook (29). A complete description of the operation and maintenance of the MS9 and vee tube is given in the Series MS9 Manual (28, 29) published by the manufacturer.

C. Stability or Drift Test

Two drift tests were performed by feeding 0.2% helium gas at 1 CFPH to the MS9 via a "T" connection and SCL. The first test lasted 80 minutes with readings taken every 10 minutes after the machine had come to equilibrium condition and the inlet flow of gas had stabilized. A maximum deviation of $\pm 4\%$ was noted for this test. A second drift test was made for a period of over five hours with readings taken every 15 minutes. The maximum deviation for this trial was $\pm 3\%$.

D. Response Time

The response time of the MS9 was determined using different size tygon (I.D.) tubing, tube lengths, and suction velocities. The time obtained included the 12-15 sec. lag time that it took for the machine to respond to a concentration obtained right at the inlet side of the standard calibrated leak (SCL). As was expected, the smaller size tubing gave the lesser response time. The best results were obtained using 1/16" tubing as shown on Fig. 61. However, in actual operation it was discovered that no readings were obtained with the standard thickness wall 1/16" tubing due to the atmospheric weight of the

ambient air pressing down on the thin wall tubing and collapsing it. Special heavy wall tubing was ordered, and this initial problem was resolved.

On all test runs a constant gas input of 1 CFPH was fed via a "T" to the SCL attached to the MS9. One side of the "T" was open to the atmosphere to have inlet conditions as close to ambient pressure as possible since the concentration readings depend both on temperature and pressure. The response time, as mentioned previously, also depended on which SCL (leak rate) was used. The largest SCL had the least response time and the largest reading for the same concentrations. This concentration reading can be again noted in Fig. 6. The largest SCL also allowed one to take concentration data far downstream from the injection source with a minimum injection mass flow. This minimum mass flow rate would prevent the ambient free-stream helium concentration from building up too rapidly.

E. Continuous Recording of Concentration

Initially, an attempt was made to obtain continuous concentration data by connecting the electrical output of the MS9 to the input of an X-Y plotter. A sample representation of the results obtained is shown in Fig. 62. With a motor speed of 12 min./20 in. or 0.6 min./in. and a distance of 9 feet between injector and sampler, a large lag time was noted in the response. By installing

slower speed motors on the traversing device (20 min./in.), much better response time and results were obtained as shown on Fig. 63. These results are with a separation distance of 2 feet with arc height up to 6½ inches. An attempt was made to use the geometry of similar triangles and geometric projections after establishing known concentrations at three known heights, but the results obtained were not sufficiently accurate due to the ever-present lag time of the machine response. However, one should note that far downstream where the concentrations are much less, the degree of accuracy obtained with the slow speed motor was fairly good.

F. Calibration of MS9 (Mass Spectrometer)

As was mentioned earlier, the MS9 was calibrated using three standard gases and three standard leaks. Two component special gases were used and consisted of helium and nitrogen. The percentages of helium (with guarantee, see Fig. 64) in the standard mixtures were 0.05% ± 0.005%, 0.2% ± 0.02%, and 0.5% ± 0.05%. In actual parts per million by volume this is 500 ± 50, 2000 ± 200, and 5000 ± 500. As can be easily found by a simple calculation, the manufacturer only guarantees the gas to have an accurate count within 20% or ± 10% from the mean concentration. The three SCL's were SCL1730 (3μCFPH), SCL1733 (15μCFPH), and SCL1735 (86μCFPH). As can be seen from Fig. 6, straight lines are obtained with a slope

approximately equal to one on log-log graph paper. Based on this and later studies, it was assumed that this linear parallel relationship would be valid for ranges above and below the calibration points.

G. Concentrations, Maximum and Minimum

A test was performed to determine the maximum concentration that could be recorded on the MS9, using a fixed injection mass flow rate. This was done to determine the limits of sampling distance both closest and furthest from the injector. This was accomplished by using the different capacity SCL's and recording readings from the upper scale limit to the smallest scale division on the leak indicator.

H. Reproducibility of Results

Many tests were performed to determine the reproducibility of results. It was found that reproducibility of results varied from $\pm 3\%$ to $\pm 30\%$. However, if one were testing over a short period of time, if the outside turbulence level was low, and if the machine was operating stably, one could then expect results to be within a range of $\pm 8\%$ to $\pm 10\%$.

I. Variation Test

A variation test was performed by letting the sampler record gas concentration (X-Y plotter on time

basis) at a fixed position. This was done only for the stable flow for this test (U_∞ = 5 fps). The probe was set at x = 65 ft (x_0 = 40) close to the floor (z = 1/8"), and readings were taken for 8 minutes -- one minute per reading. The eight-minute plot on the graph paper was divided in eight sections. The mean of the high section scale reading was 30.4, and the mean of the low section scale reading was 26.4 . The mean of the eight readings was 28.3 . The percent variation between high and low mean scale readings was about 12% when converted into concentration, or $\pm$ 6%. A similar time run (8 minutes) was made at the same x-position, but z now at 7 inches. The mean of the high scale reading was 8.80, and the mean of the low was 6.30 . The mean of the eight readings was 7.55 . The percent variation between the high and low means for this eight-minute time interval was about 35% or $\pm$ 17.5% when converted into concentration readings. This and similar studies showed that reproducibility of turbulent diffusion data was also very dependent on the sampling time as well as on the time interval between tests. A graphical picture of these results is shown on Fig. 65.

From this above test it was decided that each concentration reading should be taken for a minimum of 3 minutes after equilibrium was attained at any position. However, if the sampling time could be extended, the degree of reliability could be increased. However, then the time element became prohibitive when trying to cover a great

range of downwind distances, velocities, and other varia-
bles that were being evaluated during the research.

II. Other Studies

   A. Natural Buoyancy Effect of Helium Gas

       A study was made to determine the natural buoyancy

effect, if any, that the molecular weight of the tracer has

had on the concentration readings. A calculation was made

to determine what size heat exchanger would have to be made

to get optimum cooling of helium gas if cooled with liquid

nitrogen at -320°F. Assuming that helium was a perfect gas

at 75°F., the calculations showed that the best that could

be done would be to increase the density of helium by 2 so

that the molecular weight ratio would be about 8/29 rather

than 4/29. Assuming that the designed coil was analogous

to a single pass condenser (having a constant temperature

medium at rest -- liquid nitrogen), the cross-sectioned

area came out to be about 4 sq. inches. A coil was made to

give more than twice the calculated cooling surface required

and was installed in a one-quart dewar jar filled with liq-

uid nitrogen. The greatest reduction that actually could

be obtained was 50°F. from the ambient room temperature of

75°F. This could be due to heat gains and inefficient

"heat" transfer.

       A neutral and cooled helium test was made obtaining

C_{max} vs. x and vertical concentration profiles for both

flow conditions at 6 fps (x = 65'). The neutral

helium went through the same coil (no coolant) so that the same swirl and exit velocity (as determined by the flow-meter) could be obtained.

In Fig. 66 is plotted C_0 vs. x for neutral and cooled helium. The maximum floorline decay was found to be:

$$C_0 \propto x^{-1.51} \qquad\qquad \text{B-1}$$

When the vertical spreads were plotted against x (see Fig. 67), the following results were obtained:

$$\mathcal{R} \propto x^{0.50} \qquad \text{(cooled helium)} \qquad \text{B-2}$$

$$\mathcal{R} \propto x^{0.62} \qquad \text{(neutral helium)} \qquad \text{B-3}$$

There definitely appeared to be a difference in spreads which was more noticeable at 5 and 10 ft. The cooled helium seemed to diffuse in the vertical less readily, and this is what one would expect since its temperature was lower.

Dimensionless plots of $\dfrac{C}{C_0}$ vs. $\dfrac{z}{\mathcal{R}}$ for both cases were plotted on Figs. 68 and 69. The plot of neutral helium showed less scatter and was more closely aligned with the normal distribution than the plot of cooled helium gas.

Even though there appears to be a natural buoyancy effect in the use of helium gas as a tracer, the data was not corrected for this buoyant effect since it appears to be within the range of the day-to-day reproducibility.

B. Leakage Control of the Wind Tunnel

A study was devoted to leak-testing of the wind tunnel to reduce or minimize the creation of secondary circulation as much as possible. Seams along the walls and floor of the wind tunnel were sealed with masking tape, and this seemed to reduce some of these effects detrimental to low flow under both neutral and stable flow conditions. Smoke was also injected into the wind tunnel by means of a smoke generator. The smoke injector probe was placed on the floor at x_o = 40 ft and 18 inches to the east and then 18 inches to the west of the centerline. The smoke on the east side seemed to hug the floor for ten or more feet and then seemed to diffuse evenly toward the east wall and centerline of the tunnel. When the smoke injection probe was placed on the west side, it was noted that the smoke had a tendency to drift eastwardly after ten or more feet. This seemed to indicate that the flow was not uniformly distributed on a cross-section normal to the flow. The tunnel was run at 5 fps inversion flow conditions for this smoke study.

In line with this same study a concentration "offset" study was made. The gas injection probe was set at x = 40 ft, 19" west of the centerline on the floor. Horizontal floor concentrations were taken at 15 ft, 25 ft, and 35 ft. Vertical concentrations were also taken at the maximum floor horizontal concentration. Then, a three-dimensional plot drawn to scale was drawn of the

concentration versus distance effect. At this stable flow velocity of 5 fps, a definite effect of secondary circulation could be noted in the strange concentration profiles obtained. The effect of meandering was also noted from the indication of the movement of the horizontal floor maximum concentration. From the above portions of the second study, a good indication was obtained as to the problems that could be encountered in low velocity inversion flow.

FIGURES
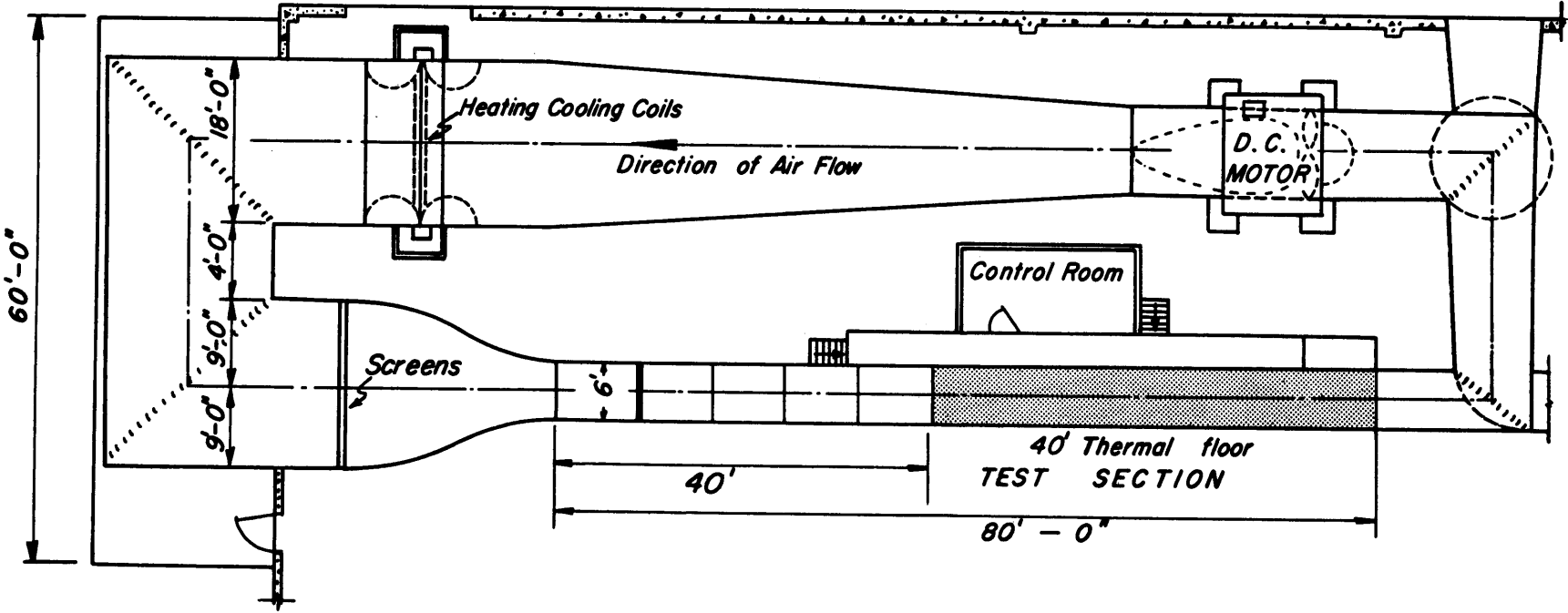
PLAN VIEW

Fig. 1 Large wind tunnel
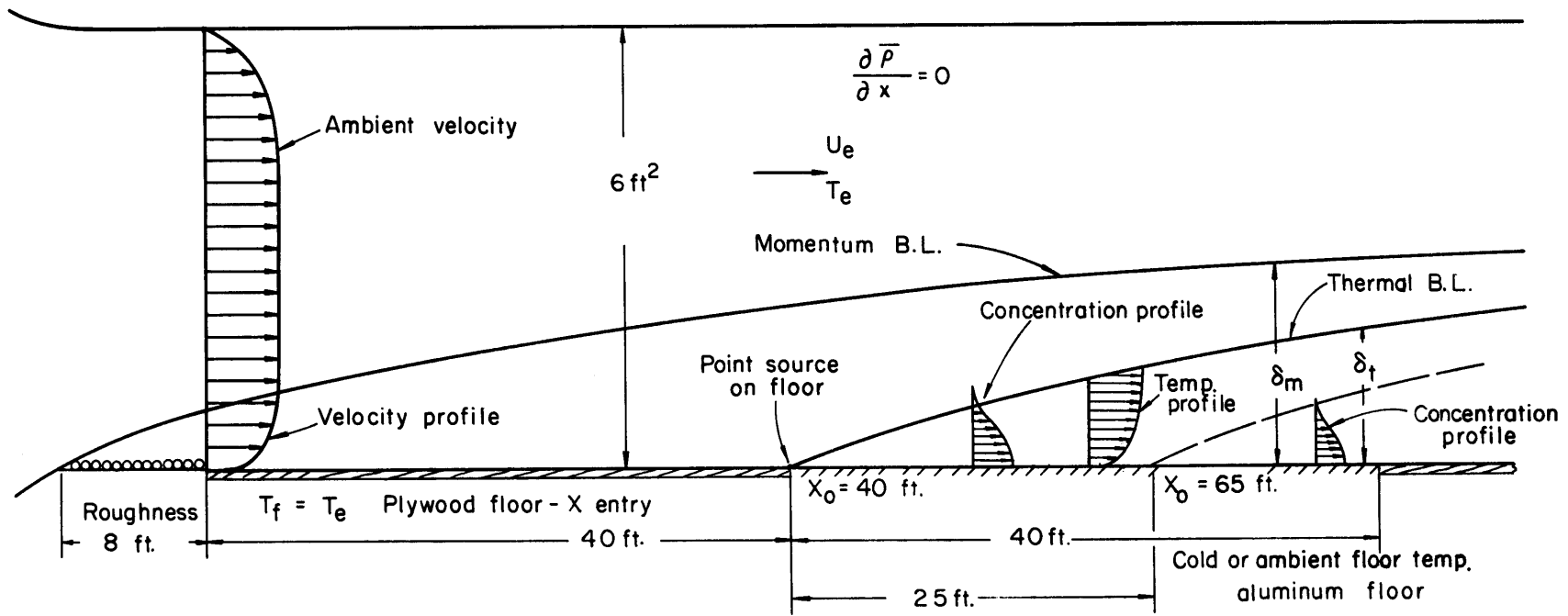
Fig. 2 Test section geometry

Ambient line (~ 36" up)

Probe positioner

Direction of air flow

Injection (feed) probe

Intake probe

$X_0 = 40'$

Wind tunnel floor

Precision flow meter with needle valve

Aluminum plate

Test line

Pressurized and bottled 99.99 % pure helium

Two-way valve

FOR CALIBRATION

Open to atmosphere

"T"

Controlled leak (SCL)

To bottles with two-constituent gas mixture $(He - N_2)$

Vacuum pump

To MS9

Welch Duo Seal Type

Mass spectrometer leak detector MS9

x-input from probe positioner

Moseley Type 135

Concentration readout on x-y plotter

Fig. 3   Schematic of gas feed system

105
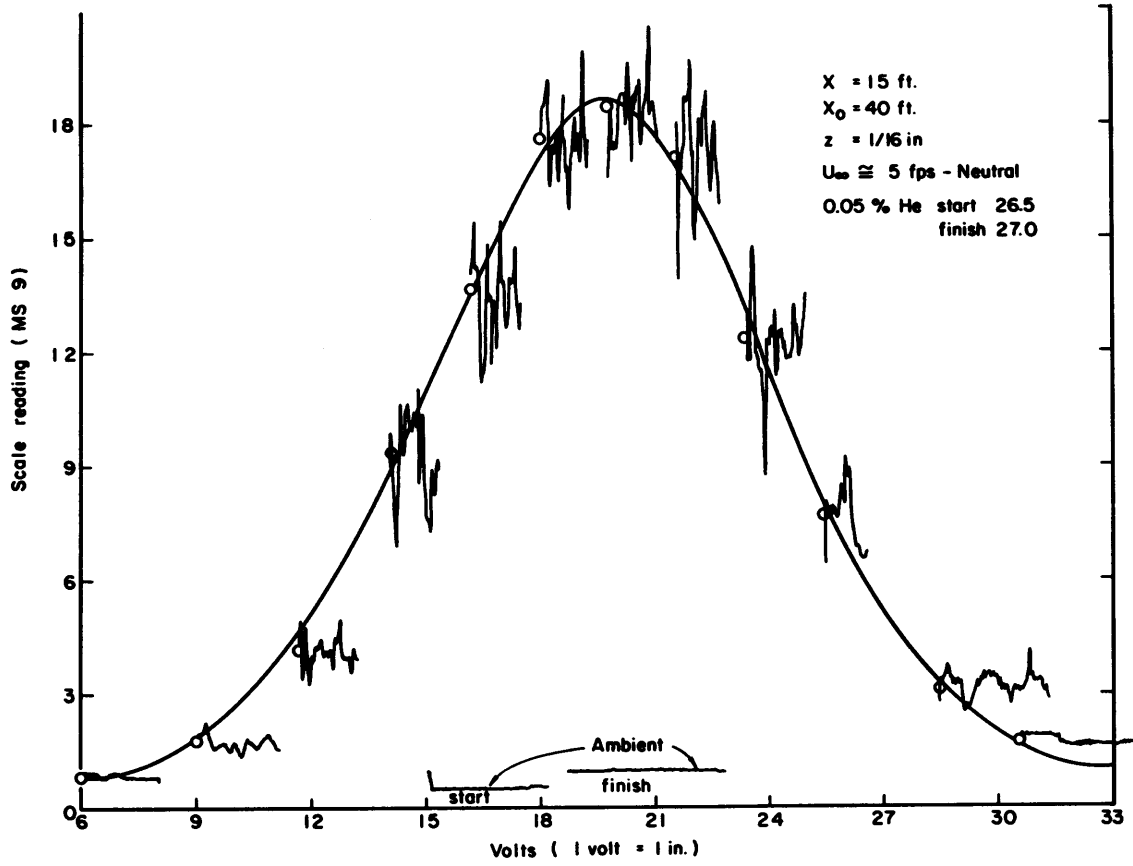
Fig. 4   Horizontal concentration profile
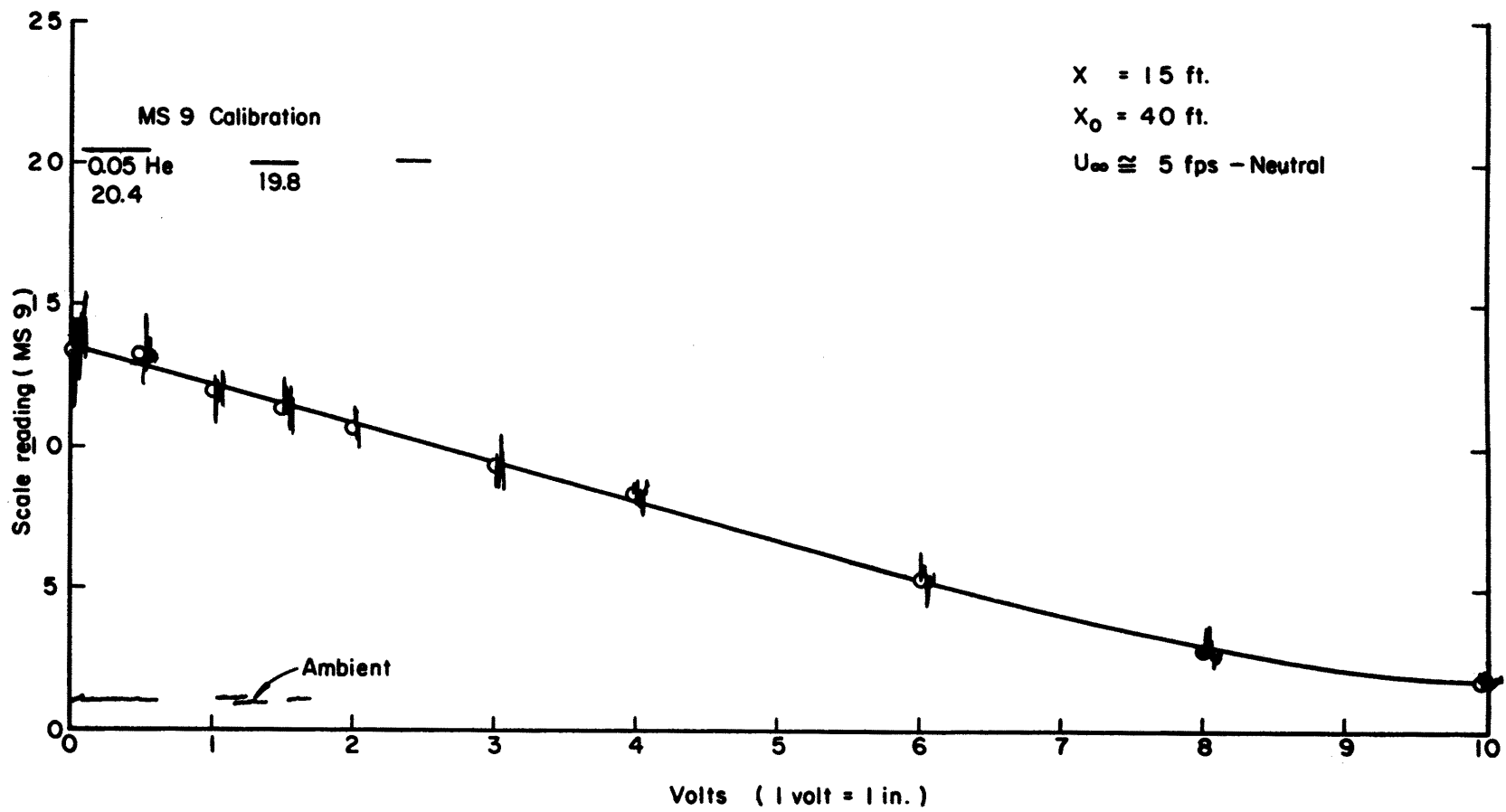
Fig. 5   Vertical concentration profile
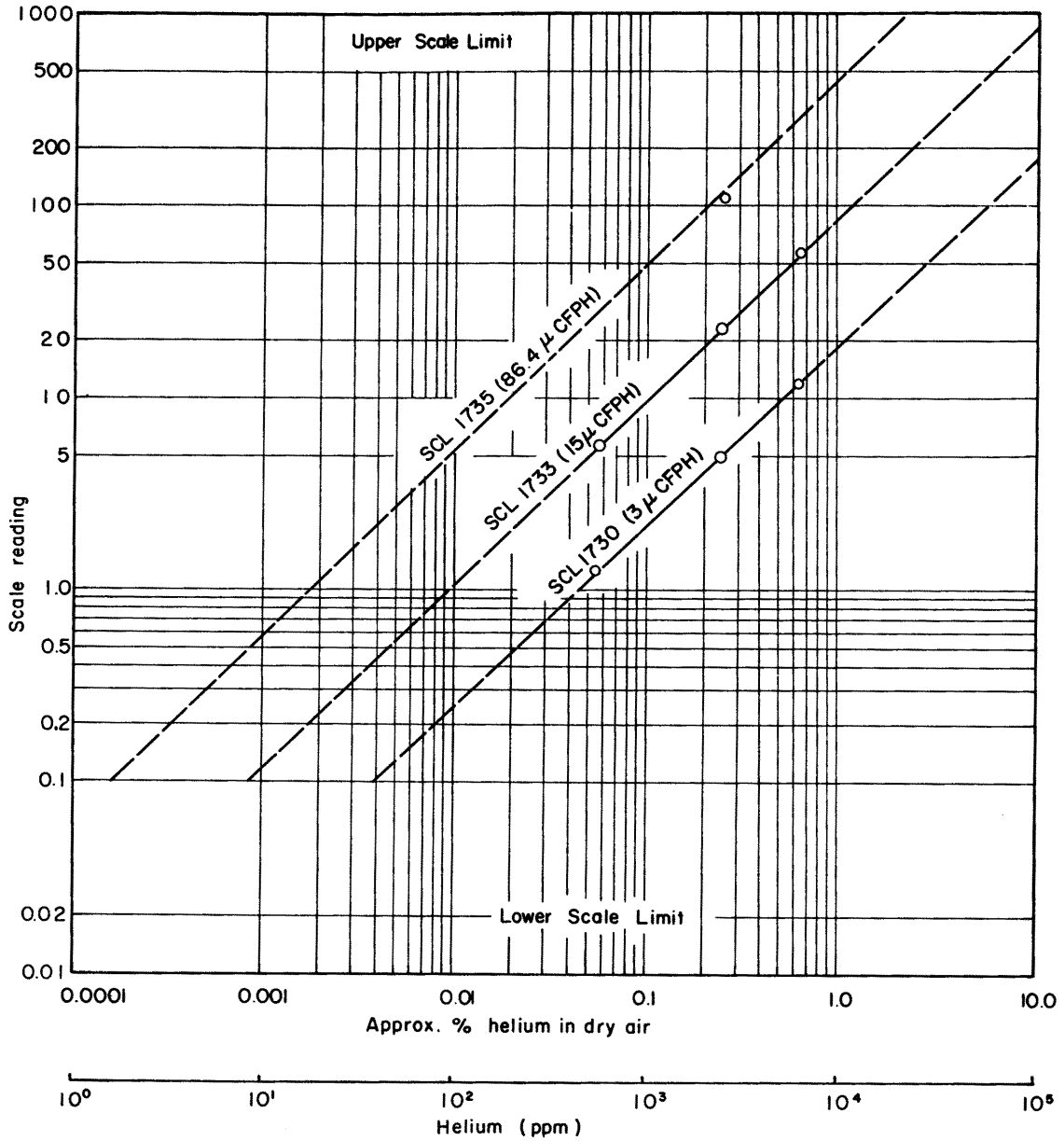
Fig. 6 Leak detector calibration
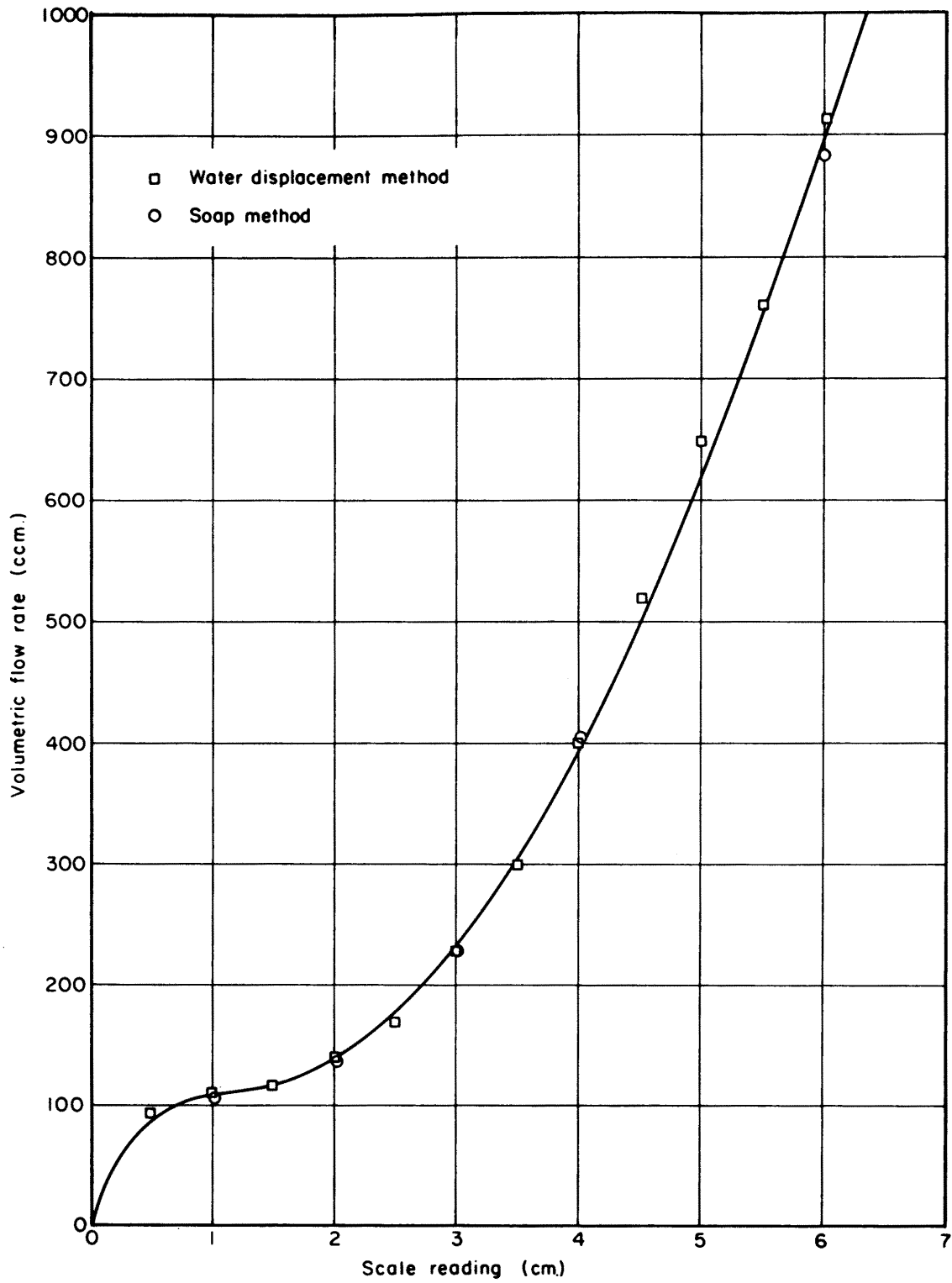
Fig. 7 Injection flowmeter calibration
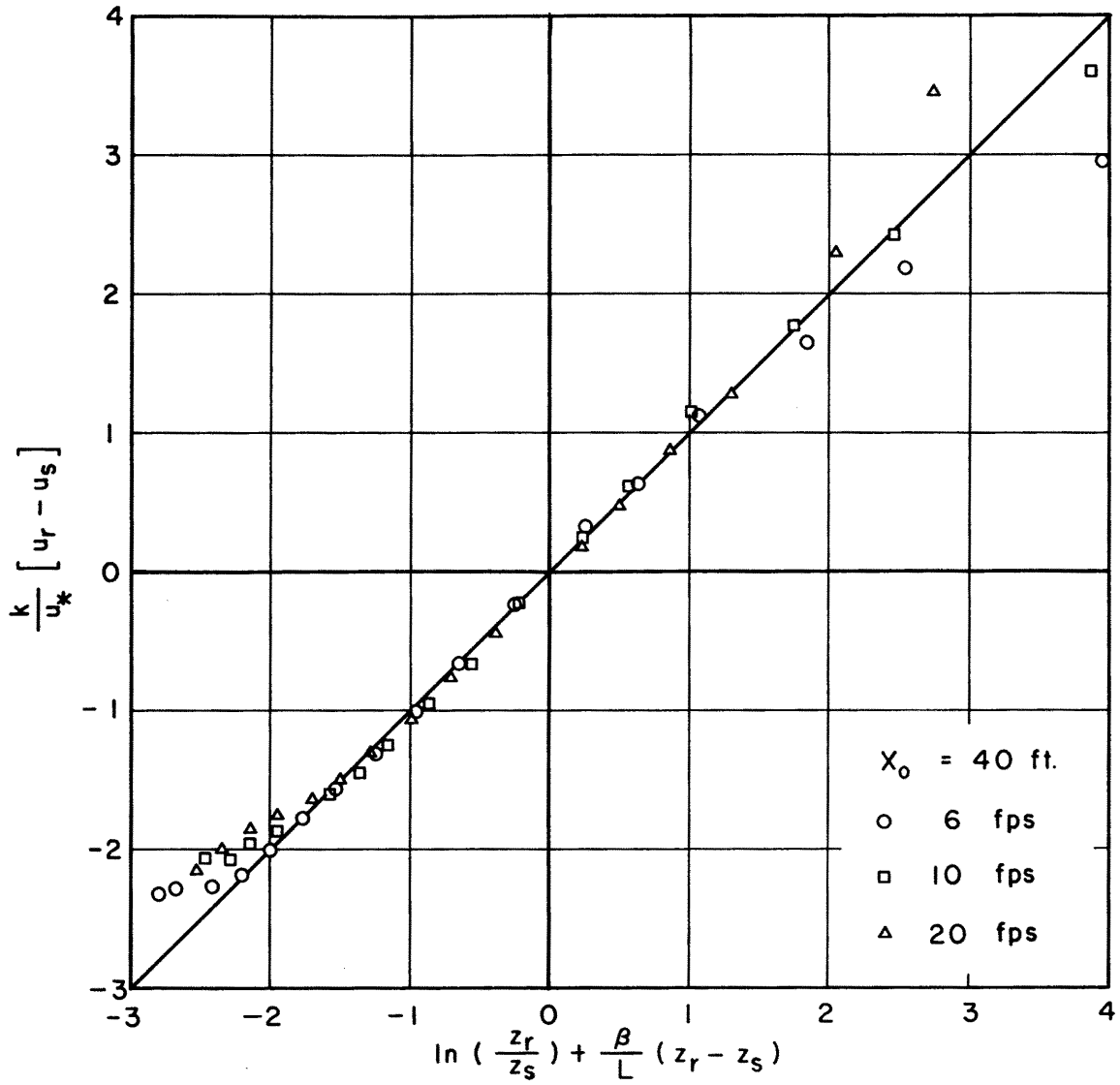
Fig. 8 Monin-Obukhov velocity model comparison (x=60ft)
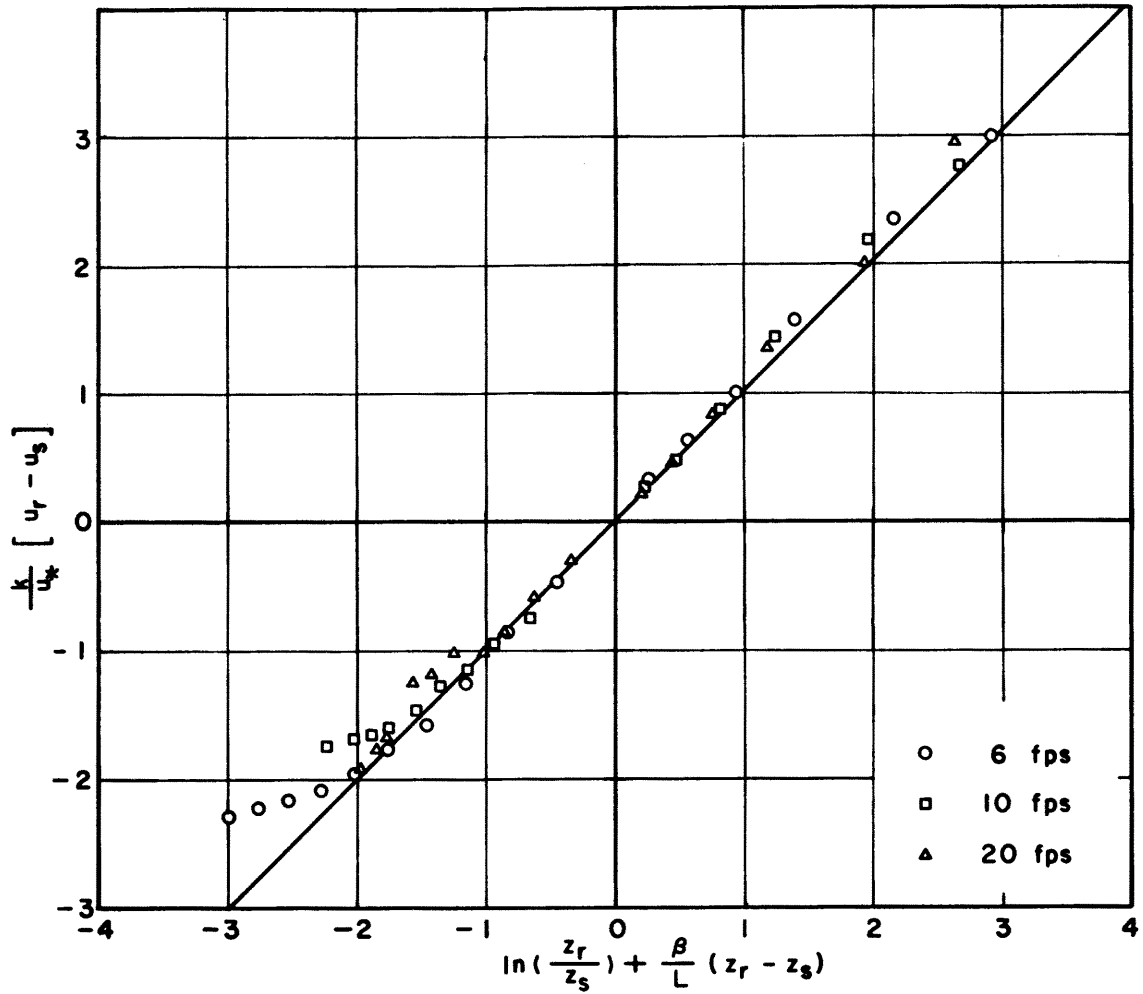
Fig. 9 Monin-Obukhov velocity model comparison (x=70ft)
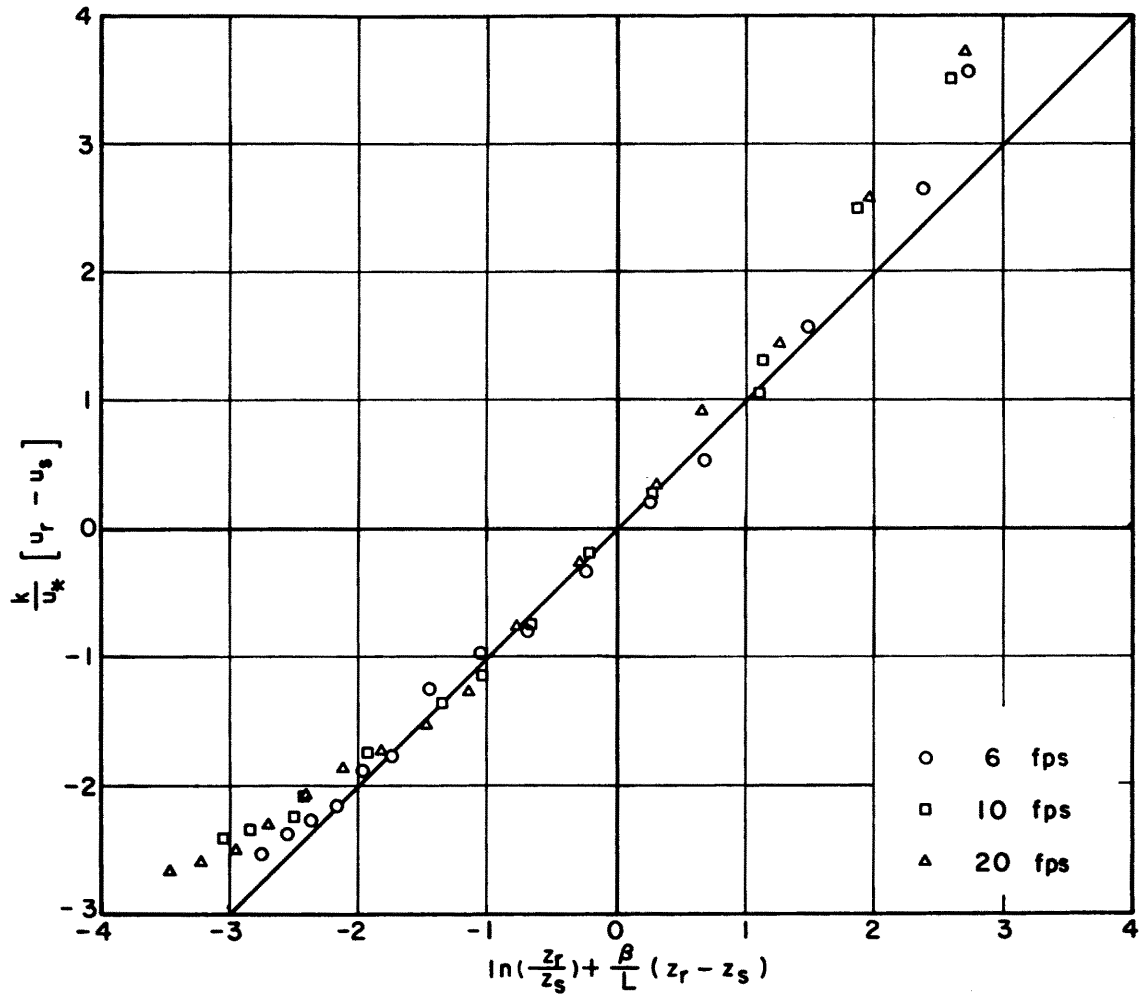
Fig. 10   Monin-Obukhov velocity model comparison (x=78ft)
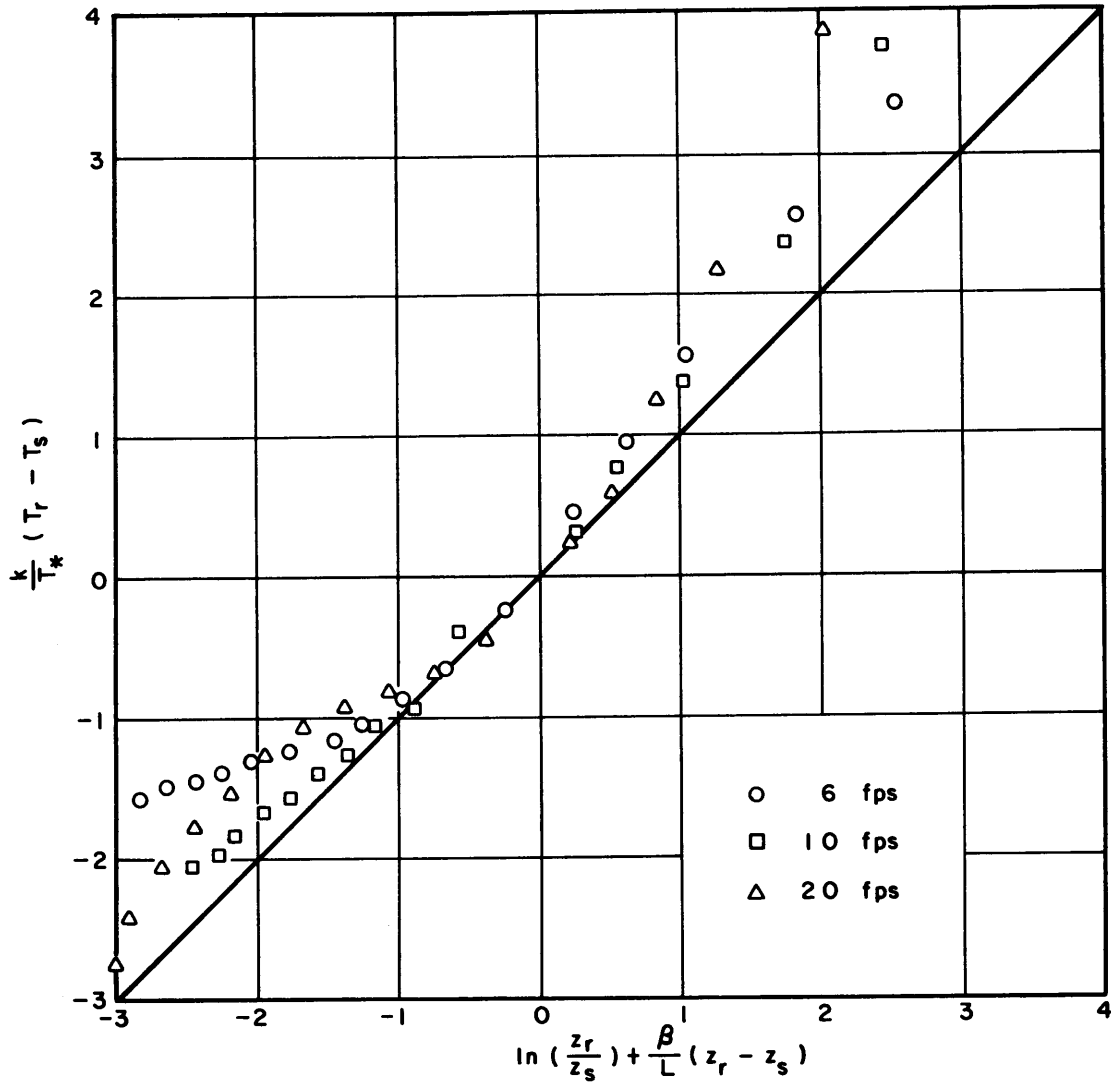
Fig. 11 Monin-Obukhov temperature model comparison (x=60ft)

114
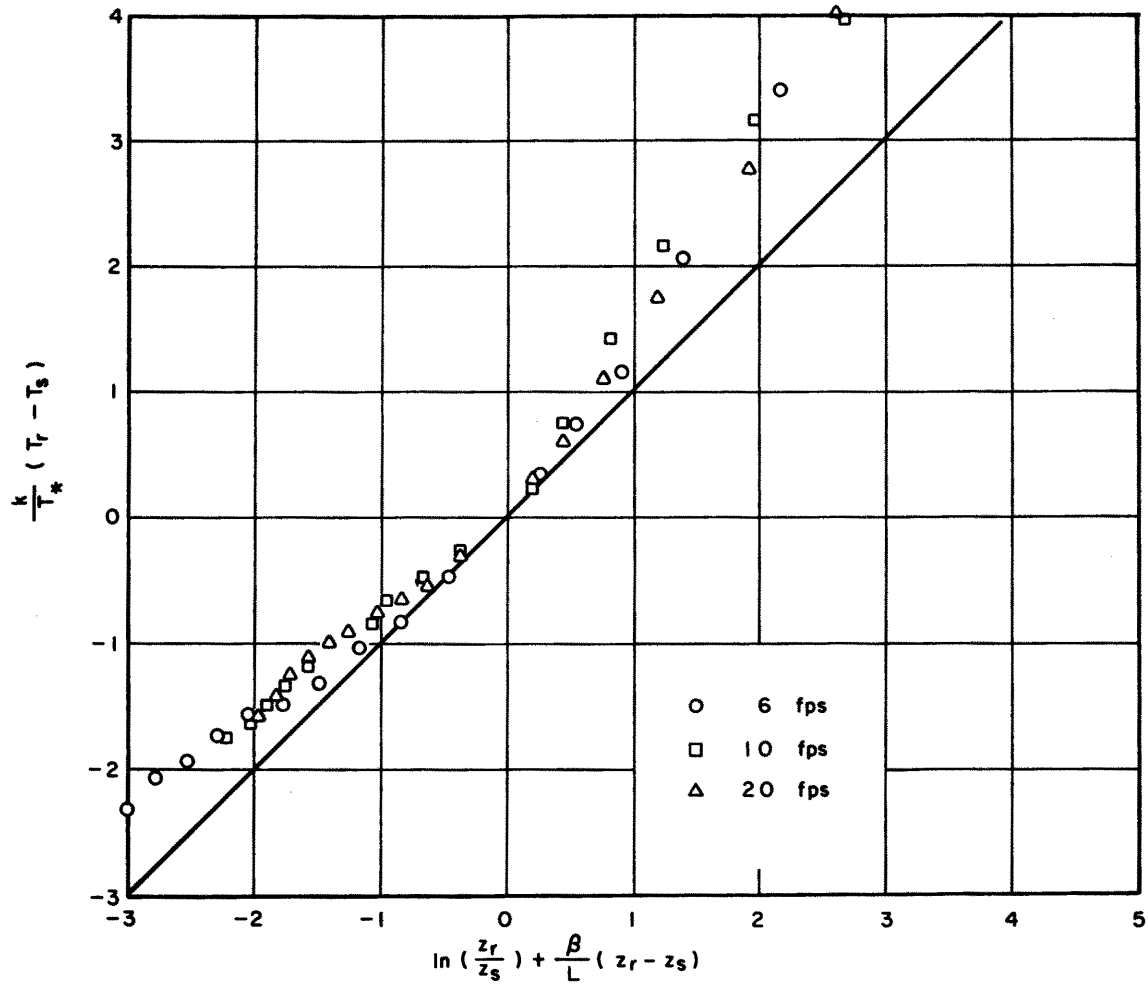
Fig. 12 Monin-Obukhov temperature model comparison (x=70ft)
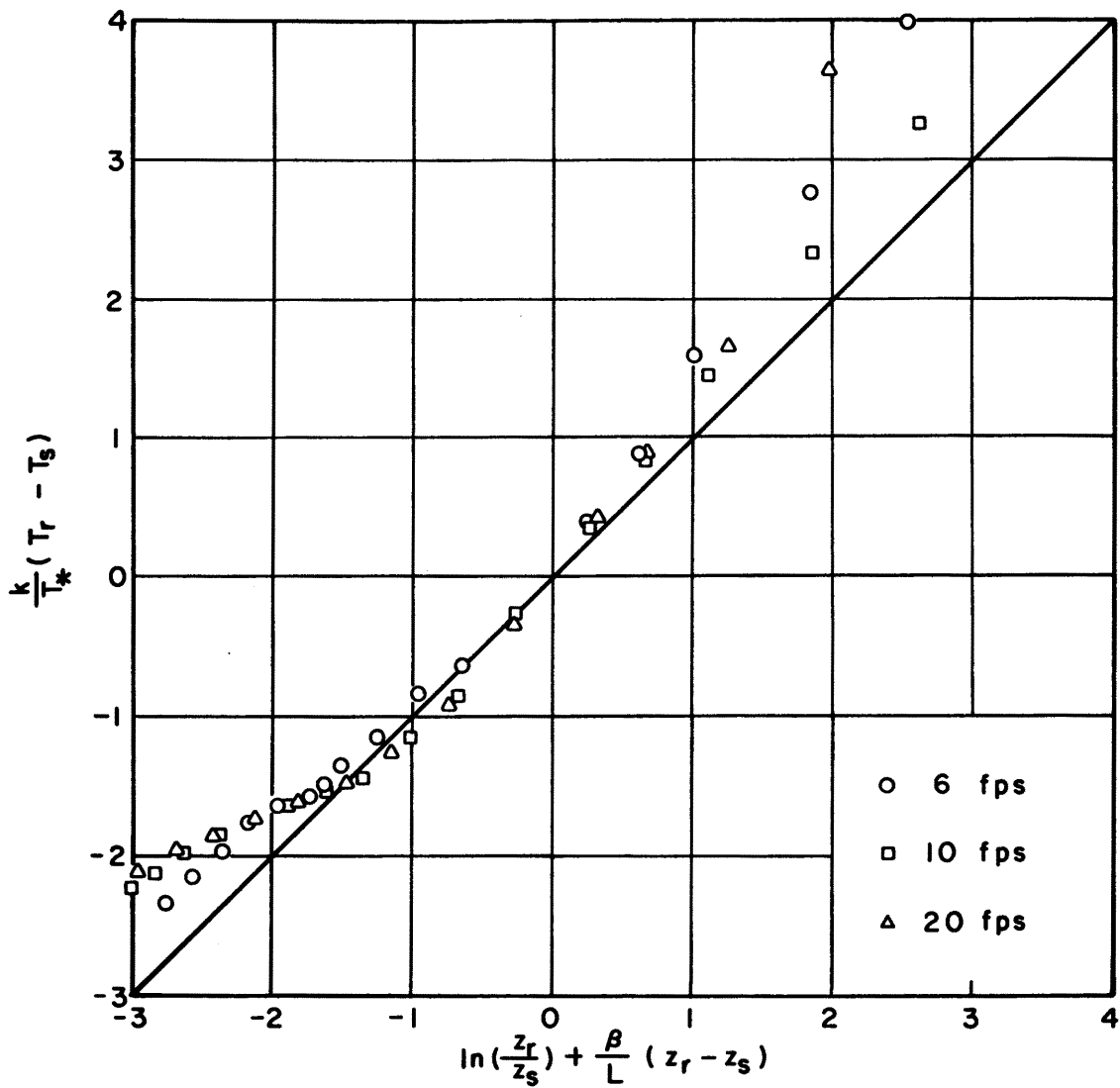
Fig. 13 Monin-Obukhov temperature model comparison (x=78ft)
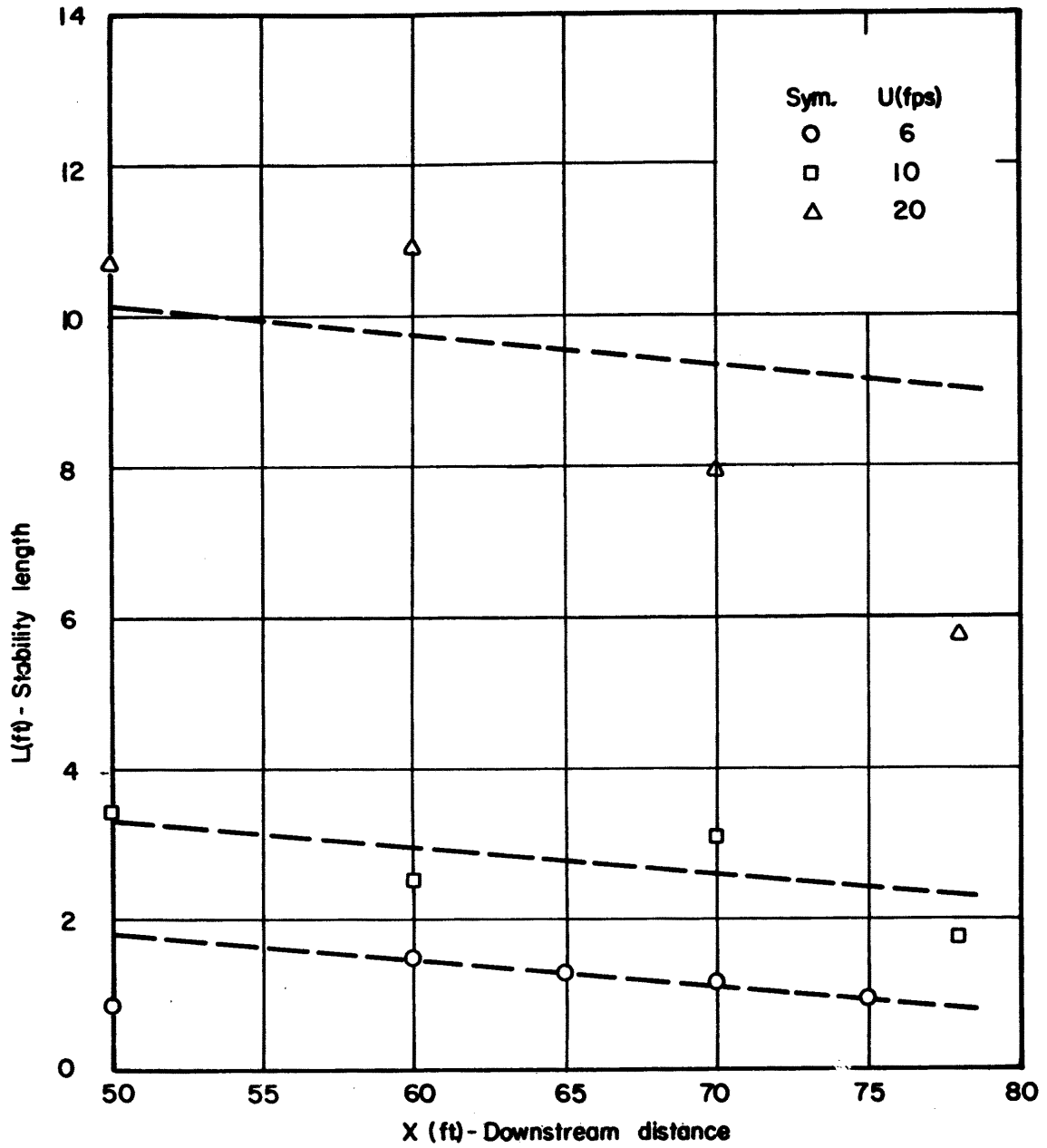
Fig. 14   Stability length (L) versus downstream
distance (x)
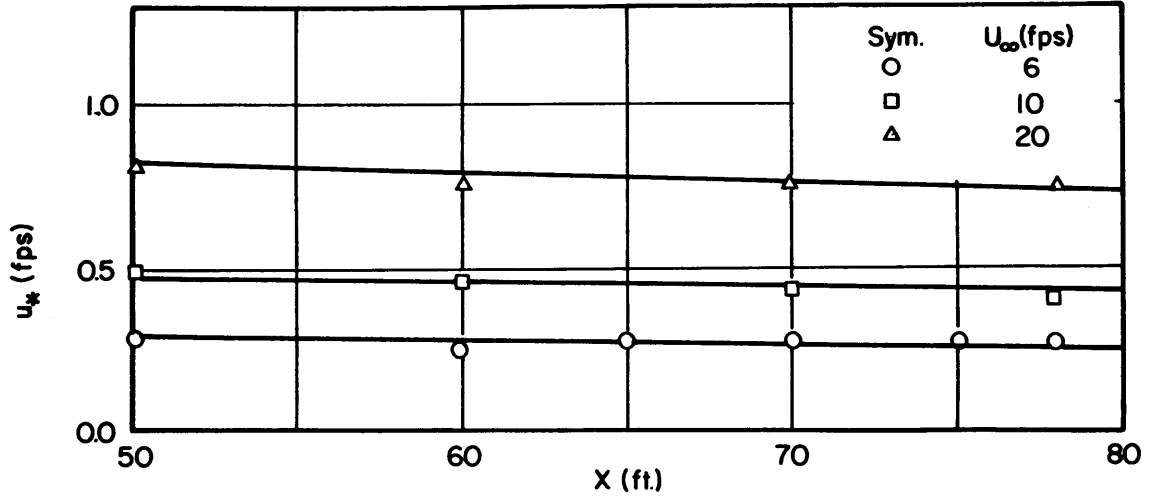
Fig. 15   Relationship between u_* and x (neutral flow)
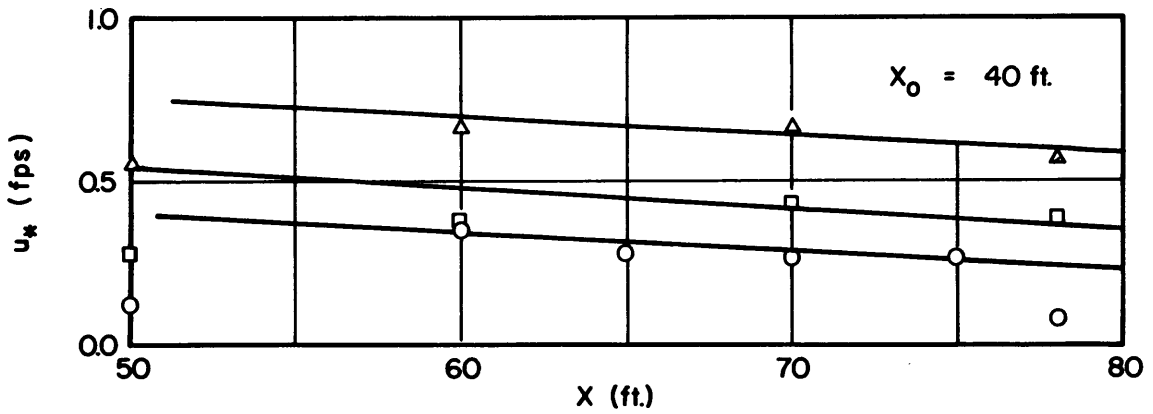
Fig. 16   Relationship between u_* and x (inversion)
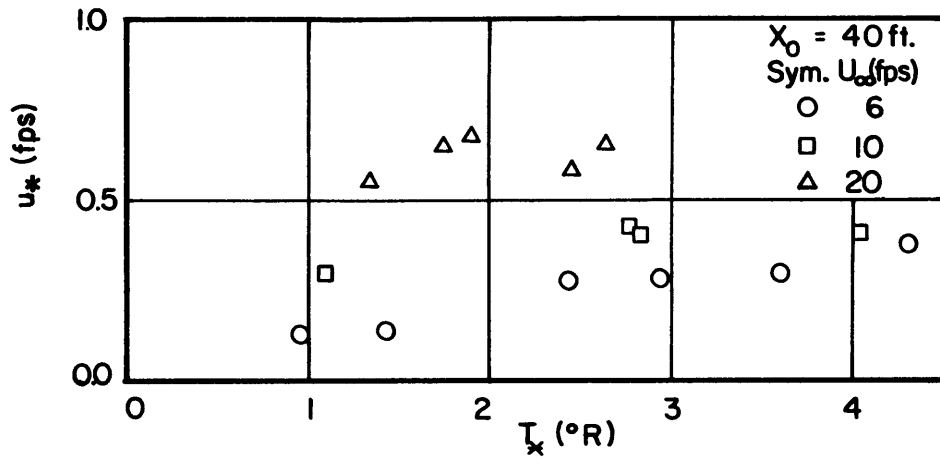
Fig. 17   Relationship between u* and T*
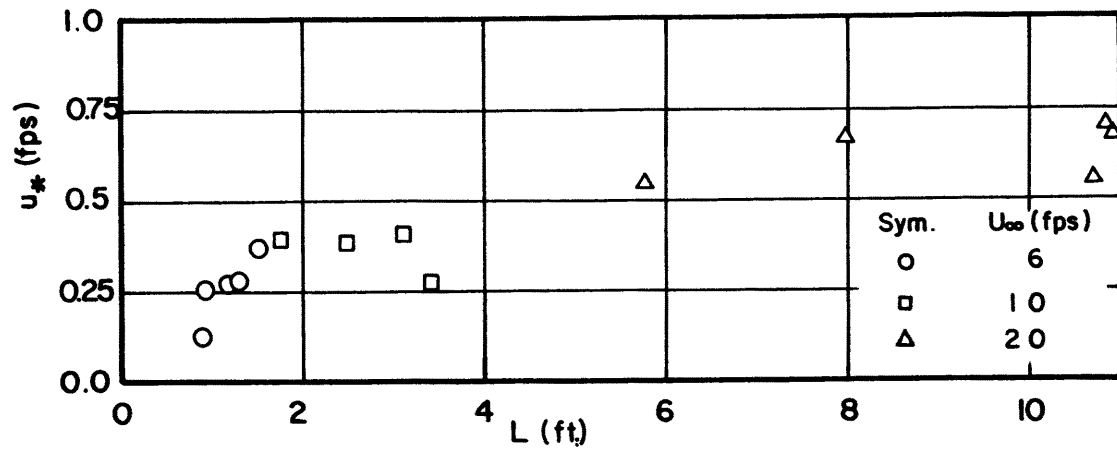
Fig. 18   Relationship between u$_*$ and L
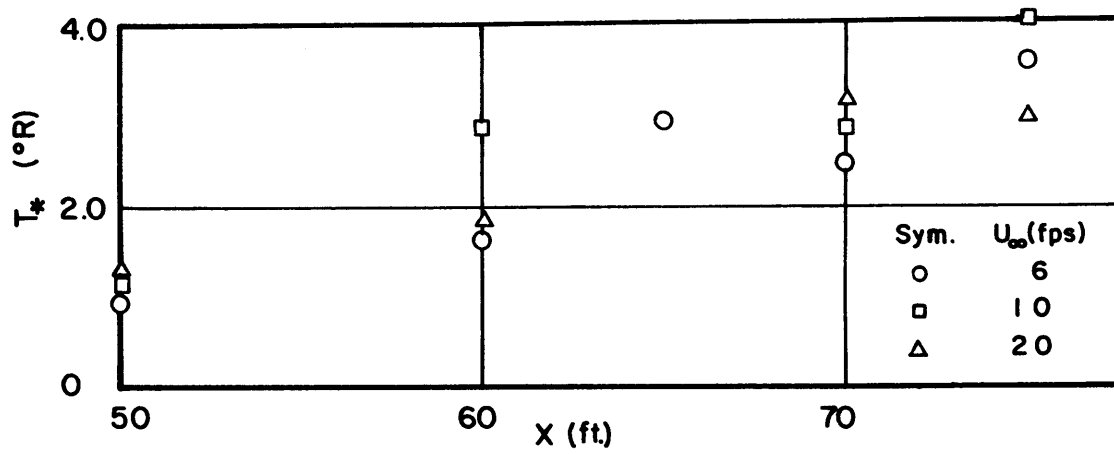
Fig. 19 Relationship between T* and x
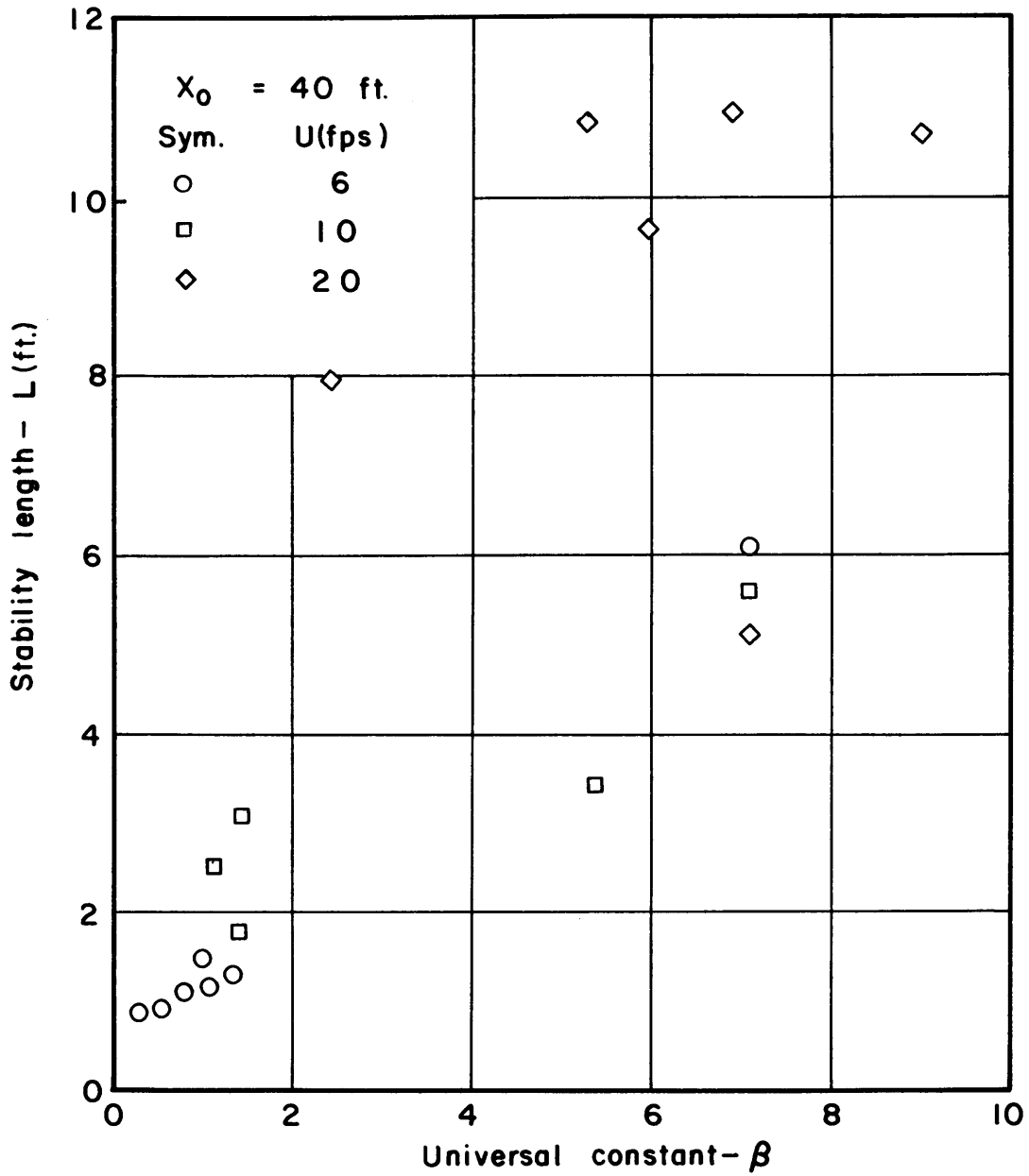
Fig. 20   Stability length (L) versus universal
constant (β)
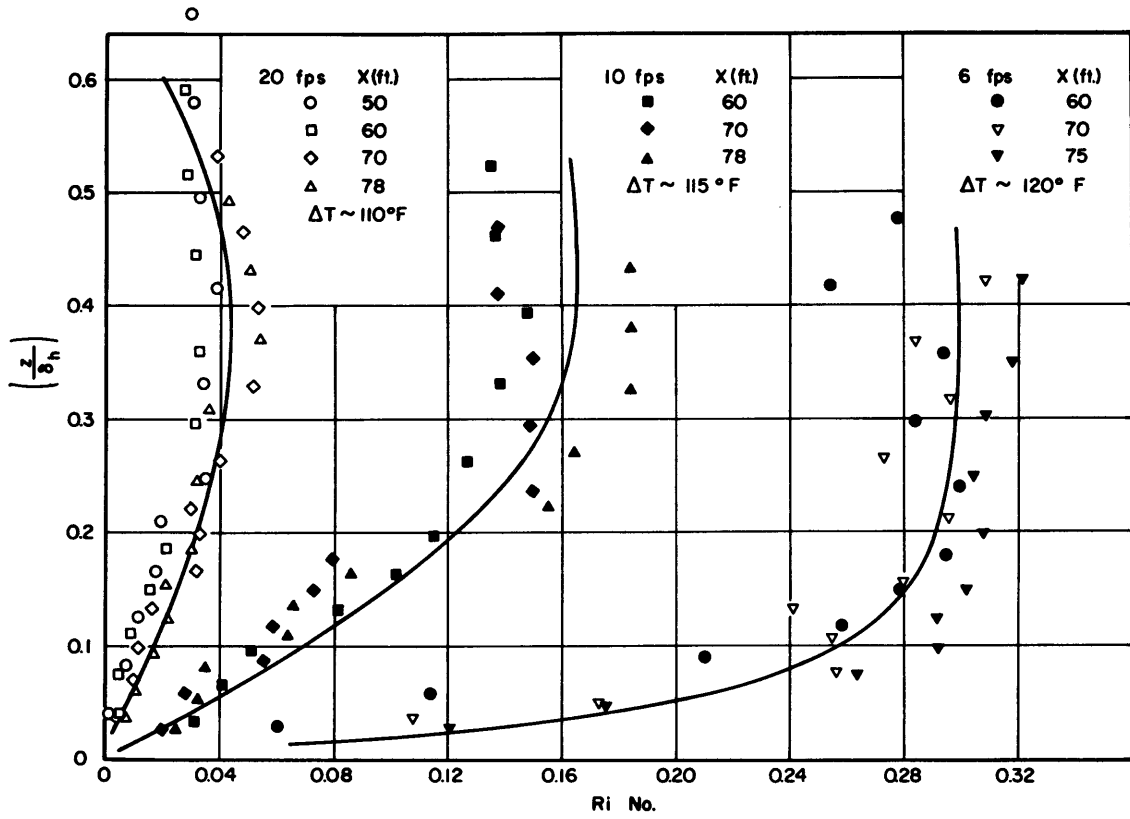
Fig. 21 Ri versus $\frac{z}{\delta_h}$ for inversion type flow
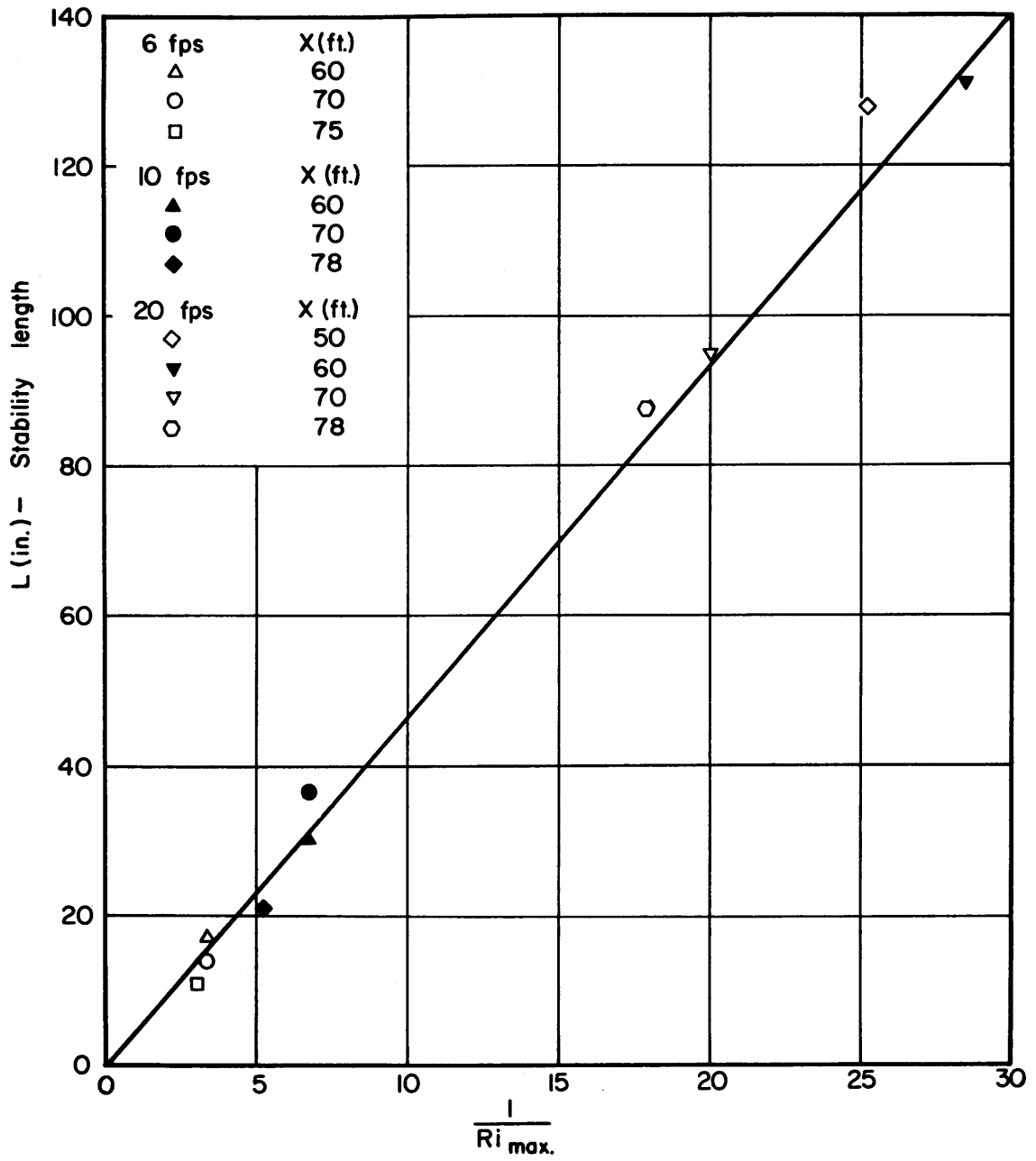
Fig. 22 Stability length (L) versus $\dfrac{1}{Ri_{max}}$
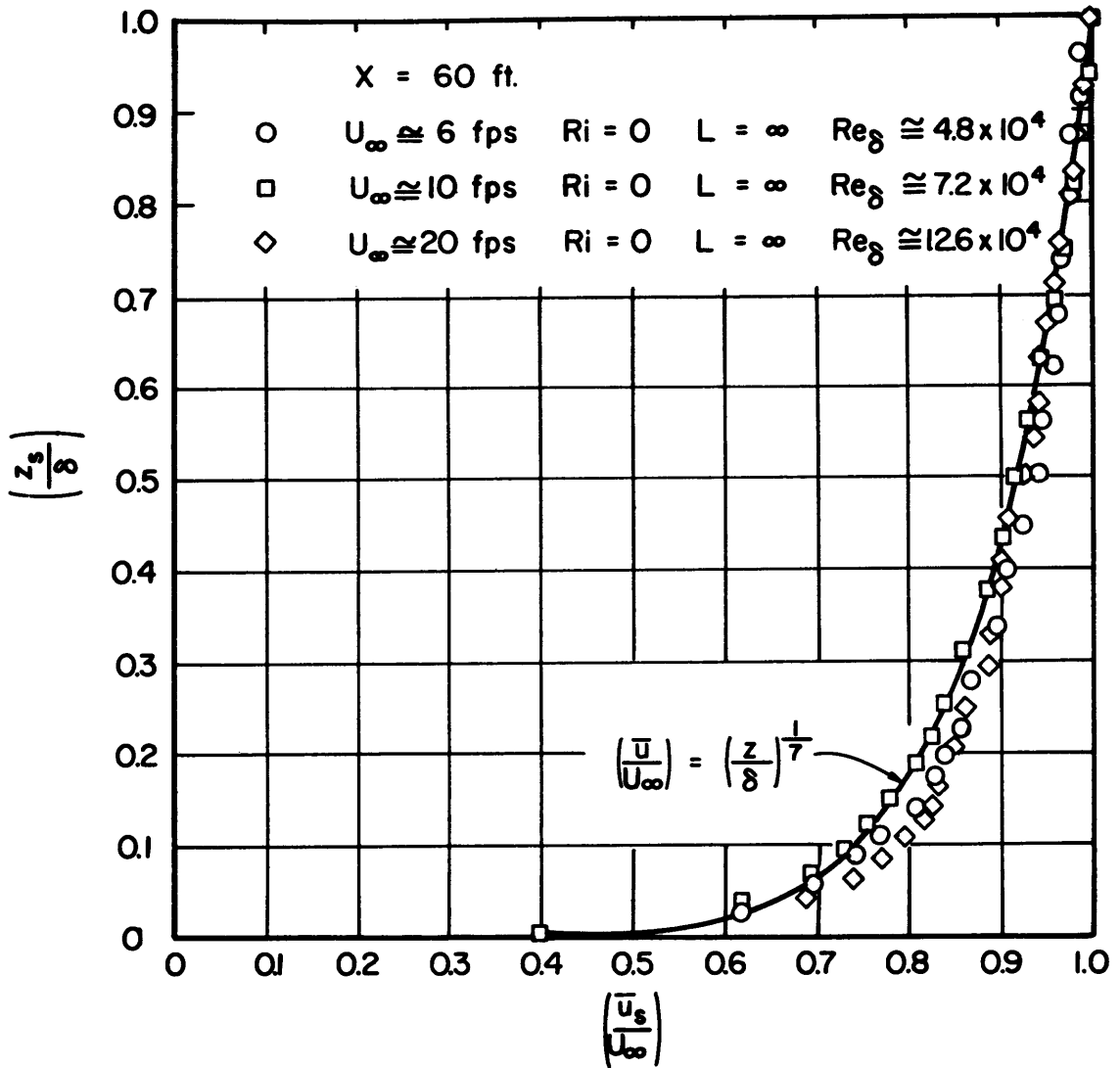
Fig. 23   Velocity profile across turbulent boundary
layer (neutral flow, x=60ft)
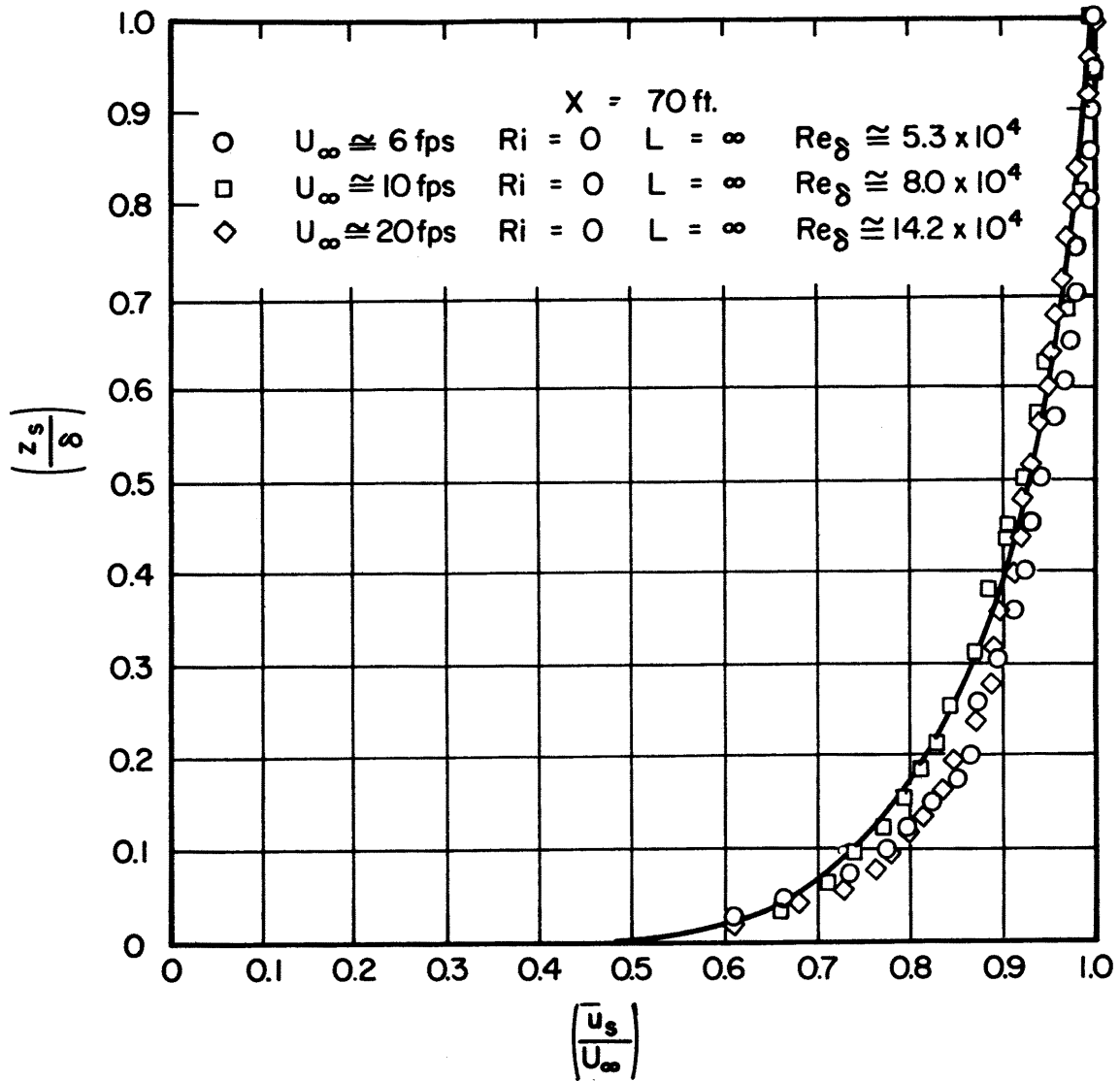
Fig. 24 Velocity profile across turbulent boundary
layer (neutral flow, x=70ft)
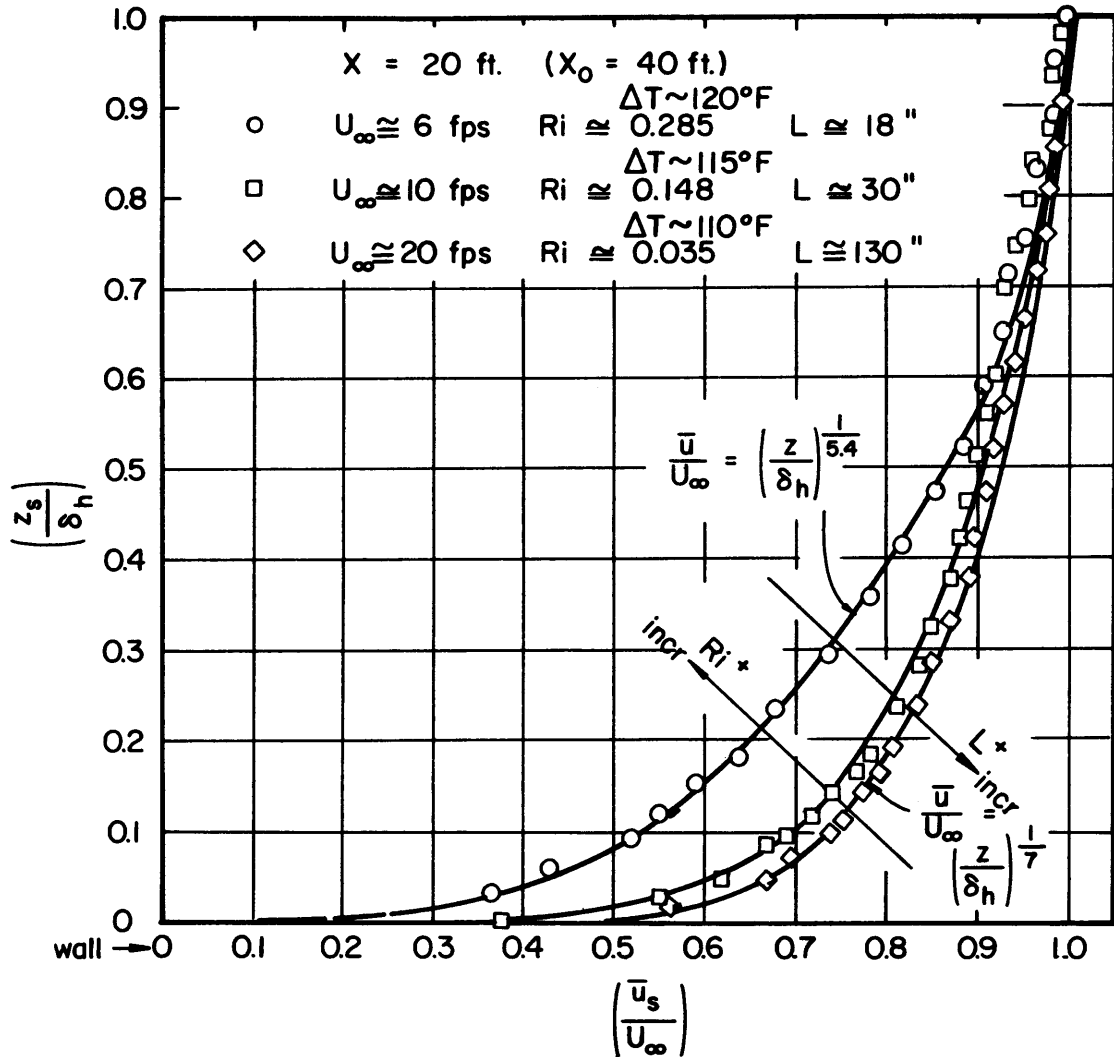
Fig. 25   Velocity profile across turbulent boundary layer (inversion, x=60ft)
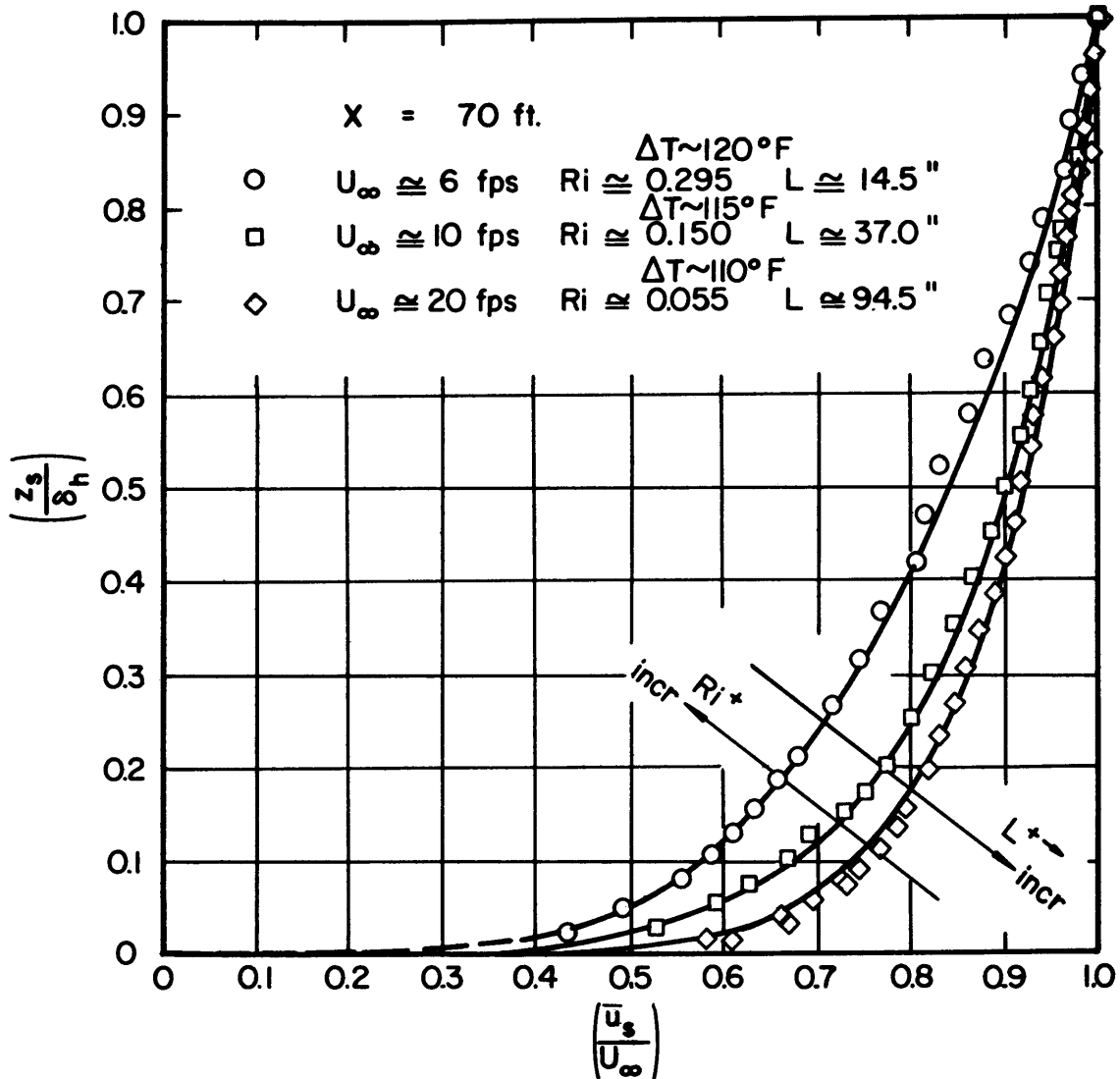
Fig. 26   Velocity profile across turbulent boundary
          layer (inversion, x=70ft)
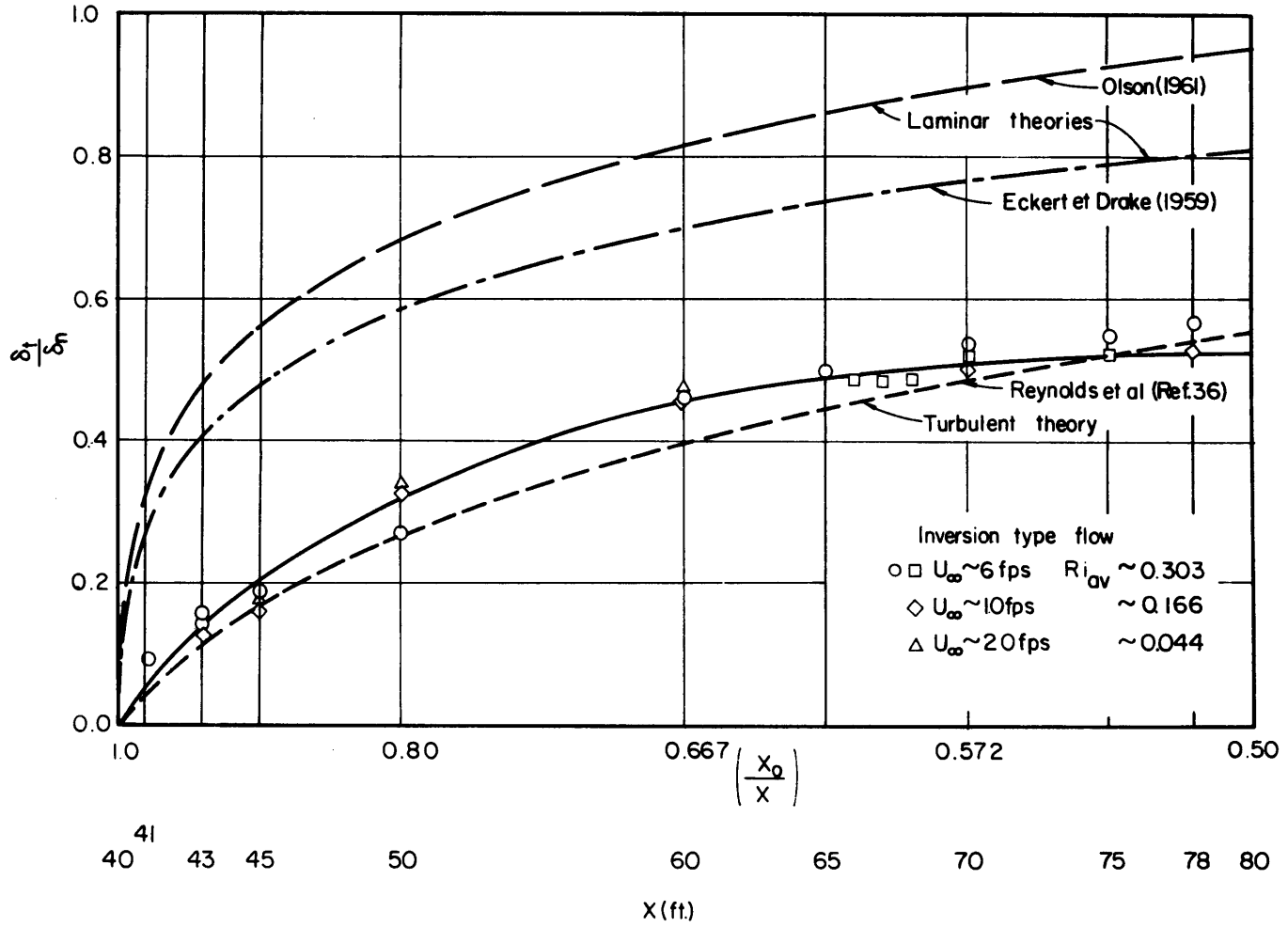
Fig. 27 Ratio of $\dfrac{\delta_t}{\delta_h}$ versus $\dfrac{x_o}{x}$

128
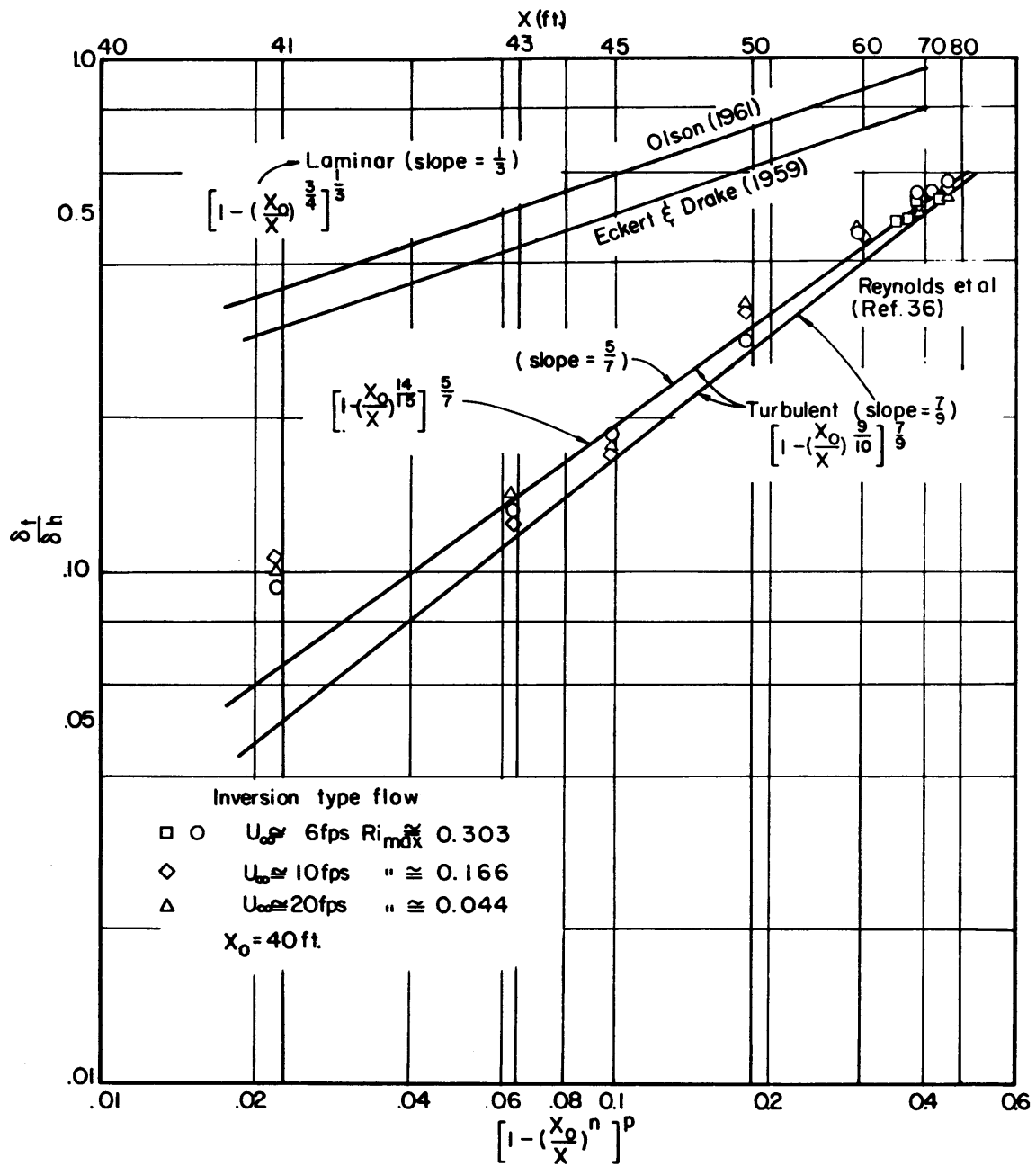
Fig. 28 Comparison of experiment $\dfrac{\delta_t}{\delta_h}$ to theory
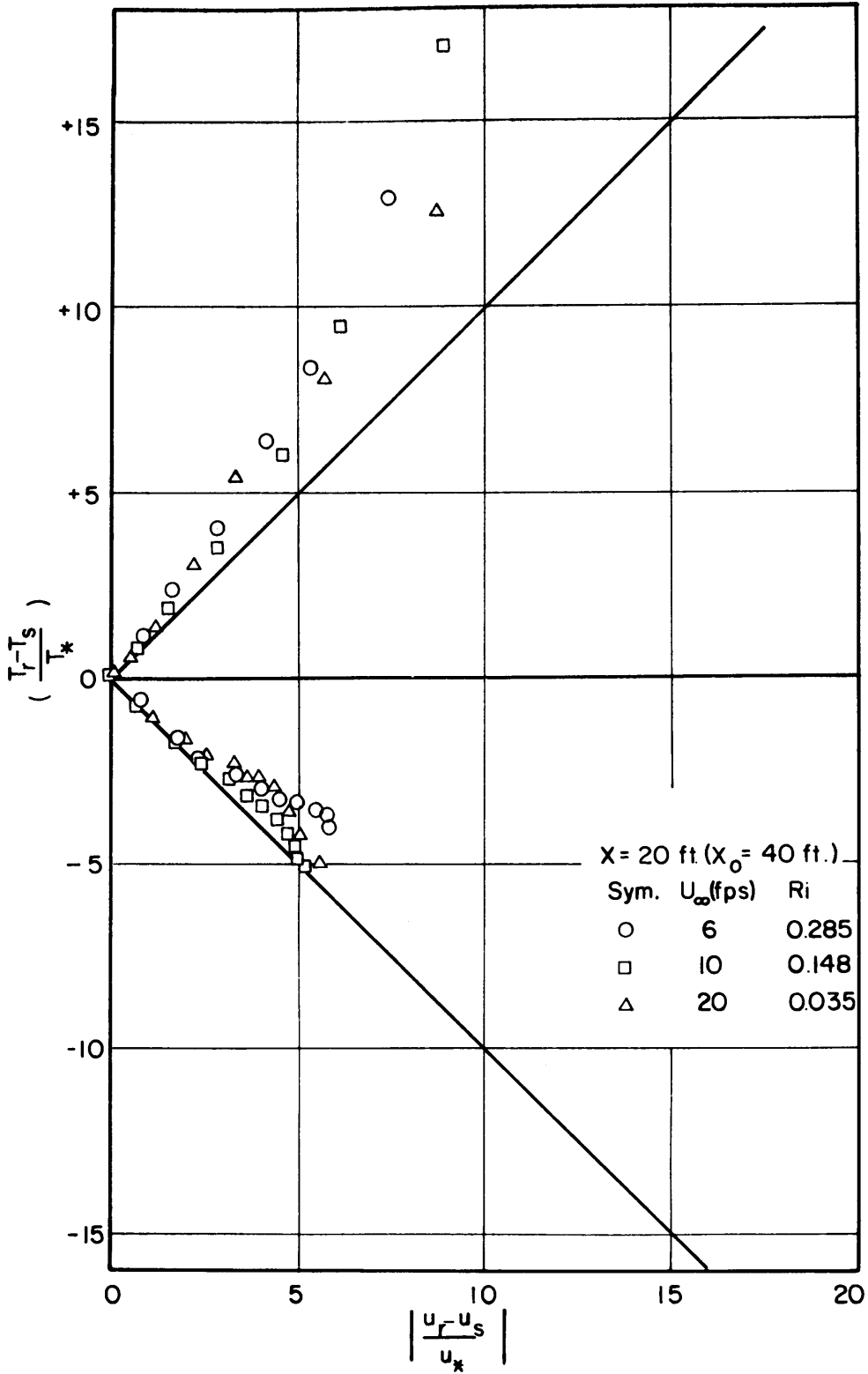
Fig. 29 Relation between velocity and temperature
distributions (x=60ft)
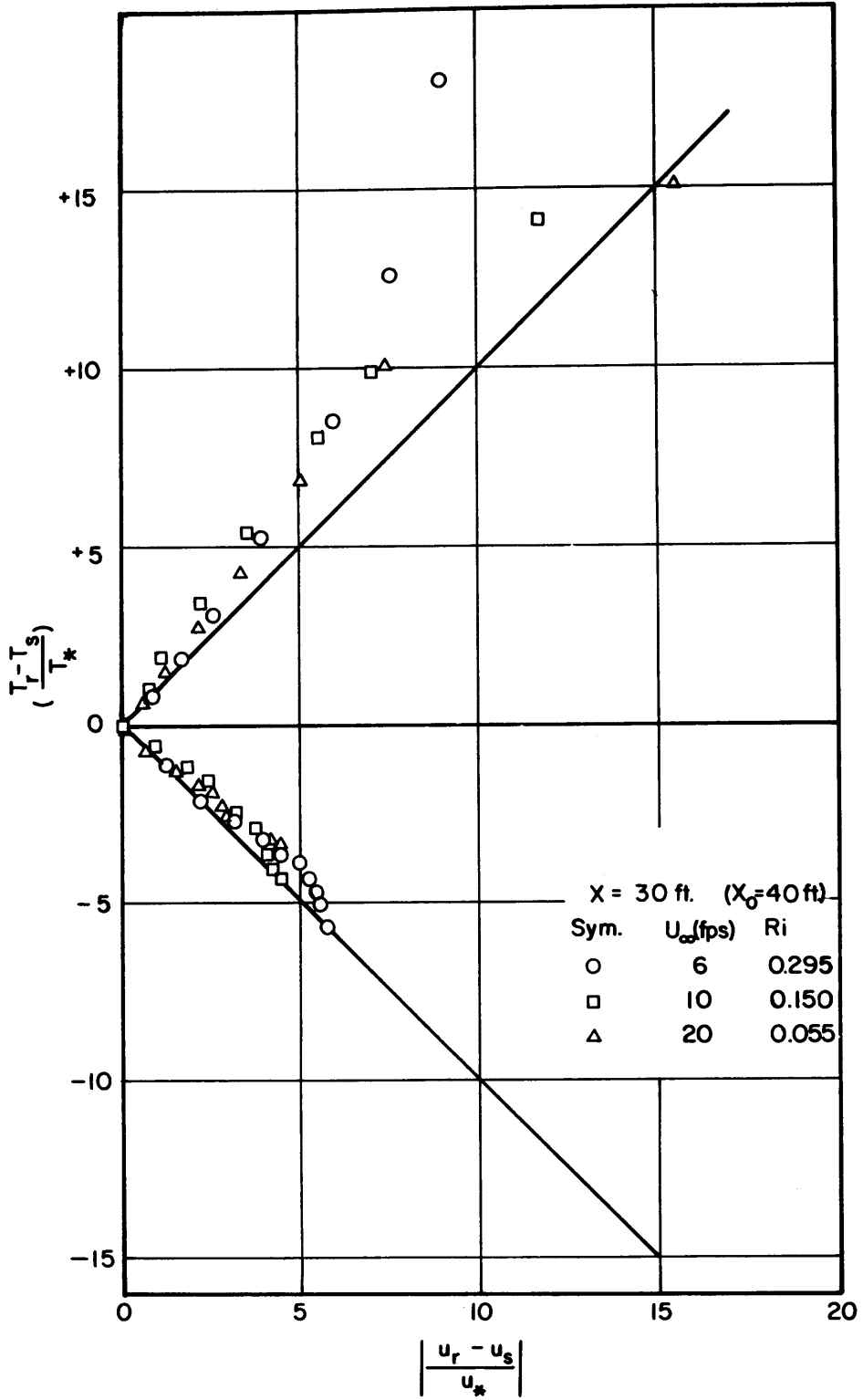
Fig. 30 Relation between velocity and temperature
distribution (x=70ft)
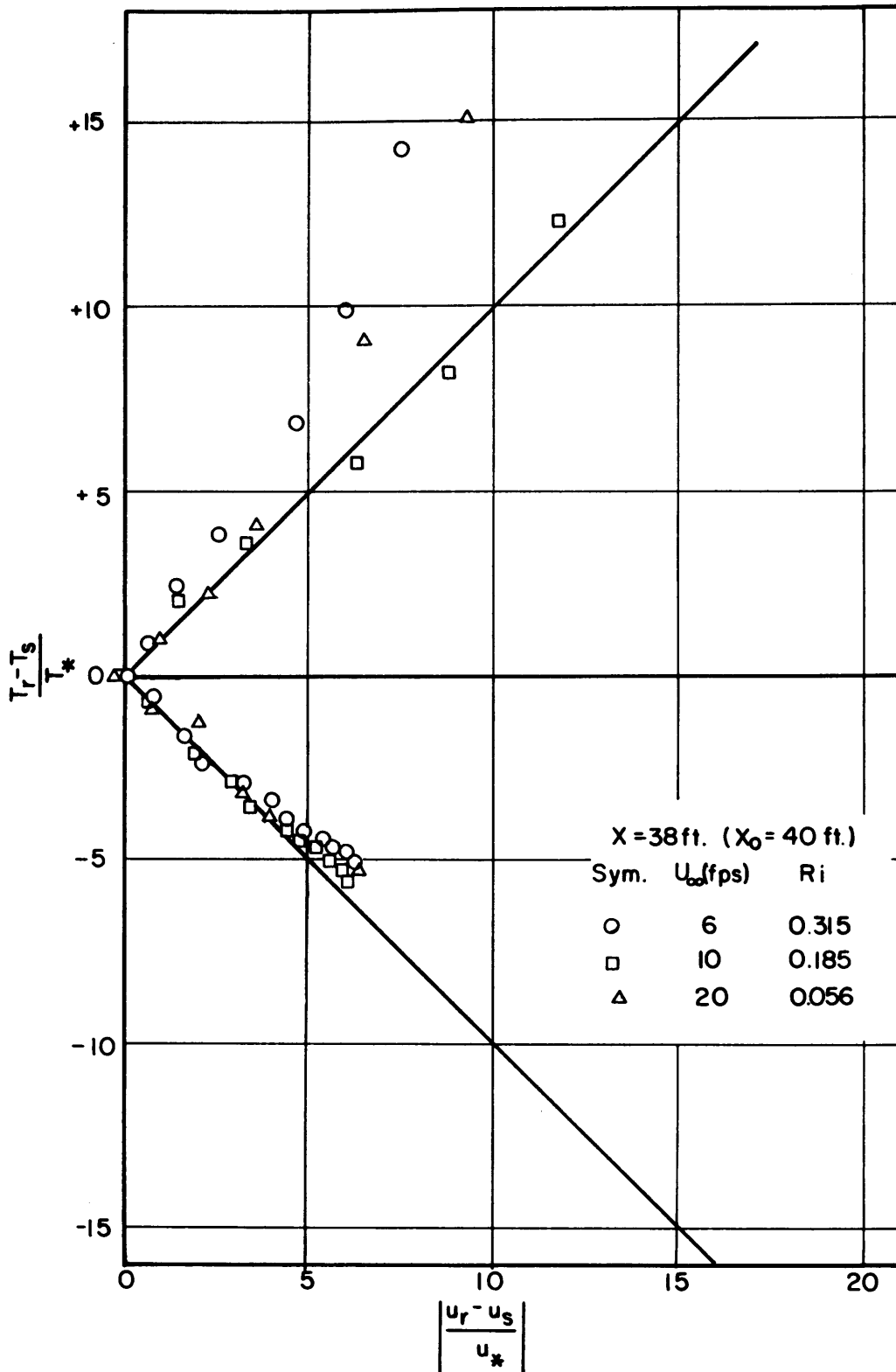
Fig. 31 Relation between velocity and temperature
distribution (x=78ft)
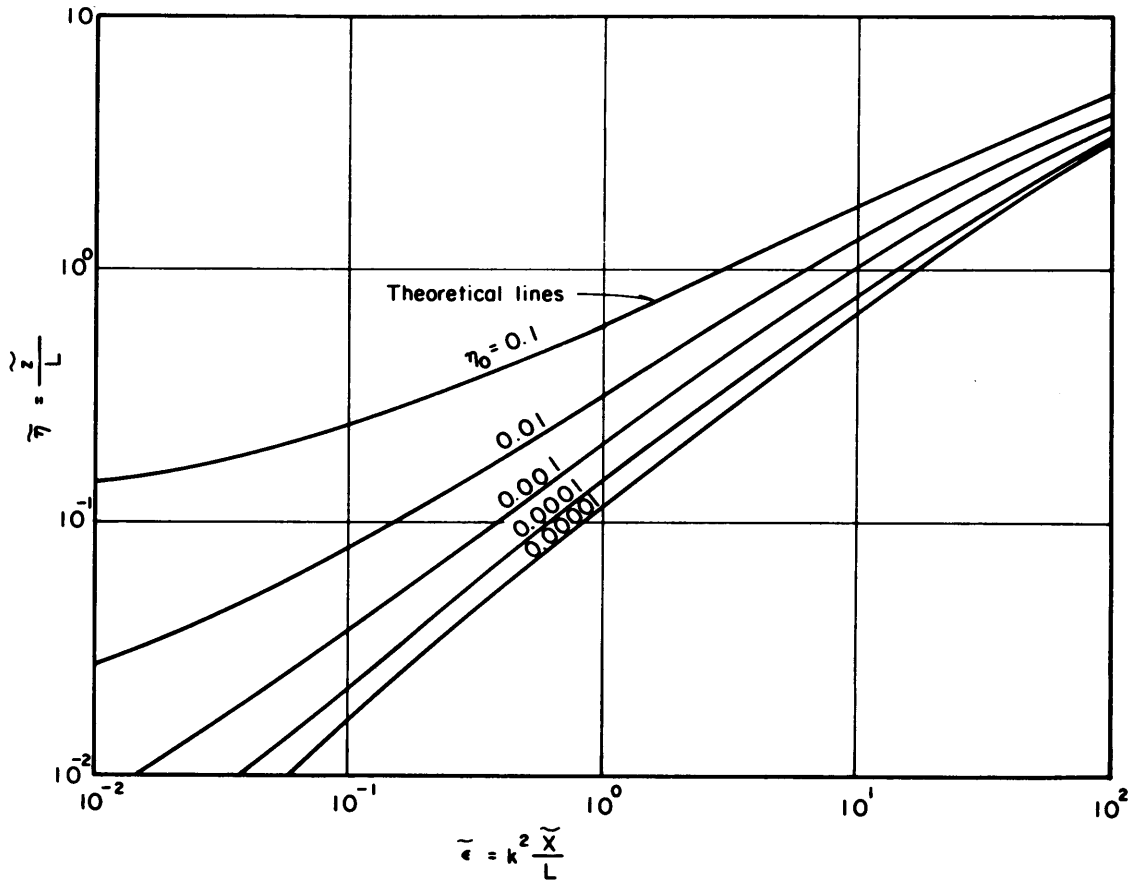
Fig. 32 Vertical spread versus x ($\beta = 1$)
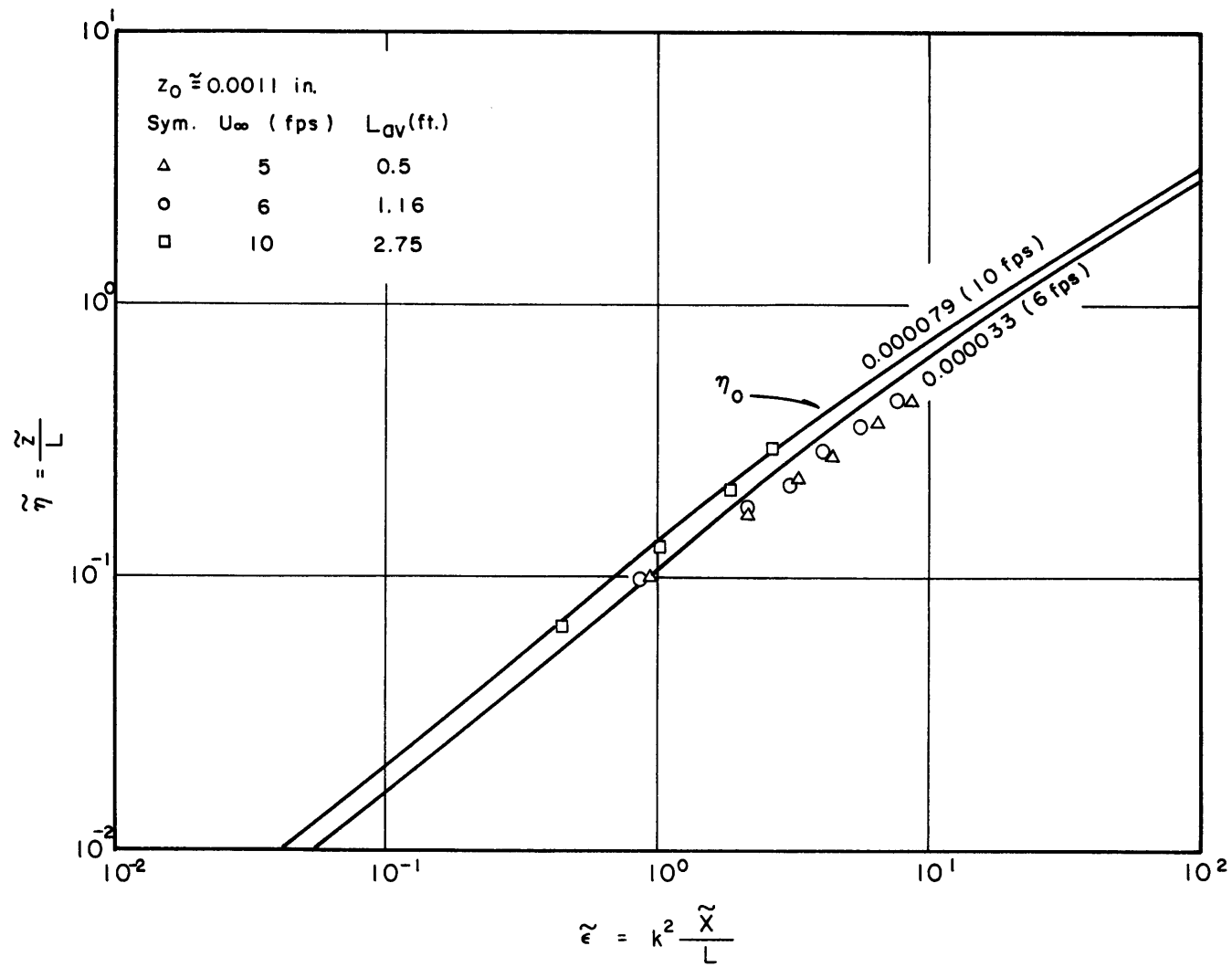
Fig. 33 Vertical spread with data points ($\mathscr{B}$ = 1)

134
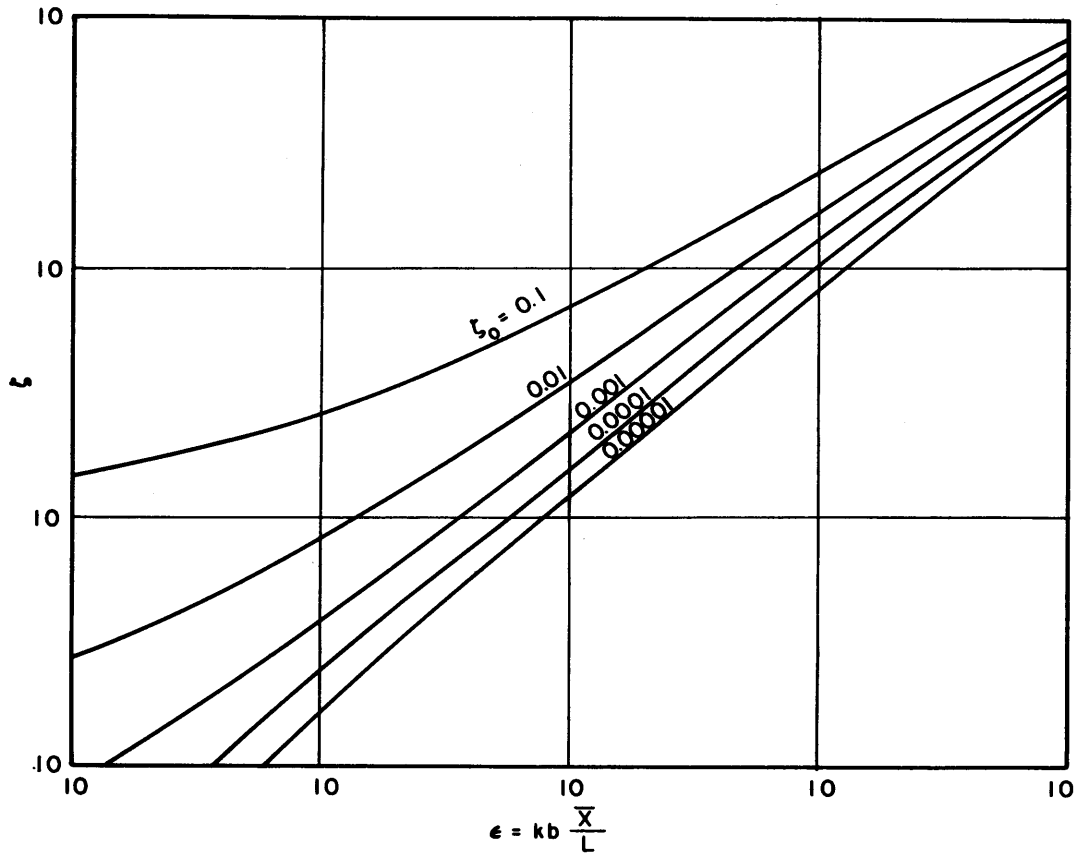
Fig. 34 Vertical spread ($\beta = 1$, Ref. 13)

$z_0 \cong 0.0011$ in.

Sym.	U_∞ (fps)	L_{av} (ft.)
△	5	0.5
○	6	1.16
□	10	2.75

$\zeta_0 \longrightarrow 0.000079$ (10 fps)

0.000033 (6 fps)

ζ

$\epsilon = kb\dfrac{\overline{X}}{L}$
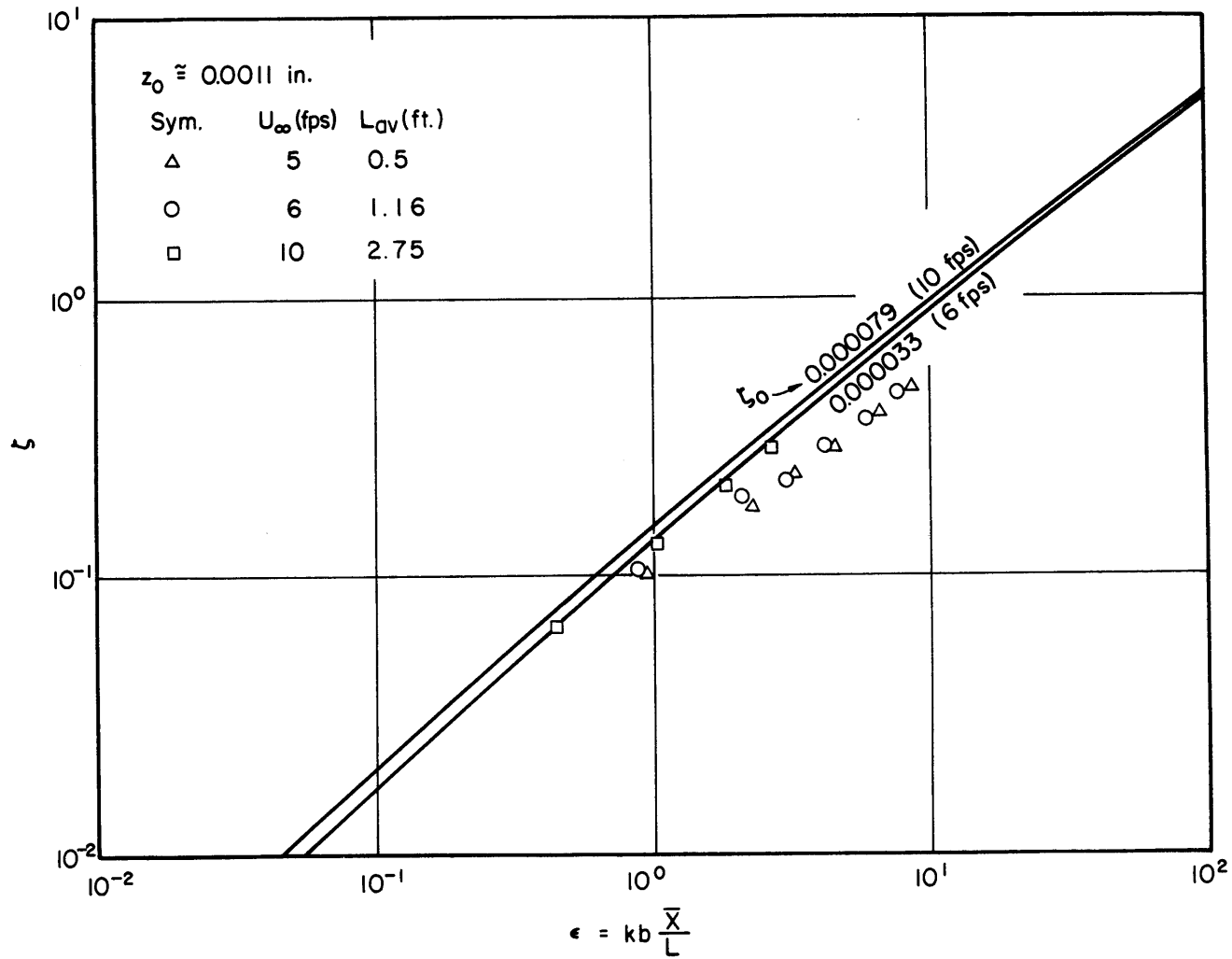
Fig. 35 Vertical spread with data points ($\beta = 1$, Ref. 13)
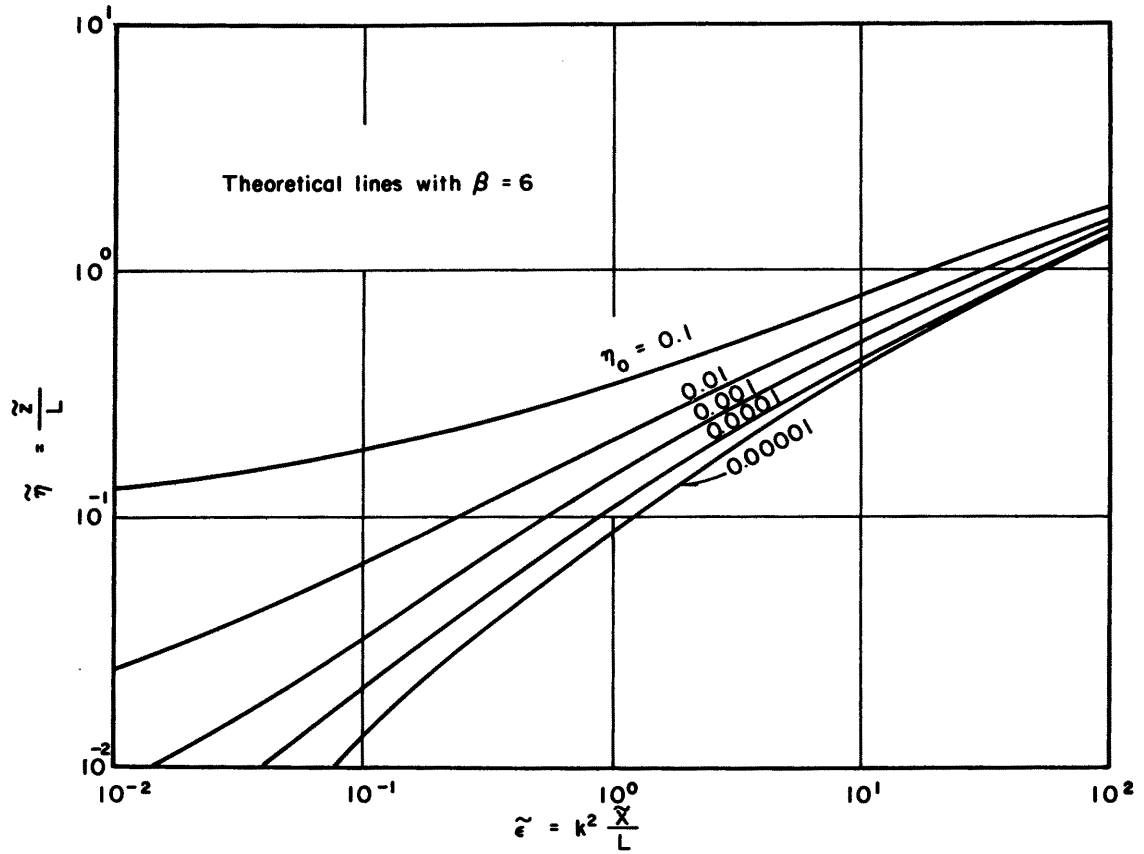
Fig. 36 Vertical spread (β = 6)
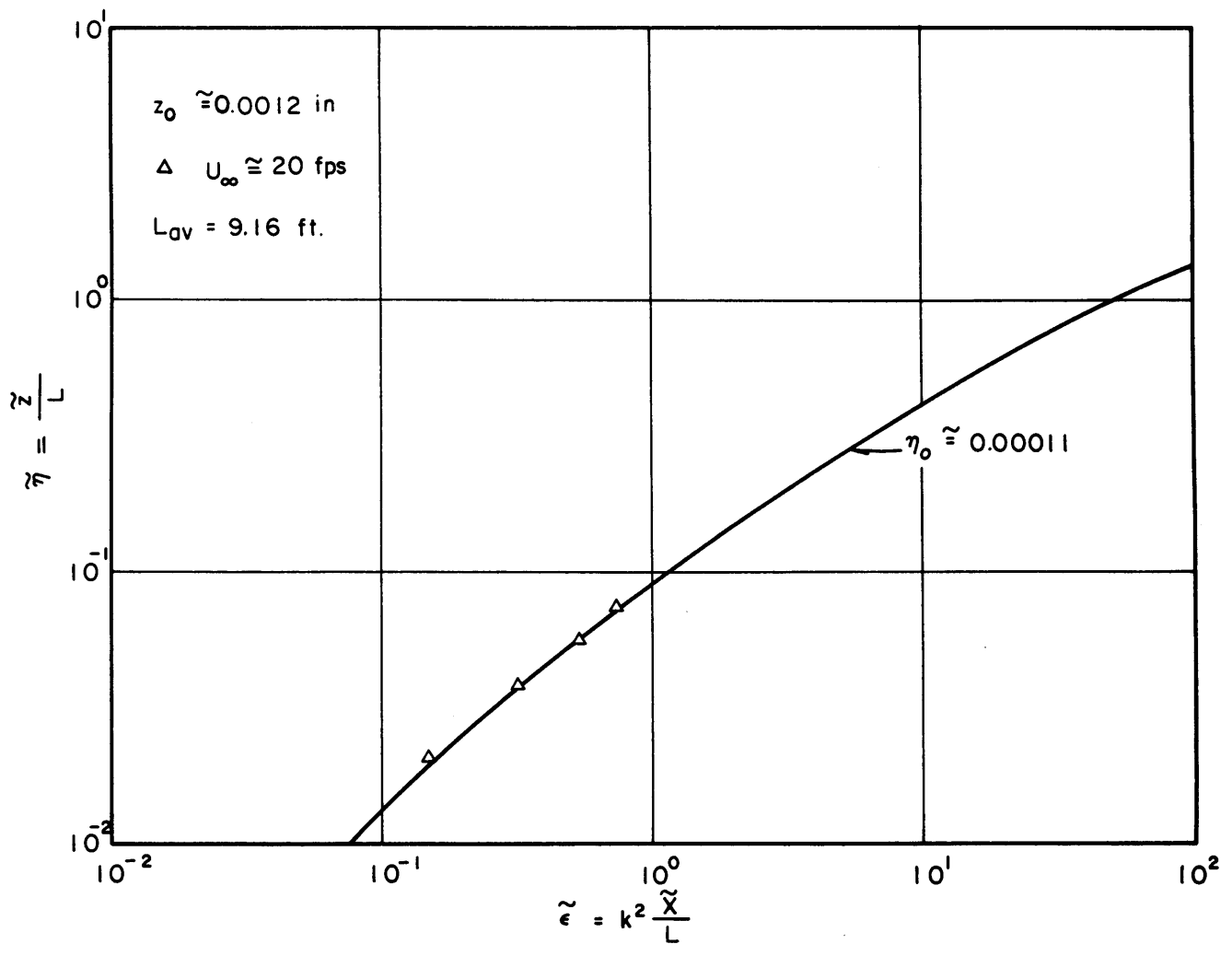
Fig. 37   Vertical spread with data points (β = 6)
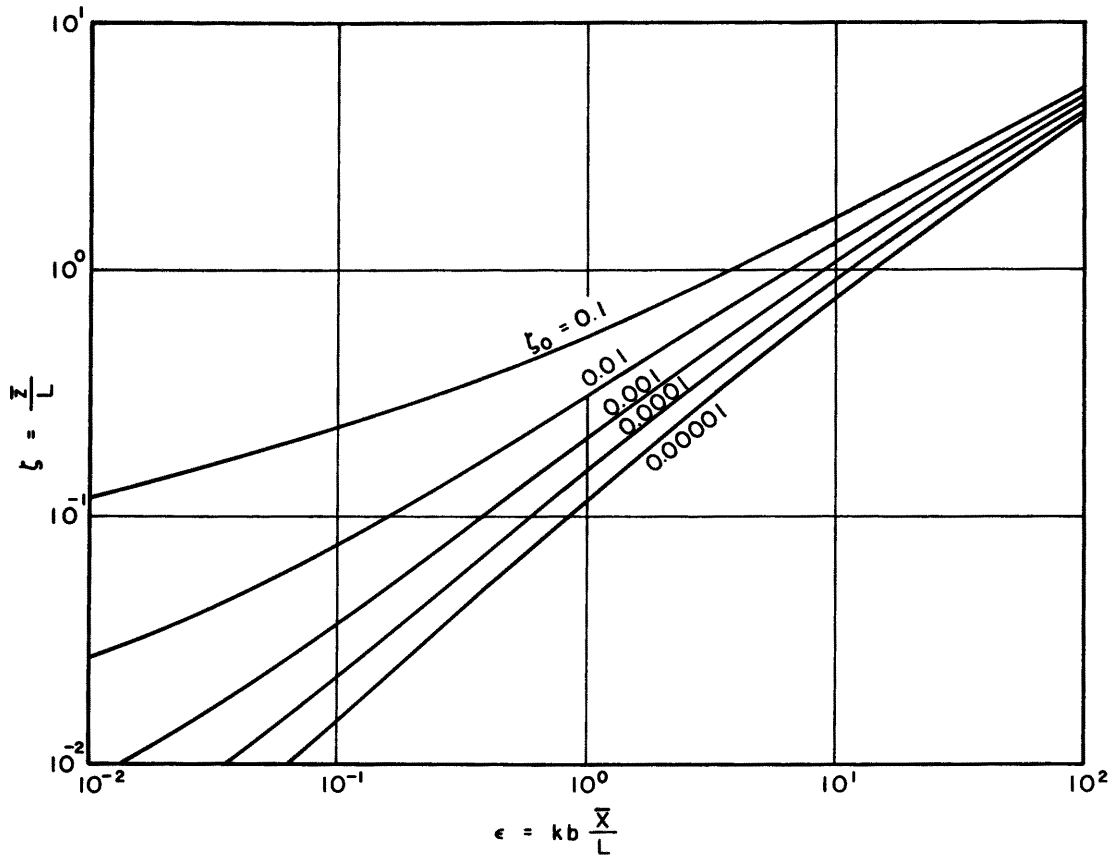
Fig. 38 Vertical spread (β = 6, Ref. 13)
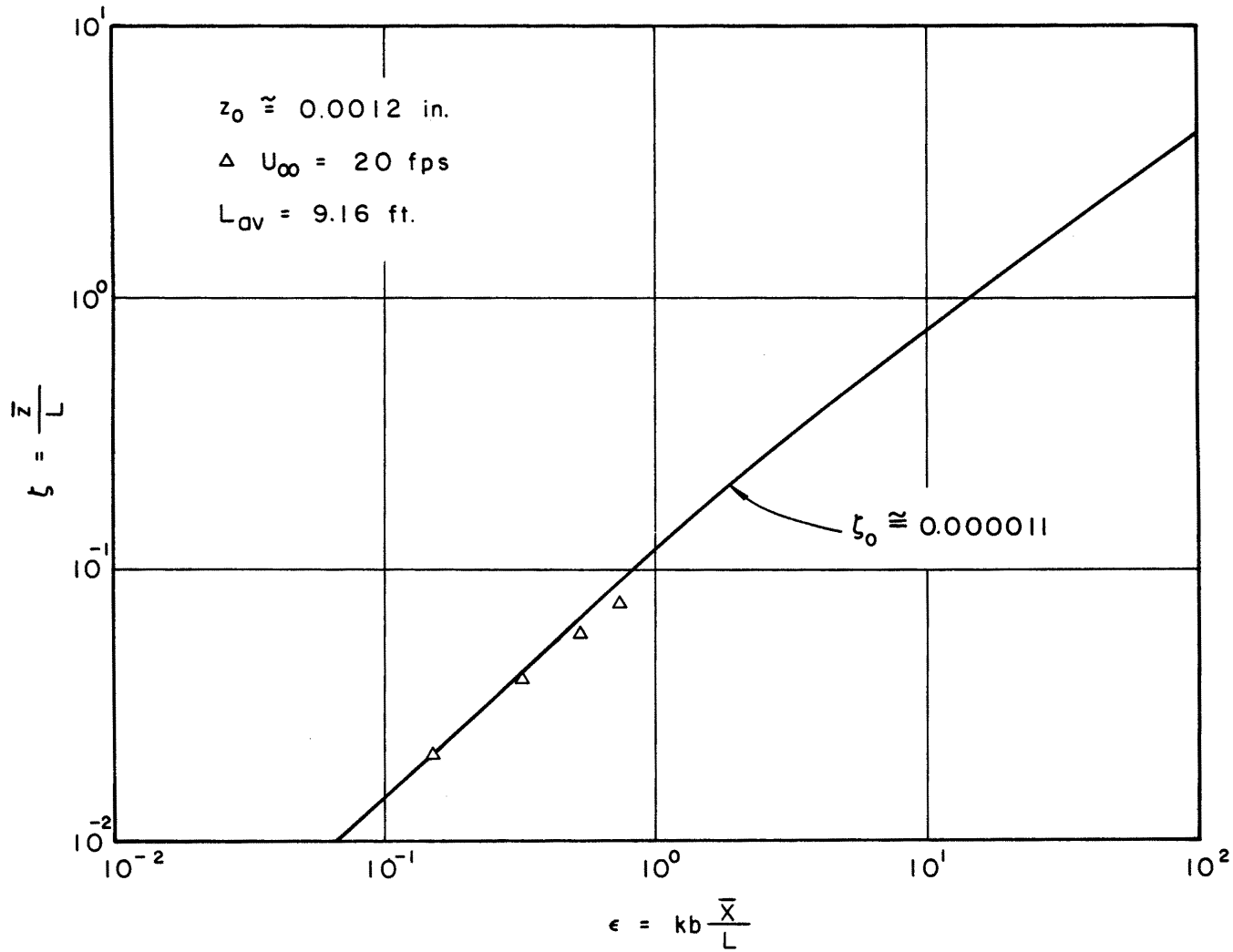
Fig. 39 Vertical spread with data points (β = 6, Ref. 13)
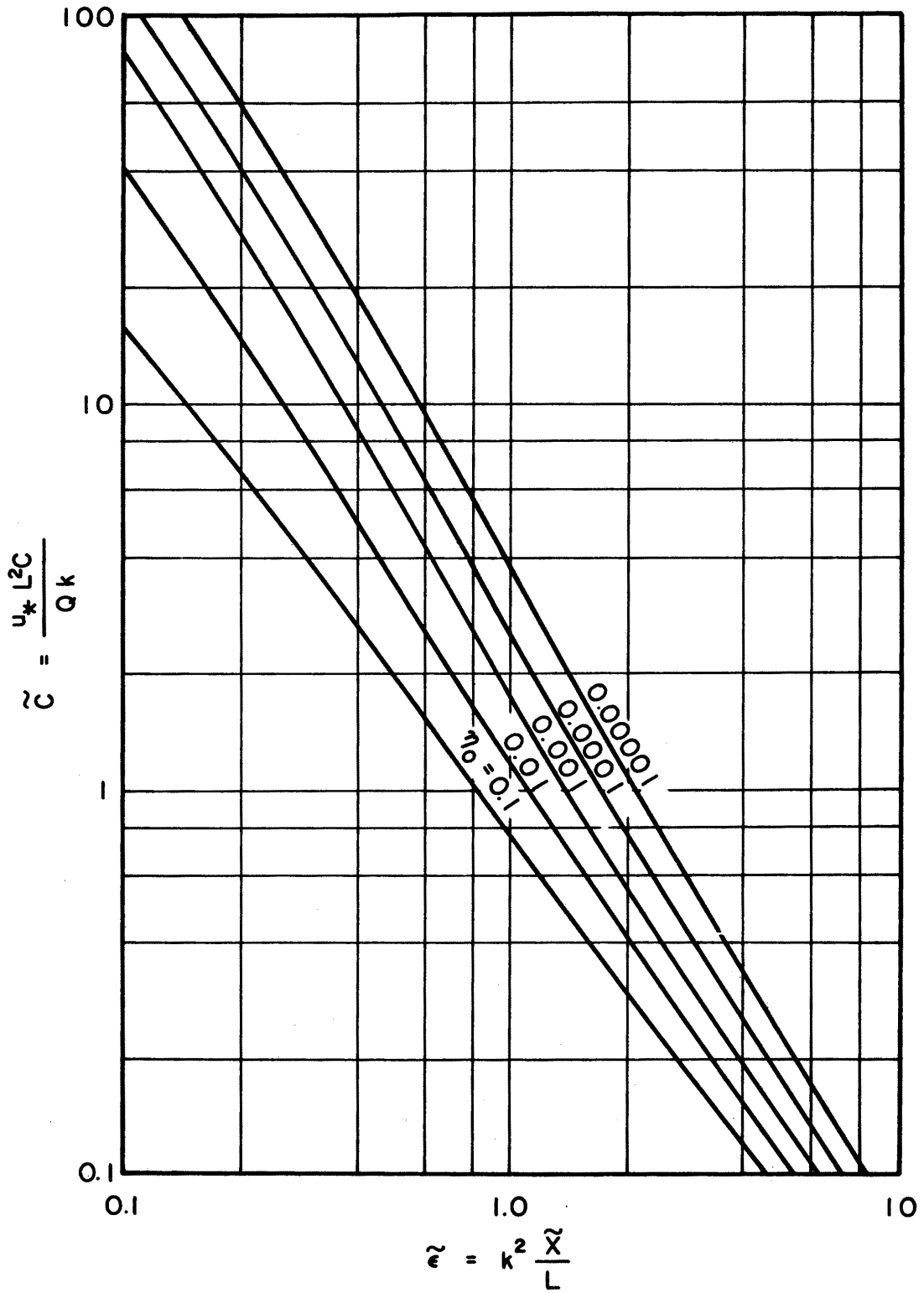
Fig. 40   Concentration lines ($\beta = 1$)
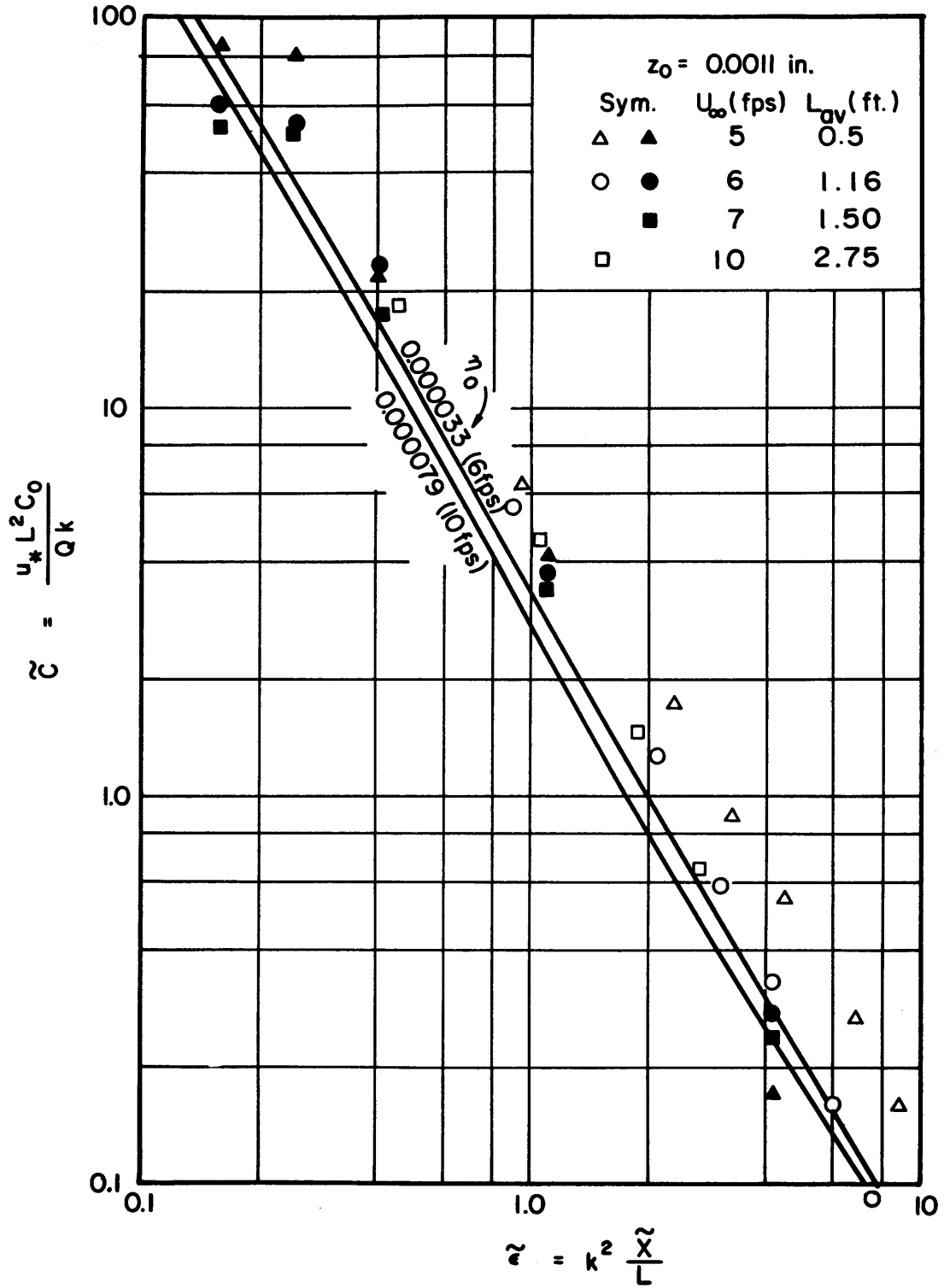
Fig. 41   Concentration lines with data points (θ = 1)

143
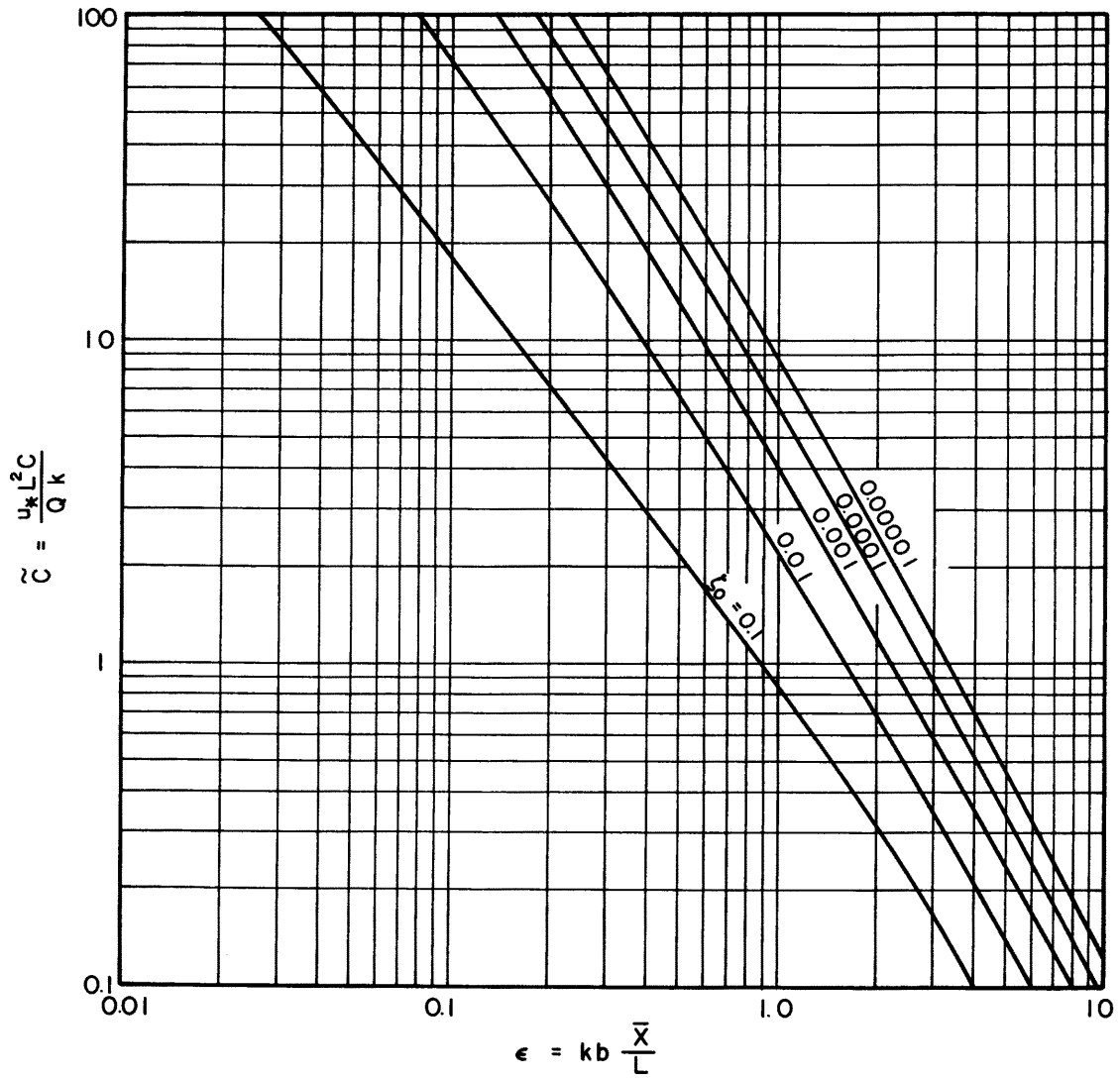
Fig. 42 Concentration lines (β = 1, Ref. 13)
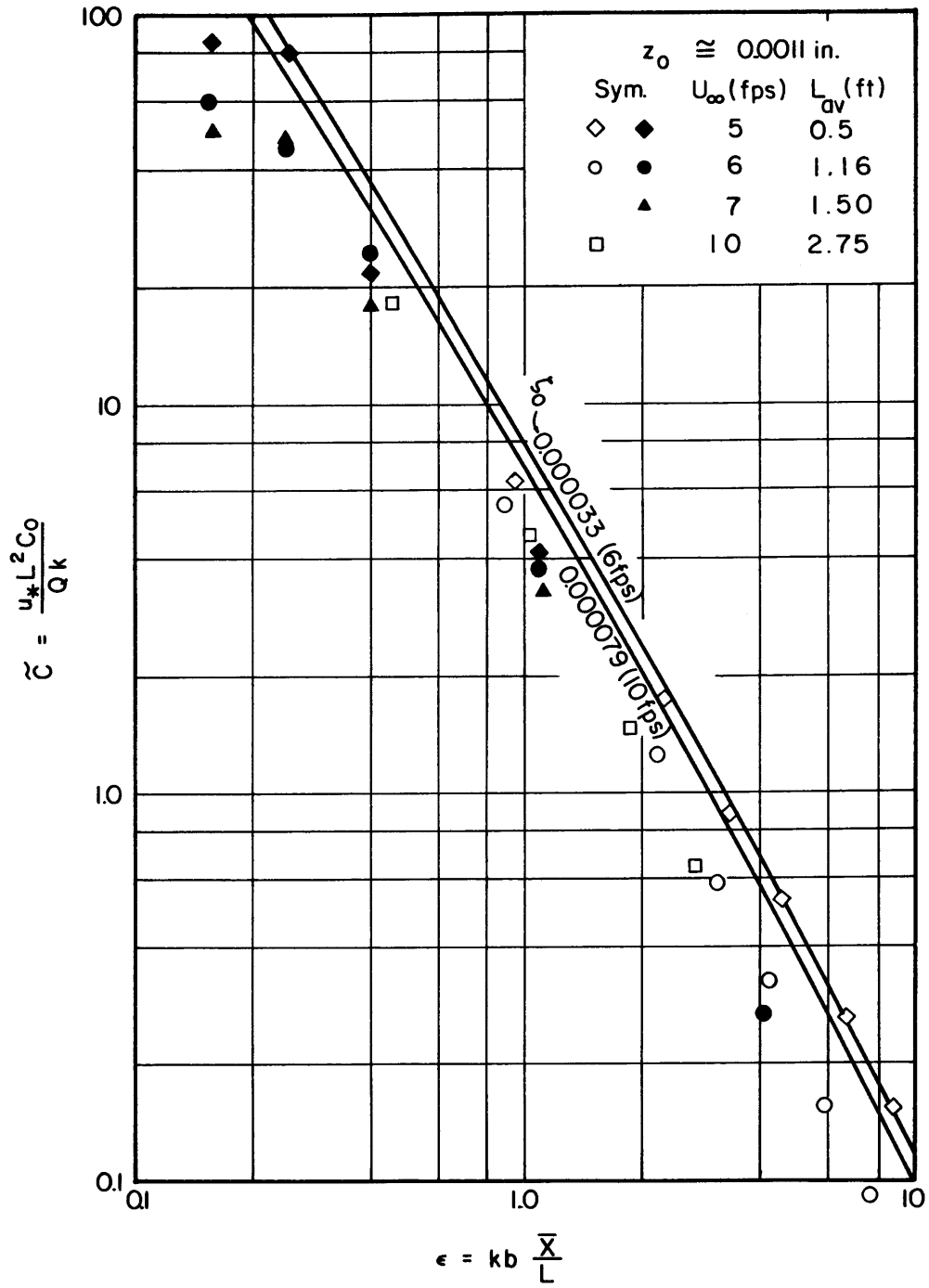
Fig. 43   Concentration lines with data points
(β = 1, Ref. 13)
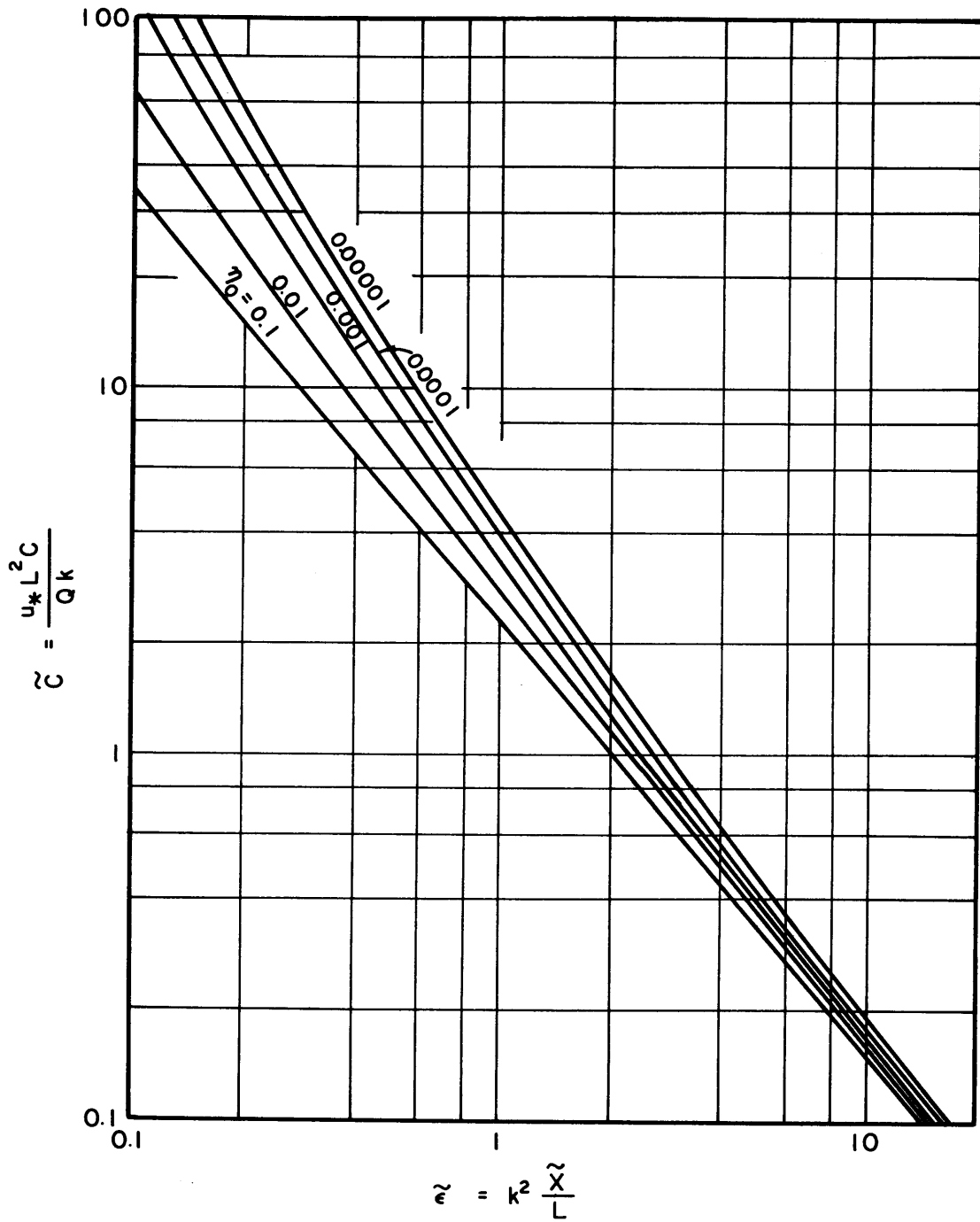
Fig. 44 Concentration lines ($\beta = 6$)

146
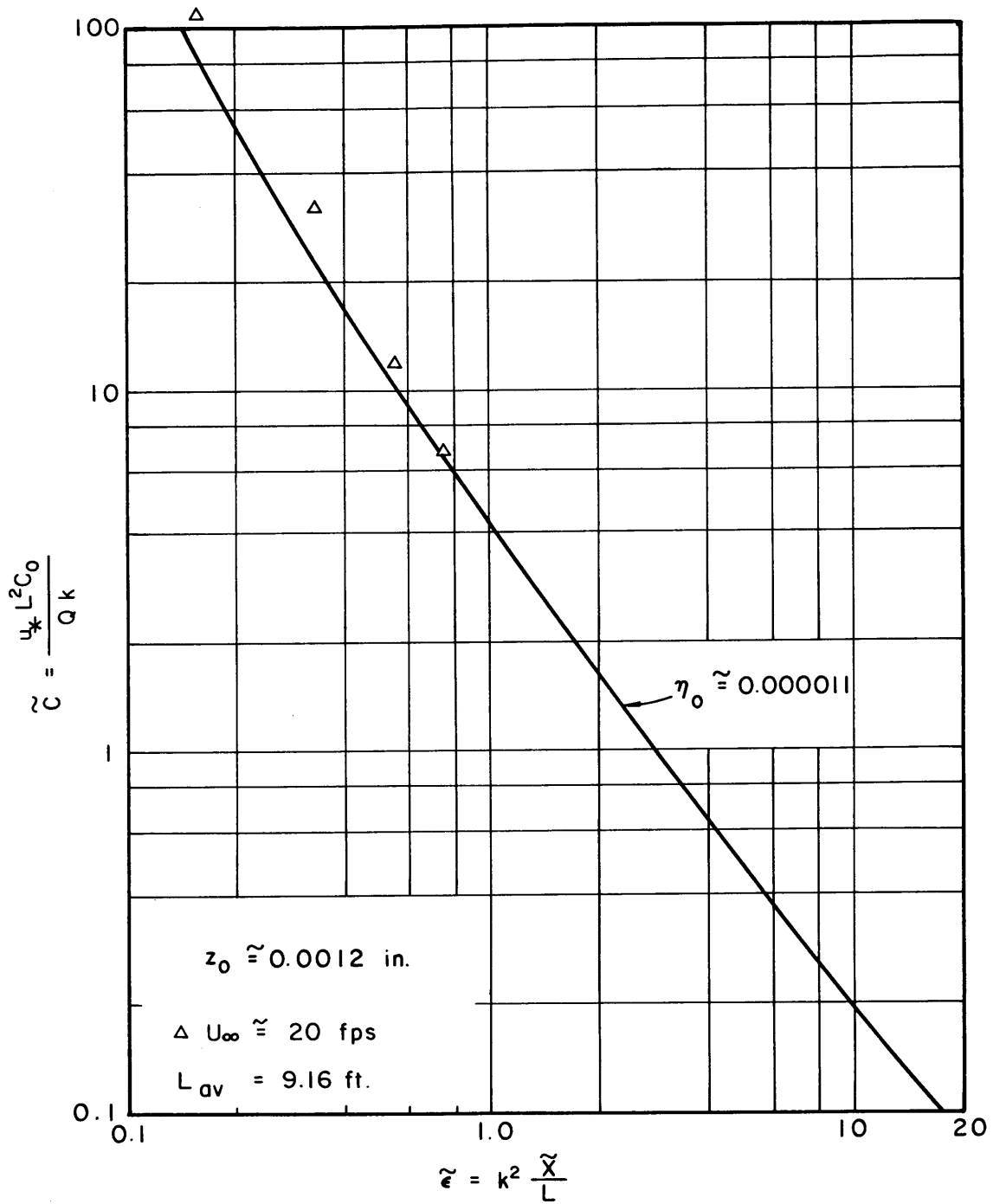
Fig. 45 Concentration line with data points (β = 6)
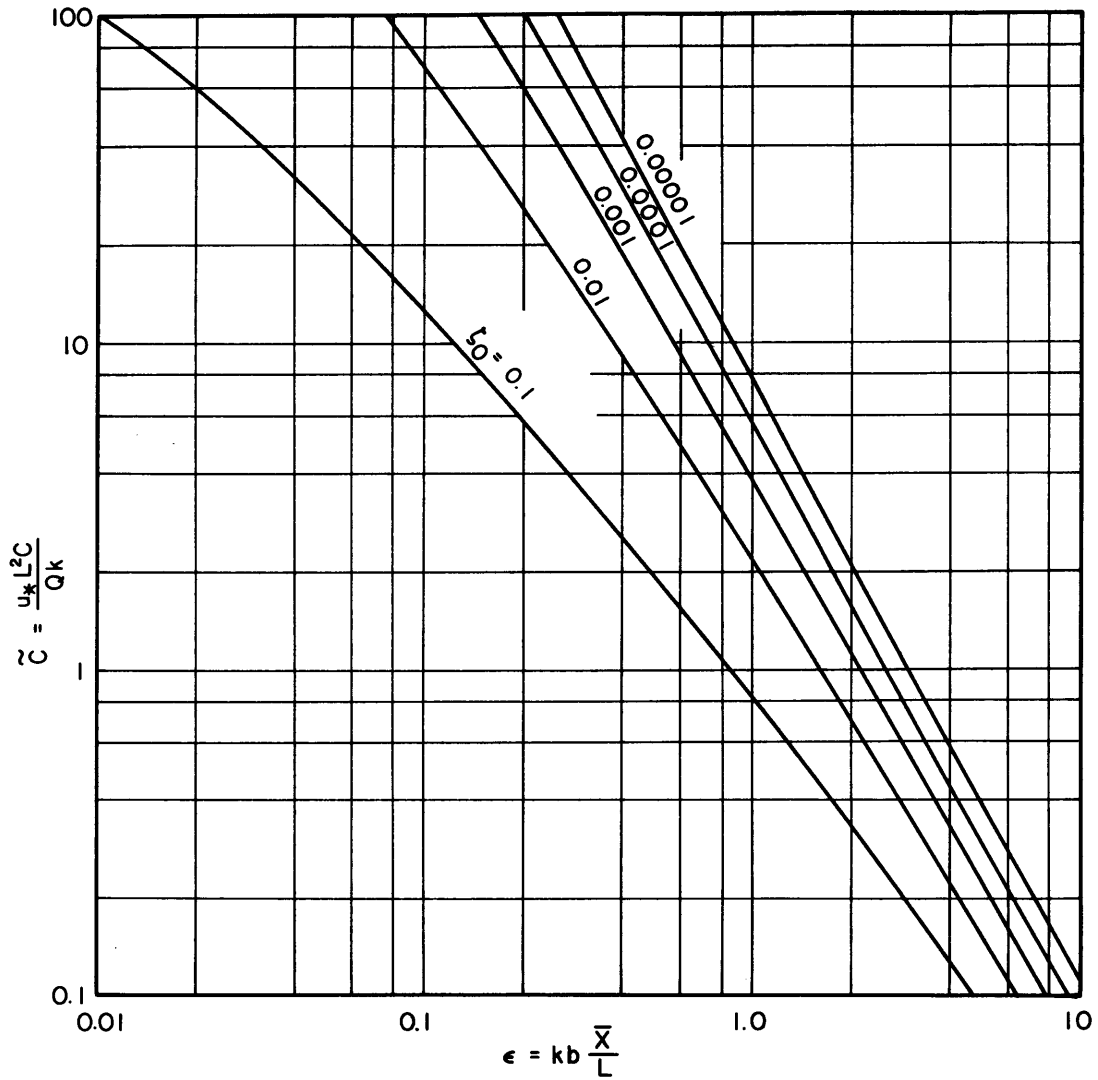
Fig. 46 Concentration lines (β = 6, Ref. 13)

148
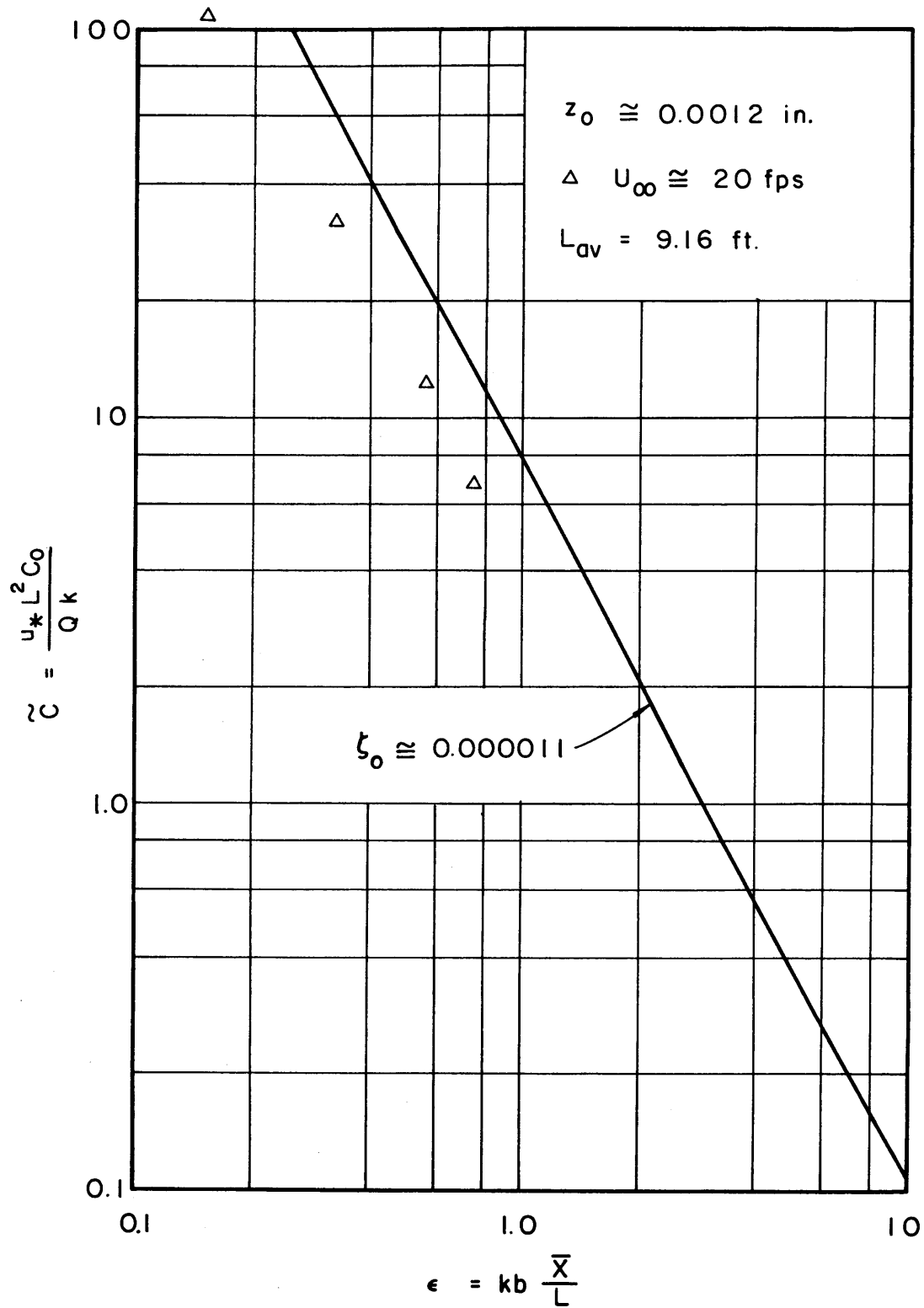
Fig. 47 Concentration line with data points
(β = 6, Ref. 13)
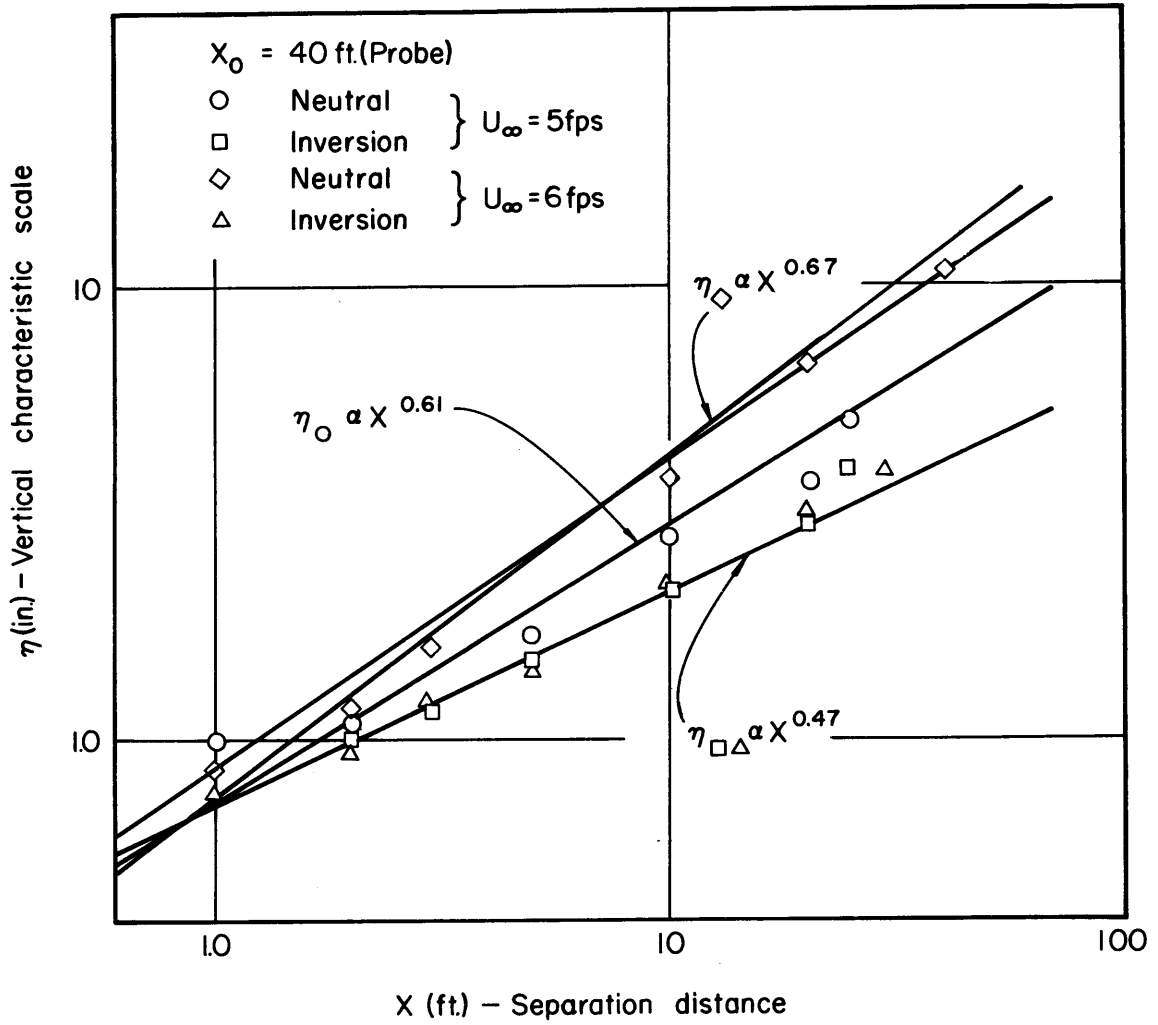
Fig. 48 Vertical spread data (u = 5, 6 fps)
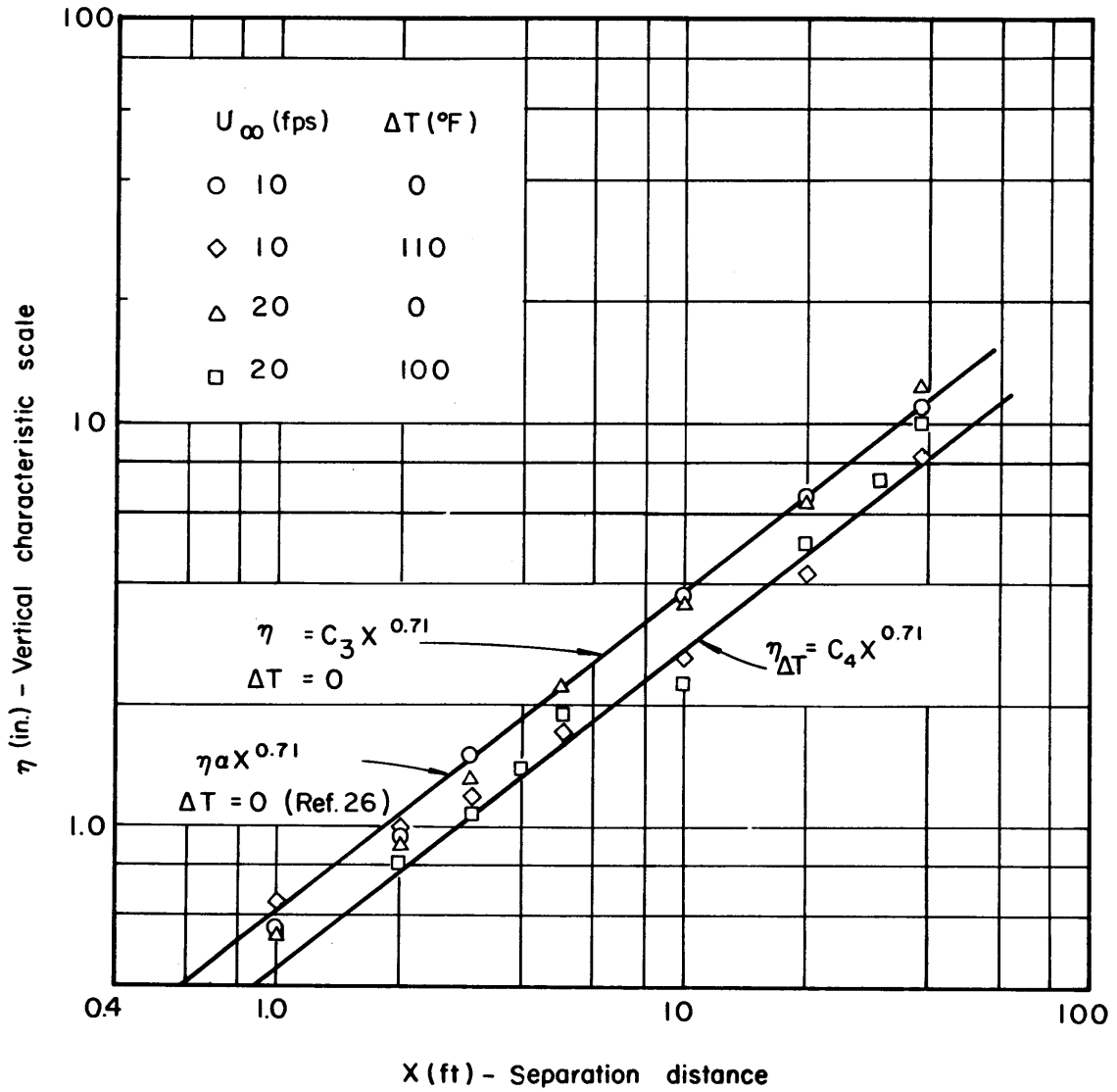
Fig. 49   Vertical spread data (u = 10, 20 fps)
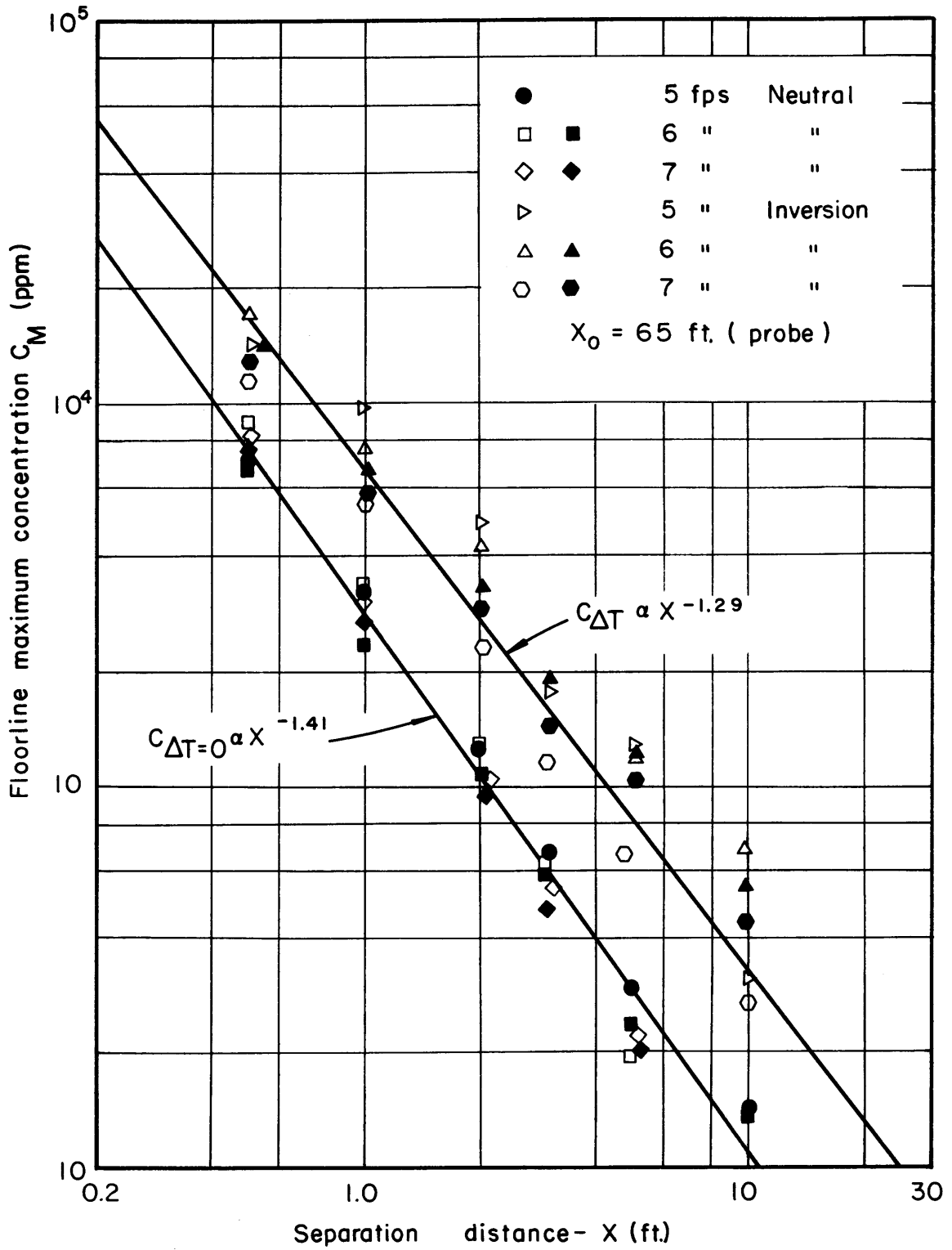
Fig. 50 Floorline concentration data (5, 6, 7 fps)
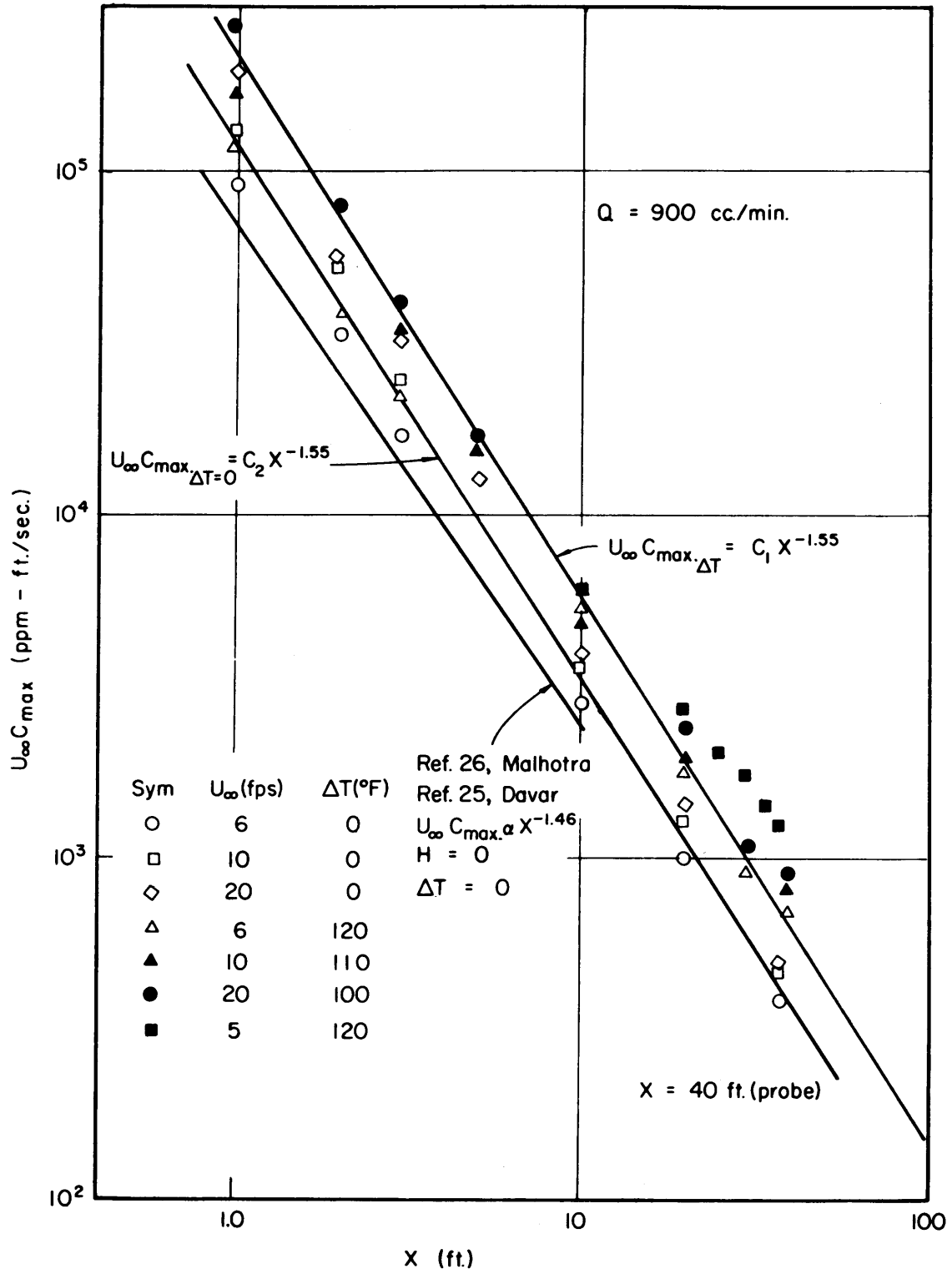
Fig. 51 Floorline concentration data (10, 20 fps)
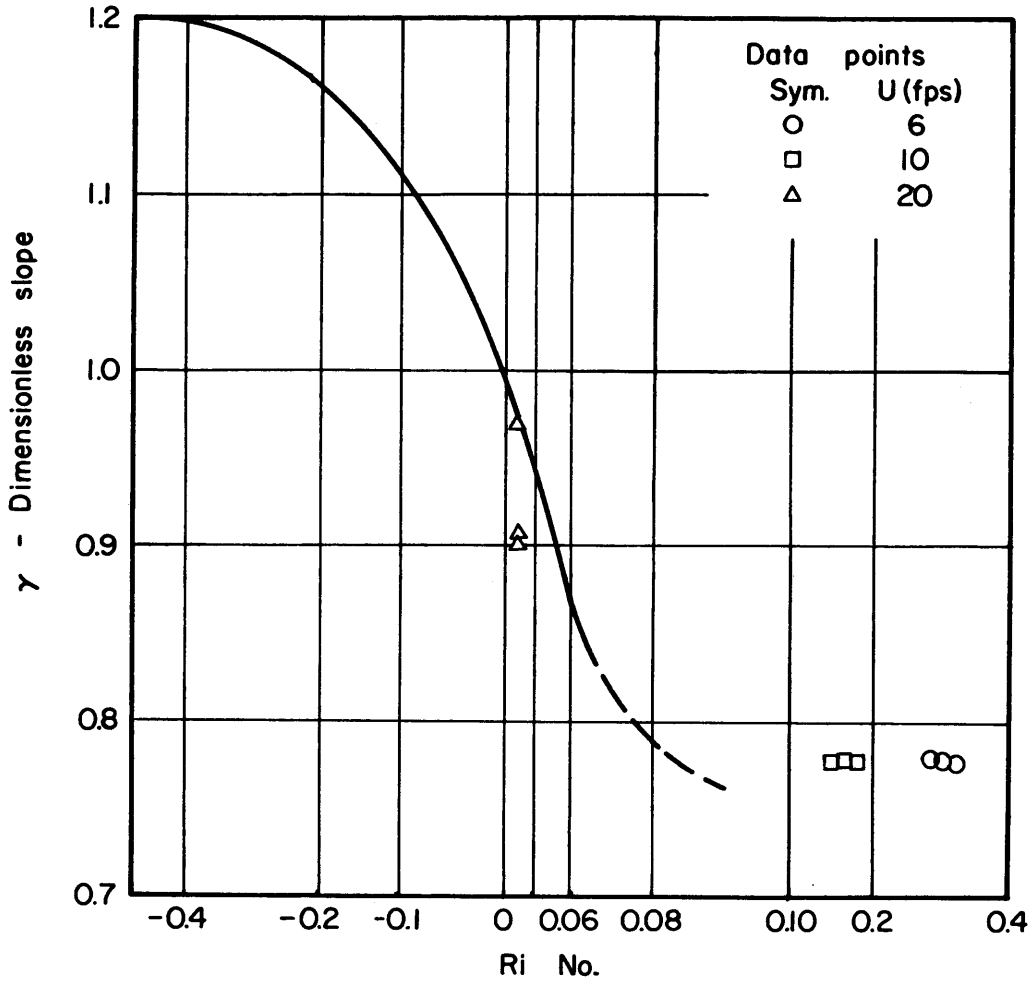
Fig. 52 The variation of γ with stability
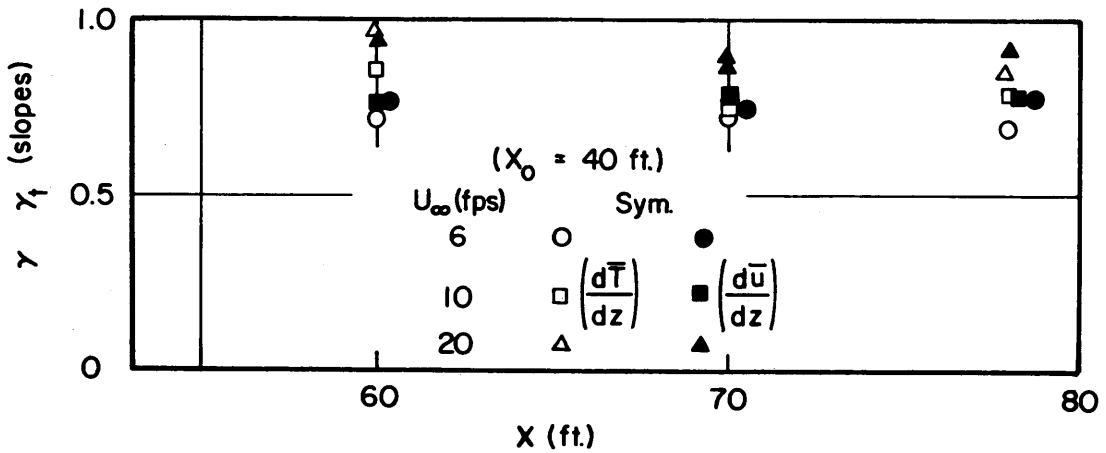
Fig. 53 Slope (γ, γ_t) in Deacon's equations
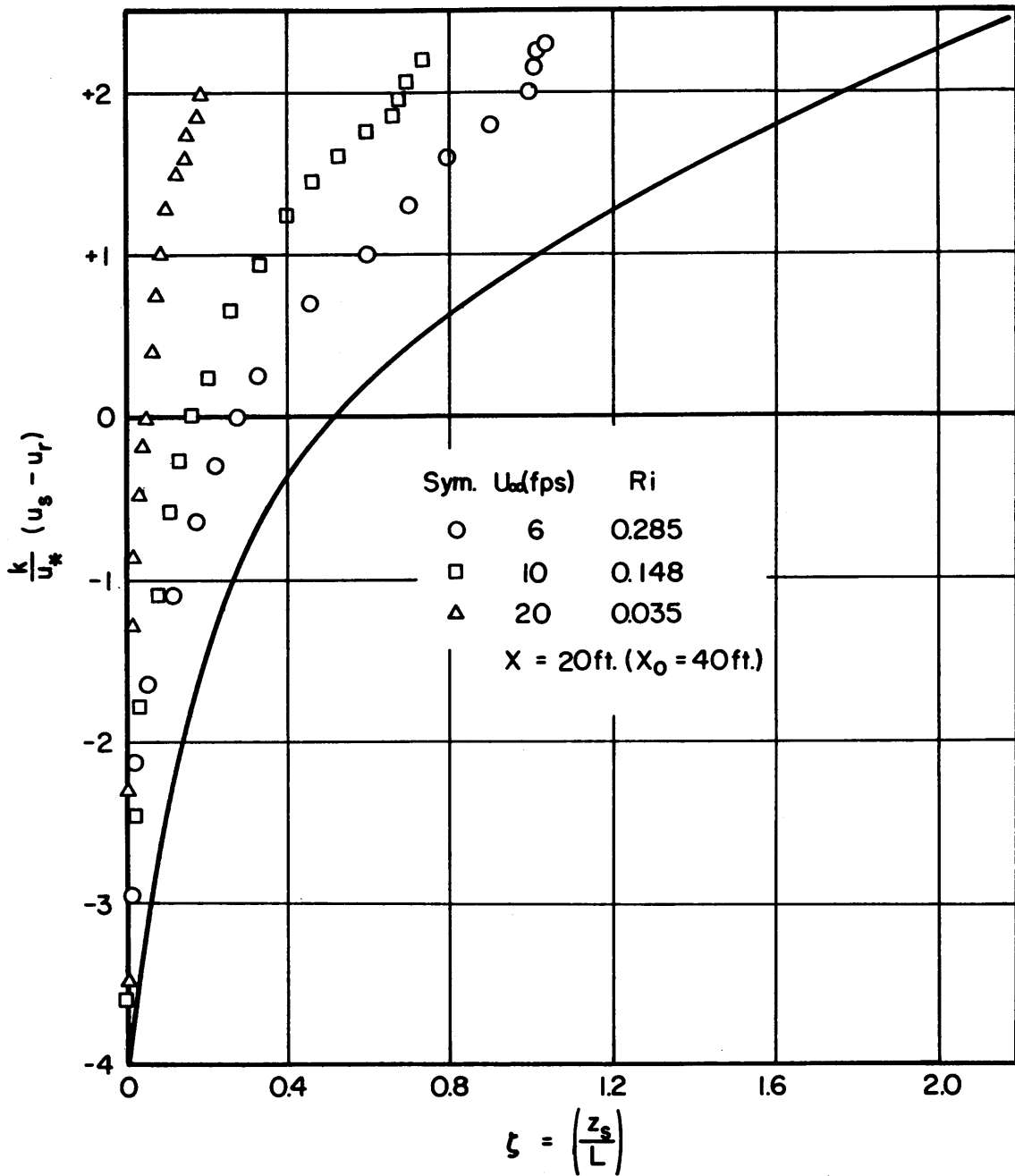
Fig. 54   Comparison of data with universal wind
profile (inversion, x=60ft)
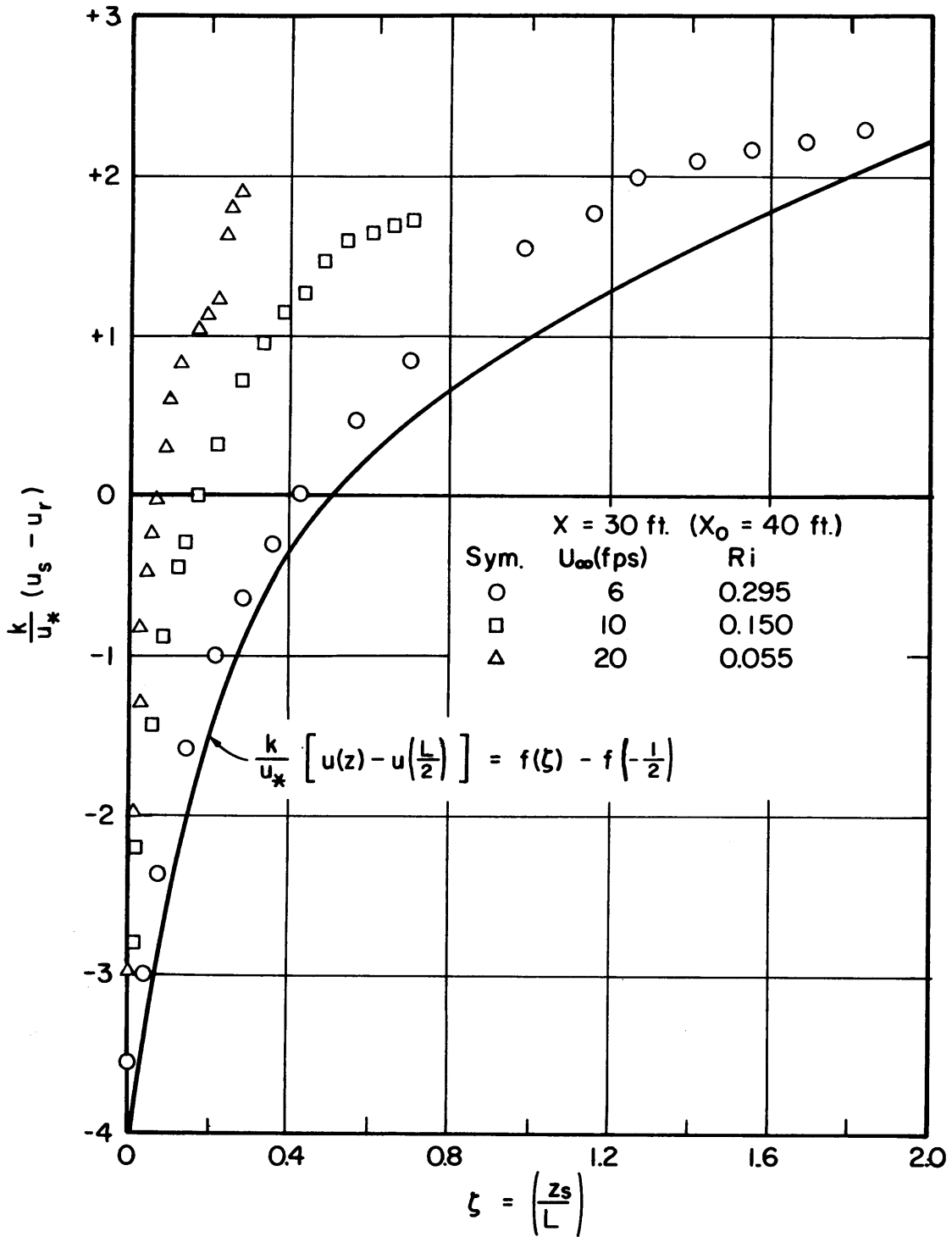
Fig. 55 Comparison of data with universal wind
profile (inversion, x=70ft)
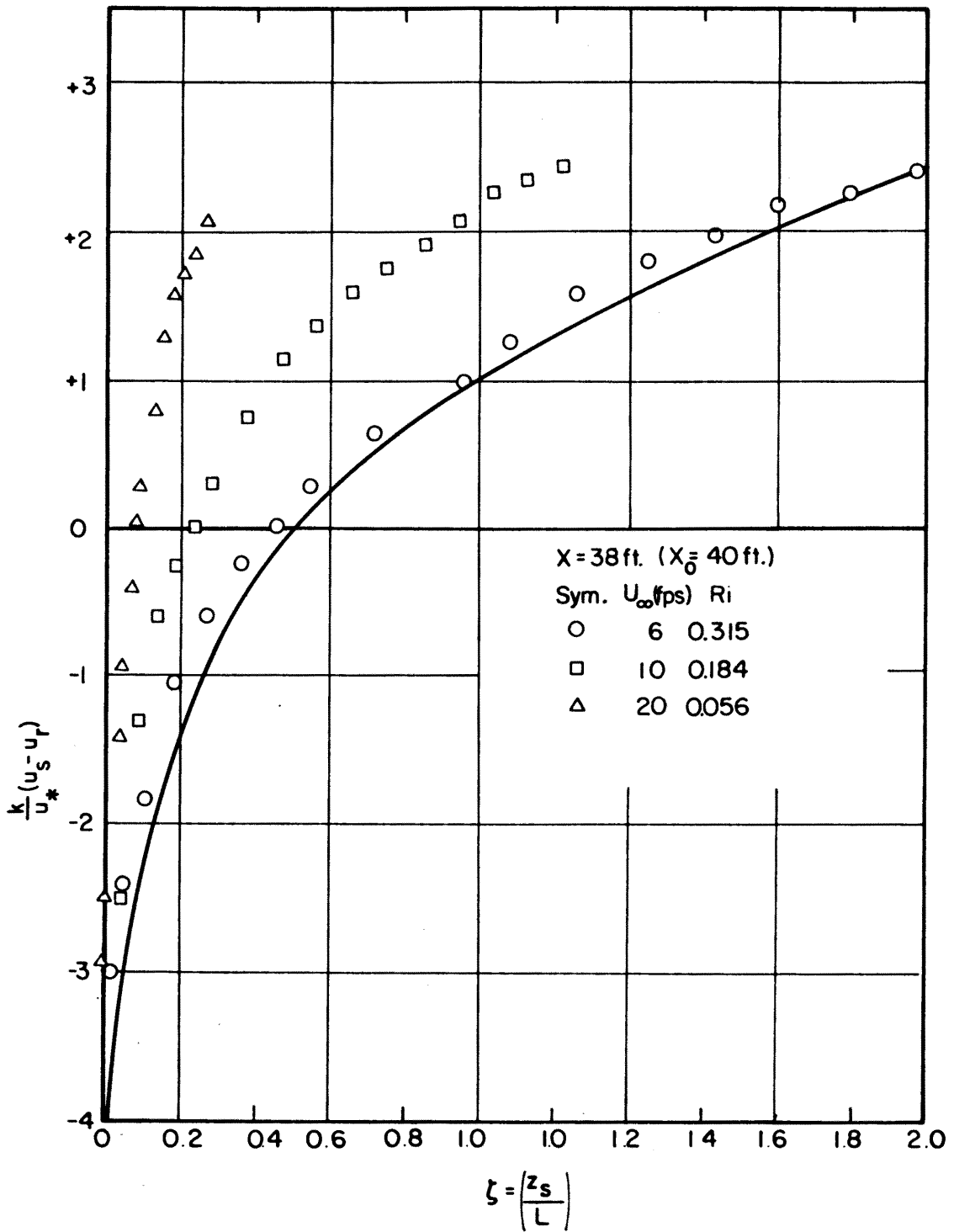
Fig. 56   Comparison of data with universal wind
profile (inversion, x=78ft)

157
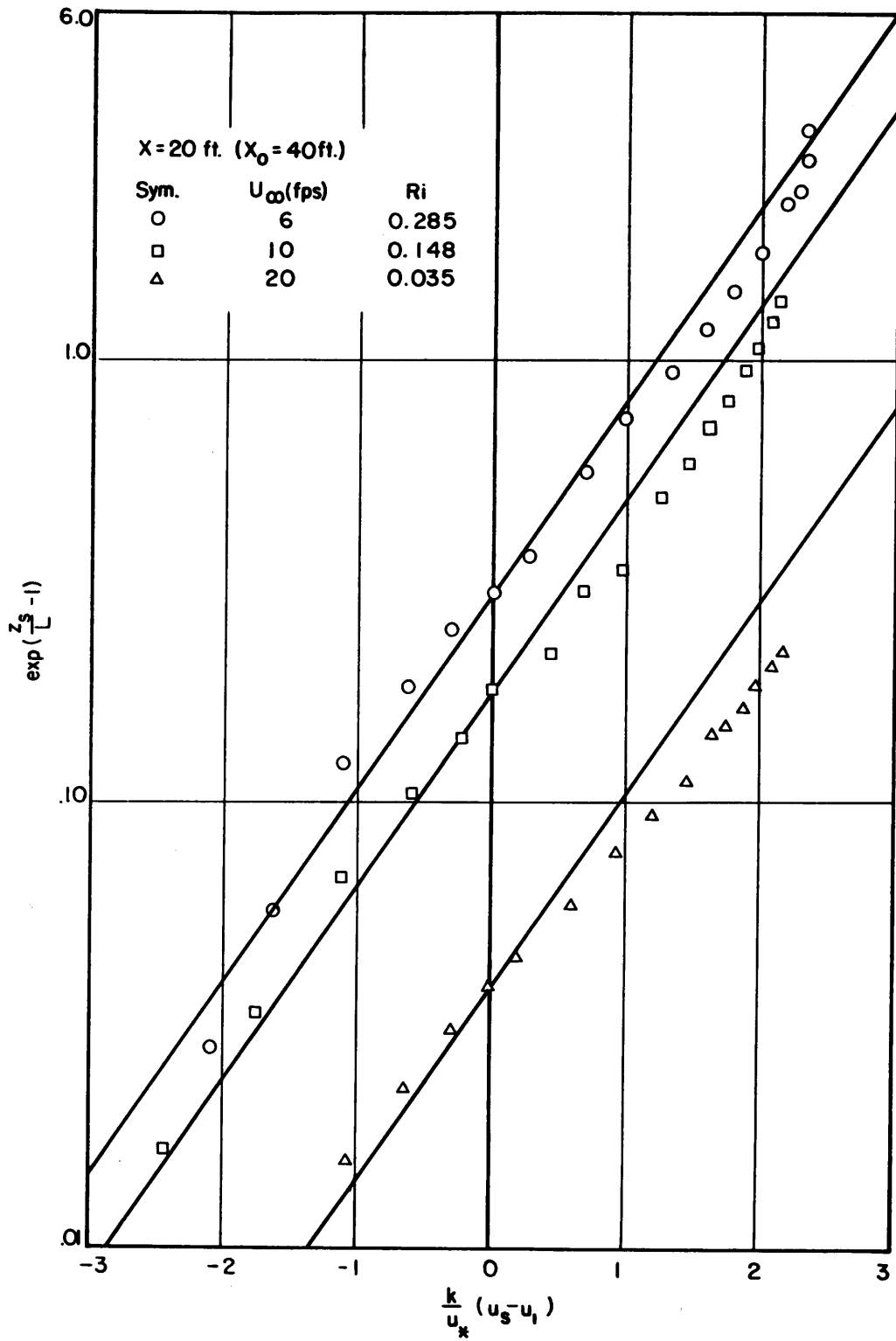
Fig. 57   Comparison of data with exponential profile
(inversion, x=60ft)
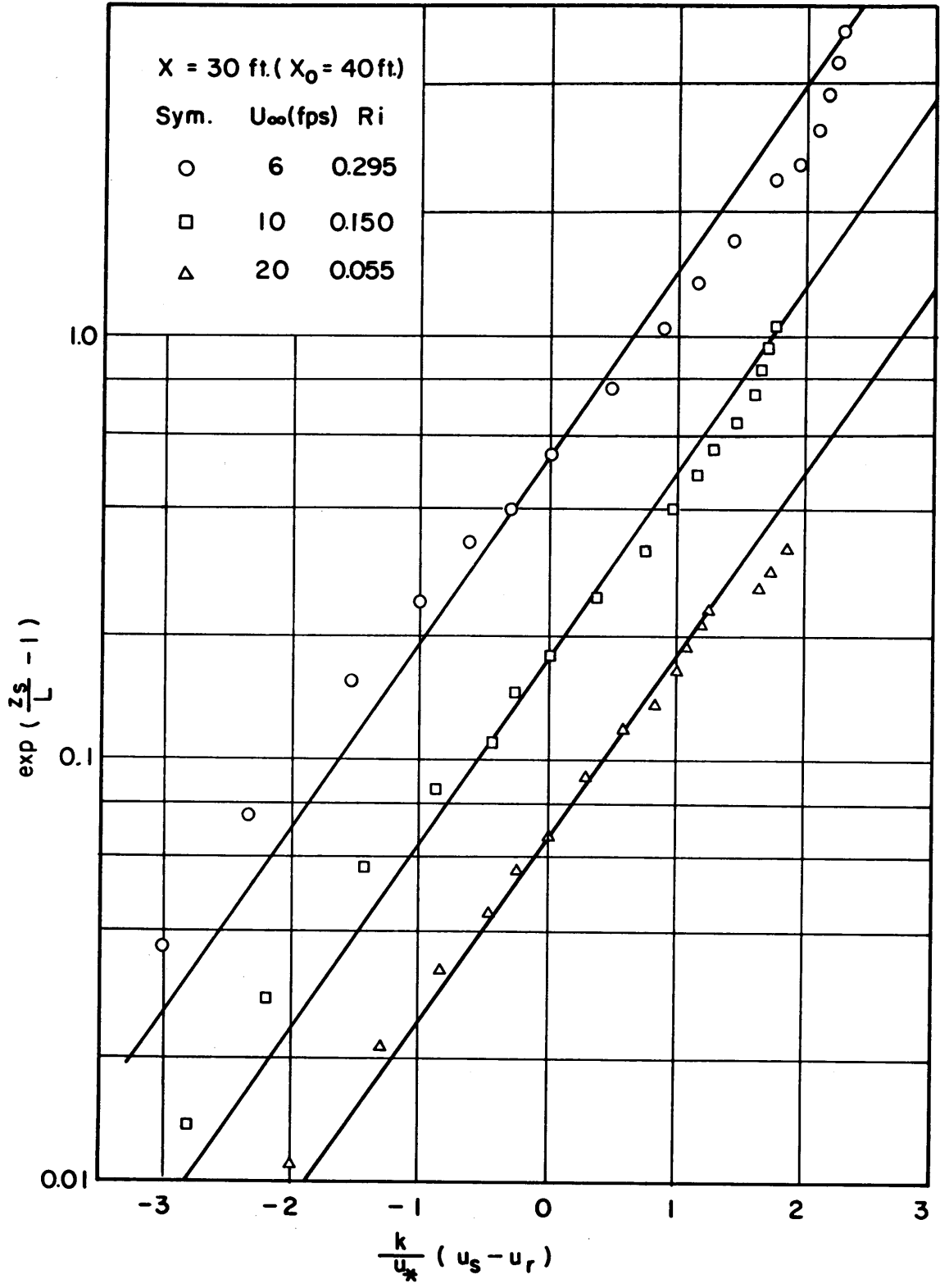
Fig. 58   Comparison of data with exponential profile
(inversion, x=70ft)

159
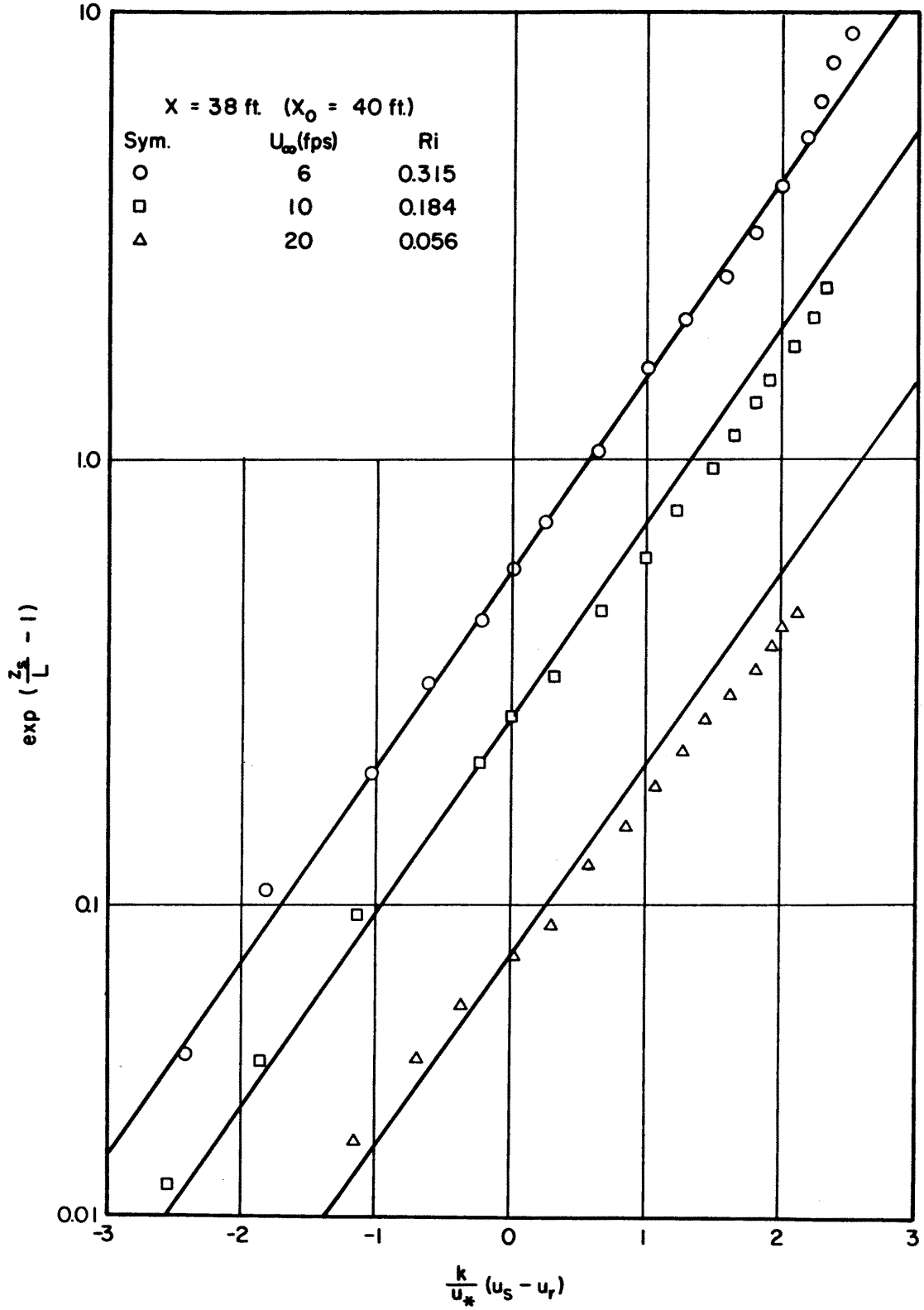
Fig. 59 Comparison of data with exponential profile
(inversion, x=78ft)
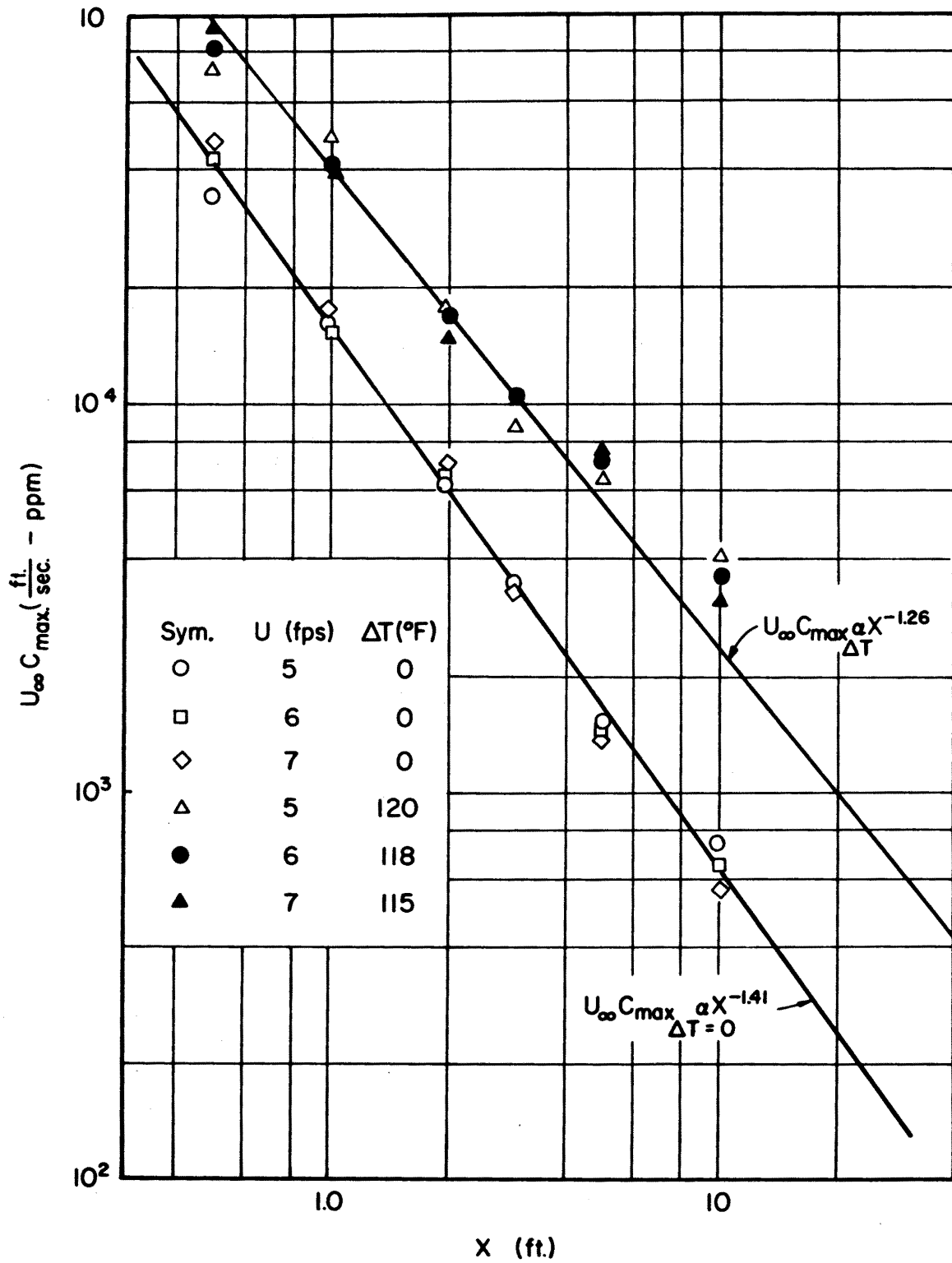
Fig. 60 Effect of stability on ($u\,C_{max}$)
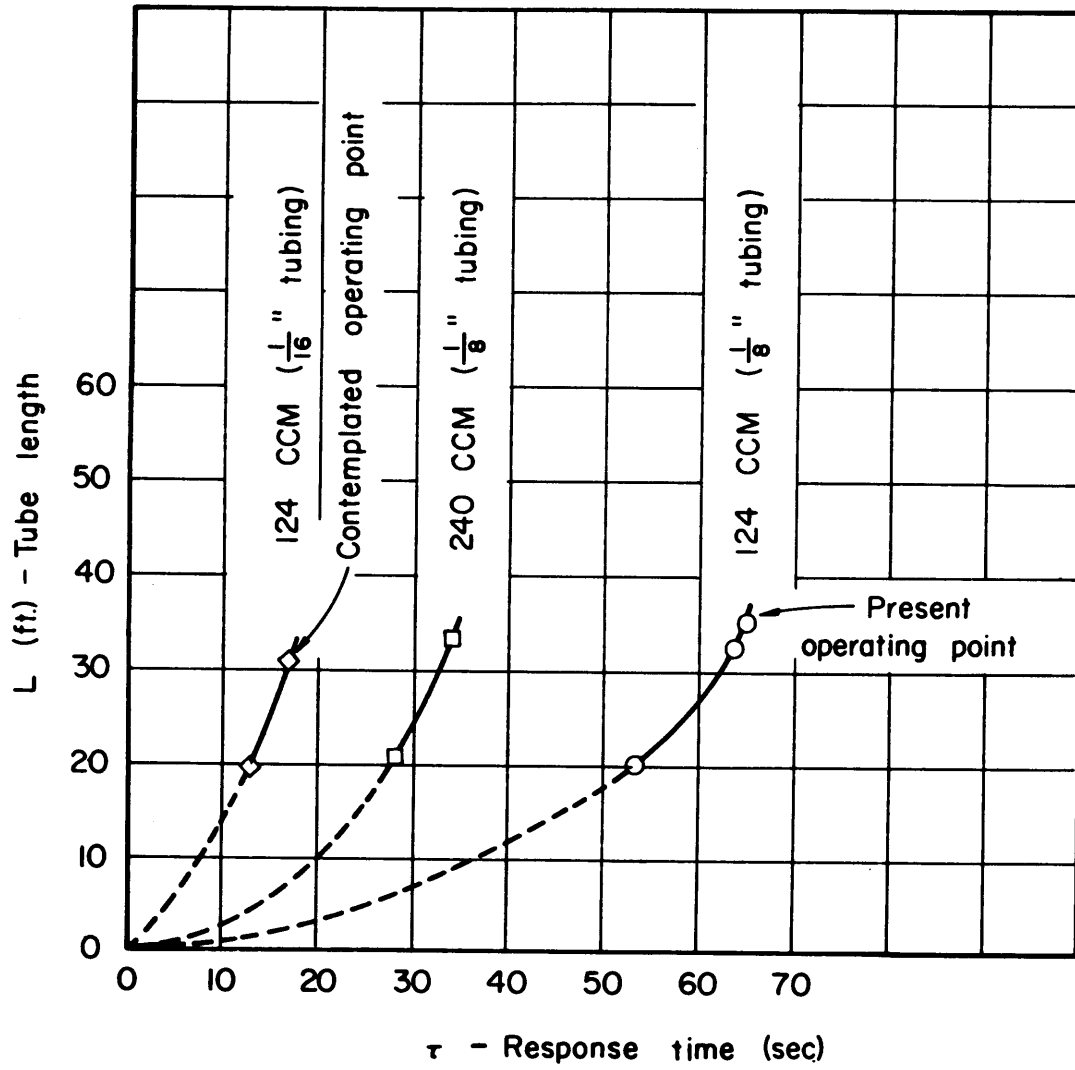
Fig. 61 Response time of MS9
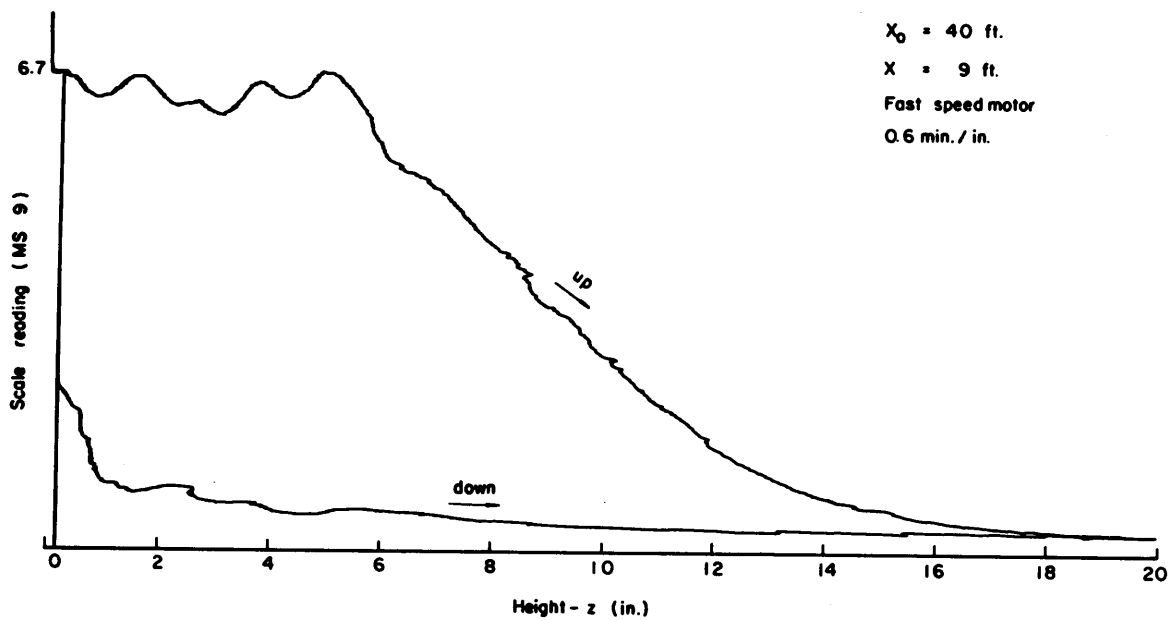
Fig. 62 Concentration plot, fast motor
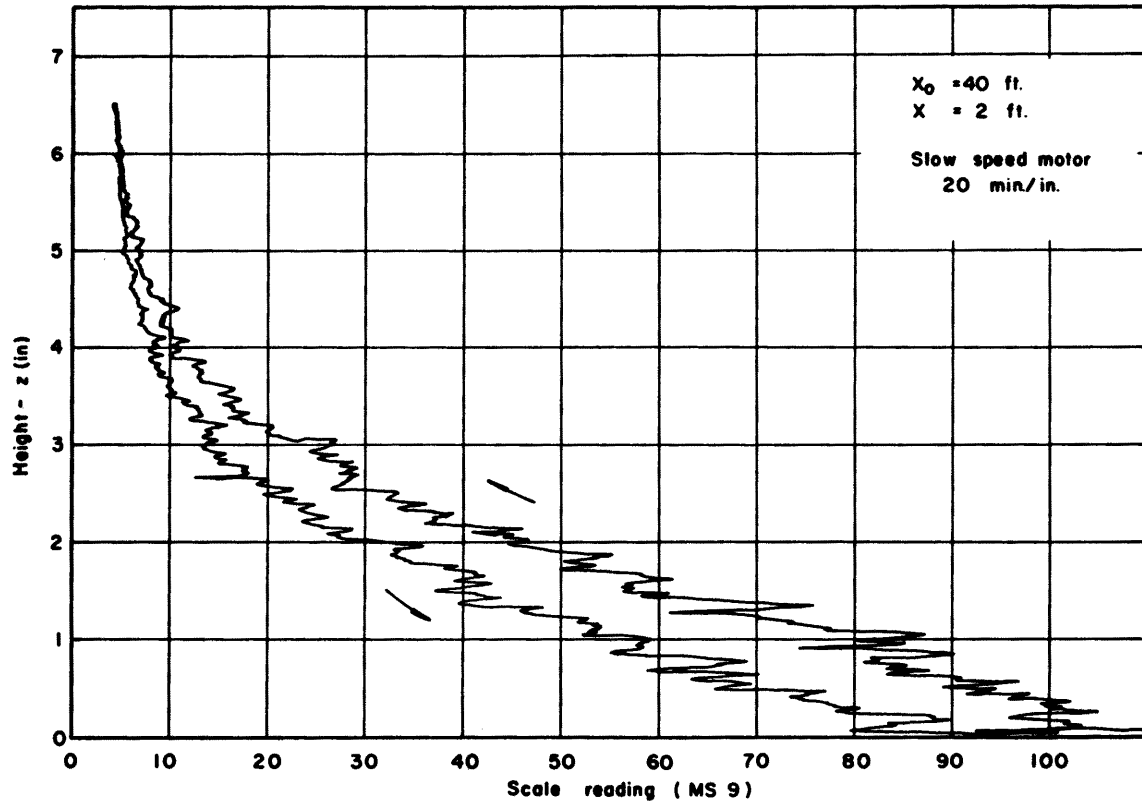
Fig. 63   Concentration plot, slow motor

164
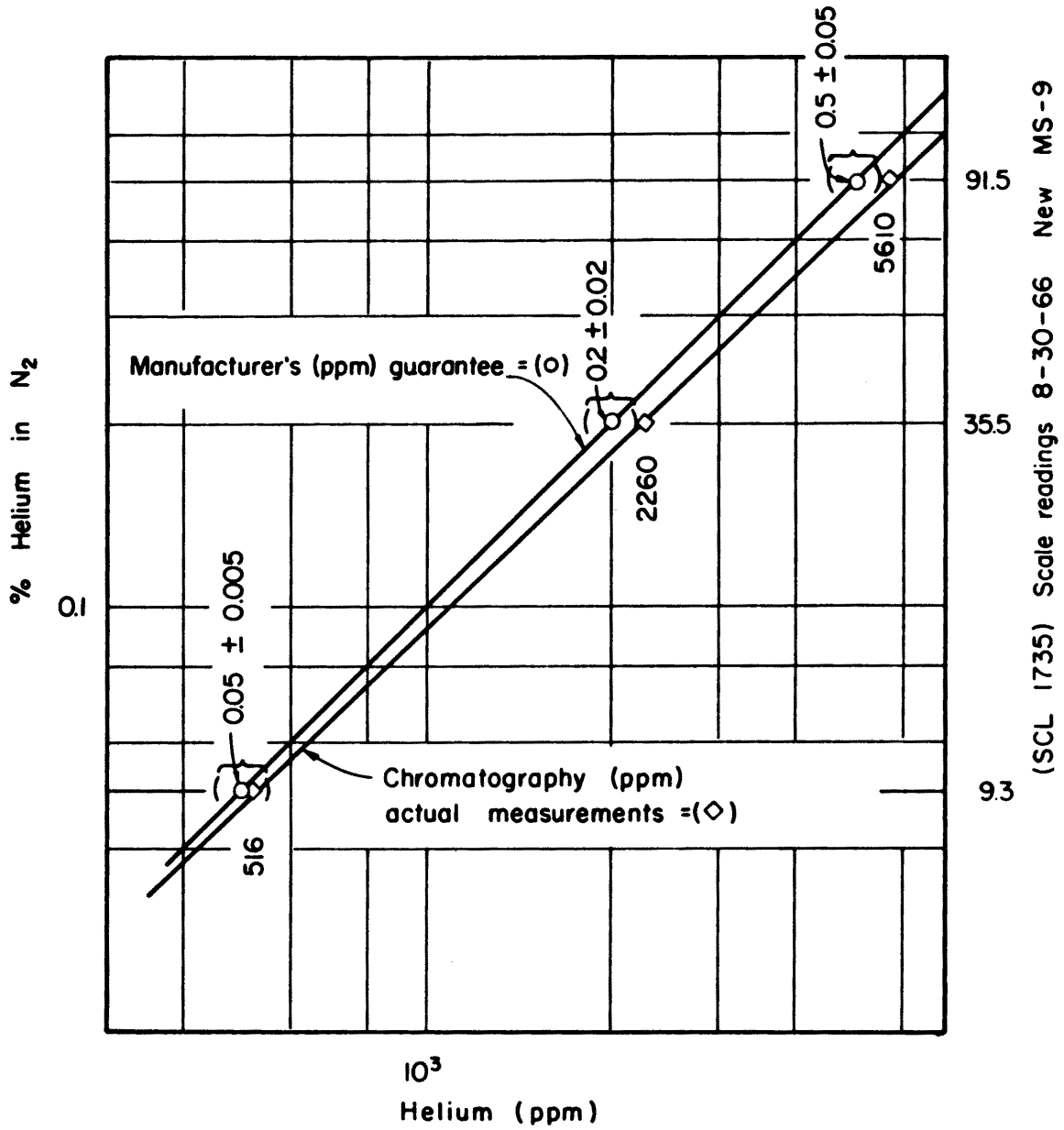
Fig. 64 Percent concentration, standard mixtures
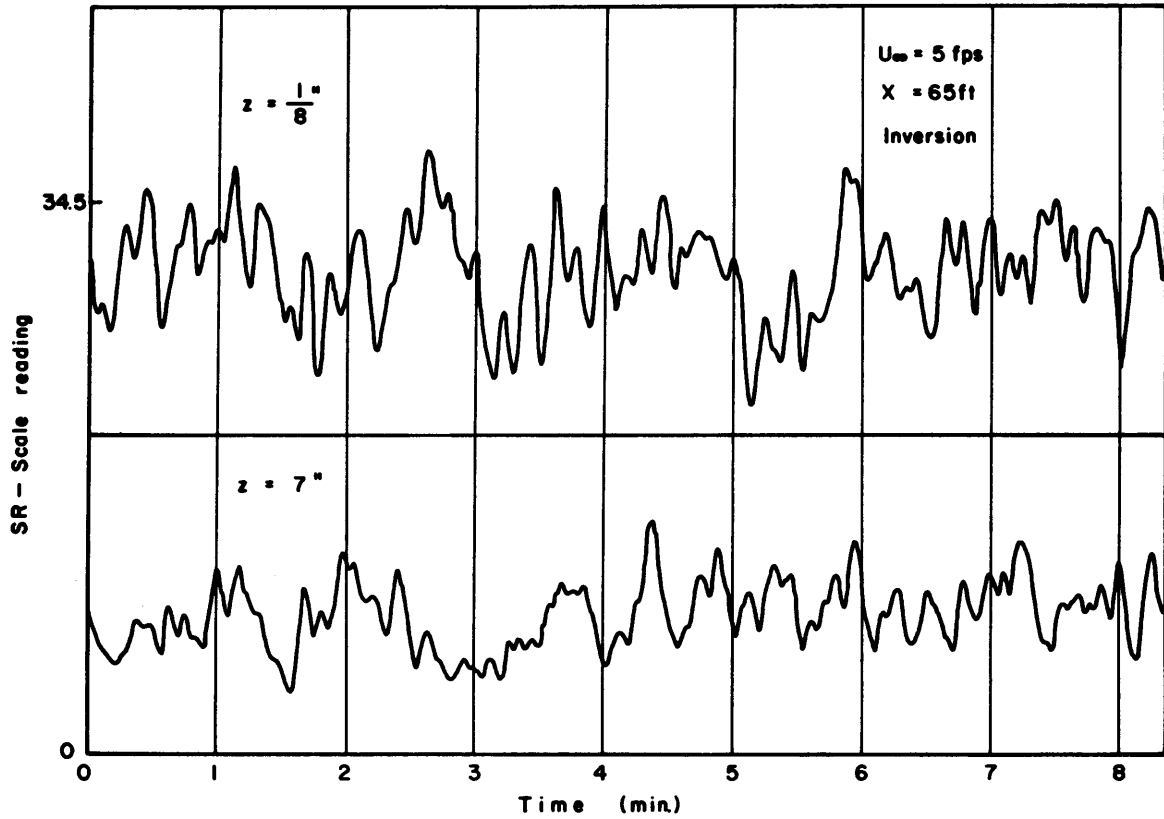
Fig. 65   Variation test
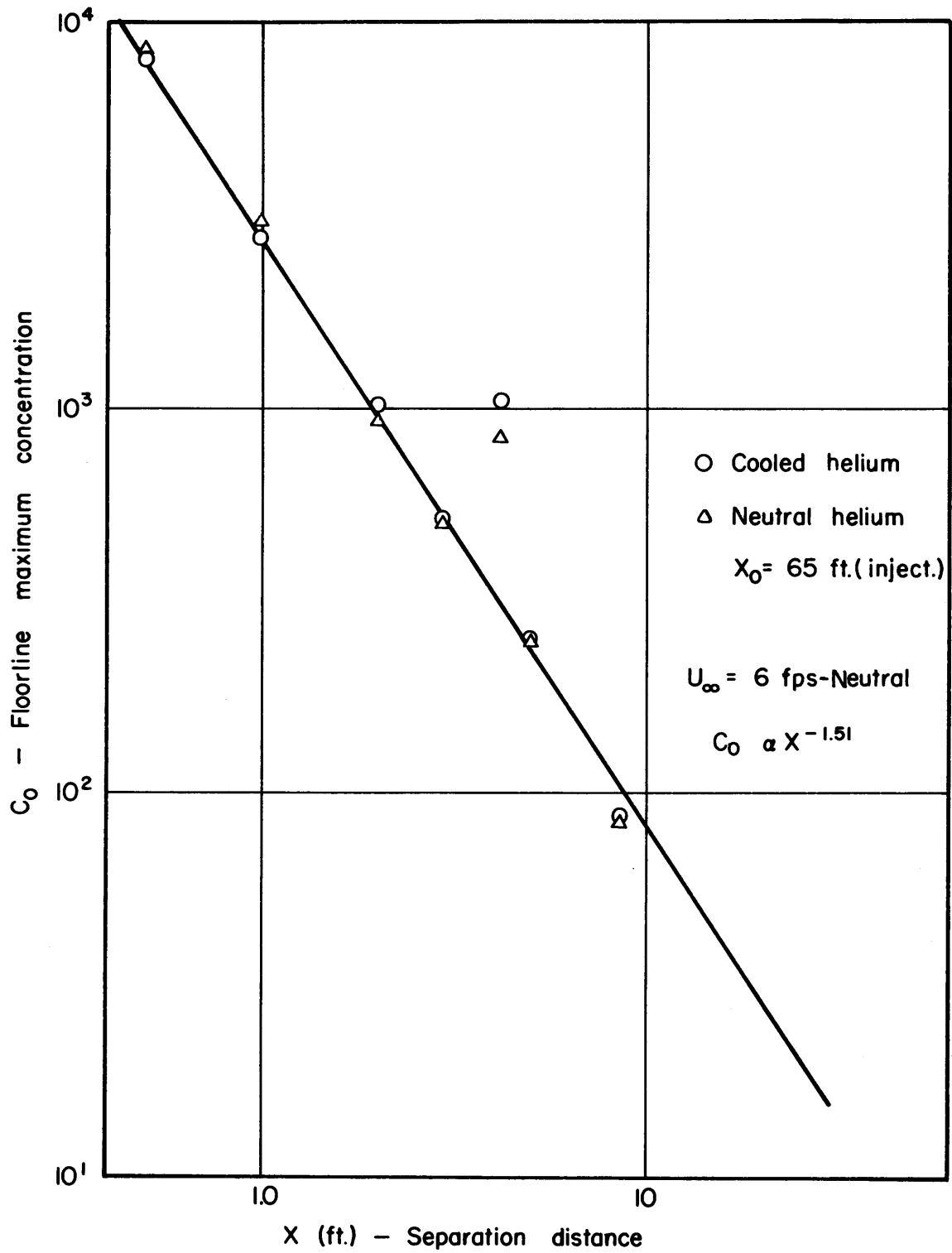
Fig. 66 Floorline concentration (neutral and cooled helium)

167
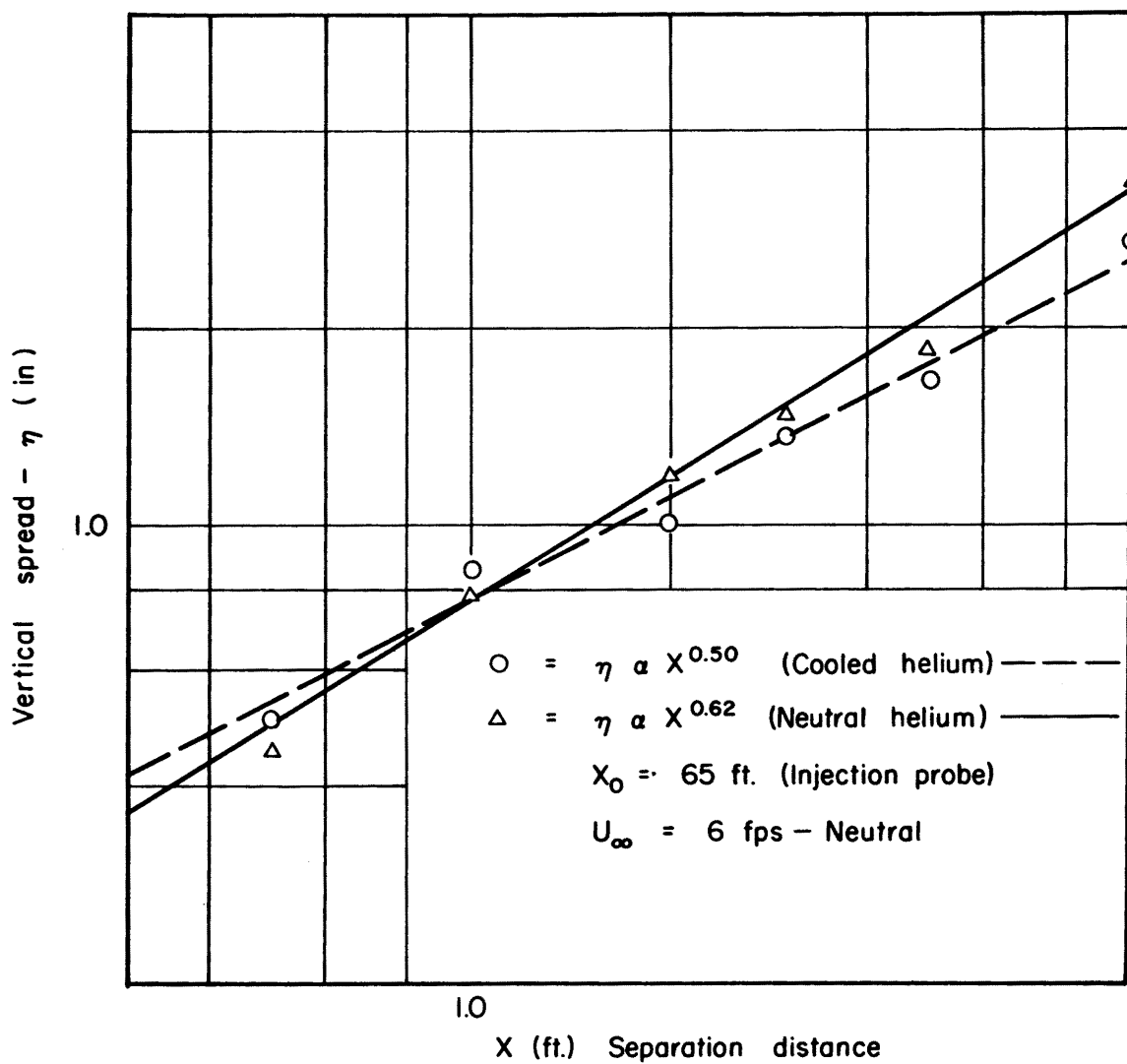
Fig. 67   Vertical spread
(neutral and cooled helium)
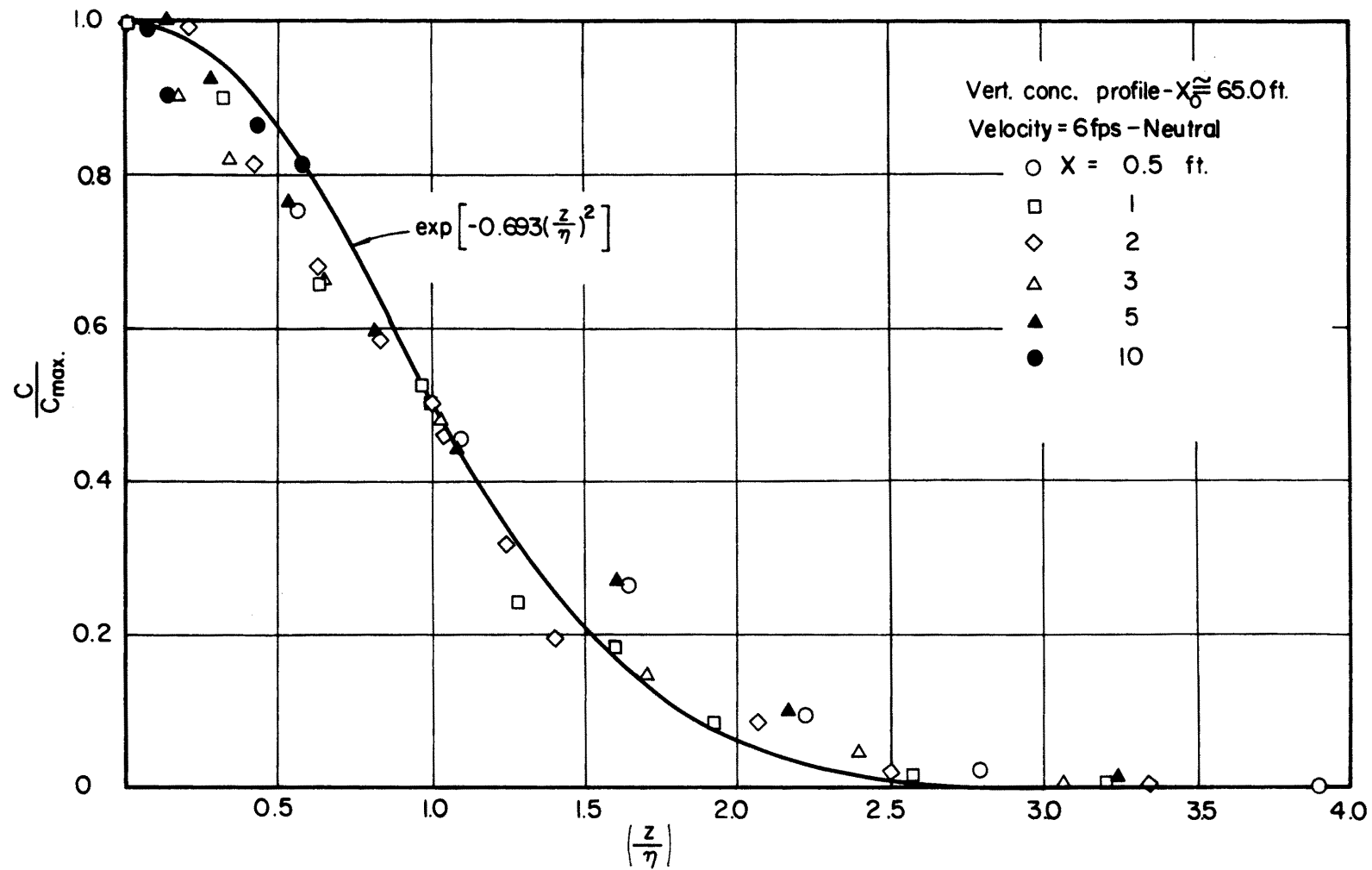
Fig. 68 Normalized vertical concentration profile (neutral helium)
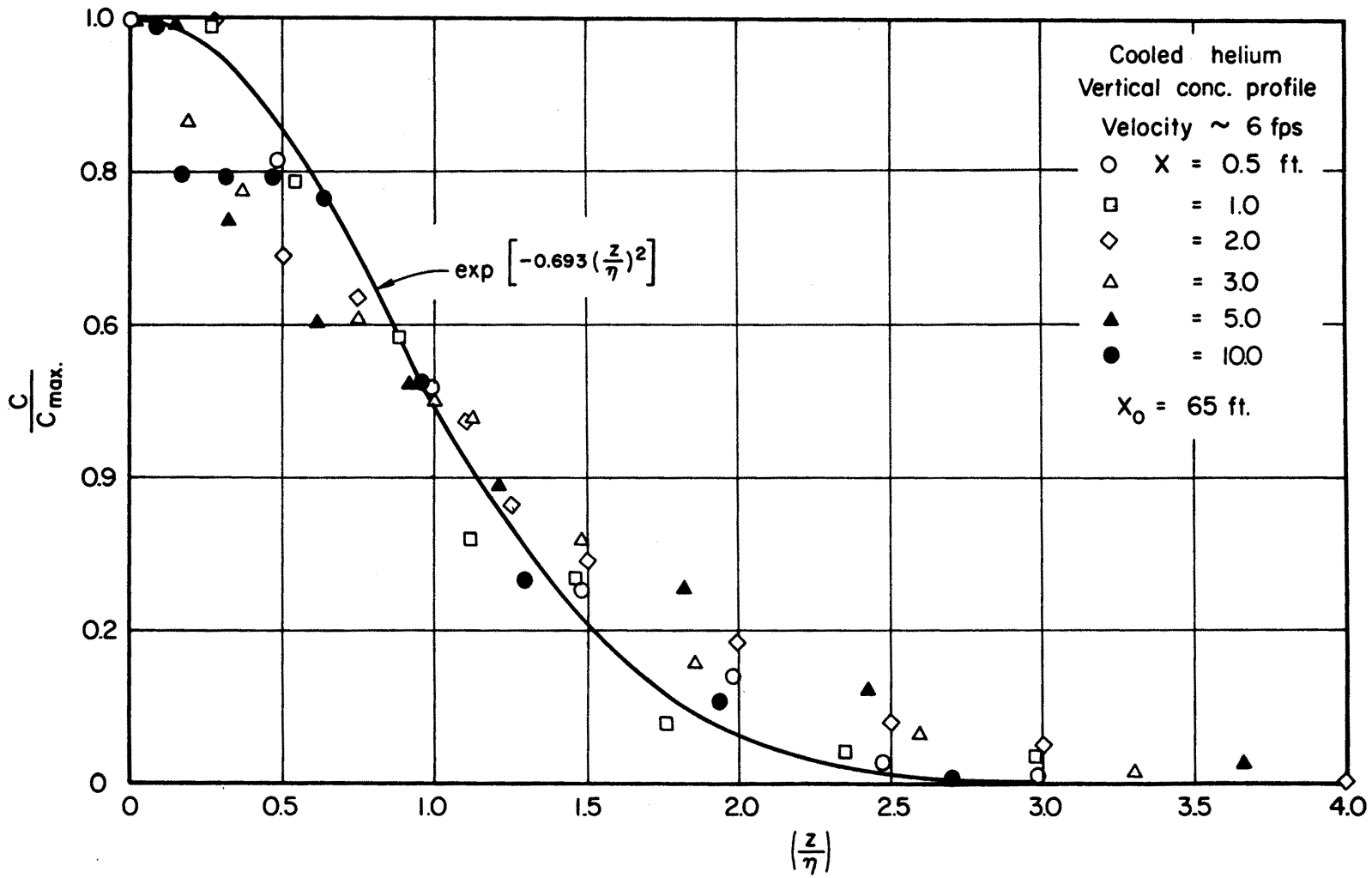
Fig. 69 Normalized vertical concentration profile (cooled helium)
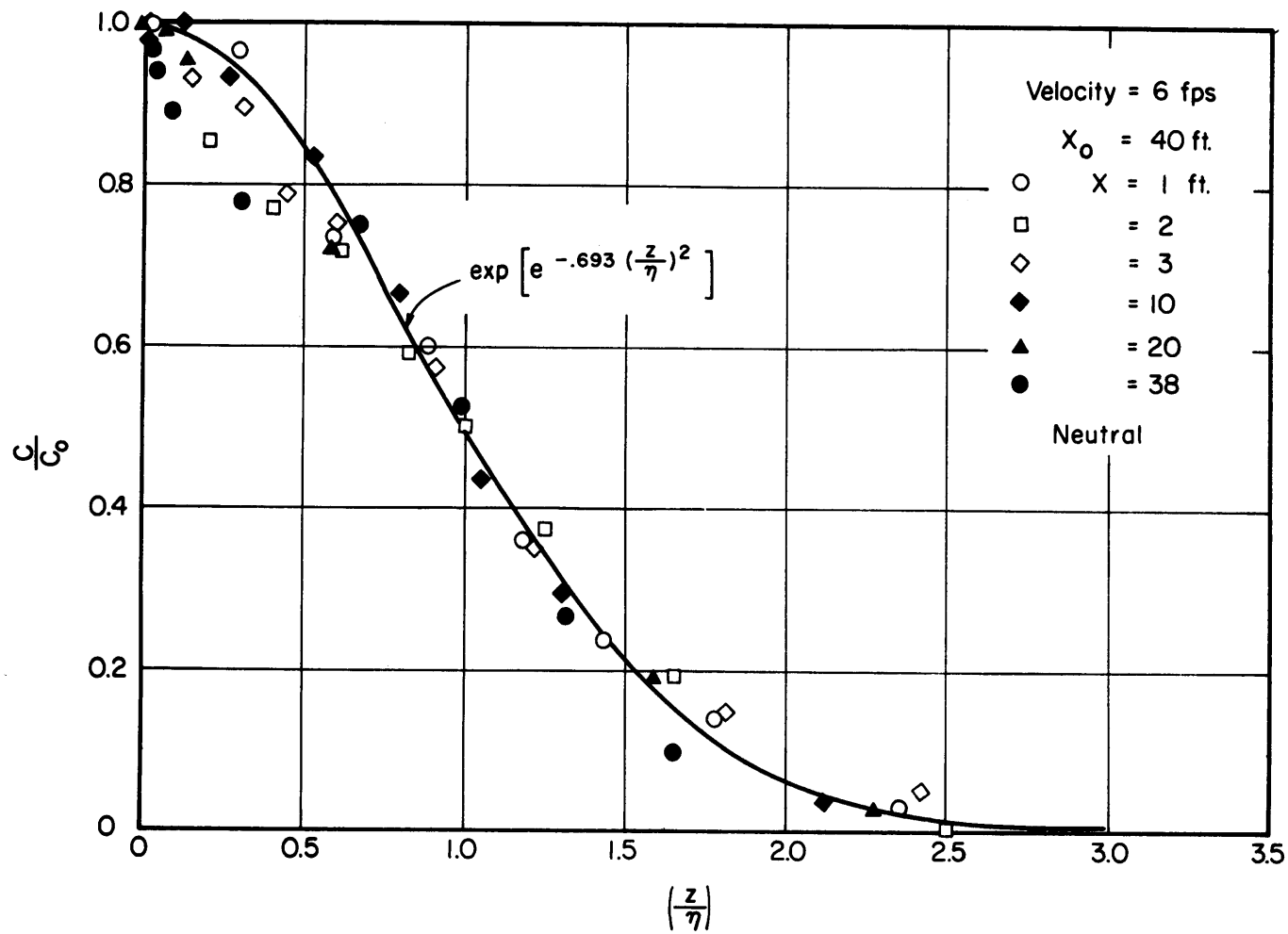
Fig. 70 Normalized vertical concentration profile (u=6fps, neutral)

$$\exp\left[-0.693\left(\tfrac{z}{\eta}\right)^2\right]$$

	X	=	1 ft.
○			
□	=	2	Velocity = 10 fps –
◇	=	3	Neutral
●	=	10	
■	=	20	X_0 = 40 ft.
◆	=	38	
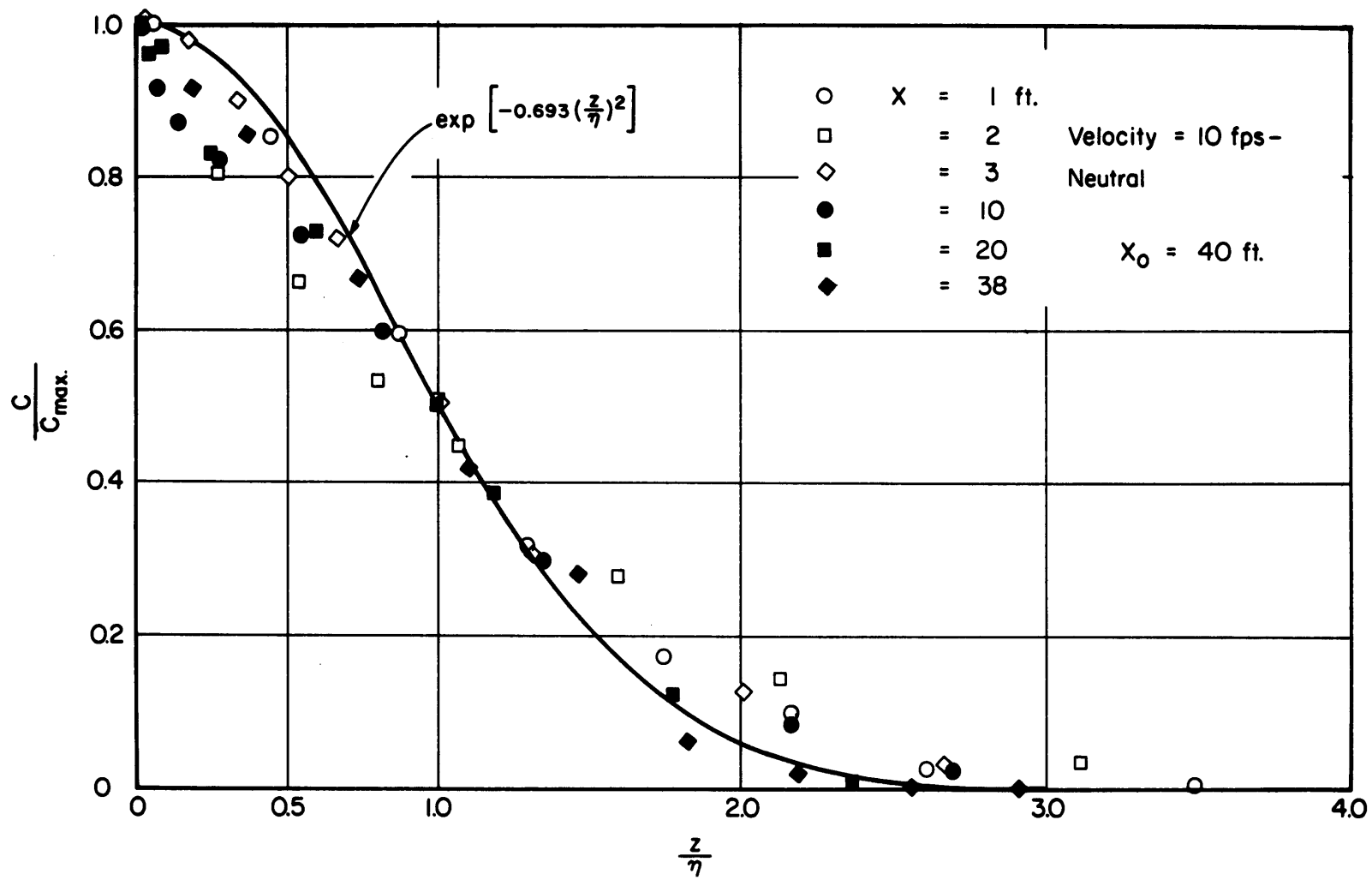
Fig. 71 Normalized vertical concentration profile (10 fps, neutral)
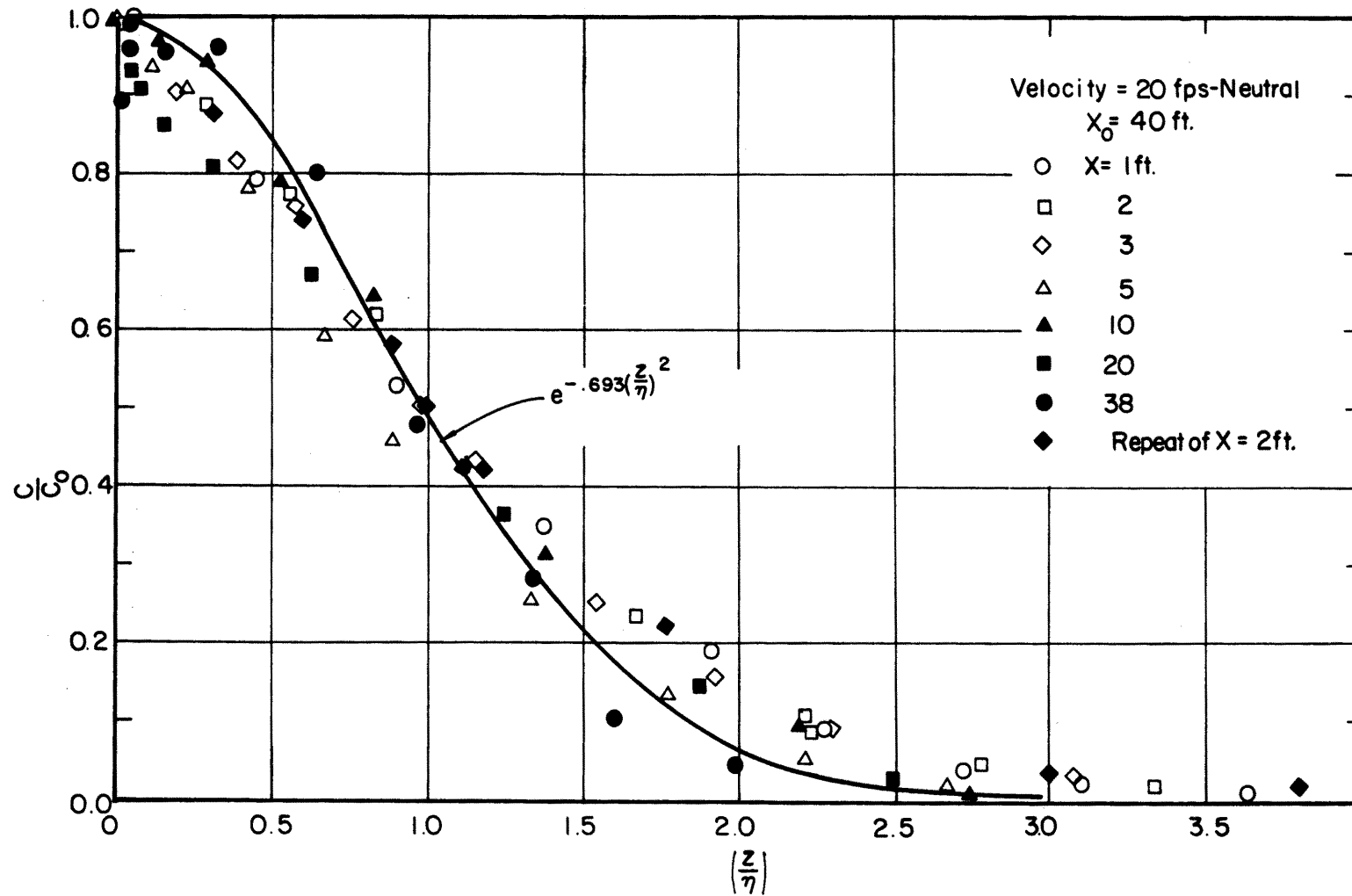
Fig. 72   Normalized vertical concentration profile (20 fps, neutral)
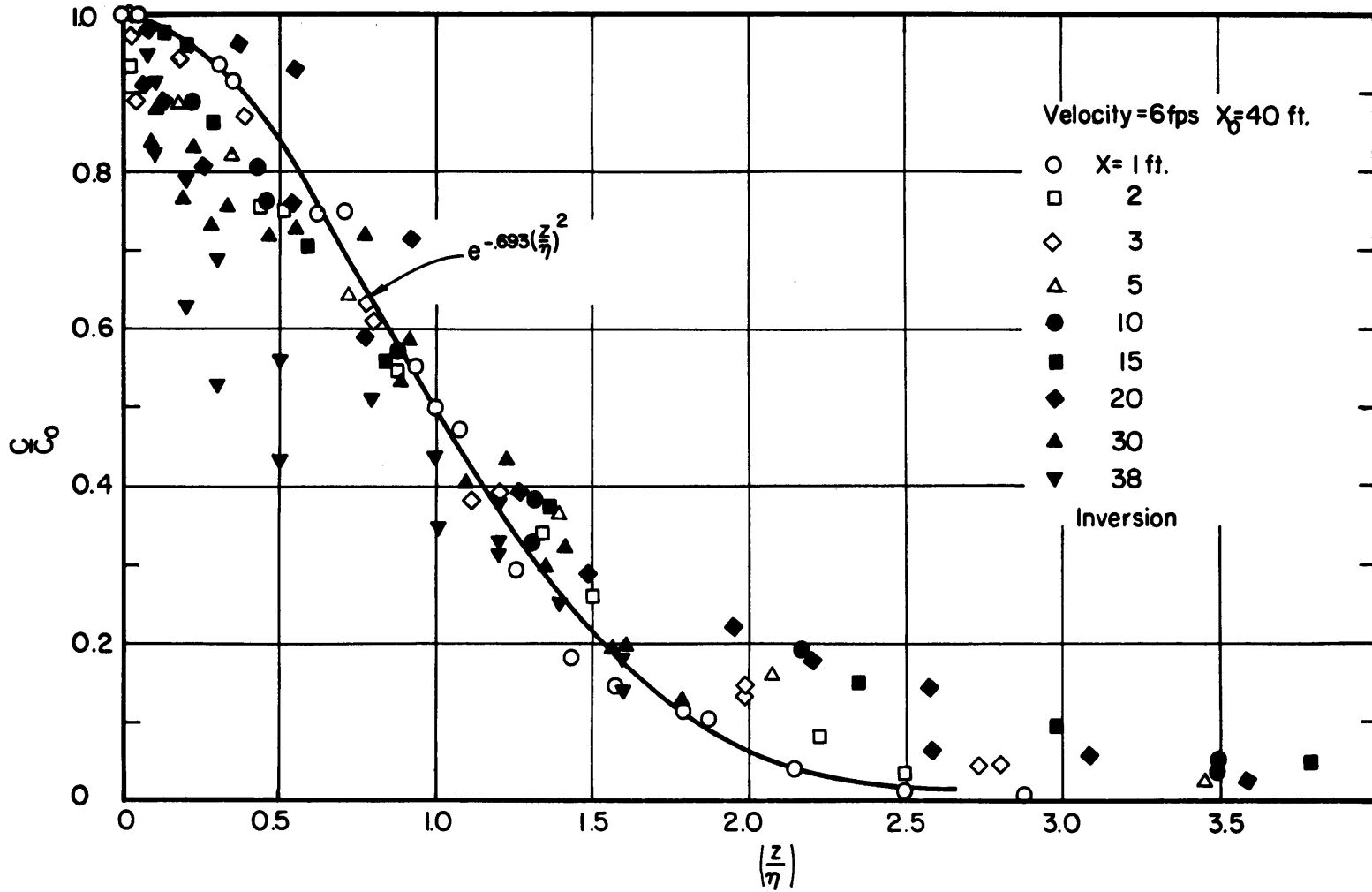
Fig. 73 Normalized vertical concentration profile (6 fps, inversion)
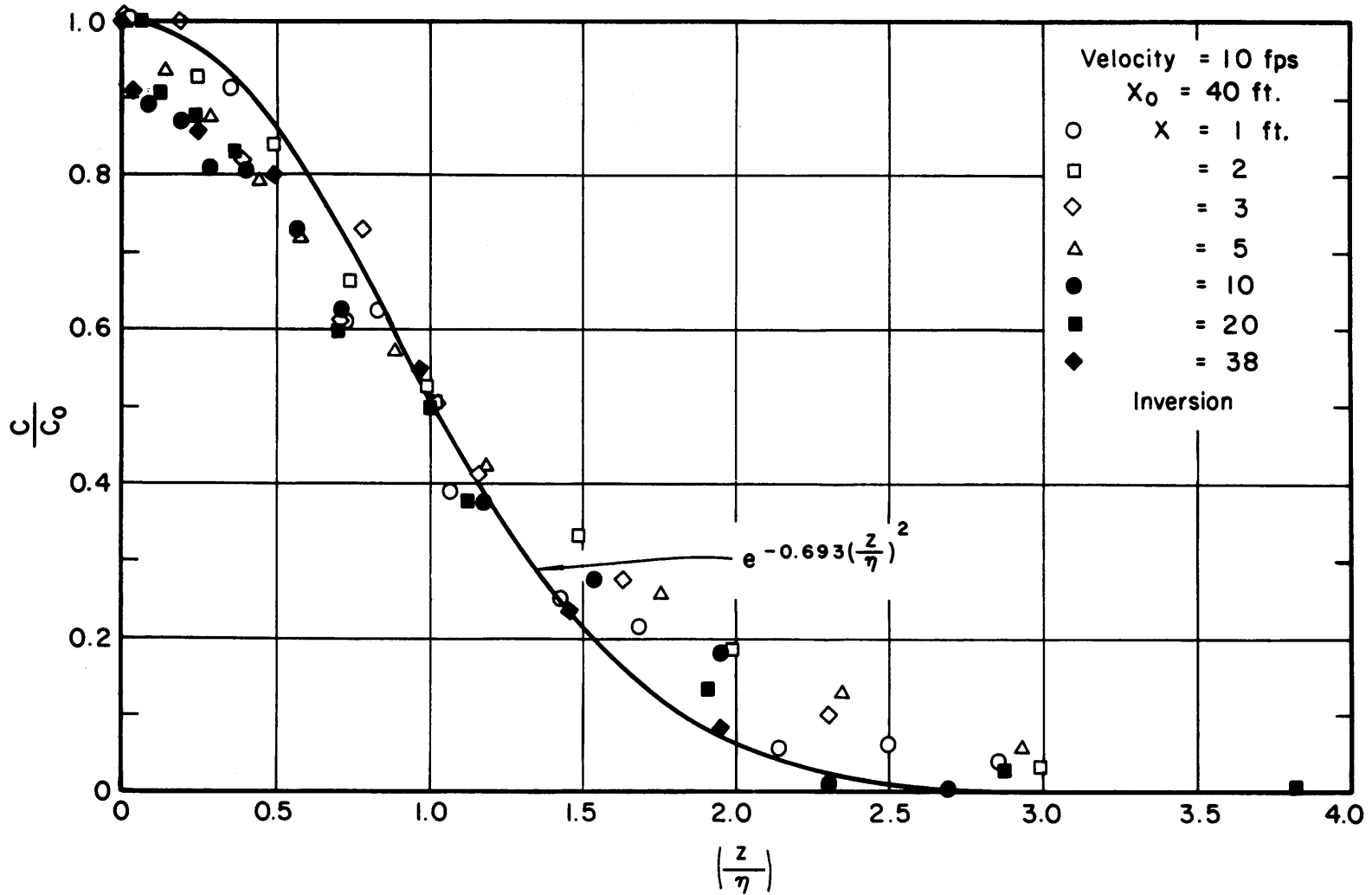
Fig. 74 Normalized vertical concentration profile (10 fps, inversion)
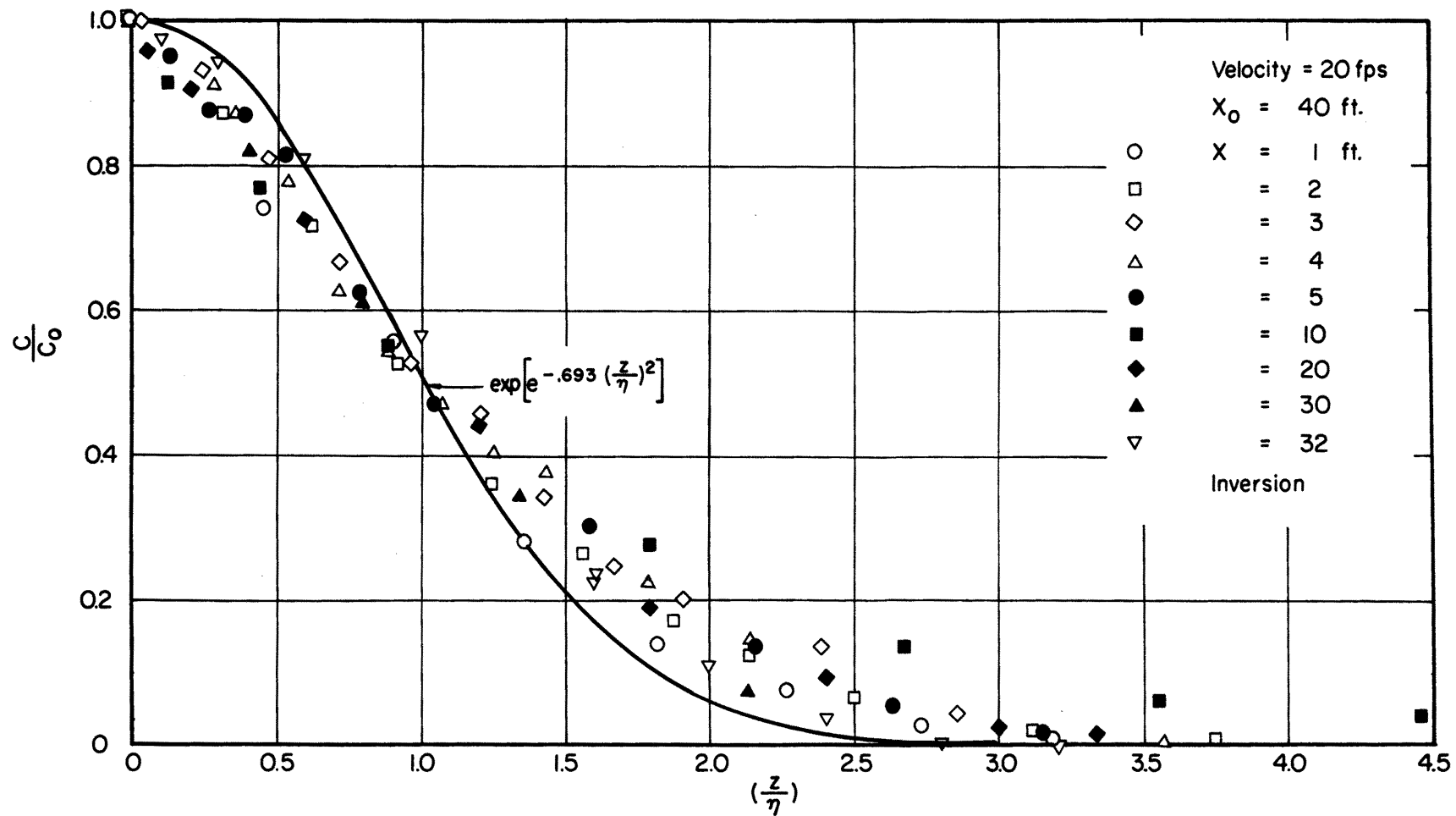
Fig. 75 Normalized vertical concentration profile (20 fps, inversion)
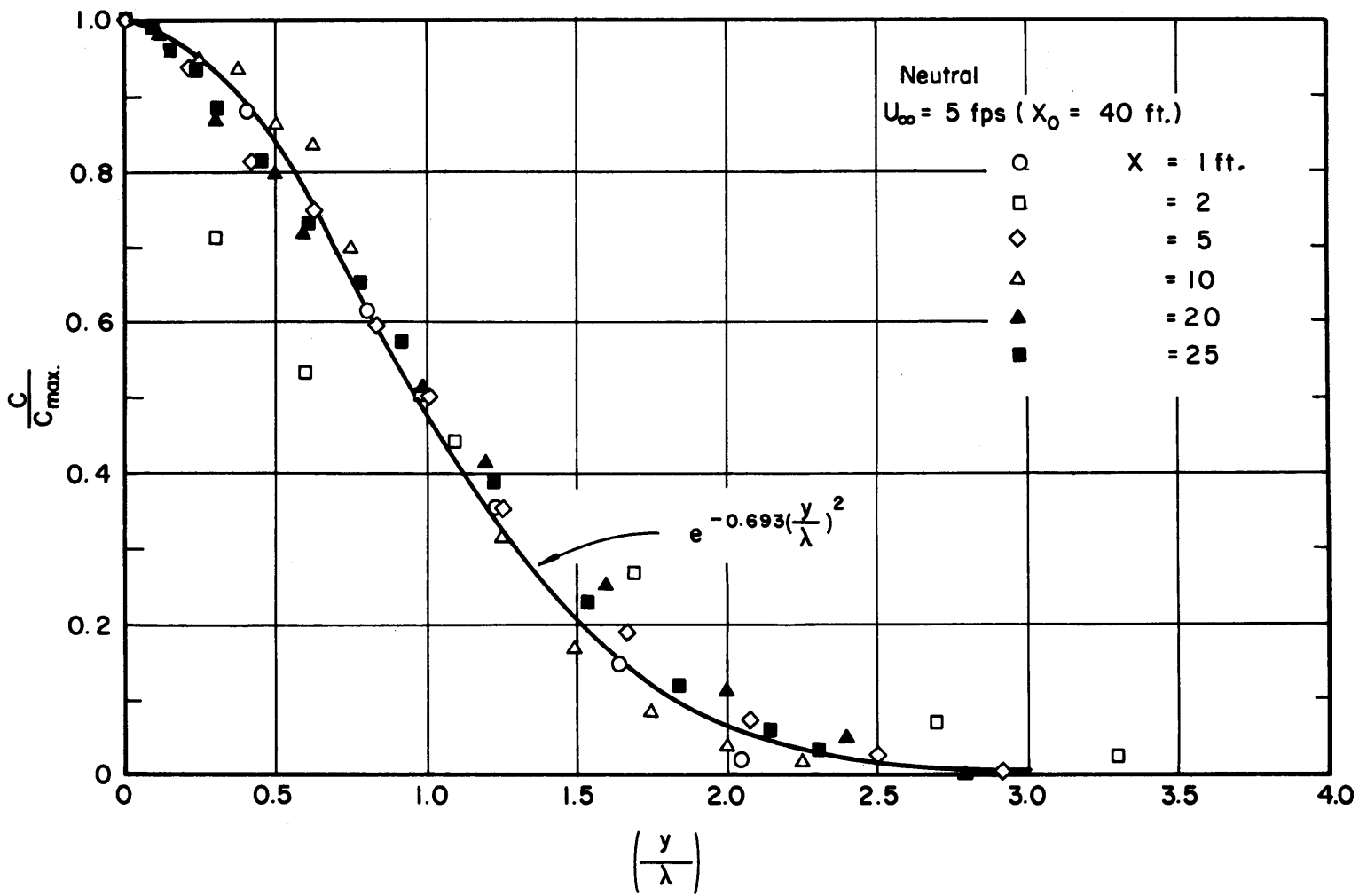
Fig. 76 Normalized horizontal concentration profile (5 fps, neutral)
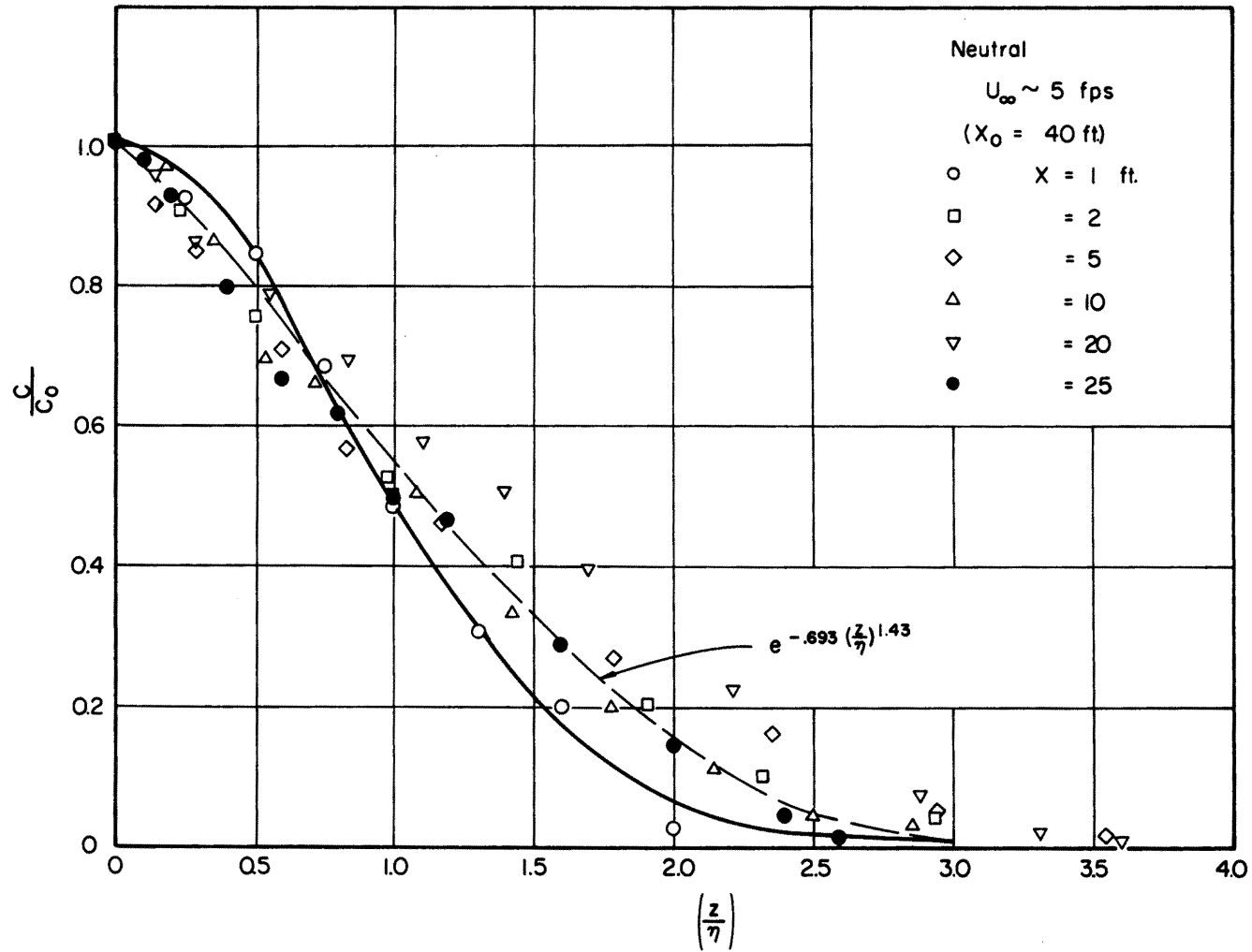
Fig. 77 Normalized vertical concentration profile (5 fps, neutral)
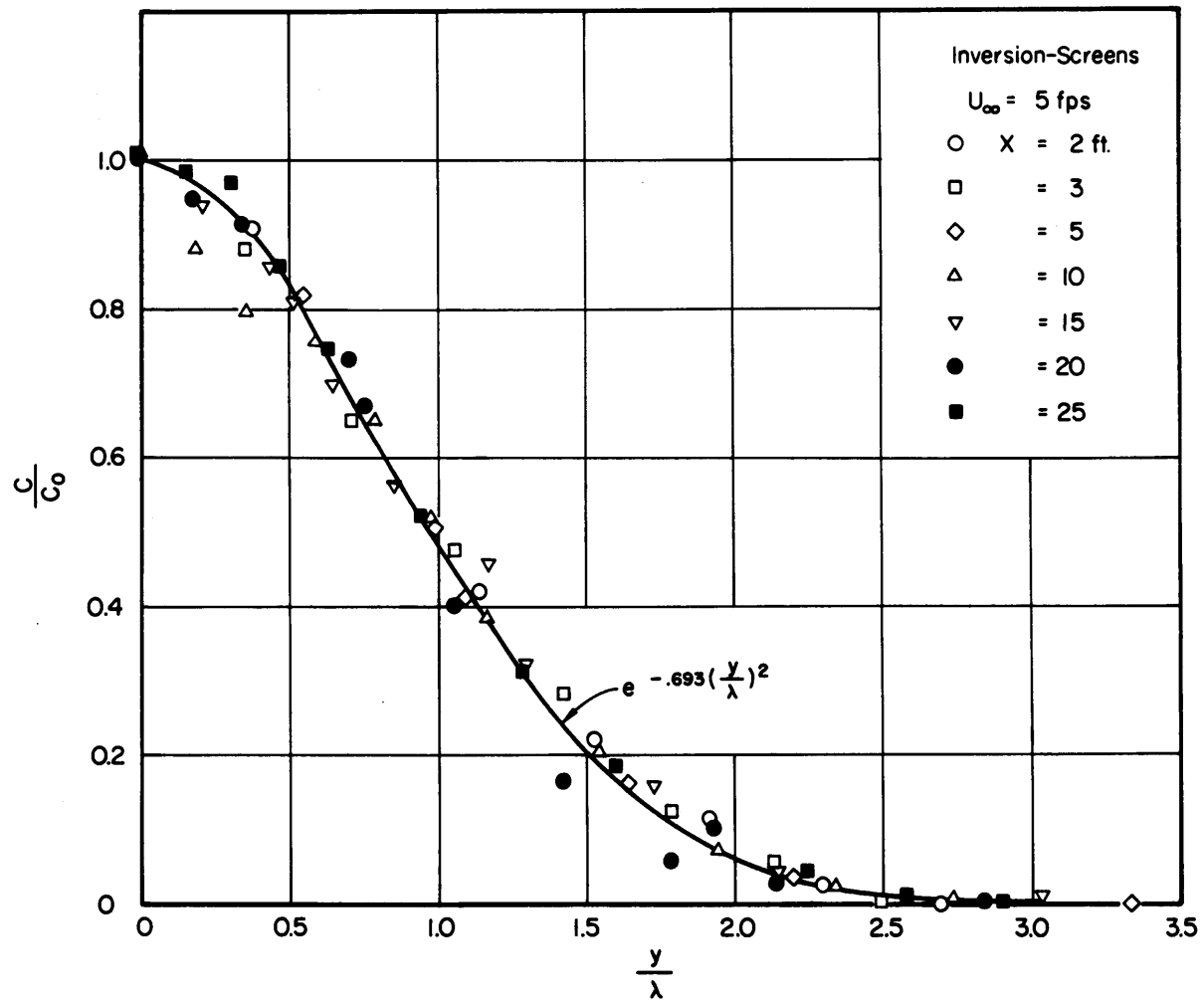
Fig. 78 Normalized horizontal concentration profile (5 fps, inversion)
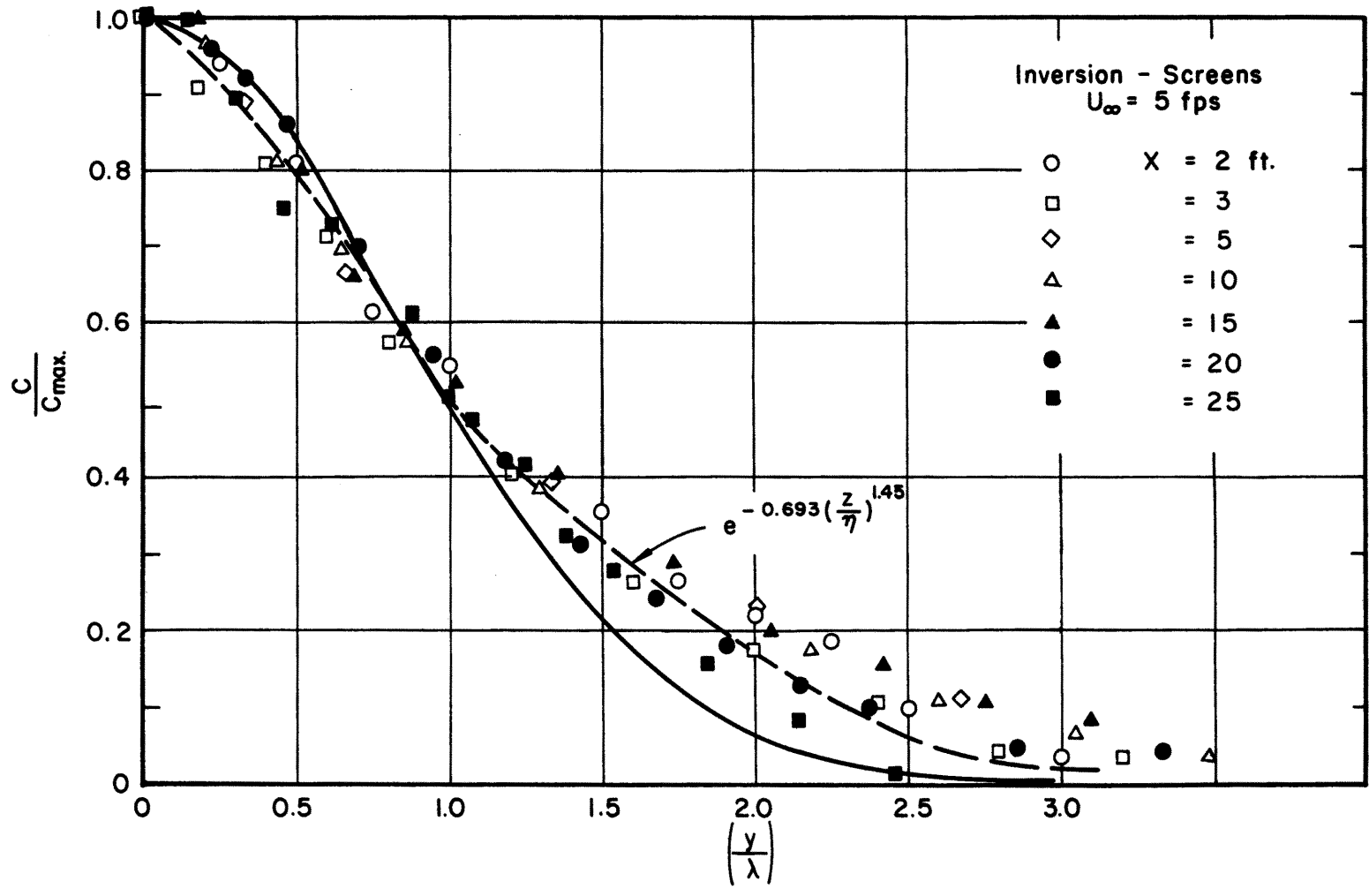
Fig. 79 Normalized vertical concentration profile (5 fps, inversion)
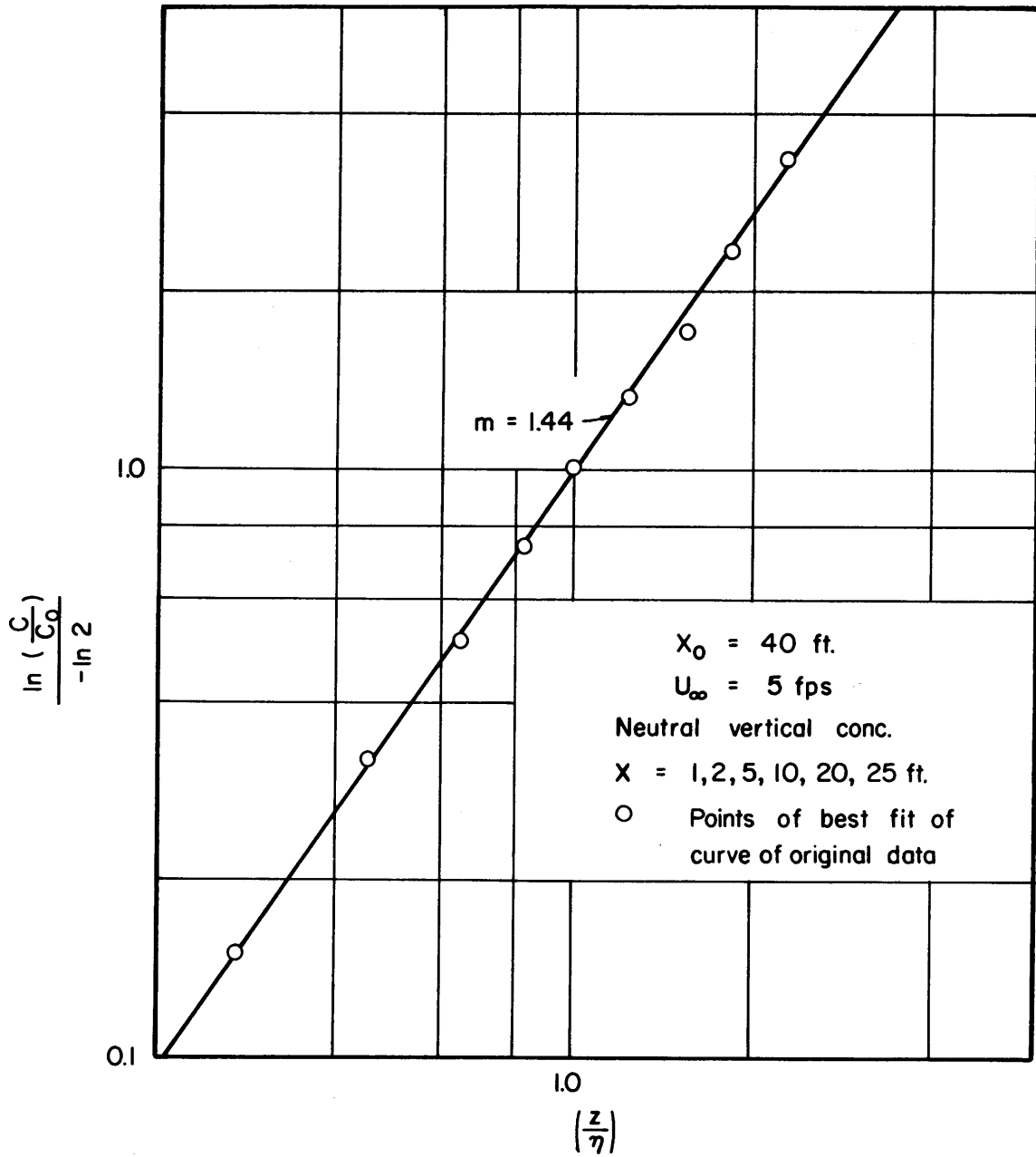
Fig. 80 Determining exponent "m"
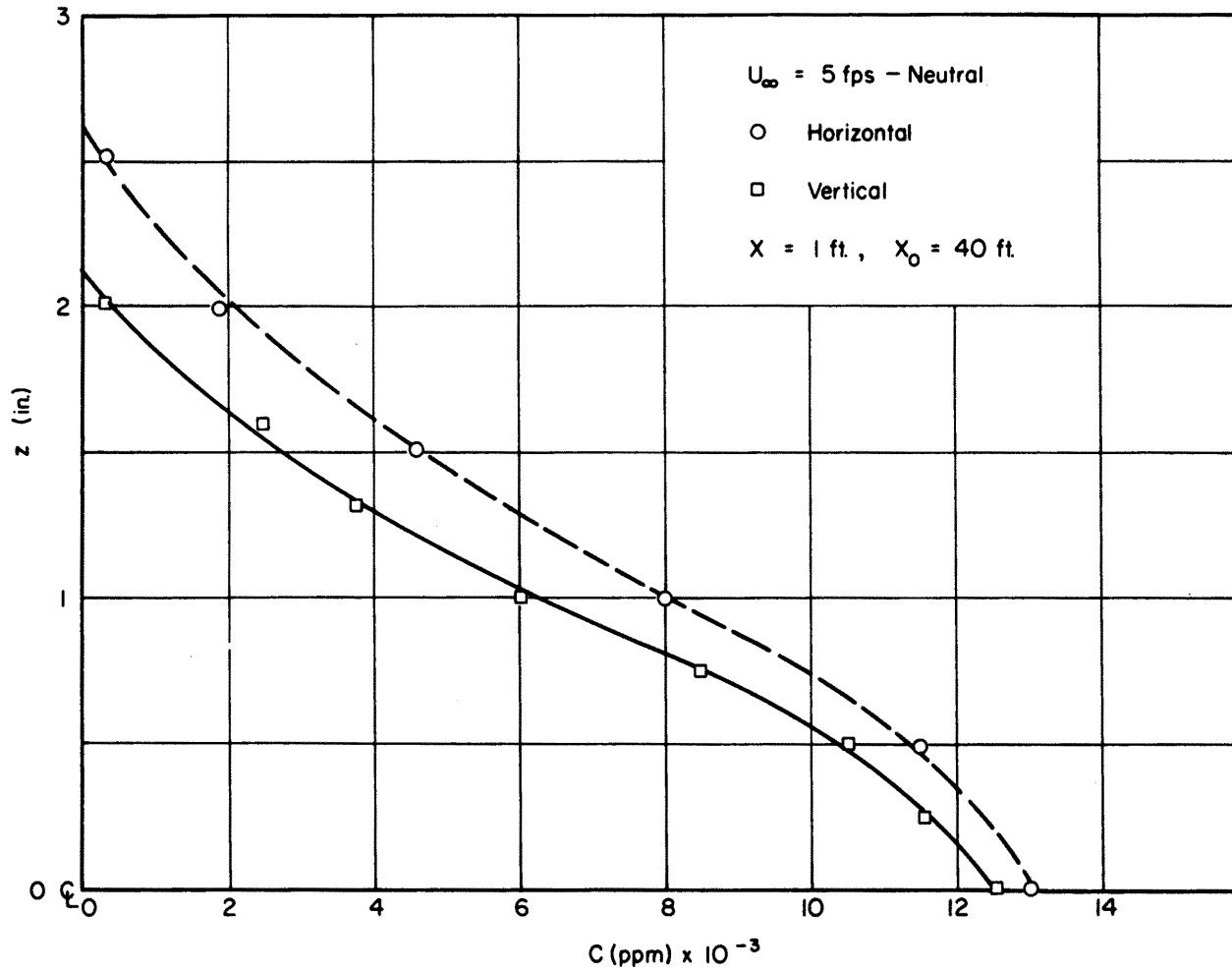
Fig. 81   Horizontal and vertical concentration profiles
(5 fps, neutral, 1 ft)
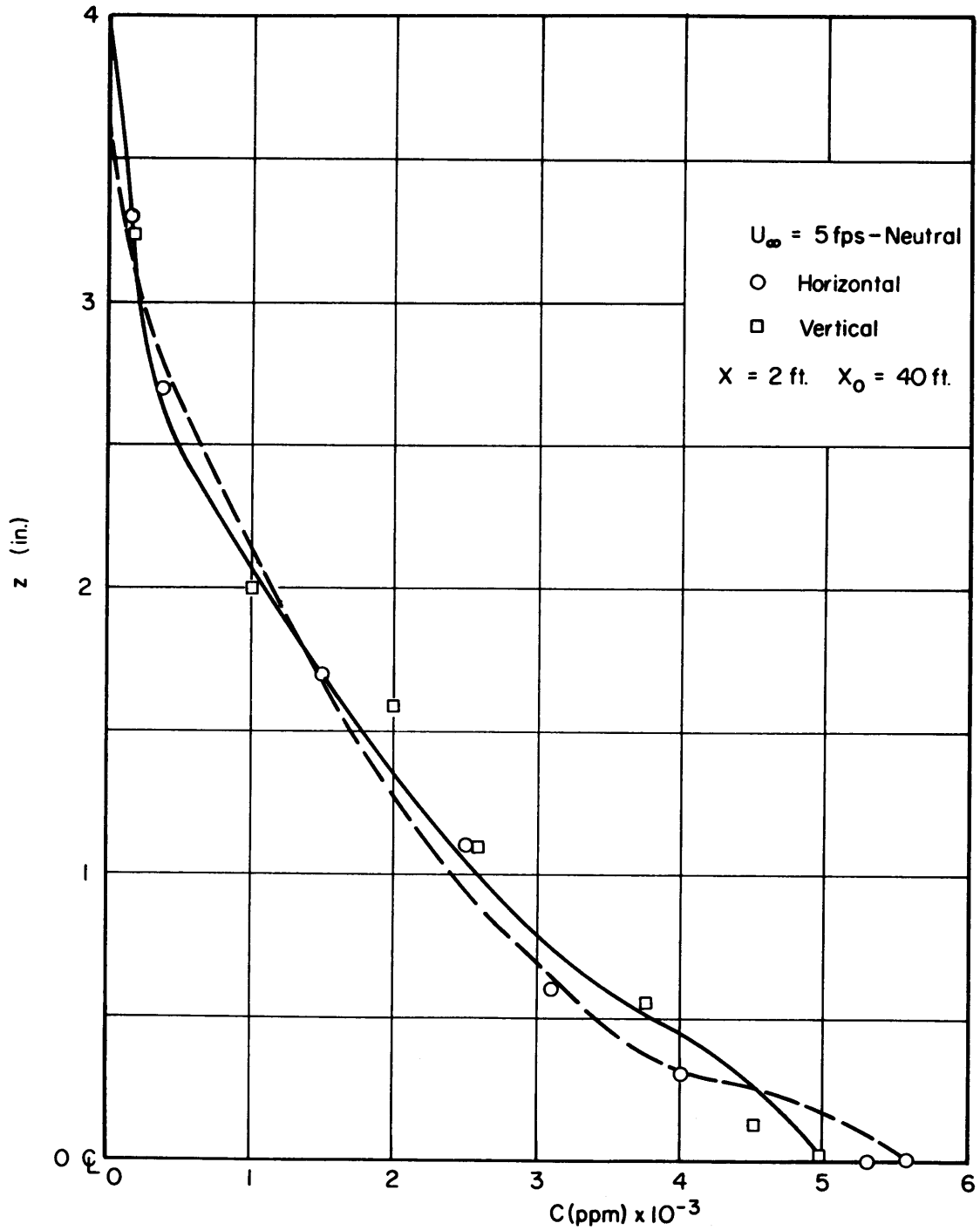
Fig. 82 Horizontal and vertical concentration profiles
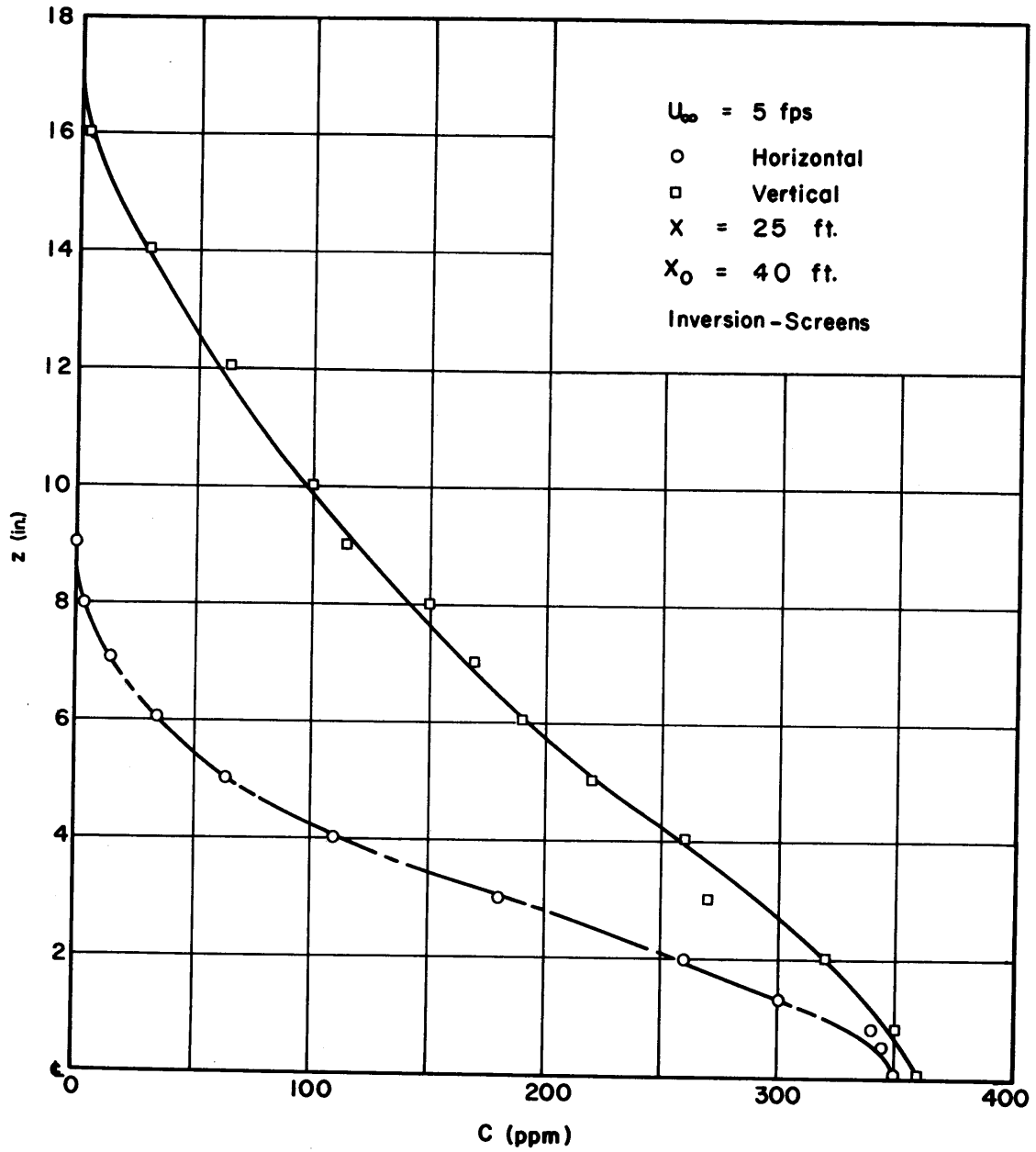(5 fps, neutral, 2 ft)
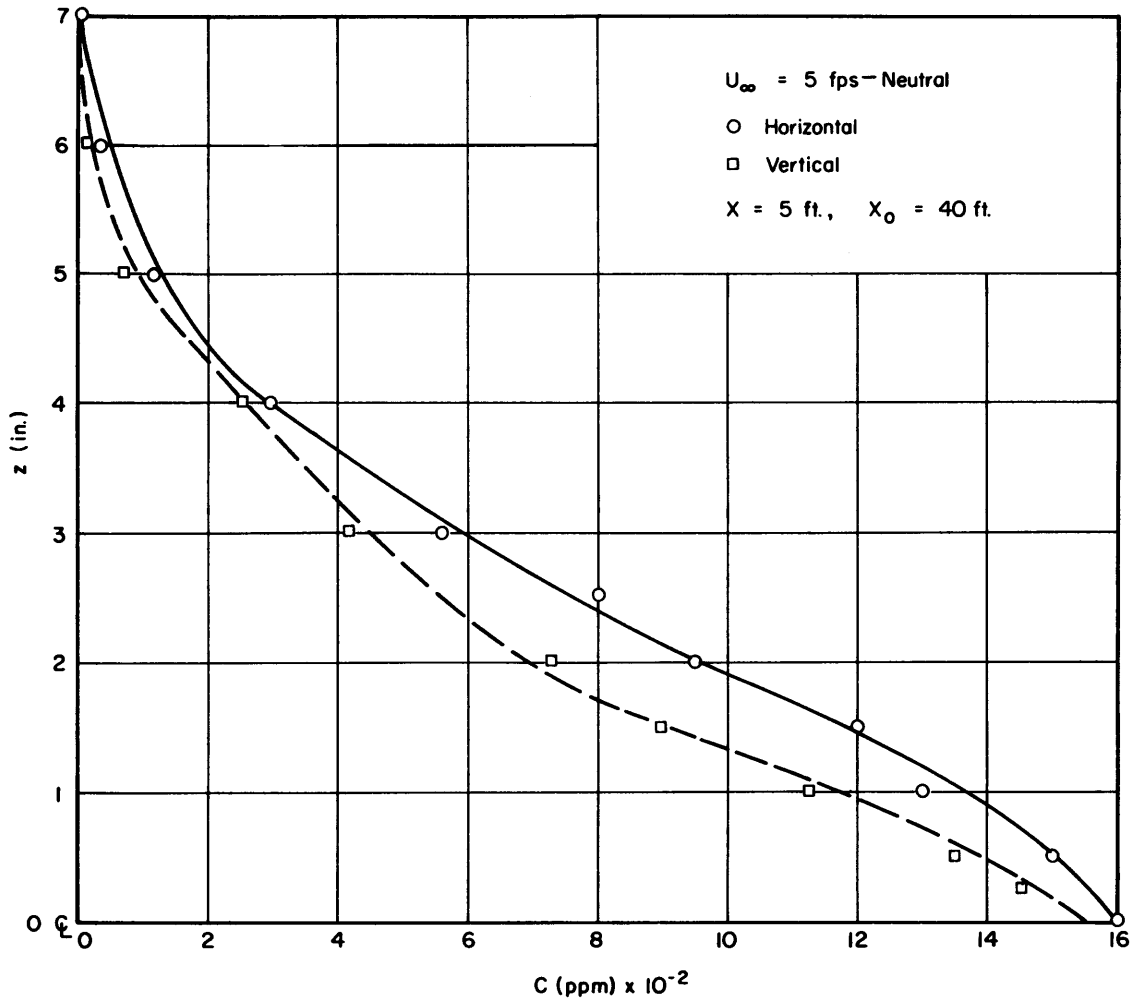
Fig. 83 Horizontal and vertical concentration profiles
(5 fps, neutral, 5 ft)
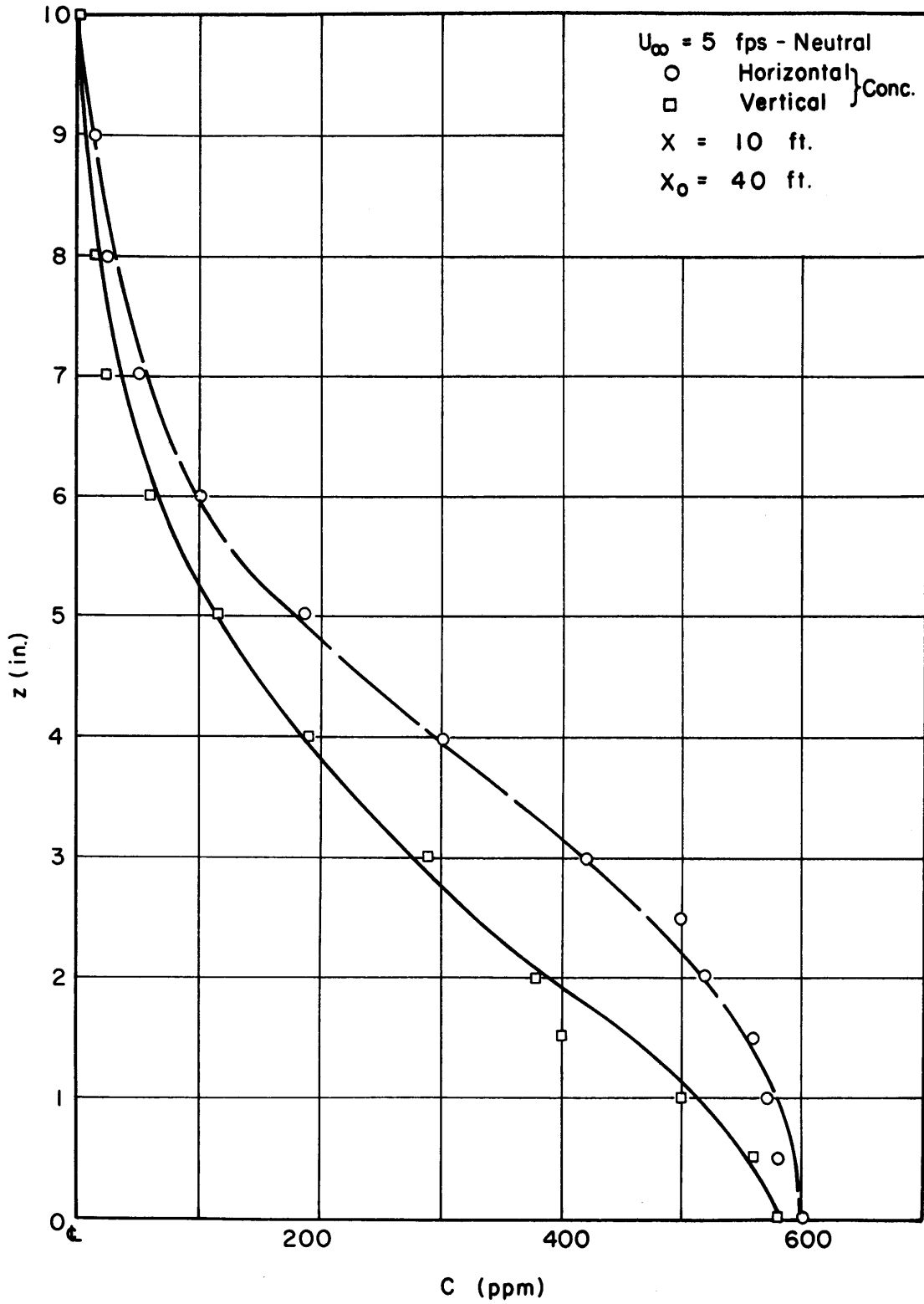
Fig. 84 Horizontal and vertical concentration profiles
(5 fps, neutral, 5 ft)
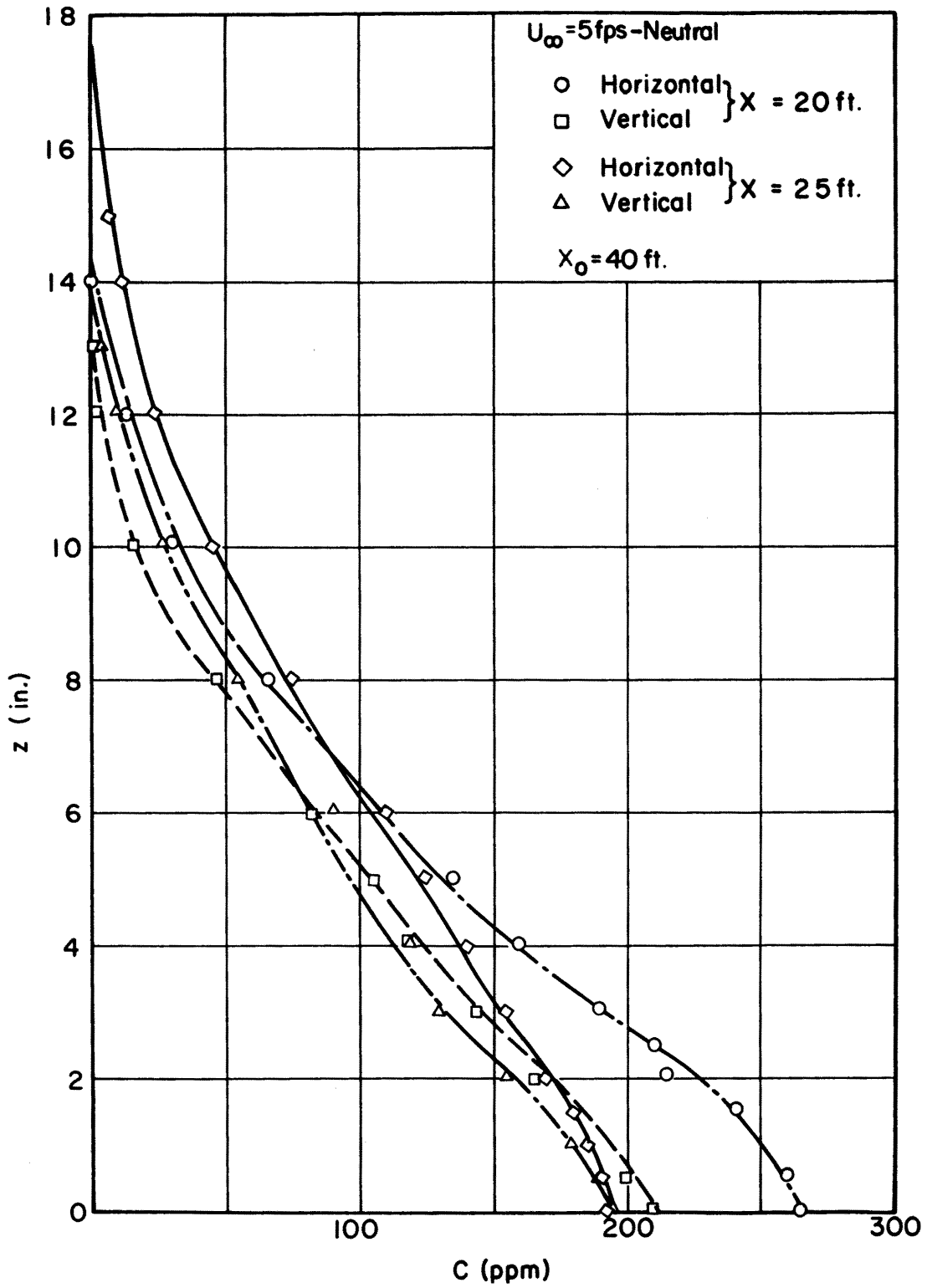
Fig. 85 Horizontal and vertical concentration profiles
(5 fps, neutral, 10 ft)
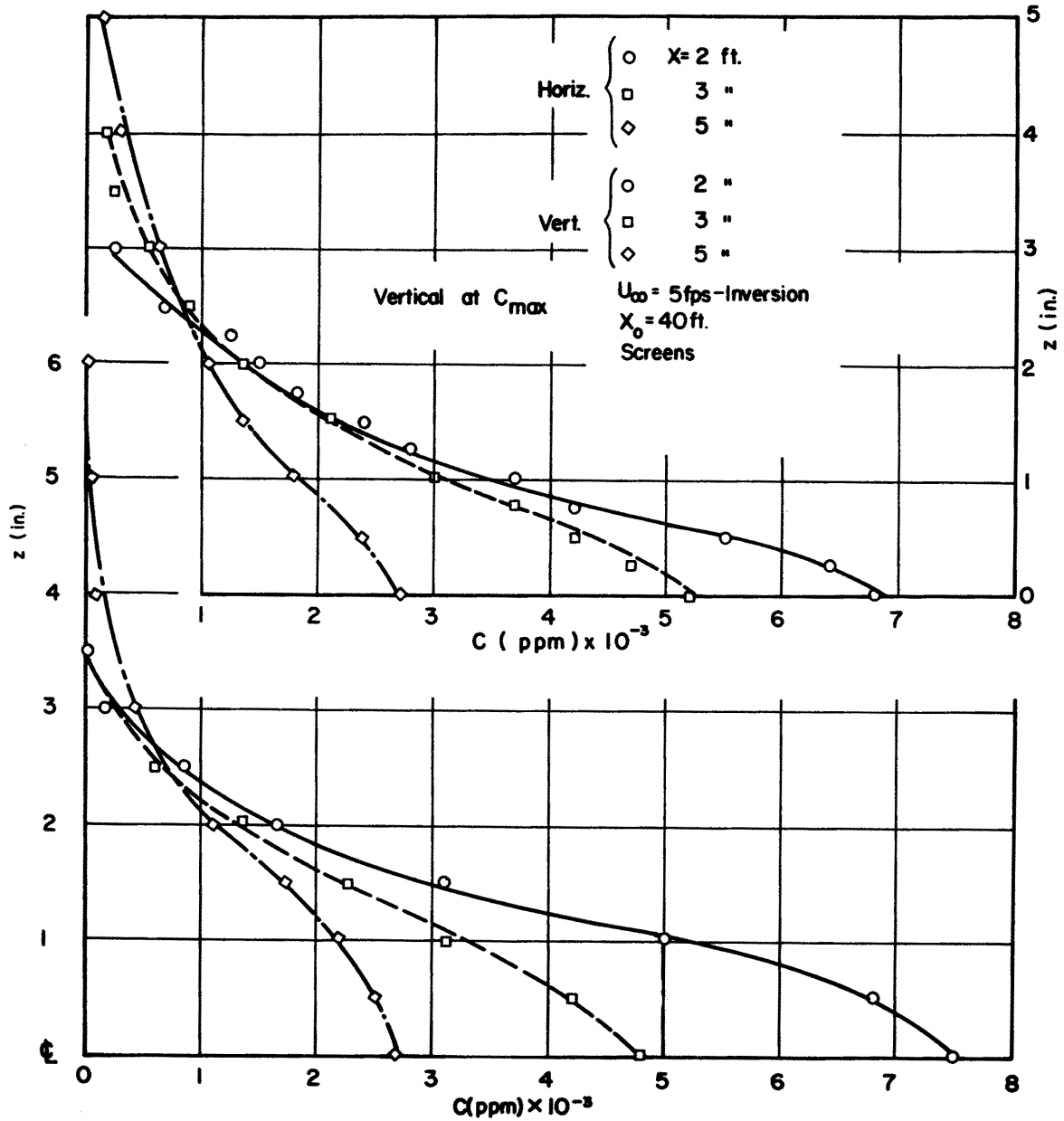
Fig. 86   Vertical concentration profiles (5 fps, stable,
           2, 3, and 5 ft) - (Top figure)

Fig. 87   Horizontal concentration profiles (5 fps,
           stable, 2, 3, and 5 ft) - (Bottom figure)
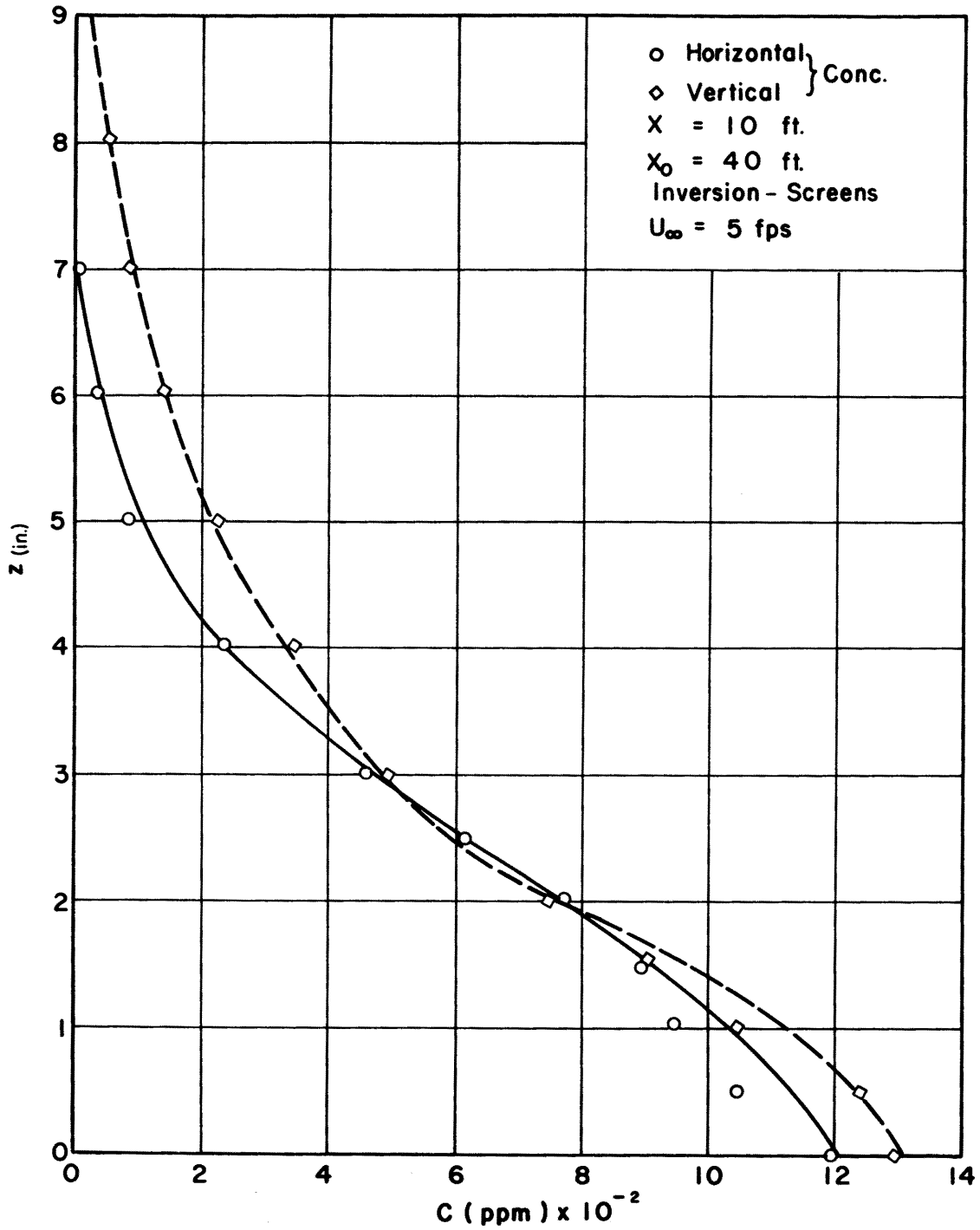
Fig. 88   Horizontal and vertical concentration profiles
(5 fps, stable, 10 ft)
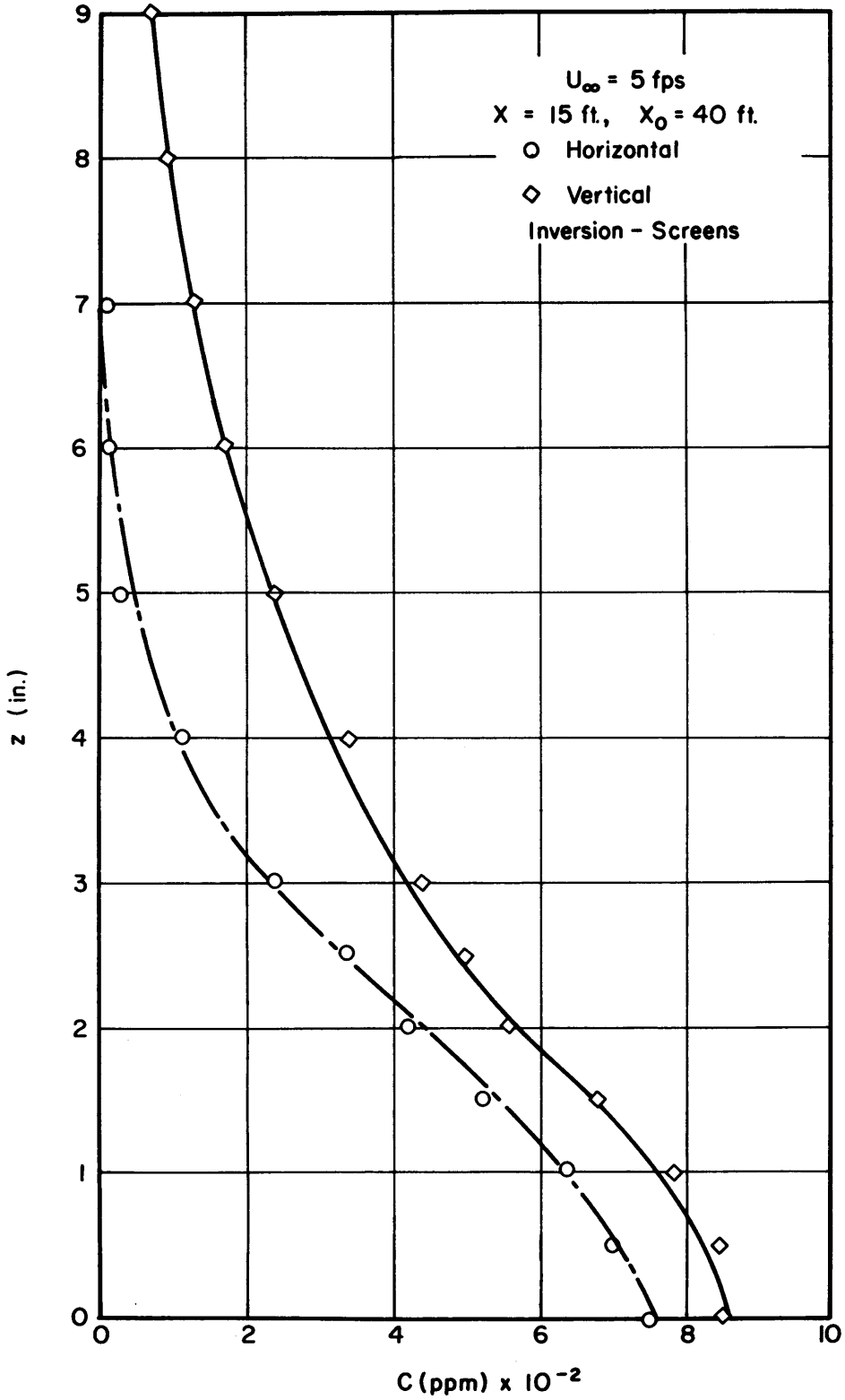
Fig. 89 Horizontal and vertical concentration profiles
(5 fps, stable, 15 ft)
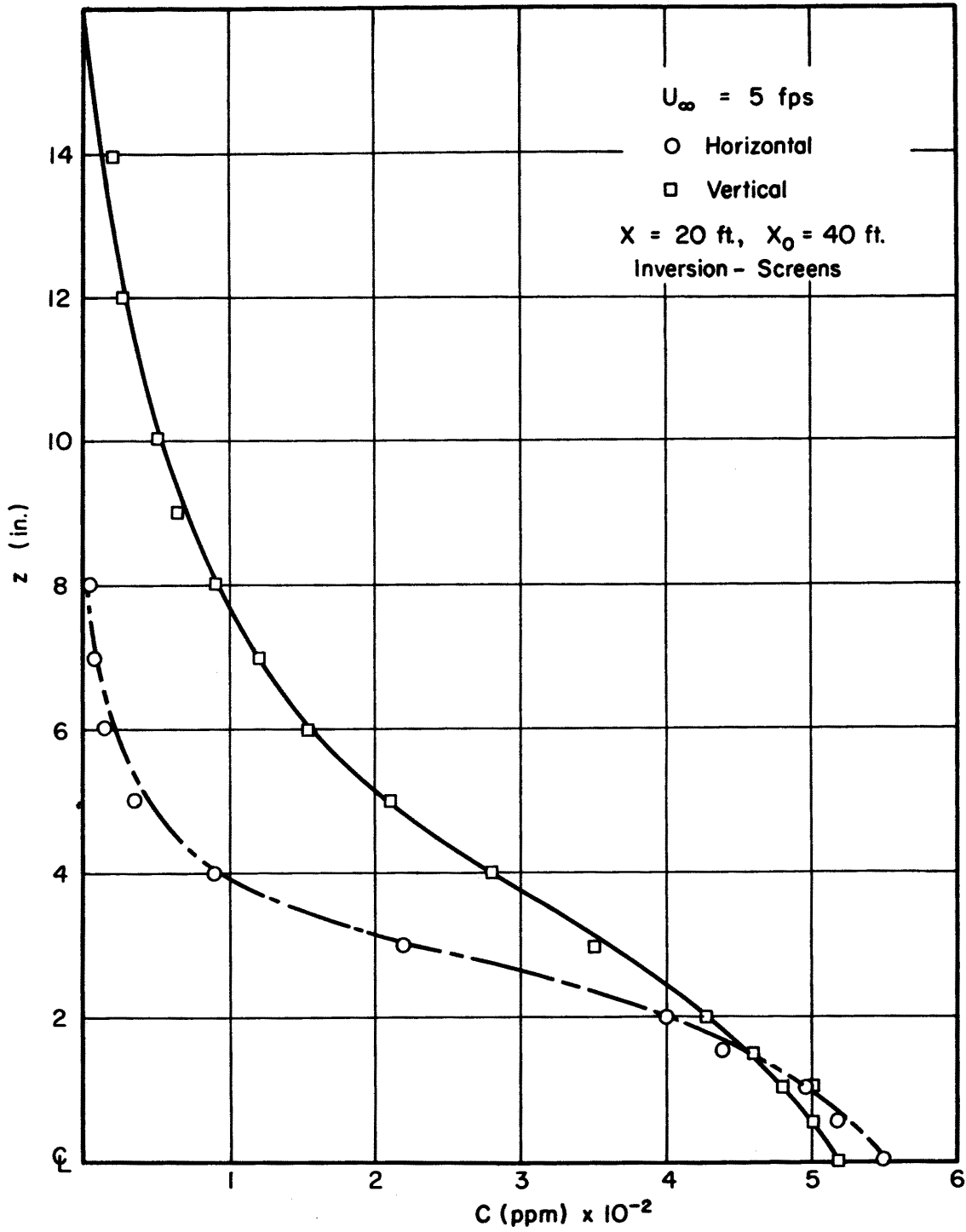
Fig. 90 Horizontal and vertical concentration profiles
(5 fps, stable, 20 ft)

Fig. 91   Horizontal and vertical concentration profiles
          (5 fps, stable, 25 ft)
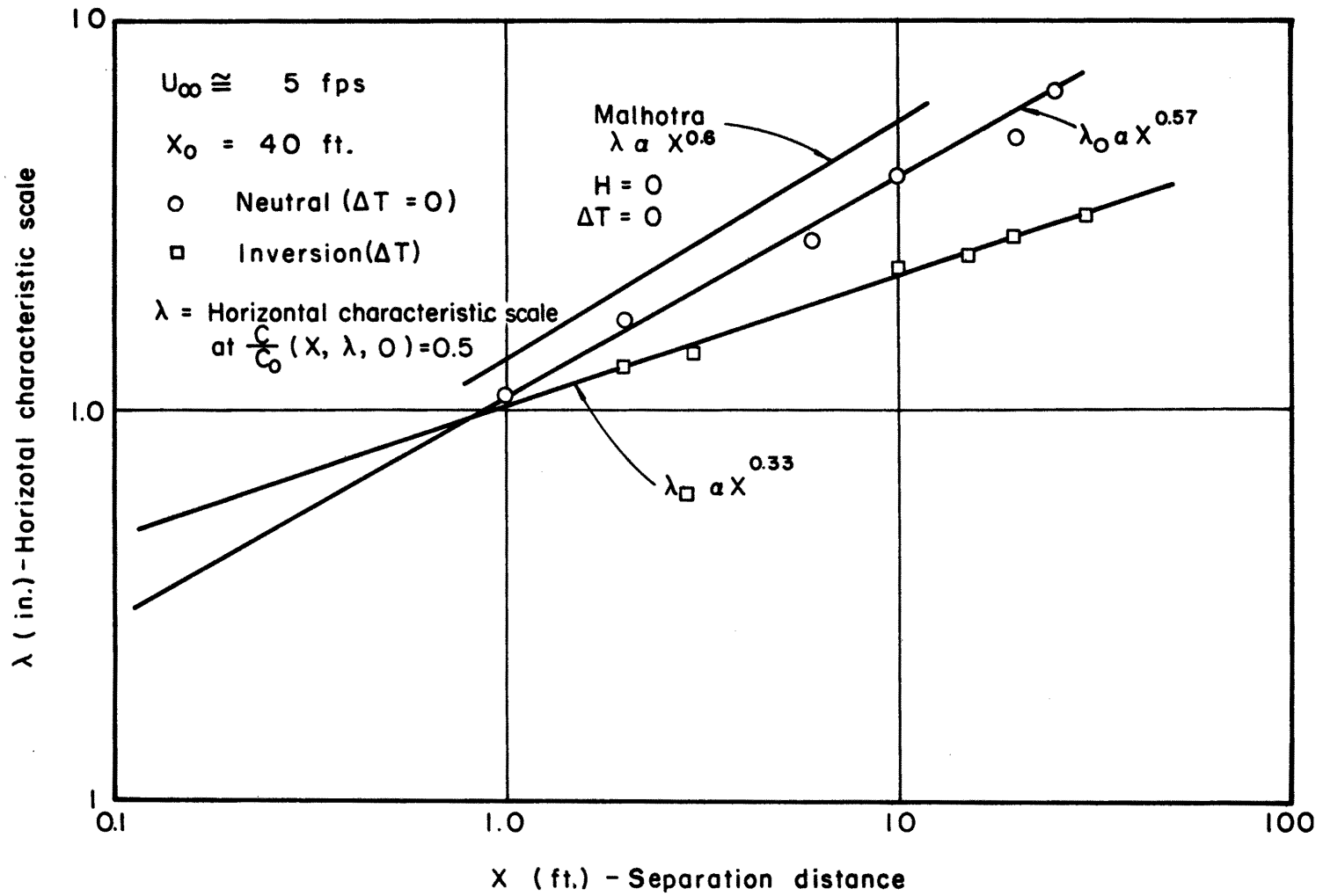
Fig. 92 Horizontal spread (5 fps, neutral and stable)
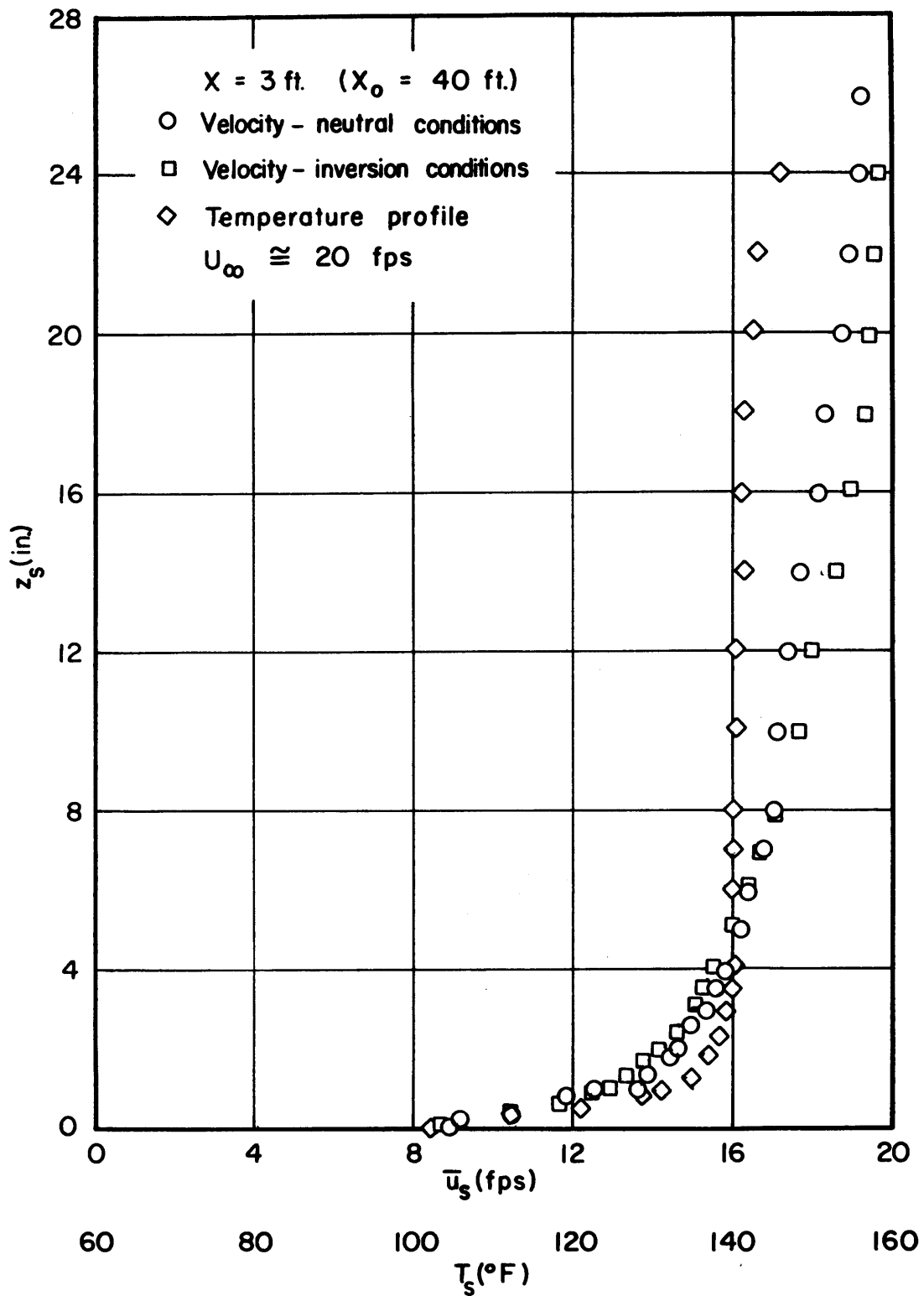
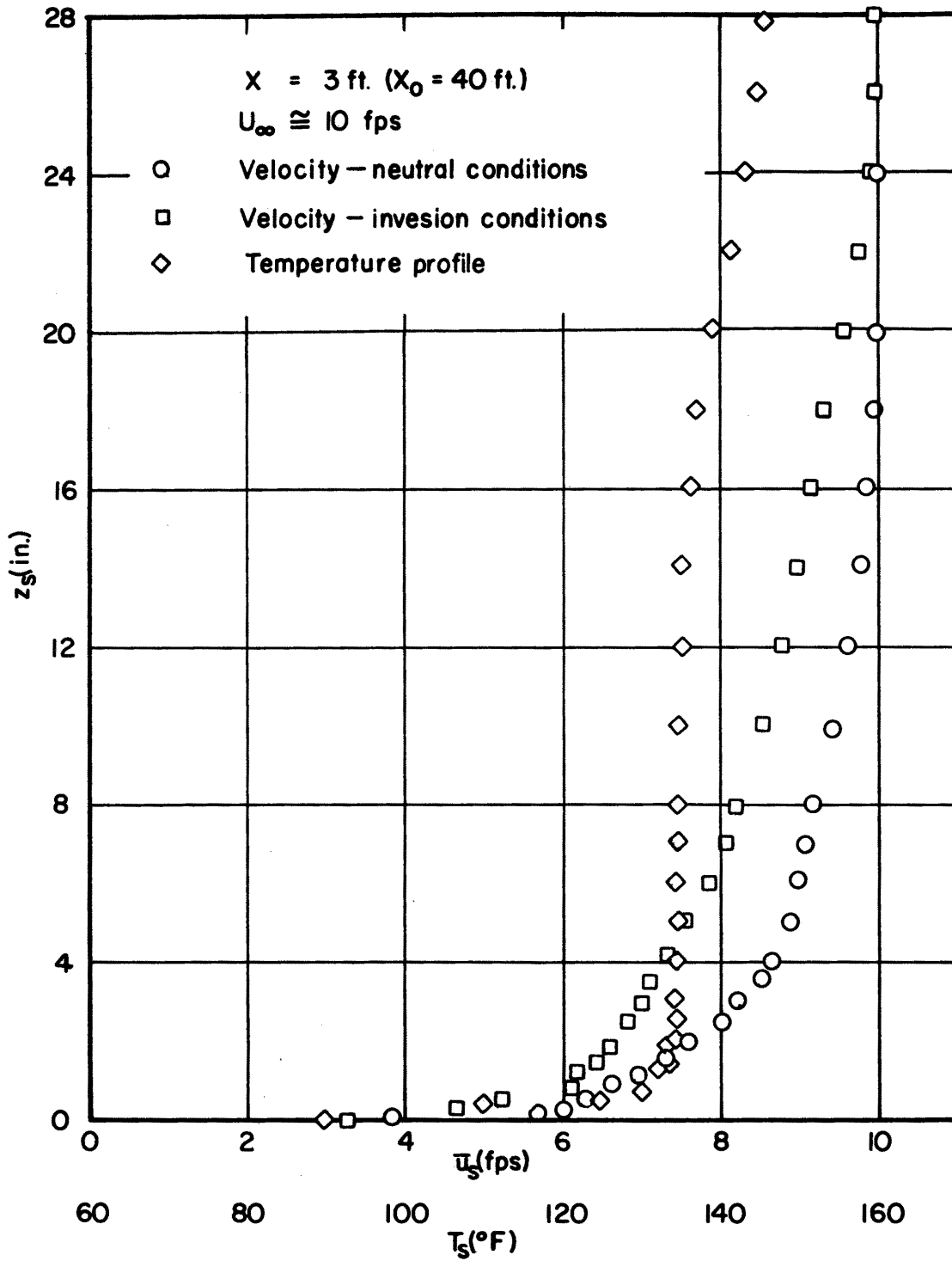Fig. 93 Velocity and temperature profiles (20 fps, x=3ft)
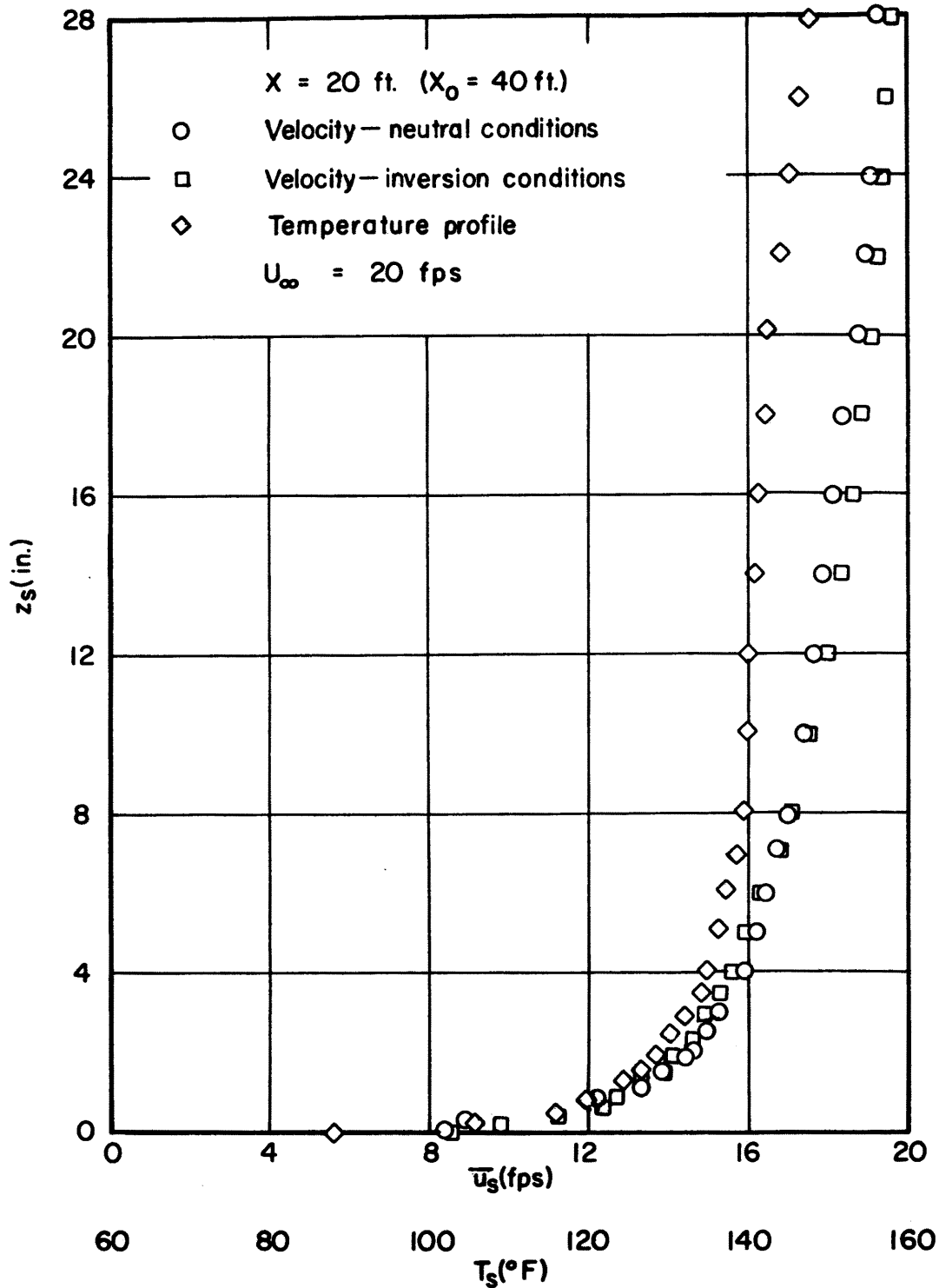
Fig. 94 Velocity and temperature profiles (20 fps, 20 ft)

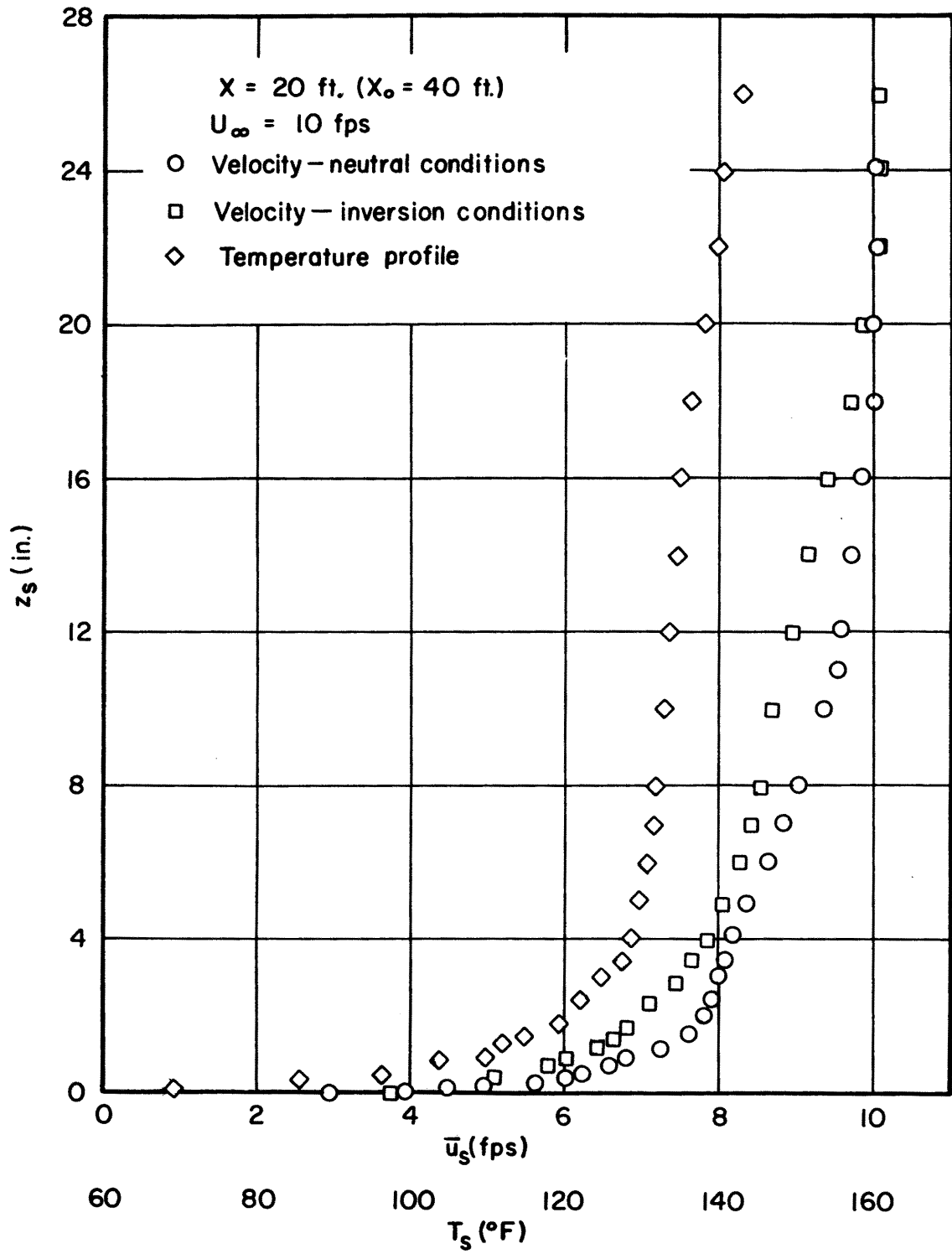Fig. 95 Velocity and temperature profiles (10 fps, 3 ft)

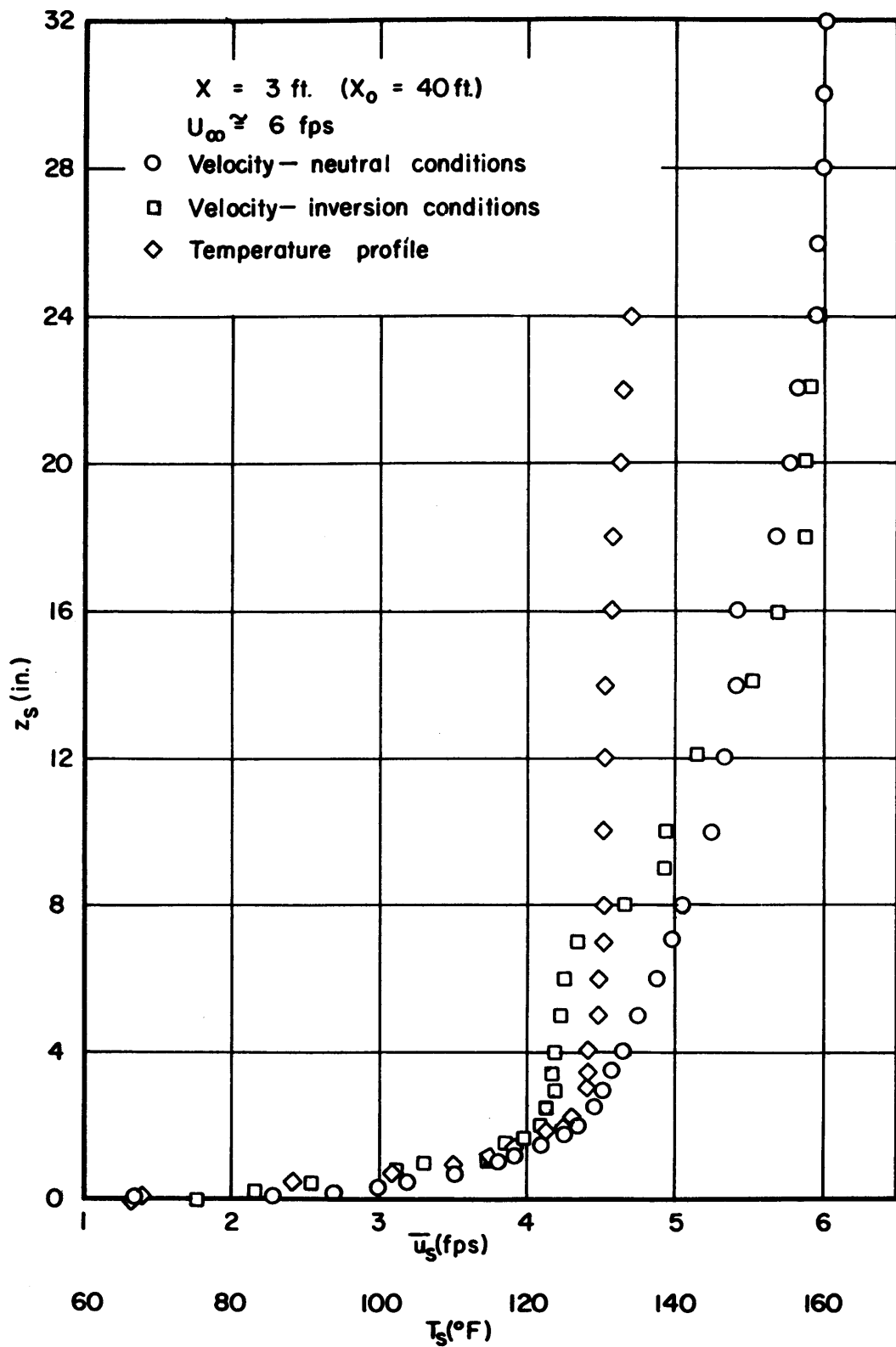Fig. 96 Velocity and temperature profiles (10 fps, 20 ft)
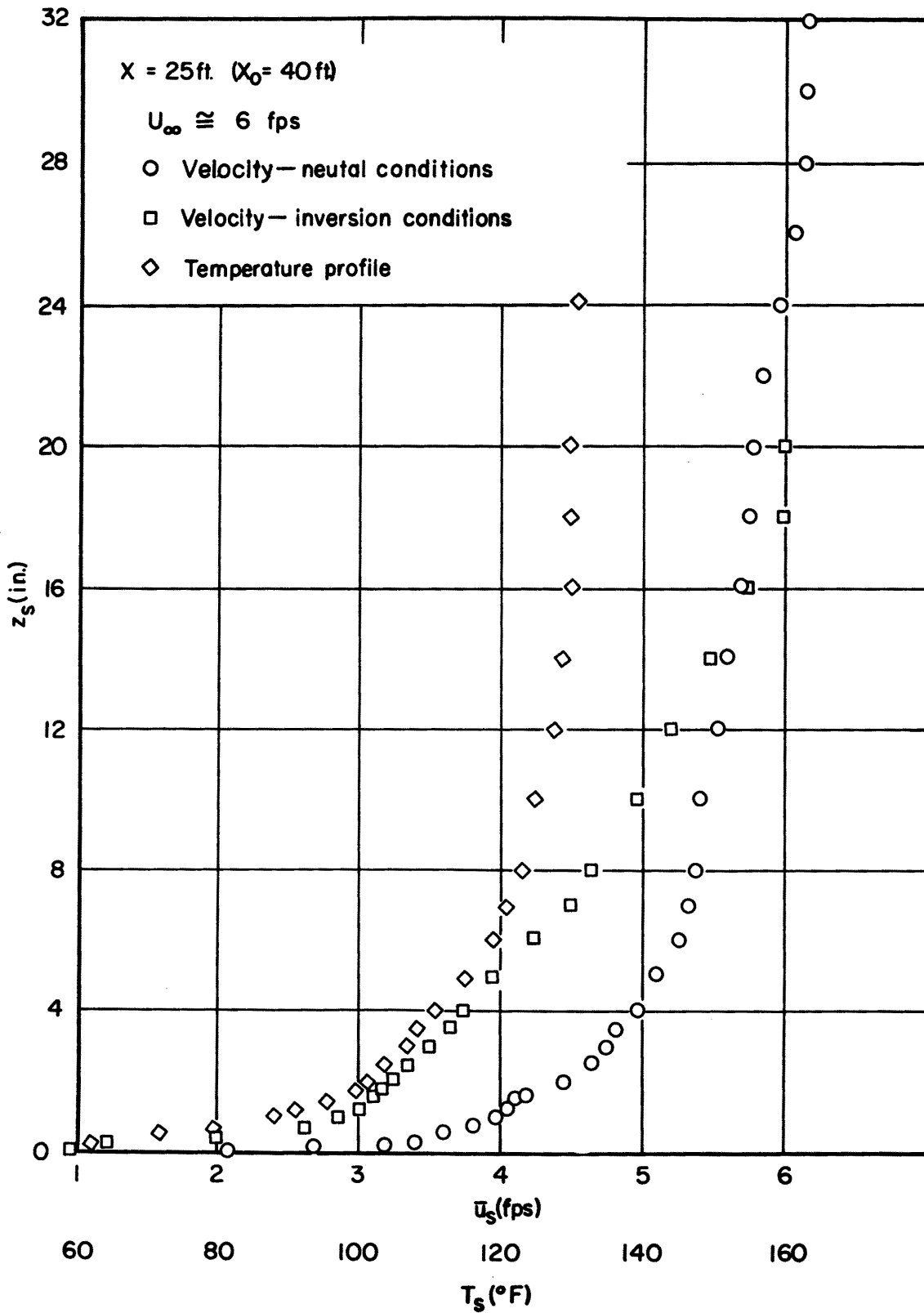
Fig. 97 Velocity and temperature profiles (6 fps, 3 ft)

197

Fig. 98 Velocity and temperature profiles (6 fps, 25 ft)